



HAL
open science

Proteomics of trans-Golgi Network subdomains revealed lipid crosstalk between sphingolipids and phosphoinositides in plants.

Nicolas Esnay

► **To cite this version:**

Nicolas Esnay. Proteomics of trans-Golgi Network subdomains revealed lipid crosstalk between sphingolipids and phosphoinositides in plants.. *Vegetal Biology*. Université de Bordeaux, 2018. English. NNT : 2018BORD0416 . tel-03035010

HAL Id: tel-03035010

<https://theses.hal.science/tel-03035010>

Submitted on 2 Dec 2020

HAL is a multi-disciplinary open access archive for the deposit and dissemination of scientific research documents, whether they are published or not. The documents may come from teaching and research institutions in France or abroad, or from public or private research centers.

L'archive ouverte pluridisciplinaire **HAL**, est destinée au dépôt et à la diffusion de documents scientifiques de niveau recherche, publiés ou non, émanant des établissements d'enseignement et de recherche français ou étrangers, des laboratoires publics ou privés.

THÈSE PRÉSENTÉE
POUR OBTENIR LE GRADE DE

DOCTEUR DE
L'UNIVERSITÉ DE BORDEAUX

ÉCOLE DOCTORALE
SCIENCES DE LA VIE ET DE LA SANTÉ

Par **Nicolas ESNAY**

**PROTEOMICS OF *TRANS*- GOLGI NETWORK
SUBDOMAINS REVEAL A LIPID CROSSTALK BETWEEN
SPHINGOLIPIDS AND PHOSPHOINOSITIDES IN PLANTS**

SOUS LA DIRECTION DE : YOHANN BOUTTÉ

Soutenue le 21 Décembre 2018

Membres du Jury :

M. JAILLAIS, Yvon	Directeur de Recherche, CNRS	Rapporteur
D'ANGELO, Giovanni	Professeur, EPFL	Rapporteur
M. MCCUSKER, Derek	Chargé de Recherche, CNRS	Président
GUYOMARC'H, Soazig	Maître de Conférences, Université Montpellier	Examineur
BOUTTÉ, Yohann	Chargé de Recherche, CNRS	Directeur de thèse

Remerciements

Je tiens particulièrement à remercier mon Directeur de Thèse, **Yohann**, qui a rendu cette incroyable aventure possible, qui a su me faire confiance et m'accompagner dans ce merveilleux voyage du transport vésiculaire. Grâce à ta bonne humeur et à ta prévoyance, ces 3 ans se sont passés dans les rires et sans encombre, malgré quelques petits couaques, tu avais toujours un plan B caché pour rattraper le coup. T'as réussi à me faire comprendre l'importance de la rigueur scientifique, de l'optimisation de son temps (et ça en a pris du temps) mais surtout qu'un directeur de thèse pouvait devenir un ami et pour ça, je t'en remercie profondément.

Je tiens également à remercier les autres membres de l'équipe, **Valérie**, qui m'a beaucoup aidé à essayer de percer les mystères de la PCR et qui a supporté mes choix musicaux douteux et **Patrick** pour tes précieux conseils et ton soutien.

Jean-Jacques, merci de m'avoir accueilli dans le laboratoire et de m'avoir permis de d'aller en congrès pour pouvoir présenter mon travail. Merci également à la FR BIE, et surtout à son directeur **Jérôme** sans qui je n'aurais pas pu partir en congrès. Merci d'ailleurs à l'ISPL team (**Seb, Jérôme** et **Fred**) pour l'ambiance de ce premier congrès au Japon qui était juste incroyable.

Marie, merci d'avoir su supporter nos débats 'ultra importants' avec **Paul**, et **Paul** merci pour ces débats. **Mag'**, je n'oublierai jamais nos moments conneries et nos 'Scary Friday' à deux voire trois (on doit toujours faire cette fusée !!). Et merci à toi, **Rodrigo** pour ces derniers mois, à finir à pas d'heures tous les deux et à ces tentatives de pranks totalement ratées.

Je remercie également tous les membres du laboratoire pour la bonne humeur et la bonne ambiance et les discussions 'intenses' de certains midis. Merci également à toi **Agnès** pour ton soutien, ainsi qu'à **Steph** et **Claire** d'avoir été là depuis mes débuts en tant que Master 2.

J'ai une pensée particulière pour **Vincent** et nos longues discussions tous les deux en fin de journée, j'aurai aimé que tu puisses être là aujourd'hui.

Je remercie également mes amis du côté obscur, **Pierre** et **Amélie** pour ces bons moments tous les trois. Également, je remercie **Hannah, Lily** et **ma famille** pour leur soutien plus qu'essentiel à la réalisation de cette thèse.

And finally, I want to thank the members of the jury **Yvon Jaillais, Giovanni D'Angelo, Dereck McCusker, Soazig Guyomarc'h** for agreeing to criticize, discuss and evaluate my thesis work.

Résumé en Français

Le système de membrane intracellulaire est un ensemble de membranes pouvant se connecter au sein d'un réseau ou être indépendantes et échanger des composants par le biais du transport vésiculaire. L'élaboration de ce système endomembranaire représente certainement l'avantage le plus réussi des cellules eucaryotes sur le plan de l'évolution et leur a permis de compartimenter les réactions biochimiques et de spécifier des voies telles que les voies sécrétoire, endocytique, de recyclage, phagocytaire, de stockage ou de dégradation. Les cellules procaryotes peuvent également présenter une certaine compartimentalisation de la membrane intracellulaire, telles que les membranes thylakoïdes photosynthétiques des cyanobactéries ou un organelle ressemblant à un noyau chez les planctomycète, un phylum de bactéries (Yee et al., 2012; Liberton et al., 2013). Cependant, le degré de diversification de la compartimentalisation endomembranaire est beaucoup plus élevé dans les cellules eucaryotes. Mis à part les mitochondries et les chloroplastes qui étaient une acquisition procaryotique de cellules eucaryotes, le réticulum endoplasmique (RE) est certainement le plus ancien compartiment endomembranaire (Garnier, 1897). Le RE est un réseau de membranes tubulaires constitué de tubules et de feuillettes fenêtrées qui sont en continuité et entourent le noyau, dans le cas du RE périnucléaire, mais qui peuvent aussi se localiser à proximité immédiate de la membrane plasmique (MP), le RE périphérique sous-cortical et établir des sites de contact membranaire avec le MP (Porter et al., 1945; Pichler et al., 2001; Shibata et al., 2006). Le RE est déjà une structure hautement spécialisée, divisée en sous-domaines distincts impliqués dans la formation de corps protéiques ou de corps lipidiques, par exemple, le RE est un endroit où la biosynthèse de lipides et de protéines se produisent. Les protéines destinées à traverser le RE sont transférées dans le lumen du RE après leur synthèse par des ribosomes associés au RE (Simon and Blobel, 1991; Görlich et al., 1992; Crowley et al., 1993).

Un autre exemple de la diversification endomembranaire est le complexe de Golgien, un organelle central conservé parmi les eucaryotes qui a été découvert par Camillo Golgi en 1897 grâce à ses observations sur le système nerveux (Golgi, 1898). Bien que les scientifiques de cette époque ne croyaient pas qu'une telle structure hautement organisée ne puisse exister dans la cellule, c'est grâce au développement révolutionnaire de la microscopie électronique qui finit bientôt par les convaincre, au début du XXe siècle (Dalton and Felix, 1956). Les scientifiques ont dû revoir leur vision des unités intracellulaires eucaryotes et les considérer comme des structures très différenciées qui ne sont pas toujours rondes mais qui peuvent

également adopter des formes vraiment intrigantes, à l'instar de l'appareil de Golgi récemment découvert qui apparaît tubulo-vésiculé (Rambourg and Clermont, 1990). L'origine évolutive du système endomembranaire reste encore un débat aujourd'hui. On pense que l'enveloppe nucléaire et le RE auraient pu provenir de l'invagination de la membrane plasmique où Sar1, le membre le plus ancestral de la famille des small-GTPase dans laquelle les membres se seraient fortement diversifiés au cours de l'évolution, aurait agi par sa propension à induire la tubulation membranaire (Barlowe et al., 1993; Saito et al., 1998; Long et al., 2010; Hanna et al., 2016). En ce qui concerne l'appareil de Golgi, les chercheurs ont peine à croire à la fusion progressive des vésicules existantes ou à l'empilement progressif du réseau tubulaire pouvant dériver de l'ER (Farquhar and Palade, 1998).

La diversification de la famille des smallGTPases aurait pu jouer un rôle crucial dans la structuration du système endomembranaire et les différencier progressivement dans des compartiments spécifiques. Dans les cellules animales, l'appareil de Golgi est une entité complexe en forme de ruban attachée au centrosome des microtubules, tandis que chez les plantes, de nombreux appareils de Golgi sont dispersés dans le cytoplasme et affichent un mouvement le long de câbles d'actine (Thyberg and Moskalewski, 1999; Akkerman et al., 2011). Dans la levure à bourgeon, les citernes du Golgi sont dispersées contrairement à la levure à fission ou à *Pichia pastoris*, où le Golgi est organisé en citernes empilées (Rossanese et al., 1999; Papanikou and Glick, 2009). Dans les cellules animales et végétales, la plus grande citerne de l'appareil de Golgi est en continue avec un compartiment tubulaire, ramifié et réticulé appelé *trans*-Golgi Network (TGN) (Rambourg et al., 1979; Griffiths and Simons, 1986). Le TGN est également perceptible dans la levure de fission ou *Pichia pastoris*, mais pas dans la levure à bourgeon ou *Saccharomyces cerevisiae*. Ce réseau est maintenant considéré comme une plaque tournante centrale pour le tri des protéines via le trafic de vésicules dérivé du TGN (Gu et al., 2001). Cependant, cette organelle diffère des animaux, des levures ou des plantes en termes de structures et de fonctions. Dans mon introduction, je décrirai ces différences entre les règnes ; néanmoins, je me concentrerai davantage sur le TGN des plantes. Comment se forme l'appareil de Golgi et, comment est géré la progression de cargos protéiques ainsi que sa structuration particulière sont différents sujets toujours débattus passionnément par les chercheurs.

De plus en plus de preuves alimentent l'idée que les lipides agissent sur le recrutement et la régulation des protéines impliquées dans la formation ou le processus de tri des vésicules. La différenciation fonctionnelle des compartiments est corrélée à la capacité des membranes eucaryotes à séparer les lipides et à créer une hétérogénéité lipidique. L'hétérogénéité lipidique

crée à son tour une ségrégation des protéines et différencie la fonction à des endroits spécifiques du système endomembranaire. En effet, deux classes de lipides, les sphingolipides et les stérols, ont fortement évolué dans les cellules eucaryotes et sont à la base de la ségrégation des lipides dans les membranes biologiques. Les stérols et les sphingolipides sont également présents dans les cellules procaryotes mais sont moins complexes. Les produits finaux de la voie de biosynthèse des stérols des bactéries sont en réalité les composés intermédiaires de la voie de biosynthèse des stérols eucaryotes et sont moins modifiés que chez les eucaryotes. Les sphingolipides existent dans les bactéries mais leur Long Chain Base (LCB) et leur acide gras (AG) sont saturés et ne dépassent pas 17-19 atomes de carb(Kato et al., 1995; Watanabe et al., 2001; Naka et al., 2003; Heung et al., 2006). Les LCB et la chaîne acyle des AG des sphingolipides eucaryotes peuvent être insaturés, hydroxylés et la chaîne acyle des AG a typiquement une longueur de 22 à 26 atomes de carbone (Kroesen et al., 2003; Buré et al., 2014). Ces particularités eucaryotes des stérols et des sphingolipides ont un impact important sur la biophysique des membranes qu'ils composent. En général, on pense que l'auto-association des glycérolipides, des sphingolipides et des stérols induit une ségrégation membranaire latérale de ces lipides en domaines distincts (Duran et al., 2012; Campelo et al., 2017). Ces domaines influencent la courbure, l'épaisseur et la phase (phase fluide, phase gel) des membranes et facilitent le recrutement des protéines impliquées dans la formation des vésicules et le tri des protéines (Duran et al., 2012; Kulakowski et al., 2018). **Si les lipides peuvent être considérés comme des régulateurs du trafic membranaire pour le tri des protéines, les mécanismes liant les lipides aux protéines dans ce processus cellulaire sont en grande partie inconnus.**

Il a été démontré que les vésicules dérivant du TGN sont enrichies en stérols et en sphingolipides. Mon laboratoire d'accueil a montré dans sa dernière étude que le TGN des plantes est également enrichi en sphingolipides et stérols (Wattelet-Boyer et al., 2016). Néanmoins, les mécanismes de tri agissant au niveau des vésicules et des tubules du TGN demeurent inconnus pour un large éventail de protéines. De plus, il reste à déterminer quels mécanismes dépendent de la composition lipidique de la membrane, en ce qui concerne le tri des protéines. **L'organisation latérale des lipides au sein d'une membrane biologique est en train de devenir un intérêt fondamental pour les biologistes cellulaires.** Existe-t-il un lien direct entre les lipides membranaires et les cargos ou des domaines lipidiques spécifiques recrutent-ils des types spécifiques de protéines encore non identifiées ? Identifier les lipides et les protéines dépendantes des lipides au niveau du TGN serait certainement utile pour comprendre la complexité des mécanismes de tri.

Au cours de ma thèse, j'ai utilisé différentes approches expérimentales pour obtenir une première réponse à ces questions. Dans cette partie de ma thèse de doctorat, je voudrais d'abord décrire plus en détail les bases conceptuelles sur lesquelles j'ai développé ma recherche.

Table of contents

ABBREVIATION	1
I. INTRODUCTION	2
A. THE GOLGI APPARATUS	5
B. THE <i>TRANS</i> -GOLGI NETWORK (TGN)	6
1. <i>The trans-Golgi Network Structure</i>	7
2. <i>Secretory pathways at trans-Golgi Network</i>	8
3. <i>The Ypt/Rab superfamily and endomembrane identity</i>	9
C. LIPID ACTING AT THE ENDOMEMBRANE IDENTITY	13
1. <i>Phosphoinositide</i>	13
2. <i>Sphingolipids</i>	15
II. MATERIALS AND METHODS	19
A. PLANT MATERIAL AND GROWTH CONDITIONS	19
1. <i>Seeds sterilization and in vitro growth</i>	19
2. <i>On-soil growth</i>	19
3. <i>Plant stable transformation</i>	19
4. <i>Plant crossing method</i>	20
B. TREATMENTS	20
1. <i>Inhibitor treatments</i>	20
2. <i>β-Estradiol induction</i>	21
C. ROOT GRAVITROPISM AND ROOT LENGTH ASSAYS	21
D. IMMUNOPRECIPITATION OF INTACT TGN AND GOLGI COMPARTMENTS.....	22
E. WESTERN BLOTTING OF IP FRACTIONS.....	23
F. PROTEOMIC ANALYSIS	24
1. <i>Sample preparation and protein digestion</i>	24
2. <i>nLC-MS/MS analysis</i>	24
3. <i>Database search and results processing</i>	25
4. <i>Label-Free Quantitative Data Analysis</i>	25
G. CLONING	26
1. <i>DNA extraction and Multisite Gateway[®]</i>	26
2. <i>Competent bacteria protocol</i>	27
H. CONFOCAL MICROSCOPY	28
I. STATISTICAL ANALYSIS	29
III. RESULTS	30

A.	METAZACHLOR: A NEW PHARMACOLOGICAL TOOL TO REDUCE THE VERY-LONG-CHAIN FATTY-ACID LENGTH OF SPHINGOLIPIDS.....	30
B.	IDENTIFICATION OF SPHINGOLIPID-DEPENDENT ACTORS.....	33
1.	<i>Compartments extraction</i>	34
2.	<i>Proteomic analyses</i>	36
3.	<i>Extraction validation by proteomic analysis</i>	37
4.	<i>Cargos traffic through specific TGN sub-domains</i>	42
5.	<i>Identifying Sphingolipid-dependent actors at TGN</i>	43
C.	CLONING OF SYP61-PROTEOME-SELECTED PROTEINS	45
D.	METAZACHLOR AFFECTS PIPs HOMEOSTASIS	46
1.	<i>Metazachlor alters PI₄P quantity at plasma membrane</i>	47
2.	<i>Metazachlor gravitropism response is affected in the pi4k61/pi4k62</i>	47
3.	<i>PI₃P fluorescence intensity is decreased upon metazachlor treatment</i>	49
4.	<i>Metazachlor not only affect PI₃P overall quantity but also alters PI₃P localization pattern</i>	49
5.	<i>Metazachlor increases the PI₃P synthesis through a distinct pathway than the PI 3-kinase</i>	51
6.	<i>SAC1 function and localization is not impaired by metazachlor</i>	52
E.	METAZACHLOR AFFECTS RAB-GTPASES PATTERNING AT TGN.....	53
IV.	DISCUSSION	55
	REFERENCES	64
	ANNEX 1	79
	ANNEX 2	80
	ANNEX 3	81
	ANNEX 4	83
	ANNEX 5: NATURE COMMUNICATION	87

Abbreviation

ACN: Acetonitrile

ADN: Acid DesoxyriboNucleic

amiRNA: artificial micro-RNA

AP: Adaptor Protein

CCV: Clathrin-Coated Vesicle

CGFB: Function Genomic Center of
Bordeaux

CHC: Clathrin-Heavy-Chain

CME: Clathrin-Mediated Endocytosis

Col-0: Columbia-0 ecotype of *Arabidopsis
thaliana*

Da: Dalton

DAG: DiAcylGlycerol

DMSO: DiMethylSulfOxide

EE: Early Endosome

EM: Electron Microscopy

ER: Endoplasmic Reticulum

FA: Fatty Acid

GIPC: GlycosylInositolPhosphorylCeramide

GMT: GIPC mannosyl transferase

GO: Gene Ontology

IEM: Immunolabeling Electron Microscopy

KCS: 3-Ketoacyl-Coenzyme A Synthase

LC-MS/MS: Liquid Chromatography
coupled to Mass Spectrometry

LDB: Lipid-Binding Domain

LE: Late Endosome

MVB: Multi-Vesicular Body

PC: PhosphatidylCholine

PI: PhosphatidyInositol

PI_{3,4,5}P₂: PhosphatidyInositole 3,4,5-
triPhospate

PI_{3,5}P₂: PhosphatidyInositole 3,5-
biPhospate

PI3K: PI 3-kinase

PI₃P: PhosphatidyInositole 3-Phospate

PI_{4,5}P₂: PhosphatidyInositole 4,5-
biPhospate

PI4K: PI 4-kinase

PI₄P: PhosphatidyInositole 4-Phospate

PIP: PhosphoInositide

PKD: Protein Kinase D

PM: Plasma Membrane

PVC: Pre-Vacuolar Compartment

RE: Recycling Endosome

RNA: RiboNucleic Acid

SDS-PAGE: Sodium Dodecyl Sulfate-
PolyAcrylamide Gel Electrophoresis

SDS: Sodium Dodecyl Sulfate

SV: Secretory Vesicle

TGN: *trans*-Golgi Network

α VLCFA: α -hydroxylated-Very-Long-Chain-
Fatty-Acid

I. Introduction

The intracellular membrane system is a set of membranes that can connect within a network or can be independent and exchange material through vesicle transport. The building of this endomembrane system certainly represents the most successful evolutionary advantage of eukaryotic cells and allowed them to compartmentalize biochemical reactions and specifies pathways such as secretory, endocytic, recycling, phagocytic, storage or degradation pathways. Prokaryotic cells can also present some intracellular membrane compartmentalization such as photosynthetic thylakoid membranes of cyanobacteria or the nucleus-like organelle of planctomycete, a phylum of bacteria (Yee et al., 2012; Liberton et al., 2013). However, the degree of diversification of membrane compartmentalization is much higher in eukaryotic cells. Aside from mitochondria and chloroplasts that were prokaryotic acquisition of eukaryotic cells, the endoplasmic reticulum (ER) is certainly the most ancient endomembrane compartment (Garnier, 1897). The ER is a tubular membrane network made of tubules and fenestrated sheets which are in continuity and surround the nucleus, in the case of the perinuclear ER, but which can also localize in close proximity of the plasma membrane (PM), in the case of the sub-cortical peripheral ER, and establish membrane contact sites with the PM (Porter et al., 1945; Pichler et al., 2001; Shibata et al., 2006). The ER is already highly specialized structure divided in distinct sub-domains involved in formation of protein bodies or lipid bodies for instance, the ER is a place where lipid and protein biosynthesis occur. Proteins destined to cross the ER are translocated in the lumen of the ER after their synthesis by ER-associated ribosomes (Simon and Blobel, 1991; Görlich et al., 1992; Crowley et al., 1993).

Another very good example of endomembrane diversification is the Golgi complex, a central organelle conserved amongst eukaryotes that was discovered by Camillo Golgi in 1897 through his observations on the nervous system (Golgi, 1898). Although scientists of that time did not believe that this highly organized structure ever exist in the cell, groundbreaking development of the electron microscope would soon convince them at the beginning of the 20th century (Dalton and Felix, 1956). Scientists had to revisit their view of eukaryotic intracellular unities and consider them as highly differentiated structures that are not always round but can also adopt really intriguing shapes as was the newly discovered Golgi apparatus that appears tubulo-vesiculated (Rambourg and Clermont, 1990). The evolutionary origin of the endomembrane system still remains a debate today. It is thought

that the nuclear envelope and ER could have appeared from invagination of the plasma membrane where Sar1, the most ancestral member of the small GTPase family, in which members strongly diversified during evolution, would have had acted through its propensity to induce membrane tubulation (Barlowe et al., 1993; Saito et al., 1998; Long et al., 2010; Hanna et al., 2016). As for the Golgi apparatus, researchers are torn to believe in either progressive fusion of existing vesicles or progressive stacking of tubular network that could derived from ER (Farquhar and Palade, 1998).

Diversification of the small GTPase family could have had a crucial role in sculpting diverse shapes within the endomembrane system and progressively specialize them in specific compartments. In animal cells, the Golgi apparatus is one ribbon-shaped complex entity attached to microtubules of the centrosomes while in plants, there are many Golgi apparatus dispersed in the cytoplasm and displaying a velocity along actin cables (Thyberg and Moskalewski, 1999; Akkerman et al., 2011). In budding yeast, the cisternae of the Golgi are dispersed in contrast to fission yeast or *Pichia pastoris* where the Golgi is organized in stacks (Rossanese et al., 1999; Papanikou and Glick, 2009). In animal and plant cells, the *trans*-most cisterna of the Golgi apparatus is continuous with a tubular, branching and reticulated compartment called *trans*-Golgi Network (TGN) (Rambourg et al., 1979; Griffiths and Simons, 1986). TGN is also discernible in fission yeast or *Pichia pastoris* but not in budding yeast. This network is now considered to be a central hub for sorting of proteins through TGN-derived vesicles trafficking (Gu et al., 2001). However, this organelle differs from animals, yeast or plants in terms of structures and functions. In my introduction, I will describe these differences between kingdoms; nevertheless I will be more focus on plant's TGN. How the Golgi apparatus stack is formed and manages progression of cargos proteins through the stack and how TGN is acquiring its specific shape is still a matter of passionate debate for cell biologists.

Growing evidences feed the idea that lipids act on recruiting and regulating proteins involved in vesicle formation or sorting process. Functional differentiation of compartments is correlated with the ability of eukaryotic membranes to segregate lipids and create lipid heterogeneity. Lipid heterogeneity in turn creates protein segregation and differentiates function at specific spots of the endomembrane system. Indeed, two classes of lipids, sphingolipids and sterols, strongly evolved in eukaryotic cells and are at the basis of lipid segregation in biological membranes. Sterols and sphingolipids are also present in prokaryotic cells but are less complex. Final products of the sterol biosynthesis pathway of bacteria are

actually the intermediate compounds of eukaryotic sterol biosynthesis pathway and are less modified than in eukaryotes. Sphingolipids exists in bacteria but both their Long Chain Base (LCB) and Fatty Acid (FA) acyl chain are saturated and do not exceed 17-19 carbons in length (Kato et al., 1995; Watanabe et al., 2001; Naka et al., 2003; Heung et al., 2006). Eukaryotic sphingolipids LCBs and FA acyl chain can be unsaturated, hydroxylated and FA acyl chain is typically 22-26 carbons in length (Kroesen et al., 2003; Buré et al., 2014). These eukaryotic parameters of sterols and sphingolipids have a strong impact on the biophysics of membranes they composed. In general, it is thought that auto-association of glycerolipids, sphingolipids and sterols induce lateral membrane segregation of these lipids into distinct domains (Duran et al., 2012; Campelo et al., 2017). These domains influence curvature, thickness and the phase (fluid-phase, gel-phase) of membranes and facilitate recruitment of proteins involved in vesicle formation and protein sorting (Duran et al., 2012; Kulakowski et al., 2018). **If lipids can be viewed as membrane traffic controller for protein sorting, the mechanisms linking lipids to proteins in this cellular process are largely unknown.**

It has been shown that TGN-derived vesicles are enriched in sterols and sphingolipids and deprived in glycerophospholipids. My host lab has shown in its last study that TGN of plants is also enriched for sphingolipids and sterols (Wattelet-Boyer et al., 2016). Still, sorting mechanisms acting at TGN vesicles and tubules still remain unknown for a wide set of proteins. Moreover, it remains unclear which mechanisms depend on lipid membrane composition in respect to protein sorting. **The lateral organization of lipids within a biological membrane is emerging as a core interest for cell biologists.** Is there a direct link between membrane lipids and cargos or do specific lipid-domains recruit specific types of yet to identify proteins? Identifying lipids and lipid-dependent proteins at TGN would definitely help but to understand the complexity of sorting mechanisms.

During my PhD thesis I employed experimental approaches to get a first answer on these questions. In this section of my PhD thesis I would like first to describe more deeply the conceptual bases on which I developed my PhD research.

A. The Golgi apparatus

Firstly describe more than 100 years ago by Camillo Golgi, the Golgi was compare as a basket-like structure surrounding the nucleus (Golgi, 1898). More than 50 years later, Electron Microscopy (EM) technology has improved and for the first time, the Golgi apparatus was described as a stack of flattened membrane sacs called cisternae (Dalton and Felix, 1956). The Golgi apparatus can contains as few as 3 or as many as 20 cisternae depending on the organism or the cell type (Becker and Melkonian, 1996). The concept of maturation appears later, thanks to a French scientist who hypothesized a plausible role of the Golgi apparatus in the secretory pathways (Grassé, 1957), however this has been proved few years later using radioactive markers which furthermore suggested a cisternae maturation for the *cis* side (ER side) to the *trans* side of the Golgi apparatus (Farquhar and Palade, 1981). From this moment, the Golgi apparatus was considered as a stack of cisternae which matures from the *cis* side (ER-side) to the *trans* side. The Golgi apparatus is divided in four different part: the *cis*, the medial, the *trans* and the TGN. These parts are defined by their morphology, their function and also by their composition. The Golgi apparatus is the place where protein modifications and protein sorting occur. Furthermore, it's a place for glucan-modification of different type of molecules as sugars, proteins or lipids by synthetizing complex polysaccharides (Stanley, 2011; Ruiz-May et al., 2012; Donohoe et al., 2013). Each enzymes of modification are located in define cisternae, allowing the cell to optimized the pH, ion composition, and substrate concentrations for each set of enzymes (Day et al., 2013). In plant cells, the Golgi apparatus is also the compartment where occurs the biosynthesis of cell wall components. The compartmentation of the cisternae prevents the agglomeration of pectic and xyloglucan polysaccharides in the secretion pathway (Zhang and Staehelin, 1992; Atmodjo et al., 2013; Dick et al., 2012).

Furthermore, the fact that the Golgi apparatus in plants plays a key role in the biosynthesis of plant's cell wall likely lead to an increase of Golgi apparatus number. Unlike yeast and animal cells, plant cells contains several Golgi apparatus, up to 600 depending on the cell type and/or development state (Mollenhauer and Morré, 1994). On the other hand, Golgi apparatus in budding yeast *Saccharomyces cerevisiae* is also different from plant and animal Golgi apparatus by its non-stacked-cisternae morphology. However, this non-stacked Golgi has still different cisternae with different functions and compositions (Papanikou and Glick, 2009). How the Golgi apparatus works is still misunderstood and is a subject of controversy. First described as a four-stage model, according the cisternae's localization,

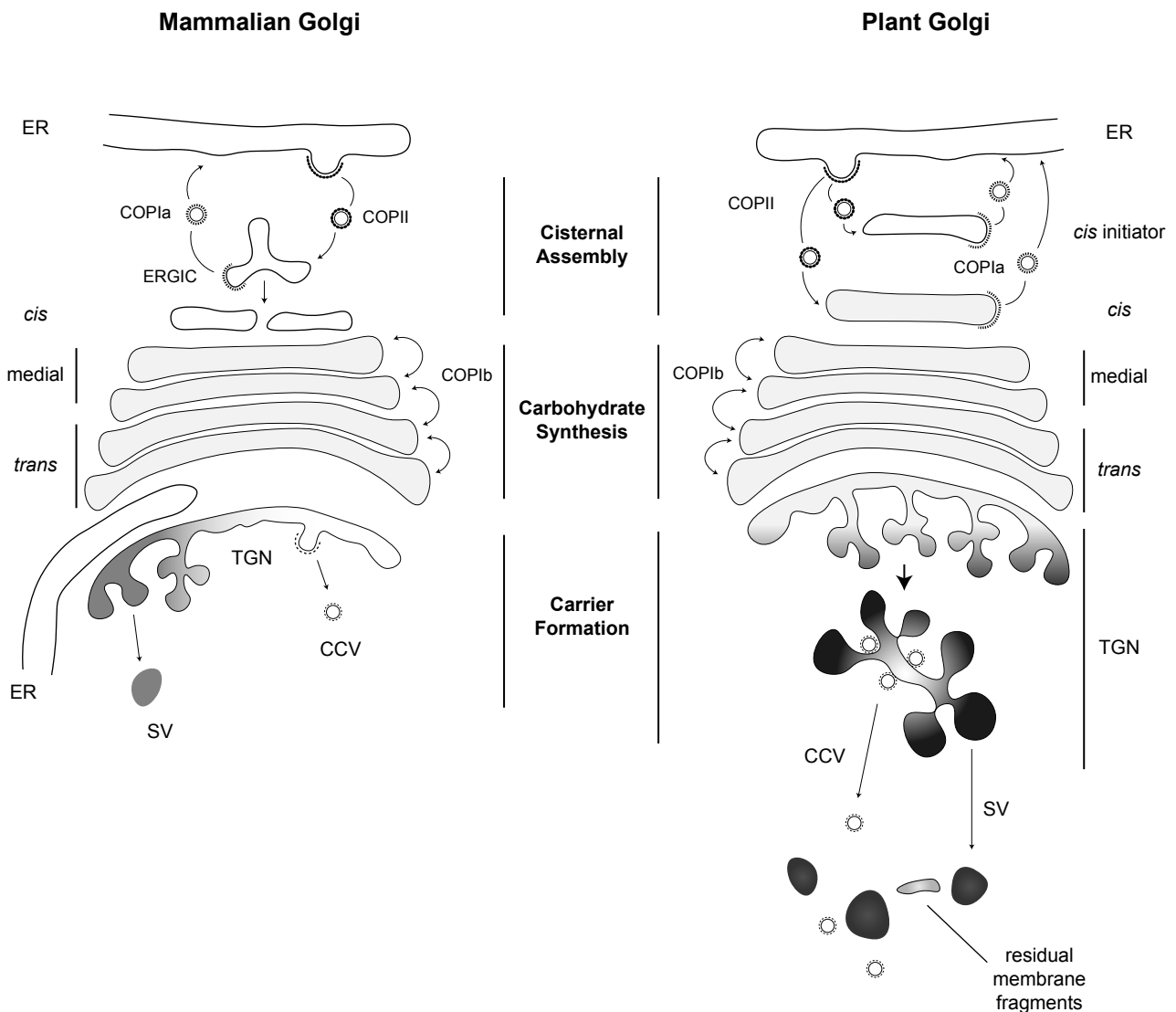


Figure 1: Difference between Mammalian and Plant Golgi, and the relevance of the Three-Stage Model. Both mammalian and plant Golgi are initiated via the trafficking of COPII vesicles from the ER to the ERGIC for mammals or the *cis* initiator for the plant. In these two organisms, retrograde transport is done by the COPIa-coated vesicles from the Golgi to the ER, and the vesicles trafficking between the Golgi cisternae are performed by COPIb vesicles. The major difference between mammals and plants is the TGN which is associated to the Golgi and the ER in mammals while in plants, the TGN can be independent and fragmented to release different cargos. ER: Endoplasmic Reticulum, ERGIC: ER-Golgi Intermediate Compartment, TGN: *trans*-Golgi Network, SV: Secretory Vesicle, CCV: Clathrin-Coated Vesicle
Adapted from Day et al. 2013

function and composition (*cis*, medial, *trans*, and TGN), recent reviews want to reconsider this model. They propose a three-stage model based on the vesicle trafficking and cisternae's function. Indeed, there is different trafficking machinery associated with specific coat protein between the cisternae: the ER to *cis*-Golgi transport uses COPII vesicles, the *cis*-Golgi to ER uses COPIa vesicles, and the transport between the Golgi's cisternae is performed *via* COPIb vesicles. All these coat proteins are described to traffic between these compartments of the Golgi apparatus (Orci et al., 1997; Scales et al., 1997; Day et al., 2013). Furthermore, the COP proteins are well conserved between yeasts, animals and plants unlike the enzymes contained in the different cisternae. However, another criterion of this novel model is the global function of each part of the Golgi apparatus. So, the three parts of the Golgi apparatus are:

- Cisternal Assembly stage: when COPII vesicles bud from the ER and fuse together to form the *cis* Golgi, and there is also the retrograde transport of ER-resident protein *via* COPIa vesicles
- Carbohydrate Synthesis stage: when the cisternae lose their ability to receive COPII vesicles and start to receive COPIb vesicles. There is also a cisternae maturation from the *cis* to medial and medial to the *trans*, and moreover the beginning of the carbohydrate synthesis and the protein maturation
- Carrier Formation stage: when the cisternae no longer receive COPIb vesicles and produce COPIb vesicles. There is the formation of secretory vesicle, and this part also corresponds to the TGN.

The advantage of the new three-stage model (figure 1 adapted from Day et al., 2013) is that all the Golgi apparatus from different species fit in, whatever the cisternae numbers or structure between the ER and the *cis* Golgi (as ERGIC, ER-Golgi Intermediate Compartment) or the morphology of the Golgi apparatus.

B. The *trans*-Golgi Network (TGN)

The Golgi apparatus is a place where occurs the maturation of different molecules (proteins, lipids, polysaccharides, etc.). Most of these molecules do not localize at the same part of the cell at the end of the secretion journey. Hence, they need to be sorted out; one of their main sorting stations is the TGN, a major secretory pathway sorting hub. The TGN is an

endomembrane compartment located at the *trans*-most side of the Golgi apparatus where a further maturation occurs and leads to the formation of the TGN (Griffiths and Simons, 1986). Thirty years ago, Griffiths G. and Simons K. already proposed a model of TGN releasing at least two types of vesicles, the Secretory Vesicles (SV) and the Clathrin-Coated Vesicles (CCV). Nowadays, the improvement of the new technologies highlights the TGN features. In plant cell, auxin carriers pass through the Golgi apparatus and are sorted by the TGN, however their final localization at the plasma membrane is different dependently on the auxin carrier looked at. For example, the auxin influx carrier AUX1 has a rather non-polar localization in the root epidermal cell whereas the auxin efflux carrier PIN2 is polarly localized at the apical membrane of root epidermal cells (Swarup and Péret, 2012; Boutte et al., 2013; Kleine-Vehn et al., 2011). These two auxin carriers, AUX1 and PIN2, are known to traffic through the TGN to be secreted to the plasma membrane but they use different TGN-mediated pathways (Kleine-Vehn et al., 2006; Robert et al., 2008; Boutte et al., 2013; Wattelet-Boyer et al., 2016). Another auxin carrier PIN1, which localization is polar at basal membrane of root central cylinder cells, is known to recycle between the PM and the TGN (Kania et al., 2014; Luschnig et al., 2014). How plant TGN acts in different sorting pathways is still misunderstood. However, there are some differences between animals, yeasts and plants TGN that could give some clues.

1. The *trans*-Golgi Network Structure

The TGN is now described as a tubulo-vesicular endomembrane compartment where occurs different sorting pathways as secretory sorting or recycling pathways. The TGN of animals, yeasts and plants is structurally different. For example, in animals (rat kidney cells), the TGN is described by EM tomography to be interconnected with the ER structure called *trans*-ER (Ladinsky et al., 1999). They suggest a possible role in lipid transfer from the TGN to the ER which is supported by recent study on ceramide transport between the TGN and the ER (Hanada et al., 2009). However, this kind of interconnection between the ER and the TGN is not described in plants, despite a lot of ultra-structural studies on plant TGN. The shape of animal TGN changes according to the secretory status of the cell, bigger are the secretory granules, smaller is the TGN and sometimes there is no TGN (Clermont et al., 1995; Gu et al., 2001). This observation suggests that the TGN is a dynamic organelle in continuous renewal. Plants have a lot of TGN specific features, the first being that there is a plethora of TGN as compared to animal cell.

In plant cells, the TGN can be classified in two types: Golgi-Associated TGN, GA-TGN, or the Golgi-Independent TGN, GI-TGN (Uemura et al., 2014). Thanks to the improvement of confocal imaging, a new type of microscope, which is only available in RIKEN (Japan), called the Super-resolution Confocal Live Imaging Microscopy (SCLIM) offers a combination between high resolution and *in silico* deconvolution, allowing a high-resolution with a high-speed acquisition. With the SCLIM, Akihiko Nakano' and Tomohiro Uemura's team has shown that TGN marked by GFP-SYP43 (Syntaxin of Plant 43) is whether associated or not with the *trans* cisternae of the Golgi apparatus marked by ST-mRFP highlighting the existence of GI-TGN in plant cell (Uemura et al., 2014). Moreover, thanks to the ability of the SCLIM to perform live cell imaging, they recorded the TGN release from the Golgi apparatus and the formation of neo-GA-TGN at the *trans* most side of the Golgi apparatus (Uemura et al., 2014). These results show that the plant TGN is a very dynamic organelle moving within the cell. According to the plant cell type, there is a relation between GA-TGN/GI-TGN ratio and the differentiation level of the cell, the more the cell is differentiated, higher is the number of GI-TGN (Uemura et al., 2014). This could reflect the mobilization of TGN to respond to the cell elongation need.

In yeast, TGN is quite different from other organisms. First, most of the time, the Golgi apparatus in *Saccharomyces cerevisiae* is unstacked so the *cis*, medial and *trans* Golgi cisternae are dispersed within the yeast and the TGN is more considered as the Late Golgi, a sort of compartment between the Golgi and the TGN (Losev et al., 2006; Matsuura-Tokita et al., 2006; Chow et al., 2008; Emr et al., 2009). Whatever the organism, animal, plant or yeast, the TGN or Late Golgi, as described before, is a highly dynamic endomembrane compartment where occurs the secretory sorting of at least two types of vesicles. Most of those vesicles are coming or going from or to the PM which can be divided in different domains depending on the cell polarity.

2. Secretory pathways at *trans*-Golgi Network

In animal epithelial cells, lateral diffusion at PM is limited by the tight junctions that physically blocked the molecule diffusion between the apical PM and the baso-lateral PM. In plant cells (as in yeast too), there is no tight junction but there is still a polarity with define apical, basal and lateral PM polar domains. Plants developed sub-cellular mechanisms to maintain polar PM domains by linking the membrane components to the cell wall, recycling

pathways and polar secretory sorting (Kleine-Vehn et al., 2008; Kania et al., 2014; Ruiz Rosquete et al., 2017; Wattelet-Boyer et al., 2016).

Moreover, plants' TGN is highly dynamic compared to animals. This feature is essential for the cell wall components secretion and formation of the cell plate, e.g. the division plane, for example. In animal cells, TGN and endosomes are separated although they can exchange materials, whereas in plants, these secretory and endosomal sorting happen both at the TGN. Indeed, the plants' TGN is the central sorting hub of cargoes but is also involved in the recycling of endosomal components and is therefore termed TGN/EE (early endosomes) which suits better than TGN. In addition, TGN releases at least two types of vesicles the SV (secretory vesicles) and the CCV (clathrin coated vesicles). For the neo-synthesized cargoes, the animals' TGN dispatches coated vesicles to RE (recycling endosomes) or LE (late endosomes) and also directly to the PM whereas the endocytosed components are first sorted in EE which send them to LE or RE. In contrary, in plants, the TGN acts as EE and RE (Dettmer et al., 2006; Viotti et al., 2010; Ruiz Rosquete et al., 2017). The mechanism of division of labor by the TGN is still being studied. However, by comparing homologous proteins from animal, some mechanisms start to be underlined, as for example the recycling endosomes (RE)-localized Rab11 which homologues in Arabidopsis, RabA2 and RabA3, localize at TGN and play a key role in endosomal recycling trafficking between the PM and the TGN (Chow et al., 2008).

3. The Ypt/Rab superfamily and endomembrane identity

The small GTPase proteins Rab, in plant and animal, and Ypt, in yeast are a super family in charge of giving specificity to vesicle transport. It has to be tightly regulated to avoid mislocalization of protein to mistargeted compartments. Several Ypt/Rab have been identified to be associated to specific transport mechanism as polar sorting mechanism through recycling (Pereira-Leal and Seabra, 2001; Rutherford and Moore, 2002; Rink et al., 2005)

a) *Ypt/Rab identification*

How the Ypt/Rab are classified in a nomenclature is different across organisms and, plants present a wide diversification of Rab classified into several subfamilies, as example:

Table representing the Rab family repartition according to the plant's Rab clades with orthologues highlighted in green:

<i>Rab Family</i>	<i>Plant Subfamily</i>	<i>Animal Subfamily</i>	<i>Yeast Subfamily</i>
A	RabA1, RabA2, RabA3, RabA4, RabA5, RabA6	Rab11, Rab25	Ypt31, Ypt32
B	RabB1	Rab2, Rab4, Rab14	
C	RabC1, RabC2	Rab18	
D	RabD1, RabD2	Rab1	Ypt1
E	RabE1	Rab8 (11 members)	Sec4
F	RabF1, RabF2	Rab22, Rab5, Rab21, Rab17, Rab24	Ypt51/52/53
G	RabG1, RabG2, RabG3	Rab7 (9 members)	Ypt7
H	RabH1	Rab6	Ypt6

This table (adapted from Rutherford and Moore, 2002) underlines the complexity of the Rab annotation amongst the species even if on this table the different isoforms (annotated with a lowercase letter after the number) do not appear. In yeast *S. cerevisiae*, 11 Ypt/Rabs have been identified and can be dispatched in 8 functionally subclasses, whereas in animal there is 60 Ypt/Rabs distributed in 40 different functional subclasses, and between yeast and animal, six subclasses show conserved functionality (Zerial and McBride, 2001; Pereira-Leal and Seabra, 2000, 2001; Rutherford and Moore, 2002). Within the *A. thaliana* genome, 57 genes have been identified coding for Rab-GTPases, they are classified in eight clades according to their sequence homology (table above, Pereira-Leal and Seabra, 2001; Rutherford and Moore, 2002). And there are still the same six subclasses in common with the three kingdoms (plants, animals and fungi) suggesting these six Ypt/Rab subclasses (A, D, E,

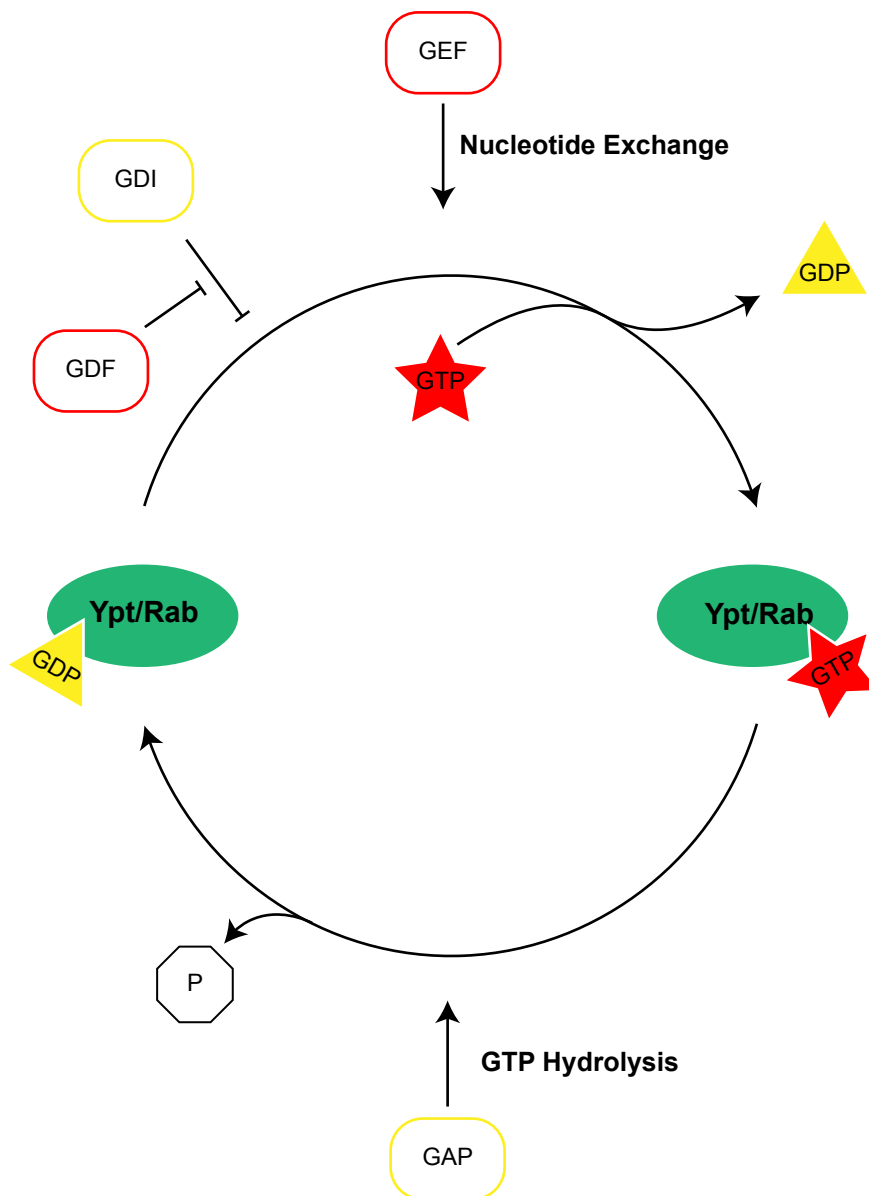


Figure 2: Ypt/Rab regulation cycle. The Ypt/Rab inactivated form (Ypt/Rab-GDP) is maintained in the cytosol by the GDI which is dissociated from the Ypt/Rab-GDP by the GDF, allowing its membrane localization and its activation by the GEF that change the GDP in GTP (active form). The Ypt/Rab-GTP go back to its inactivated form by the action of the GAP that hydrolyzes the GTP in GDP, leading to the Ypt/Rab deactivation.

In yellow, the different deactivator, GDI: Guanine nucleotide Dissociation Inhibitor, GAP: GTPase Activating Protein. And in red, the activators, GDF: GDI Dissociation Factor, GEF: Guanine nucleotide Exchange Factor.

Adapted from Segev N., 2001

F, G and H) are the minimal set of eukaryotic Rab functions. This conservation is observed as well in the sequence homology as in the subcellular localization, *e.g.* RabD2, Rab1 and Ypt1 share more than 80% homology (including conservative exchange) and all three localize between the ER and the Golgi apparatus, and moreover the Rab1 complements the *Ypt1* mutant in yeast underlying the conservation of Ypt/Rab across eukaryotic kingdoms (Haubruck et al., 1987; Segev et al., 1988; Haubruck et al., 1989; Batoko et al., 2000). All these publications suggest a strong conservation amongst the kingdoms of the Ypt/Rab paralogues in their functionality and their localization.

b) The Ypt/Rab features

Ypt/Rab is attached to the membrane *via* lipid tails and recruits a plethora of effectors which mediate vesicular transport. Due to their conservation, the homology between the kingdoms facilitates the identification of their putative function (Rutherford and Moore, 2002). The Ypt/Rab are described as compartment-specific small GTPase more than transport-step specific, and their activity are regulated by a set of Guanine nucleotide Exchange Factor (GEFs) and GTPase Activating Protein (GAPs) that switch on and off the Ypt/Rab by changing their GDP in GTP and their GTP in GDP respectively (figure2, Segev, 2001; Blümer et al., 2013). A lot of vesicular elements as tethers or motor proteins are acting downstream effectors of Ypt/Rab and these effectors are activated by Ypt/Rab-GTP, the active form of Rab.

The mechanisms associated with the Ypt/Rab are very complex because they are involved in the compartment identity, vesicles fusion/fission, cargos recruitment and coating mechanism. Moreover, when associated to their two different forms GDP- or GTP-form, they could have either a cytosolic or a membrane localization (inactive or active respectively, Hutagalung and Novick, 2011). This different localization allows a better control of the small GTPase activity and allows the recycling of Ypt/Rab along the sorting pathways. The localization at membranes of Ypt/Rab is mediated by a lipid anchor through a prenylation reaction that fix a geranylgeranyl isoprenoid (20 carbon) on their C-terminus part (Casey and Seabra, 1996). This Ypt/Rab membrane-anchoring is controlled by a Guanine nucleotide Dissociation Inhibitor (GDI) which recognizes the Ypt/Rab-GDP and extract it from the membrane until the GDI/Ypt/Rab-GDP complex is broken by a GDI Dissociation Factor

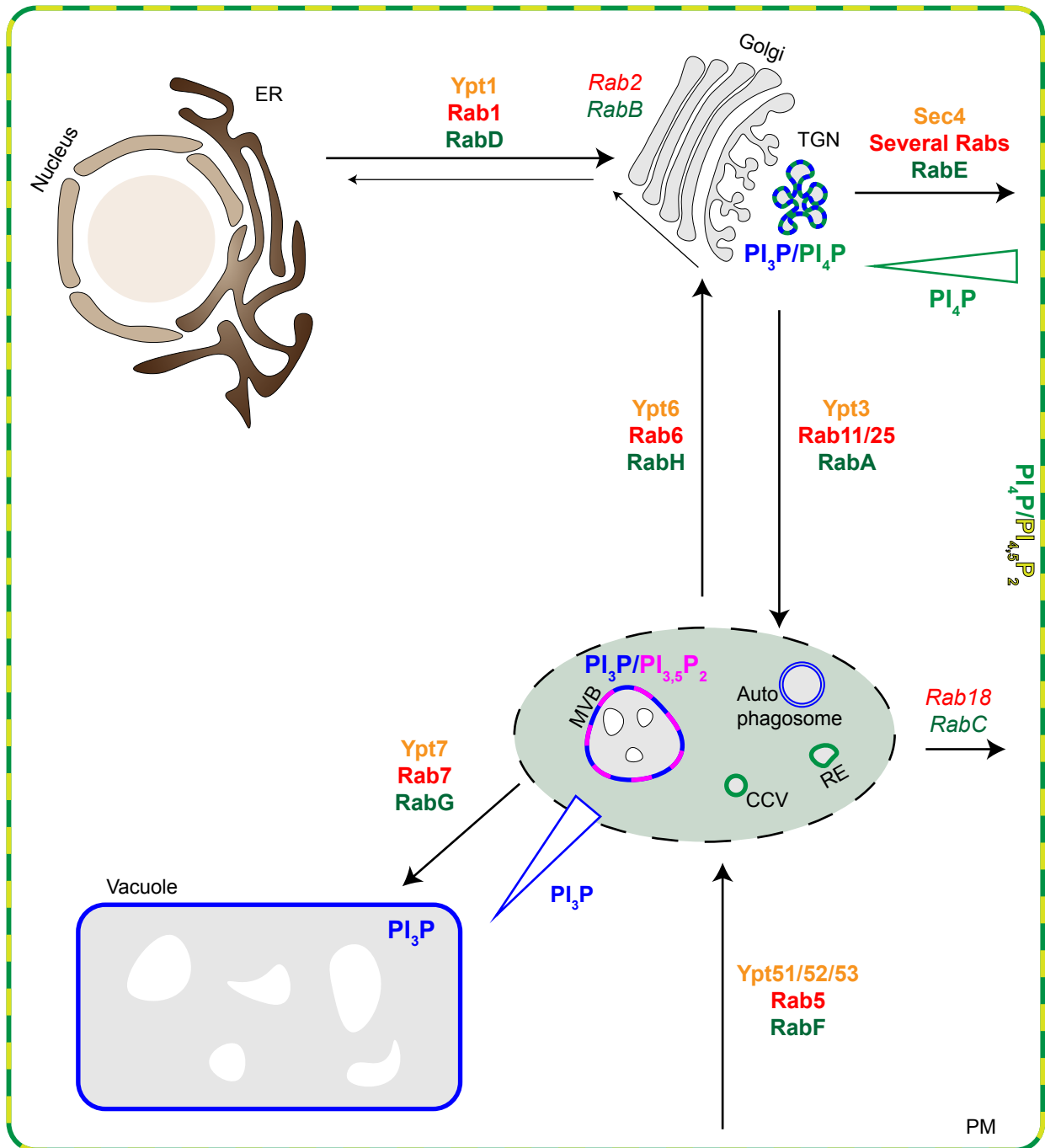


Figure 3: Schematic repartition of the eight clades of Plant's Rabs according to their trafficking pathways involvement and localization of the different phosphoinositides species in plant cells. The phosphoinositides localization in plant is different from animals cells, in plant the PI₄P (in green) is mainly localized at the PM with the PI_{4,5}P₂ (in light-green), and also a little amount is found in the TGN and endosomes (as CCV and RE). While the PI₃P (in blue) is found in the TGN too and mainly at the MVB/LE membrane and at the tonoplast. The PI_{3,5}P₂ (in purple) is found at the MVB/LE too. Their is a gradient of the PI₃P and the PI₄P amount between the vacuole to the MVB/LE, and the TGN to the PM represented by the triangle. The Ypt/Rab's color is linked to the organism: yeast in orange, animal in red and plant in green, moreover, the Ypt/Rab in **bold** are the six groups in commun amongst the eukaryote. Each Ypt/Rab class is responsible of a specific transport like the ER-Golgi, the TGN-PM, TGN-endosome, endosome-vacuole, endosome-PM by either recycling or secretory pathways. The different compartments are represented with the nucleus and the Endoplasmic Reticulum (ER), the Golgi apparatus, the trans-Golgi Network (TGN), the vacuole and, the endosomes with the MultiVesicular Bodies (MVB), Clathrin-Coated Vesicles (CCV), the Recycling Endosome (RE) and the autophagosome. *Freely adapted from the reviews of Rutherford S. et al., 2002 and Noack L. et al., 2017.*

(GDF) allowing the recycling of the Ypt/Rab and its activation by a Rab-GEF changing the GDP for a GTP.

The vesicular trafficking can be divided in transport substeps including 1) vesicle formation at the donor compartment, 2) vesicle movement, 3) vesicle docking at the acceptor compartment and the finally 4) vesicle/compartment fusion. These substeps have different machinery components as the Adaptor Proteins (AP) that recruits the cargos, coating elements, motor proteins, tethers and SNAREs proteins. All of these machinery elements were identified as Ypt/Rab effectors by interacting with the active form of Ypt/Rab-GTP. However, as I said before, the Ypt/Rab are compartment-specific rather than transport-specific, these different mechanisms are controlled by all the Ypt/Rab effectors leading to transport-specificity itself (figure 3). For instance, in animals, the Rab11 plays a role in four distinct transport pathways depending on its effectors-environment. Associated with KIF13, Rab11 acts on the transport of endosomes to the PM through microtubules whereas associated with SNX4, Rab11 leads endosomes to the RE still *via* microtubules (Campa and Hirsch, 2017). Moreover, the Ypt1 was first described as ER-to-Golgi transport (Segev et al., 1988) nevertheless, it has been shown that Ypt1 also plays a role in ER-to-autophagosome and intra-Golgi transport suggesting Ypt1 is more ER-derived membrane specific (Segev, 2001).

Several studies as well in animals, yeast or plants confirm the compartment/membrane-specific localization (figure 3) (Segev, 2001; Campa and Hirsch, 2017; Geldner et al., 2009). In animals, the Rab localization is well described. As example, Rab1 is localized at the ER-derived membrane (ER, ERGIC, *cis*-Golgi) whereas the Rab6 is localized at the TGN, Rab11 at the RE, Rab5 at the EE and Rab7 at the LE.

Interestingly, a concomitant localization of the Ypt/Rab with particular phosphoinositide (PIP) species has been highlighted (Jean and Kiger, 2012). This PIP-specific localization may be linked to the Ypt/Rab effectors as some of them are PIP-metabolizing enzymes or link to the PIP homeostasis (Rink et al., 2005; Shin et al., 2005; Naramoto et al., 2009; Scott et al., 2014; Singh et al., 2014; Casanova and Winckler, 2017). Furthermore, recent *in vitro* works show a membrane fluidity affinity of some animal Rabs (Rab1, Rab5 and Rab6) through their prenylation status. This fluidity affinity is also associated with a curvature affinity probably sensed by the geranylgeranyl anchor (Kulakowski et al., 2018). Moreover, in this interesting study, they suggest a plausible role of the positive electrostatic charges of the C-terminus of the Ypt/Rab as for Rab35 which preferentially binds to negatively charged lipids mostly found in endosomal membranes (Kulakowski et al., 2018).

This work underlines physicochemical properties of membranes that could define the Ypt/Rab specificity of anchoring (Kulakowski et al., 2018). However, most of Rabs, with the exception of RAB-F1/ARA6 are prenylated (farnesylfarnesyl or geranylgeranyl) but still showing distinct localization, pinpointing that the localization specificity is probably regulated through other means out of which membrane lipids could represent an important class to look at.

C. Lipid acting at the endomembrane identity

During a long time, lipids were considered as passive structural components of membranes. However, it is now well accepted that lipids play an active role in vesicle identity and maturation. All the lipid classes found in the cell: glycerolipids (phospholipids, anionic phospholipids, and galactolipids), sphingolipids and sterols are involved in membrane shape and fluidity. The lipids can be involved in the membrane curvature during vesicle budding that occurs during endocytosis, exocytosis or vesicle formation (Roux et al., 2005). Nowadays, lipids are more considered at the base of membrane identity and the first class described as a key component of endomembrane identity are the phosphoinositides (PIPs) (Simon et al., 2016; Jackson et al., 2016; Noack and Jaillais, 2017).

1. **Phosphoinositide**

Whatever the organisms, PIPs are composed by a DiAcylGlycerol (DAG) backbone and an inositol head that can be phosphorylated at three different carbon (3, 4 and 5). By a set of kinase, the phosphatidylinositol can be phosphorylated to give PI₃P, PI_{3,5}P₂, PI₄P or PI_{4,5}P₂ (also in PI_{3,4,5}P₃ and PI₅P) and specific phosphoinositides phosphatase dephosphorylate them at specific position. In animals, PIPs species are known to define the membrane electrostatic signature and recruit downstream machinery involved in vesicle trafficking. Each PIP species is localized at specific membrane: PI_{4,5}P₂ and PI₄P are localized at PM but also at Golgi membrane for PI₄P, whereas PI₃P is mainly localized at EE and PI_{3,5}P₂ at LE (Martin, 2001; De Matteis et al., 2002; De Matteis and Godi, 2004; Rink et al., 2005). During clathrin-mediated endocytosis (CME) there is a conversion of PM-localized PI_{4,5}P₂ into PI₃P thanks to a phosphorylation/dephosphorylation cascade using intermediate PIP species and enzymes (Posor et al., 2015).

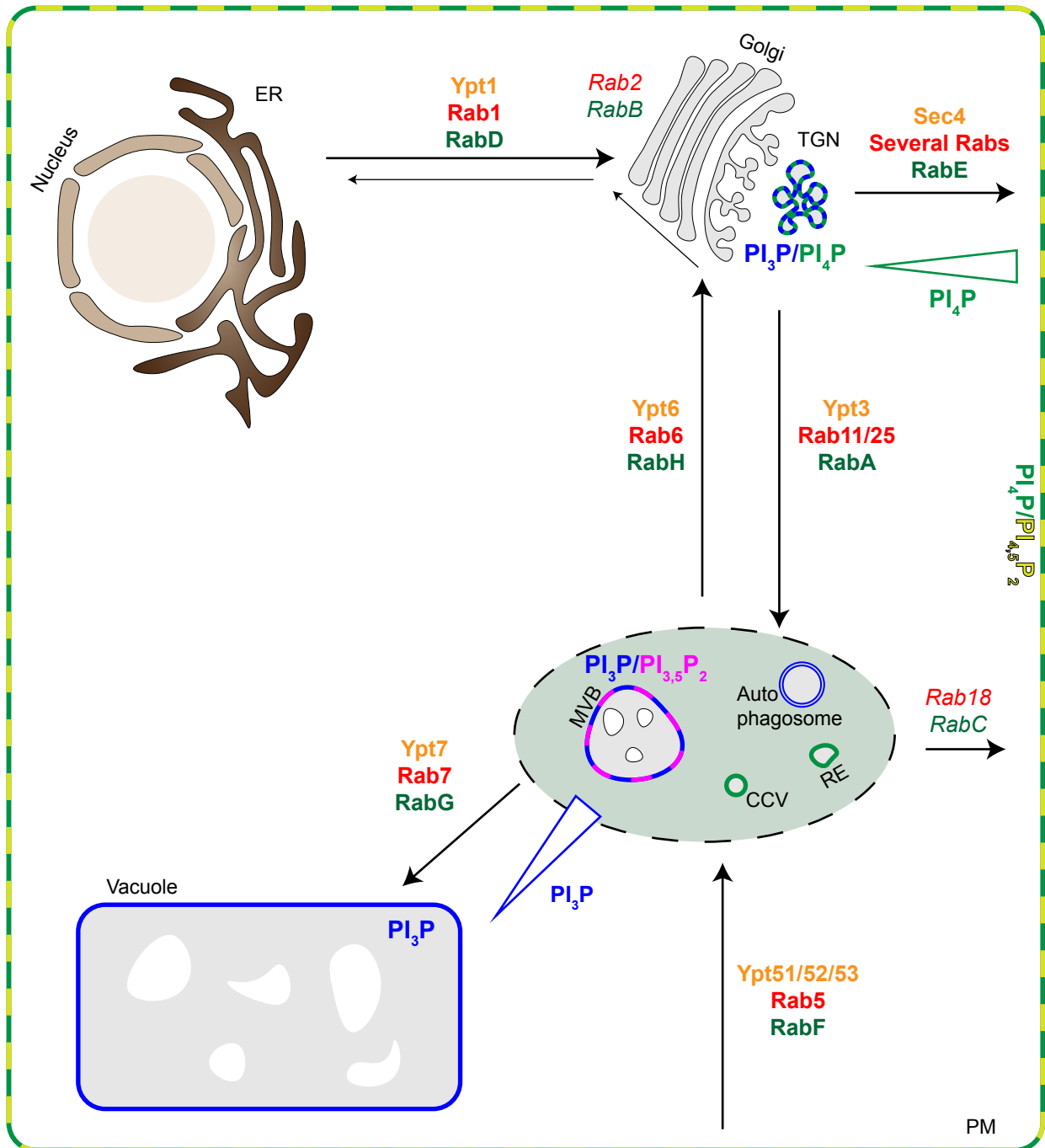


Figure 3: Schematic repartition of the eight clades of Plant's Rabs according to their trafficking pathways involvement and localization of the different phosphoinositides species in plant cells. The phosphoinositides localization in plant is different from animals cells, in plant the PI_4P (in green) is mainly localized at the PM with the $PI_{4,5}P_2$ (in light-green), and also a little amount is found in the TGN and endosomes (as CCV and RE). While the PI_3P (in blue) is found in the TGN too and mainly at the MVB/LE membrane and at the tonoplast. The $PI_{3,5}P_2$ (in purple) is found at the MVB/LE too. Their is a gradient of the PI_3P and the PI_4P amount between the vacuole to the MVB/LE, and the TGN to the PM represented by the triangle. The Ypt/Rab's color is linked to the organism: yeast in orange, animal in red and plant in green, moreover, the Ypt/Rab in **bold** are the six groups in commun amongst the eukaryote. Each Ypt/Rab class is responsible of a specific transport like the ER-Golgi, the TGN-PM, TGN-endosome, endosome-vacuole, endosome-PM by either recycling or secretory pathways. The different compartments are represented with the nucleus and the Endoplasmic Reticulum (ER), the Golgi apparatus, the *trans*-Golgi Network (TGN), the vacuole and, the endosomes with the MultiVesicular Bodies (MVB), Clathrin-Coated Vesicles (CCV), the Recycling Endosome (RE) and the autophagosome. *Freely adapted from the reviews of Rutherford S. et al., 2002 and Noack L. et al., 2017.*

This PIPs patterning at membrane is highly dynamic due to rapid phosphorylation that can occur to redefine the electrostatic signature of the membrane identity and induce a maturation from EE to LE by changing PI₃P in PI_{3,5}P₂ (Rink et al., 2005; Casanova and Winckler, 2017; Noack and Jaillais, 2017). The most predominant difference between animals and plants is that TGN acts as well as EE. This involvement of PIPs in endosomal trafficking is also present in plant despite some differences as the most abundant PIP species is the PI₄P which is found mainly at TGN/EE and at PM, together with PI_{4,5}P₂, whereas PI₃P is found in LE/MVB (Multi-Vesicular Body) and at tonoplast, and PI_{3,5}P₂ is found at LE/MVB only (figure 3) (Hirano et al., 2017; Singh et al., 2014; van Leeuwen et al., 2007). Hence, each PIPs have a unique subcellular distribution with a predominant localization in certain subsets of membranes.

The phosphorylation of PIPs creates a “code”. This “lipid code” is created by a set of PIP-metabolizing enzymes (PIP kinases and phosphatases) and is read by a batch of proteins containing Lipid-Binding Domain (LBD). These LBD-containing proteins that can either be GEF, GAP, PIP-metabolizing enzyme or Adaptor Protein (AP). Those proteins play a key role in the cargo recruitment, small GTPase turnover and vesicle maturation to allow vesicle trafficking and proteins sorting (Rink et al., 2005; Di Paolo and De Camilli, 2006; Posor et al., 2015). There is a feedback loop between PIP species and PIP-metabolizing enzymes activities but also a tight relationship between PIPs and small GTPases *via* the recruitment of GEFs or GAPs. As mentioned earlier, the APs are also described containing an LBD. For instance, the AP-2 complex is composed of four subunits, and two of them are able to bind to PI_{4,5}P₂ and to recruit cargos containing a tyrosine-based motif recognized by the AP-2 complex, leading to the Clathrin-Mediated Endocytosis initiation (Beck et al., 1991; Martin, 2001; Milosevic et al., 2011; Posor et al., 2015).

Several detection and regulation mechanisms have been underlined. For example, PIPs themselves recruit PIPs-metabolizing enzymes like the PI₃P recruits its PI₃P 5-kinase that contains a LBD. Moreover, some PIPs recruit GEFs or GAPs and act on targeted small GTPases activation/deactivation turnover. Alternatively, one small GTPase can regulate the PIPs by recruiting PIP-metabolizing enzymes, like Rab-A4b that recruits the PI 4-kinase β s to produce PI₄P at TGN/EE (Preuss et al., 2004, 2006; Kang et al., 2011). All of these mechanisms are well illustrate in the review of Noack L. (2017).

Furthermore, as the Rab, each PIP species has a proper localization and recently, it has been reported a concomitant localization between Rab type and PIP species. The PIP turnover

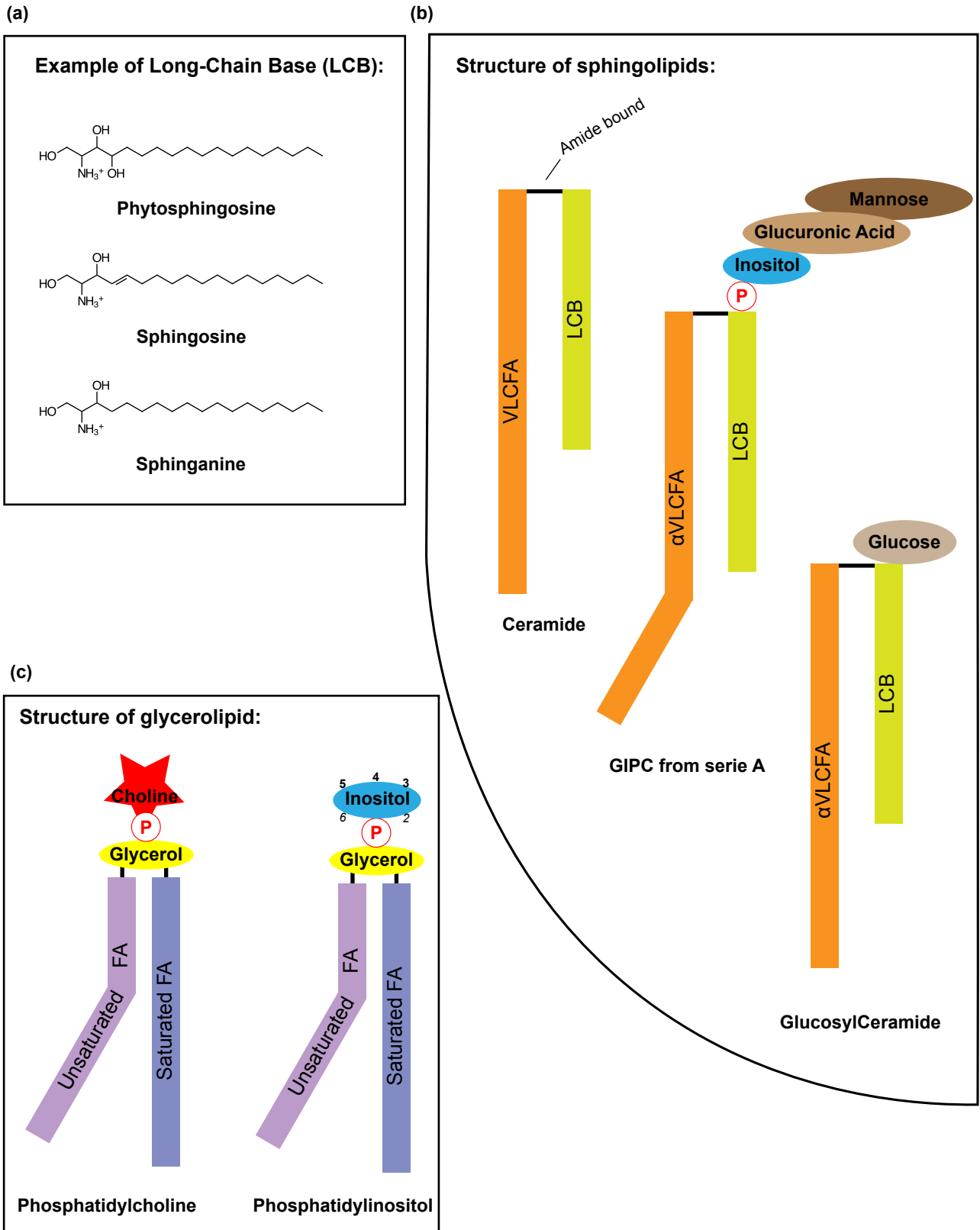


Figure 4: Structure of Long-Chain Base and schematic representation of two different sphingolipids and two different glycerolipids, with in bold the position where the inositol head can be phosphorylated. The three LCB in (a) are the most abundant amongst the organism and they can be linked to a (VLC)FA *via* an amide bond to form ceramide (b) which can be either glycosylated through an inositolphosphate to form a GIPC or directly bound to a glucose to form GluCer. These three (ceramide, GIPC and GluCer) are the most abundant sphingolipids in plant. Another class of lipid is the Glycerolipid which is composed by glycerophospholipid like phosphatidylcholine where the choline could be either an ethanolamine, a serine or an inositol. The last one can be phosphorylated in different positions to form the different phosphoinositides species.
 LCB: Long-Chain Base; VLCFA: Very-Long-Chain Fatty-Acid, P: Phosphate, FA: Fatty-Acid

allows membrane maturation, and the Rab are implied in this turnover by activating or not PIP-metabolizing enzymes (Jean and Kiger, 2012). In addition, the Rab proteins and PIP can recruit their correct downstream effectors which can be another Rab or a PIP-metabolizing protein to control the membrane maturation and the cargo routing. There is a very interesting phenomenon with the Rab and the PIP in animals and yeasts called “Rab conversion”. Rab conversion is described during EE to LE maturation (Rink et al., 2005; Nordmann et al., 2010; Poteryaev et al., 2010; Casanova and Winckler, 2017). PI₃P and Rab5 which are contained in the EE recruit the Mon1-Ccz1 complex that acts as a Rab7 GEF and blocks a Rab5 GEF leading to the activation of Rab7 and inhibition of Rab5 (Nordmann et al., 2010; Poteryaev et al., 2010). The Rab5 is further inactivated when the active Rab7 recruits a Rab5-inactivating GTPase-activating (GAP) protein leading to disruption of Rab5 effectors and recruitment of Rab7 effectors such as PI₃P 5-kinase that will convert the PI₃P to PI_{3,5}P₂ at LE (Rink et al., 2005; Shin et al., 2005; Nordmann et al., 2010; Poteryaev et al., 2010; Scott et al., 2014; Casanova and Winckler, 2017). In animal cells, the Rab GTPase Rab11 has a lot of effectors that lead to different vesicle trafficking pathways:

- Secretory sorting from endosomes to PM relies on microtubule binding ability of the effector (KIF13) (Delevoeye et al., 2014)
- Recycling sorting from endosomes to endocytic recycling compartment hinges on microtubule binding ability of the effector (SNX4) (Traer et al., 2007)
- Secretory sorting from RE to PM occurs through actin/myosin binding ability of the effector (FIP2) (Naslavsky et al., 2006)

In addition, Rab11 is also involved in trafficking from Golgi to PM due to an effector that binds PI₄P and actin/myosin (Ng et al., 2013; Campa and Hirsch, 2017). All of these works highlight an intimate relationship between PIP composition and the Rab which lead to different sorting pathways or regulation mechanisms through different recruitment strategies.

2. Sphingolipids

Unlike the PIPs which are composed by a DAG backbone and a polar head, sphingolipids are lipids resulting from the condensation of one Long-Chain Base (LCB) with a Fatty Acid chain (FA). Free LCB chains can be found and are as well classified as sphingolipids, such as sphingosine, sphinganine and phytosphingosine (figure 4). The LCB chain of sphingolipids can be hydroxylated and unsaturated. The FA of the plant

sphingolipids has the particularity to be hydroxylated on the second carbon leading to the formation of an α -OH-FA or α FA (Marquês et al., 2018). Sphingolipids biosynthesis starts at the ER by the formation of ceramide which is transported to the Golgi apparatus to be further modified (Mandon et al., 1992; Ichikawa et al., 1996; Gault et al., 2010).

In plants, ceramide is modified by the addition of a phosphoryl-inositol group by the Inositol Phosphoryl-Ceramide (IPC) Synthases (IPCS) enzymes which have been suggested to localize at TGN (Wang et al., 2008; Mina et al., 2010; Wattelet-Boyer et al., unpublished data). The transfer of glucuronic acid and sugars on IPC occurs as well in the Golgi complex (Bown et al., 2007; Rennie et al., 2012, 2014). After glycosylation, the sphingolipids are called GlycosylInositolPhosphorylCeramide (GIPC). These lipids are most probably localized at the luminal leaflet of the Golgi membrane due to that glycosylation occurs in the lumen. In *Arabidopsis*, the polar head of sphingolipids is composed from an inositol-phosphate group on which a glucuronic acid is grafted and further modified by addition of sugars such as glucose or mannose. In animals, the sugars can be galactose, glucose or N-acetyl-galactosamine. Moreover, in animal, the gangliosides support one or several sialic acids on the galactose and the number of sialic acids on the first galactose determines the 'series' of the sphingolipids (a:1, b:2 and c:3) (Komba et al., 1999; Traving and Schauer, 1998; Chen and Varki, 2010; Schnaar et al., 2014). The gangliosides are involved in a plethora of physiological processes such as the determination of blood groups and their recognition by autoantibodies or microbial factors lead to several known diseases such as leprosy or Guillain-Barré syndrome (Ribeiro-Resende et al., 2010; Nachamkin et al., 2008). Moreover, they are great cancer markers due to that tumor cells produce specific gangliosides (Schnaar et al., 2014)

I described before that the PIPs define membrane electrostatic identity as well as vesicle trafficking specificity and maturation. Similar to the PIP species, there is also a gradient of sphingolipids from ER to PM through Golgi apparatus and TGN where the sphingolipids play a critical role in organizing the order of membranes and inducing the formation of microdomains together with other lipids (Holthuis and Menon, 2014). In animal cells, sphingolipids flow through endomembrane compartments by vesicles trafficking from ER to PM *via* Golgi apparatus and TGN, or membrane maturation processes or alternatively by transfer from Golgi complex to other compartments *via* membrane-contact sites and lipid-transfer proteins (Kumagai et al., 2005; Hanada, 2006; van Meer et al., 2008; Hanada et al., 2009; Sugiki et al., 2018).

In animal cells, PI₄P is mostly localized at TGN and act as a recruitment factor for lipid-transfer proteins such as CERT and FAPP2, which transfer ceramide from ER to TGN, and OSBP1, which transfer sterols from ER to TGN (D'Angelo et al., 2008). Hence, PI₄P promotes the synthesis of sphingolipids at TGN, but during this process PI₄P is exchanged against ceramide or sterols and is thus transferred to ER. However, the beauty of homeostasis mechanisms at TGN is such that TGN-localized sphingomyelin synthase produces a DAG molecule while adding a polar head on the ceramide. DAG can activate protein kinases D (PKD) that phosphorylate PI₄KIII β involved in the production of PI₄P (Hausser et al., 2005). Meanwhile, PKD can also phosphorylates OSBP1 which enhances PI₄P relocation to ER and the PI₄P dephosphorylation by the ER-localized SAC1 phosphatase (Capasso et al., 2017). This complex crosstalk between sphingolipids, sterols and phosphoinositides establish waves of PI₄P and sphingolipids production and consumption at TGN which keep in check the amount of phosphoinositides and sphingolipids present at TGN (Capasso et al., 2017; Mesmin et al., 2017).

The role of sphingolipids in animal cell biology is very well studied. However, sphingolipids in plant deserve more attention as plant TGN might have specificities as compare to animal TGN due to the merging nature of plant TGN with EEs. In *Arabidopsis* roots, the sphingolipids pool is raftly composed of about 60% of GIPC, 38% of glycosylceramide (gluCER) and 2% of ceramides (Markham et al., 2006; Wattelet-Boyer et al., 2016). When two plant ceramide synthases are knock-down (LOH1 and LOH3), the plants contain a reduced amount in the VLCFA-containing ceramides and an increased amount in C16-FA-containing ceramides which seem to impact the recycling of the auxin carriers AUX1 and PIN1, probably *via* RabA2a compartments which form aggregate in this mutant (Markham et al., 2011).

Recent study in the laboratory on α VLCFA-containing sphingolipids has shown that they are mainly localized in Syp61/SV compartment and highlighted the specificity of metazachlor to alter the GluCer and GIPC compositions by shortening the length of the α FA from C24 and C26 to C16 and C20 carbon atoms (Wattelet-Boyer et al., 2016). When the α FA length of GIPC/GluCer is altered, it leads to a blocking of the secretory sorting of the auxin carrier PIN2 through the Syp61/SV and a loss of PIN2 polarity while no effect is observed on PIN1 and AUX1 sorting. Altogether, these results underlined two different pathways, the endosomal recycling sorting and the secretory sorting which probably rely on two distinct sphingolipids species: the VLCFA-containing ceramides and the α VLCFA-

containing GIPC and GluCer, respectively (Markham et al., 2011; Wattelet-Boyer et al., 2016).

The morphology of the TGN is also impacted by reversal reduction of the acyl-chain length in the GluCer and GIPC pools; it sports bigger SVs and less tubular interconnections between SVs which reflects the structural role of the α VLFCA-containing sphingolipids. Very-long-chains FAs can physically interact with the opposite leaflets in a mechanism called interdigitation that is cholesterol-dependent in animals (Róg et al., 2016). Interestingly, plants Syp61/SV compartment is enriched in both phytosterols and α VLCFA-containing sphingolipids (Wattelet-Boyer et al., 2016). Nevertheless, such mechanism has been characterized only *in silico* by modeling but has not been shown *in planta* (Cacas et al., 2016; Gronnier et al., 2016). The crosstalk between PI₄P and sphingolipids is also not described in plants compared to animals where it is characterized, as described before (D'Angelo et al., 2008; Capasso et al., 2017; Mesmin et al., 2017). It is important to note that there is a difference between plants and animals in respect to PI₄P localization, where in animals it mainly localizes at TGN, in plants its localization is mainly at the PM and a few amounts is present at TGN, so the regulatory mechanism between sphingolipids and PI₄P might not be the same (D'Angelo et al., 2008; Simon et al., 2014).

My PhD project is to identify the α VLCFA-containing sphingolipid-related mechanism by using metazachlor as pharmacological tool to alter GIPC composition without altering the total quantity of GIPCs. During a first part of my PhD thesis, I was focused on the metazachlor effects on root gravitropism response in different sphingolipids-biosynthesis mutant lines. During the first and second parts of my PhD I extracted TGN subdomains upon metazachlor treatment to perform proteomics analysis allowing the quantification of proteins without any labeling to identify sphingolipids-dependent actors at SV. In a third part of my PhD, I used metazachlor to observe *in vivo* effects of sphingolipids on identified protein and lipid actors.

II. Materials and Methods

A. Plant material and growth conditions

1. Seeds sterilization and *in vitro* growth

The *Arabidopsis thaliana* ecotype Colombia-0 (Col-0) and the mutants in annex 1 were used. Seeds were left at 4°C for 2 days in water then washed by immersion with a quick bath (few seconds) in ethanol 95% and then sterilized in chloride bleaching solution 3,2% (v/v) during 20min. Once sterilized the seeds were rinsed 3 times in water and sown on ½ Murashige and Skoog (MS) agar medium plates (0.8% plant agar, 1% sucrose and 2.5nM morpholinoethanesulfonic (MES) acid (Sigma) pH 5.8 with KOH), and grown in 16h light/8h darkness for 6 days before all experiments, exception made when obtaining plant material for immunoprecipitation (described hereafter).

2. On-soil growth

For seeds replication, crossing and plant transformation, on-soil growth is needed to allow the flower bar development. The seeds were either directly sown on loam:vermiculite (3:1) mix or transferred after selection from agar plate in soil, then a greenhouse was putted on the top to maintain humidity during 2 weeks. The culture conditions are the same than *in vitro* culture described above.

3. Plant stable transformation

While waiting the flower development, the different plasmids were created (described hereafter). To transform the plants, I used floral dip method (Clough and Bent, 1998) and the C58C1 *Agrobacterium tumefaciens* strain containing the plasmid. The agrobacteria were resuspended in transformation solution (5% sucrose, 0.05% silwet L-77) then the flower was dipped twice in the solution for 30s. After a high humidity was maintained during 24h then dry step by step by breaking the humidity chamber (plastic bag) 48h after transformation and 72h after transformation the plants recover normal culture condition. After senescence, the seeds were harvested and sown on agar plate containing the good antibiotic/herbicide

according to the resistance gene contained in the plasmid. All the stable lines generated are in the annex 2.

4. Plant crossing method

The chosen female plant is always the one containing a gene mutation and the male with a fluorescent marker. To do the cross, female plant with a few inflorescences was chosen and the male plant with few siliques already formed. To process, remove some siliques (3-4) formed below the flower (on the female plant) and remove the flower meristem and the flower already open. Then choose 3 closed flowers and with an ultra-thin tweezer, take off the different parts of the flower (sepals, petals and stamens) to keep only the carpel containing unfertilized oocytes. Once all these parts removed, take an open flower on the male plant and tap the anthers on the carpel to start the fertilization. Wait until the formation of the silique is finished and then harvest the seeds. All the stable lines generated are in the annex 3.

B. Treatments

1. Inhibitor treatments

For metazachlor (Greyhound Chromatography and Allied Chemicals) treatment, seedling were grown on MS plates containing the herbicide at 50 nM in most experiments, except when specified. Metazachlor was added from a 100 mM stock in dimethylsulfoxide (DMSO), an intermediate stock concentration at 100 μ M (in water) was used extemporarily to make the plates.

For Wortmannin (WN) treatment, 6-days-old-seedling grown on $\frac{1}{2}$ MS agar plate were treated in 6-wells plate with liquid $\frac{1}{2}$ MS (1% sucrose, 2.5mM MES acid pH 5.8) up to 90min at 30 μ M. The YM₂₀₁₆₃₆ pre-treatment was done as the WN treatment and 2h before the WN treatment as 1 μ M. The YM₂₀₁₆₃₆ is kept during the WN treatment. The following table represent the schedule of the WN treatment pretreated with the YM₂₀₁₆₃₆. Seven different incubation times were observed to make a kinetic study of the response to the WN.

- | | | | |
|----------|----------|----------|----------|
| 1) 5min | 3) 15min | 5) 45min | 7) 90min |
| 2) 10min | 4) 30min | 6) 60min | |

N°	Hour	Manipulation
1	11:55	Put 3 seedlings in YM ₂₀₁₆₃₆
6	12:00	Put 3 seedlings in YM ₂₀₁₆₃₆
2/7	12:10	Put 6 seedlings in YM ₂₀₁₆₃₆
3	12:25	Put 3 seedlings in YM ₂₀₁₆₃₆
4	12:50	Put 3 seedlings in YM ₂₀₁₆₃₆
5	13:15	Put 3 seedlings in YM ₂₀₁₆₃₆
	13:55	Transfer plants 1 in WN/ YM ₂₀₁₆₃₆
	14:00	Observation plants 1 and transfer 6 in WN/ YM ₂₀₁₆₃₆
	14:10	Transfer plants 2/7 in WN/ YM ₂₀₁₆₃₆
	14:20	Observation plants from 2
	14:25	Transfer plants 3 in WN/ YM ₂₀₁₆₃₆
	14:40	Observation plants 3
	14:50	Transfer plants 4 in WN/ YM ₂₀₁₆₃₆
	15:00	Observation plants 6
	15:15	Transfer plants 5 in WN/ YM ₂₀₁₆₃₆
	15:20	Observation plants 4
	15:40	Observation plants 7
	16:00	Observation plants 5

2. β -Estradiol induction

The ami-IPCS lines are upon a β -Estradiol inducible promotor (pER8). To induce the expression, the seeds were sown on $\frac{1}{2}$ MS agar plate containing β -Estradiol at 5 μ M final concentration diluted either in DMSO or 95% ethanol.

C. Root gravitropism and root length assays

Seedlings were grown on agar plates, vertically at 22°C under a 16 h light/8 h dark cycle for 3 days. They were then transferred to darkness under the same growth conditions and incubated during 24 h, maintaining the same growth plate orientation. Next, plates were turned counter-clockwise through 90° angle and incubated vertically in the dark for 24 h under the same growth conditions. The plates were then photographed, and the last curvature of the root was measured using imageJ. The new gravity vector was labelled as 0 while all the root angles were ranked into 24 classes of 15° angles. The gravitropism graphs were made

using Excel® to make the histograms and Adobe Illustrator® to make the circle gravitropism representation.

For the root length analysis, the roots were quantified using imageJ too after 6 days after seeding.

D. Immunoprecipitation of intact TGN and Golgi compartments

For immunoprecipitation, seedlings were grown in 500 ml flasks containing 250 ml of liquid medium containing full MS, 1% sucrose, 2.5 mM morpholinoethanesulfonic acid pH 5.8 for 9 days. Metazachlor was added at day 4 at 50 nM final concentration. We used pSYP61::CFP-SYP61 (Robert et al., 2008), pRAB-A2a::YFP-RAB-A2a (Chow et al., 2008) and pUB10::YFP-MEMB12 (Geldner et al., 2009) as secretory vesicles, clathrin-coated vesicles or Golgi markers respectively. *Arabidopsis* seedlings are grown under 120r.p.m. shaking and 16h light/8h darkness cycle. Seedlings are transferred to a mortar pre-cooled on ice and then grinded with a pillar in three times more (w/v) vesicle isolation buffer: HEPES 50 mM pH 7.5, 0.45 M sucrose, 5 mM MgCl₂, 1 mM dithiothreitol, 0.5% PVP (Sigma) and 1 mM phenylmethylsulfonyl fluoride (added just before the grinding).

The homogenate is then filtered through a Miracloth mesh and centrifuged at 1,600g for 20min at 4°C. The supernatant is transferred into a new tube and centrifuged two more times at 1,600g for 20 min at 4°C. Supernatant is then loaded on 38% sucrose cushion (the sucrose is dissolved in 50 mM HEPES pH 7.5) and centrifuged at 150,00g for 3h at 4°C. The total pool of membranes is located at the interface between the sucrose and the supernatant. After removing the supernatant, a step-gradient sucrose is built on the top of the total membrane interface with 33 and 8% sucrose solutions (dissolved in 50 mM HEPES pH 7.5) successively. Tubes are centrifuged overnight at 150,000g at 4°C. Bands of membranes appears at the 33/8% and 33/38% sucrose interfaces and are harvested, diluted in 2-3 volume of 50 mM HEPES pH 7.5, centrifuged at 150,000g for 2h at 4°C. The pellet is resuspended in the resuspension buffer (50 mM HEPES pH 7.5, 0.25 M sucrose, 1.5 mM MgCl₂, 150 mM NaCl, 0.2 mM EDTA, 1 mM phenylmethylsulfonyl fluoride and protease inhibitor cocktail from Sigma). This resuspend fraction is the Total Membrane (TM) fraction we used as input for the IPs.

Immunoprecipitation is performed with magnetic Dynabeads coupled to proteinA according to the manufacturer's instructions (Invitrogen). For each IP, 75 µL of beads are first

washed with PBS-Tween (137 nM NaCl, 2.7 nM KCl, 10 nM Na₂HPO₄, 1.8 nM KH₂PO₄ and 0.02% Tween-20), then incubated with 7.5 µL of rabbit anti-GFP antibodies (Invitrogen, A-11122) and 500 µL of PBST for 1h with shaking at 4°C. After to cross-link beads and antibodies, beads are washed with BS³ conjugaison buffer (20 mM Sodium Phosphate, 150 mM NaCl pH 7.9) and then, are incubated with 5 mM BS³ in BS³ conjugaison buffer during 30 min at room temperature under agitation. The cross-linking is stopped by adding 1/20 (v/v) of BS³ quenching buffer (1 M Tris-HCl, pH 7.5) and with an incubation of 15 min at RT under agitation. The beads are then washed three times with PBST and then incubated with resuspension buffer during 10 min. Beads are then incubated with 1 mL of equilibrated TM fractions (BCA kit from Sigma) for 1 h with shaking at 4°C. After incubation, four washes are performed with 1 mL of wash buffer (50 mM HEPES pH 7.5, 0.25 M sucrose, 1.5 mM MgCl₂, 150 mM NaCl, 0.2 mM EDTA) for 5 min with shaking at 4°C for each wash. After removal of wash buffer, beads bound to targeted vesicles are eluted with 25 µL of 1% SDS, 0.3 µL of 2M DTT, 2.3 µL of 1M Iodoacetamide and 6.9 µL of 6X Loading Buffer. Between each addition, an incubation for 30 min at 37°C (excepted after iodoacetamide, it is room temperature) is done.

E. Western blotting of IP fractions

Polyacrylamide gels were casted using the TGX Stain-Free FastCast premixed acrylamide solution manufactured by Bio-Rad. After gel activation of 5 min, proteins were visualized and imaged using the ChemiDoc MP imaging system (Bio-Rad). Initial step-gradient-purified TM fractions (IP input) and beads-IP fractions (IP output) were loaded at equal quantity on SDS-PAGE gel and subjected to western blotting. To equally load TM fractions and IPs fractions, we quantified the whole individual tracks using ImageJ software and adjusted the quantity of proteins loaded in each track to reach equal loading. For western blotting, the following antibodies and dilutions were used: mouse anti-GFP recognizing CFP, GFP and YFP (Roche, 118144600001) 1/1,000, rabbit anti-Memb11(Marais et al., 2015) 1/1,000 and rabbit anti-V-ATPase-E (Agrisera, AS07 213) 1/2,000. Secondary antibodies were as follows: goat anti-mouse IgG-HRP conjugate (1/3,000, Bio-Rad, 1721011) and goat anti-rabbit IgG-HRP conjugate (1/5,000, Bio-Rad, 1706515). Pictures were acquired using a ChemiDoc MP imaging system (Bio-Rad).

F. Proteomic analysis

1. Sample preparation and protein digestion

Protein samples were solubilized in Laemmli buffer and were deposited onto SDS-PAGE gel for concentration and cleaning purposes. Separation was stopped once proteins have entered the resolving gel. After colloidal blue staining, bands were cut out from the SDS-PAGE gel and subsequently cut into 1 mm x 1 mm gel pieces. Gel pieces were destained in 25 mM ammonium bicarbonate 50% acetonitrile (ACN), rinsed twice in ultrapure water and shrunk in ACN for 10 min. After ACN removal, gel pieces were dried at room temperature, covered with the trypsin solution (10 ng/μl in 50 mM NH₄HCO₃), rehydrated at 4 °C for 10 min, and finally incubated overnight at 37 °C. Spots were then incubated for 15 min in 50 mM NH₄HCO₃ at room temperature with rotary shaking. The supernatant was collected, and an H₂O/ACN/HCOOH (47.5:47.5:5) extraction solution was added onto gel slices for 15 min. The extraction step was repeated twice. Supernatants were pooled and concentrated in a vacuum centrifuge to a final volume of 100 μL. Digests were finally acidified by addition of 2.4 μL of formic acid (5%, v/v) and stored at -20 °C.

2. nLC-MS/MS analysis

Peptide mixture was analyzed on an Ultimate 3000 nanoLC system (Dionex, Amsterdam, The Netherlands) coupled to an Electrospray Q-Exactive quadrupole Orbitrap benchtop mass spectrometer (Thermo Fisher Scientific, San Jose, CA). Ten microliters of peptide digests were loaded onto a 300-μm-inner diameter x 5-mm C₁₈ PepMap™ trap column (LC Packings) at a flow rate of 30 μL/min. The peptides were eluted from the trap column onto an analytical 75-mm id x 25-cm C₁₈ Pep-Map column (LC Packings) with a 4–40% linear gradient of solvent B in 108 min (solvent A was 0.1% formic acid in 5% ACN, and solvent B was 0.1% formic acid in 80% ACN). The separation flow rate was set at 300 nL/min. The mass spectrometer operated in positive ion mode at a 1.8-kV needle voltage. Data were acquired using Xcalibur 2.2 software in a data-dependent mode. MS scans (*m/z* 350–1600) were recorded at a resolution of $R = 70\,000$ (@ *m/z* 200) and an AGC target of 3×10^6 ions collected within 100 ms. Dynamic exclusion was set to 30 s and top 12 ions were selected for fragmentation in HCD mode. MS/MS scans with a target value of 1×10^5 ions were collected with a maximum fill time of 100 ms and a resolution of $R = 17\,500$.

Additionally, only +2 and +3 charged ions were selected for fragmentation. Other settings were as follows: no sheath nor auxiliary gas flow, heated capillary temperature, 250°C; normalized HCD collision energy of 25% and an isolation width of 2 m/z.

3. Database search and results processing

Data were searched by SEQUEST through Proteome Discoverer 1.4 (Thermo Fisher Scientific Inc.) against Araport v11 protein database (40782 entries). Spectra from peptides higher than 5000 Dalton (Da) or lower than 350 Da were rejected. The search parameters were as follows: mass accuracy of the monoisotopic peptide precursor and peptide fragments was set to 10 ppm and 0.02 Da respectively. Only b- and y-ions were considered for mass calculation. Oxidation of methionines (+16Da) was considered as variable modification and carbamidomethylation of cysteines (+57Da) as fixed modification. Two missed trypsin cleavages were allowed. Peptide validation was performed using Percolator algorithm (Käll et al., 2007) and only “high confidence” peptides were retained corresponding to a 1% False Positive Rate at peptide level.

4. Label-Free Quantitative Data Analysis

Raw LC-MS/MS data were imported in Progenesis QI for Proteomics 2.0 (Nonlinear Dynamics Ltd, Newcastle, U.K). Data processing includes the following steps: (i) Features detection, (ii) Features alignment across the samples to compare, (iii) Volume integration for 2-6 charge-state ions, (iv) Normalization on features ratio median, (v) Import of sequence information, (vi) Calculation of protein abundance (sum of the volume of corresponding peptides), (vii) A T-test was calculated for each group comparison and proteins were filtered based on p-value<0.05. Noticeably, only non-conflicting features and unique peptides were considered for calculation at protein level. Quantitative data were considered for proteins quantified by a minimum of 2 peptides.

G. Cloning

1. DNA extraction and Multisite Gateway®

The Multisite Gateway® technology have been chosen to generate the clones and this technique uses recombination to create the vectors and the plasmid. The first step consists of cloning the gene with two recombination sites at the 5'- and 3'- end called *attB*_x-*attB*_y (x-y can be 4-1r, 1-2, 2r-3 depending on the vector targeted and the wanted position in the final plasmid). The recombination sites have different names depending on the steps of cloning:

- *attB*₄-*B*_{1r}, *attB*₁-*B*₂, *attB*_{2r}-*B*₃: PCR Fragment
- *attP*₄-*P*_{1r}, *attP*₁-*P*₂, *attP*_{2r}-*P*₃: pDONR™ (empty vector)
- *attL*₄-*R*₁, *attL*₁-*L*₂, *attR*₂-*L*₃: entry clone, pDONR™ with the PCR fragment
- *attR*₄-*R*₃: pDEST, the final plasmid (empty).

When the *attB*-PCR fragment is obtained, the BP clonase reaction is done. It consists of replacing the control cassette (in the pDONR™ empty vector) by the PCR fragment. The control cassette (containing *ccdB* gene and chloramphenicol resistance gene) is flanked by the *attP*_x-*attP*_y site and the role of the BP clonase is to recombine the *attB* and *attP*. The entry clone is obtained, LR cloning (recombination between *attL* and *attR*) is done by mixing the chosen pDEST and the 3 entry clones to create the final vector.

The primers designed according to the Multisite Gateway® protocol are in the annex 4 and using the gene sequences identified in The Arabidopsis Information Resource (TAIR database). The gene cloning was done on genomic DNA to keep all the splicing mechanism. The DNA was extracted by grinding seedling or leaves in cold mortar and pestle from *A. thaliana* in liquid nitrogen then the poulder obtained was mixed with cold 80µL chloroform:isoamy alcohol (24:1) and 400µL of genomic DNA isolation buffer (200mM TrisHCl pH 7.5, 250mM NaCl, 25mM EDTA and 0.5% SDS). After shaking, the tubes were centrifuged at 14,000rpm for 3min at 4°C and the supernatants were harvested and mixed with 1 (v/v) cold isopropanol (-20°C). The DNA precipitation occurred at least for 30min in -20°C and then pelleted at 14,000rpm for 5min at 4°C. The pellets were rinsed with 70% ethanol and centrifuged 14,000rpm for 3min. After removal of ethanol, the pellets were dried in speed vacuum or on the bench and the DNA were resuspended in water.

The cloning PCRs were done with the Takara PrimeStar® Max DNA Polymerase according to their protocols with the following run: 1) 98°C for 10s, 2) 55°C for 5s then 3)

N°	Construction	pDONR™
0	p35S	P4/P1r
1	pUB10	P4/P1r
3	MSBP ₁	P1/P2
4	MSBP ₂	P1/P2
5	MSBP ₃	P1/P2
6	CFP	P1/P2
7	IPCS ₁	P1/P2
8	IPCS ₂	P1/P2
9	mVenus	P1/P2
10	Cornichon	P2r/P3
11	MSBP ₁	P2r/P3
12	MSBP ₂	P2r/P3
13	MSBP ₃	P2r/P3
14	CFP	P2r/P3
15	IPCS ₁	P2r/P3
16	IPCS ₂	P2r/P3
17	mVenus	P2r/P3
19	pENTR-TagBFP2	P1/P2
20	Sec14p	P1/P2
20'	Sec14p	P1/P2
21	Sec14p	P2r/P3
21'	Sec14p	P2r/P3
22	DGK7	P1/P2
22'	DGK7	P1/P2
23'	DGK7	P2r/P3
24	MATE3	P1/P2
25	MATE3	P2r/P3
25'	MATE3	P2r/P3
26	MATE2	P1/P2
26'	MATE2	P1/P2
27	MATE2	P2r/P3
27'	MATE2	P2r/P3

N°	Construction	pDONR™
28	SAC1	P1/P2
28'	SAC1	P1/P2
29	SAC1	P2r/P3
30	RhoGAP	P2r/P3
30'	RhoGAP	P2r/P3
32	eGFP	P1/P2
33	eGFP	P2r/P3
35	RhoGAP	P1/P2
35'	RhoGAP	P1/P2
35''	RhoGAP	P1/P2
38	TagRFP	P1/P2
38'	TagRFP	P1/P2
39	TagRFP	P2r/P3
39'	TagRFP	P2r/P3
40	TagBFP2	P1/P2
40'	TagBFP2	P1/P2
43	eGFPopt	P1/P2
43'	eGFPopt	P1/P2
44	eGFPopt	P2r/P3
44'	eGFPopt	P2r/P3
46	TagBFP2	P2r/P3
46'	TagBFP2	P2r/P3
58	3rd Sec14p (at1g75170)	P2r/P3
59	2nd Sec14p (at1g14820)	P2r/P3
59'	2nd Sec14p (at1g14820)	P2r/P3
61	2nd ENTH (at3g26990)	P2r/P3
62	Actin Cross Like (at1g27100)	P2r/P3
62'	Actin Cross Like (at1g27100)	P2r/P3
64	3rd Sec14p (at1g75170)	P1/P2
64'	3rd Sec14p (at1g75170)	P1/P2
65	2nd ENTH (at3g26990)	P1/P2
65'	2nd ENTH (at3g26990)	P1/P2

Table 2: Entry clones generated for the Multisite Gateway®. Almost all the gene are cloned twice (number with a «'») to avoid cloning trouble as bad purification or bad sequencing.

72°C for 5s/kb and repeat these 3 steps 35 times. The amplicons were verified by DNA electrophoresis by migration in 1% agar gel of 12µL of the PCR product. Then, the rest of the PCR products were purified using the Monarch® PCR & DNA Cleanup kit (New England BioLabs® Inc.). The purified PCR products were insert into the corresponding pDONR™ according to the Multisite Gateway® protocol by doing a BP reaction.

The plasmids were integrated into thermo-competent *E. coli* (DH5α strain) by thermal shock, 1) 5min on ice, 2) 90s at 42°C, 3) 90s on ice then 4) 1h at 37°C with LB and spread on LB agar plate containing 50µM kanamycin. The plasmids were replicated by picking some colonies from the plate and by resuspending them in liquid LB medium with 50µM kanamycin. After overnight growth at 37°C, 200r.p.m. shaking, the plasmids were extracted using the NucleoSpin® Plasmid kit (from Macherey-Nagel) and sent to sequencing analysis to verify the sequence of the gene inserted (see Table 2). After this control of the plasmid sequences, the plasmids are recombined according to the final plasmid wanted (see Table 3) with the LR reaction according to the Multisite Gateway® protocol. The final plasmids were replicated in *E. coli* as describe before however the antibiotic used was the 50µg/mL spectinomycin:streptomycin (1:1). After colonies selection, the plasmids were extracted thanks to the NucleoSpin® Plasmid kit (from Macherey-Nagel), and transformed in *A. tumefaciens* (C58C1 strain) by thermal shock 1) 30min on ice with the plasmid, 2) 5min in liquid nitrogen, 3) 5min at 37°C, 4) 5min on ice then 5) recovery at 25°C, 250r.p.m. with LB during 3h. At the end, the agrobacteria were spread on LB agar plate containing 50µg/mL of Rifampicin, 20µg/mL of Gentamycin, 100µg/mL of Spectinomycin and 2.5µg/mL of Tetracyclin , to select the plasmid and maintain all the different plasmids in the agrobacteria (as the Ti, Helper, etc.).

2. Competent bacteria protocol

The *Escherichia coli* bacteria have been made thermocompetent by growing them in 100mL LB and waiting their exponential phase. When the OD⁶⁰⁰ reach 0.5-0.6, the culture was put on ice during 10min and then centrifuge 10min, 4°C, 2500r.p.m. to pellet the bacteria. The pellet was resuspended in 30mL of TFBII¹ at 4°C. After an incubation on ice (15min to 2h max) the bacteria were pelleted again (10min, 4°C, 2500r.p.m.) and then resuspend in 4mL TFBII² and finally aliquoted and throw in liquid nitrogen before been stored in -80°C.

Table 3: List of plasmids generated by Multisite Gateway® and their transformation status.

pDest	L4 / R1	L1 / L2	R2 / L3	Construction			pDEST	Resistance	LR	E Coli	Transformation Status			
				L4/R1	L1/L2	R2/L3					Glycerol Stock	Plasmid	Agro-bacteria	In Planta
K	0	3	14	p35S	MSBP1	CFP	pK7m34GW	KANA	✓	✓	✓	✓		
K	0	4	14	p35S	MSBP2	CFP	pK7m34GW	KANA	✓	✓	✓	✓		
K	0	5	14	p35S	MSBP3	CFP	pK7m34GW	KANA	✓	✓	✓	✓		
K	0	6	11	p35S	CFP	MSBP1	pK7m34GW	KANA	✓	✓	✓	✓		
K	0	6	12	p35S	CFP	MSBP2	pK7m34GW	KANA	✓	✓	✓	✓		
K	0	6	13	p35S	CFP	MSBP3	pK7m34GW	KANA	✓	✓	✓	✓		
B	0	9	17	p35S	mVenus	mVenus	pB7m34GW	BASTA	✓	✓	✓	✓		
B	0	7	17	p35S	IPCS1	mVenus	pB7m34GW	BASTA	✓	✓	✓	✓		
B	0	9	15	p35S	mVenus	IPCS1	pB7m34GW	BASTA	✓	✓	✓	✓		
B	0	8	17	p35S	IPCS2	mVenus	pB7m34GW	BASTA	✓	✓	✓	✓		
B	0	9	16	p35S	mVenus	IPCS2	pB7m34GW	BASTA	✓	✓	✓	✓		
B	1	7	17	pUB10	IPCS1	mVenus	pB7m34GW	BASTA	✓	✓	✓	✓	✓	✓
B	1	20	17	pUB10	Sec14p	mVenus	pB7m34GW	BASTA	✓	✓	✓	✓	✓	✓
B	1	22	17	pUB10	DGK7	mVenus	pB7m34GW	BASTA	✓	✓	✓	✓	✓	✓
B	1	24	17	pUB10	MATE3	mVenus	pB7m34GW	BASTA	✓	✓	✓	✓	✓	✓
B	1	26	17	pUB10	MATE2	mVenus	pB7m34GW	BASTA	✓	✓	✓	✓	✓	✓
B	1	28	17	pUB10	SAC1	mVenus	pB7m34GW	BASTA	✓	✓	✓	✓	✓	✓
B	1	9	15	pUB10	mVenus	IPCS1	pB7m34GW	BASTA	✓	✓	✓	✓	✓	✓
B	1	9	16	pUB10	mVenus	IPCS2	pB7m34GW	BASTA	✓	✓	✓	✓	✓	✓
B	1	9	21	pUB10	mVenus	Sec14p	pB7m34GW	BASTA	✓	✓	✓	✓	✓	✓
B	1	9	23	pUB10	mVenus	DGK7	pB7m34GW	BASTA	✓	✓	✓	✓	✓	✓
K	1	9	29	pUB10	mVenus	SAC1	pK7m34GW	KANA	✓	✓	✓	✓	✓	✓
K	1	9	30	pUB10	mVenus	RhoGAP	pK7m34GW	KANA	✓	✓	✓	✓	✓	✓
B	1	35	17	pUB10	RhoGAP	mVenus	pB7m34GW	BASTA	✓	✓	✓	✓	✓	✓
B	1	3	14	pUB10	MSBP1	CFP	pB7m34GW	BASTA	✓	✓	✓	✓	✓	✓
B	1	4	14	pUB10	MSBP2	CFP	pB7m34GW	BASTA	✓	✓	✓	✓	✓	✓
B	1	6	11	pUB10	CFP	MSBP1	pB7m34GW	BASTA	✓	✓	✓	✓	✓	✓
B	1	6	12	pUB10	CFP	MSBP2	pB7m34GW	BASTA	✓	✓	✓	✓	✓	✓
B	1	6	13	pUB10	CFP	MSBP3	pB7m34GW	BASTA	✓	✓	✓	✓	✓	✓
B	1	24	39	pUB10	MATE3	TagRFP	pB7m34GW	BASTA	✓	✓	✓	✓	✓	✓
B	1	26	39	pUB10	MATE2	TagRFP	pB7m34GW	BASTA	✓	✓	✓	✓	✓	✓
B	1	20	39	pUB10	Sec14p	TagRFP	pB7m34GW	BASTA	✓	✓	✓	✓	✓	✓
B	1	22	39	pUB10	DGK7	TagRFP	pB7m34GW	BASTA	✓	✓	✓	✓	✓	✓
B	1	28	39	pUB10	SAC1	TagRFP	pB7m34GW	BASTA	✓	✓	✓	✓	✓	✓
B	1	35	39	pUB10	RhoGAP	TagRFP	pB7m34GW	BASTA	✓	✓	✓	✓	✓	✓
B	1	38	25	pUB10	TagRFP	MATE3	pB7m34GW	BASTA	✓	✓	✓	✓	✓	✓
B	1	38	27	pUB10	TagRFP	MATE2	pB7m34GW	BASTA	✓	✓	✓	✓	✓	✓
B	1	38	21	pUB10	TagRFP	Sec14p	pB7m34GW	BASTA	✓	✓	✓	✓	✓	✓
B	1	38	23	pUB10	TagRFP	DGK7	pB7m34GW	BASTA	✓	✓	✓	✓	✓	✓
B	1	38	29	pUB10	TagRFP	SAC1	pB7m34GW	BASTA	✓	✓	✓	✓	✓	✓
B	1	38	30	pUB10	TagRFP	RhoGAP	pB7m34GW	BASTA	✓	✓	✓	✓	✓	✓
B	1	5	14	pUB10	MSBP3	CFP	pB7m34GW	BASTA	✓	✓	✓	✓	✓	✓
B	1	9	25	pUB10	mVenus	MATE3	pB7m34GW	BASTA	✓	✓	✓	✓	✓	✓
B	1	9	27	pUB10	mVenus	MATE2	pB7m34GW	BASTA	✓	✓	✓	✓	✓	✓
K	0	26	17	p35S	MATE2	mVenus	pK7m34GW	KANA	✓	✓	✓	✓	✓	✓
K	0	9	21	p35S	mVenus	Sec14p	pK7m34GW	KANA	✓	✓	✓	✓	✓	✓
K	0	9	25	p35S	mVenus	MATE3	pK7m34GW	KANA	✓	✓	✓	✓	✓	✓
K	0	22	17	p35S	DGK7	mVenus	pK7m34GW	KANA	✓	✓	✓	✓	✓	✓
K	0	9	30	p35S	mVenus	RhoGAP	pK7m34GW	KANA	✓	✓	✓	✓	✓	✓
K	0	9	27	p35S	mVenus	MATE2	pK7m34GW	KANA	✓	✓	✓	✓	✓	✓
B	1	9	29	pUB10	mVenus	SAC1	pB7m34GW	BASTA	✓	✓	✓	✓	✓	✓
B	1	9	30	pUB10	mVenus	RhoGAP	pB7m34GW	BASTA	✓	✓	✓	✓	✓	✓
B	1	24	14	pUB10	MATE3	CFP	pB7m34GW	BASTA	✓	✓	✓	✓	✓	✓
B	1	6	25	pUB10	CFP	MATE3	pB7m34GW	BASTA	✓	✓	✓	✓	✓	✓
B	1	26	14	pUB10	MATE2	CFP	pB7m34GW	BASTA	✓	✓	✓	✓	✓	✓
B	1	6	27	pUB10	CFP	MATE2	pB7m34GW	BASTA	✓	✓	✓	✓	✓	✓
B	1	8	17	pUB10	IPCS2	mVenus	pB7m34GW	BASTA	✓	✓	✓	✓	✓	✓
B	0	9	30	p35S	mVenus	RhoGAP	pB7m34GW	BASTA	✓	✓	✓	✓	✓	✓
B	0	35	17	p35S	RhoGAP	mVenus	pB7m34GW	BASTA	✓	✓	✓	✓	✓	✓

¹TFBI: Potassium Acetate (KAc) 30mM, Manganese (II) Chloride tetrahydrate (MnCl₂, 4H₂O) 50mM, Rubidium Chloride (RbCl) 100mM, Calcium Chloride (CaCl₂) 10mM, 15% glycerol and pH 5.8 with acetic acid

²TFBII: MOPS sodium salt (NaMOPS) 10mM, CaCl₂ 75mM, RbCl 10mM and 15% glycerol

The *Agrobacterium tumefaciens* bacteria have been made thermocompetent by growing them in 200mL LB and waiting their exponential phase. When the OD⁶⁰⁰ reach 0.5-0.7, always keep them in ice. The culture was dispatched in pre-cooled falcon and store on ice during 10min. After a centrifugation (3,500r.p.m., 10min, 4°C), the pellet was resuspended in 50mL of sterile ice cold 10% glycerol and centrifuged again (4,000r.p.m., 10min, 4°C). This step was repeated twice by resuspending the pellet in 25mL and then 10mL sterile ice cold 10% glycerol but for the last one (10mL), all the tubes were pooled together. And after the last centrifugation, the pellet was resuspended in 800μL sterile ice cold 10% glycerol and dispatched in 40μL aliquots and store at -80°C.

H. Confocal Microscopy

Confocal laser scanning microscopy was performed using a Zeiss LSM 880 with Zen Blue software (Zeiss). For live-cell imaging, seedlings were mounted with liquid ½MS (with or without drugs) between cover glass and 24 x 24mm coverslip separated with a double-side tape. All the acquisitions were done with a frame size of 1160x1160, 16bits pixel depth, with an oil-corrected x40 objective, 1.3 numerical aperture (APO 40x/1.3 Oil DIC UV-IR). Laser excitation wavelengths for the different fluorophores were 488nm for YFP and mVenus, and 561nm for mCherry. The photon emissions were detected with a spectral detector spliced in two detection windows, 491-585nm for the YFP/mVenus and 588-695nm for the mCherry. All the acquisitions were done in sequential line-scanning mode with a pixel dwell time of 1.96μs.

Co-localization analyses were performed using the geometrical (centroid) object-based method (Bolte and Cordelières, 2006). Images were segmented, subcellular compartments were delineated, and the distance between the centroids (geometrical centers) of two objects was calculated using the 3D objects counter plugin in imageJ. If the distance was below the resolution limit of the objective used, in both X and Y, the colocalization was accepted. Whereas if the distance was above the resolution limit, in either X or Y, the colocalization

was rejected. For each colocalization experiment, 5 zones from each 10 roots were analyzed (n=50).

Fluorescence quantification analysis were done using exactly the same acquisition for each line without any change in the laser power or the detector amplification (gain). Moreover, each line was sown at the same hour and observed at the same hour too (exactly 6 days old). For the WN and YM₂₀₁₆₃₆ inhibitors experiment, 6 snaps were done for each 3 roots per time-treatment due to the limitation in the observation time (20min per conditions).

I. Statistical analysis

All the data analyzed were unpaired (samples independent from each other). Normal distribution (Gaussian distribution) of data set was tested using Shapiro-Wilk normality test. On data normally distributed, sample homoscedasticity was assessed using Bartlett and Brown-Forsythe test before performing parametric tests. On data that were not normally distributed (or on data sets for which $n < 10$), non-parametric tests were performed. To compare multiple data sets, Dunn's test was used as non-parametric test. Tukey's test was used as a single-step multiple comparison procedure to find means significantly different from each other. All statistical tests were two-tailed (two-sided test). All statistical analyses were performed with Prism GraphPad 6.0 software. P-values were as follows: * $P < 0.05$, ** $P < 0.01$, *** $P < 0.001$ and **** $P < 0.0001$. Variances between each group of data were either represented in scatter dot plot with a representation of the mean \pm S.D.

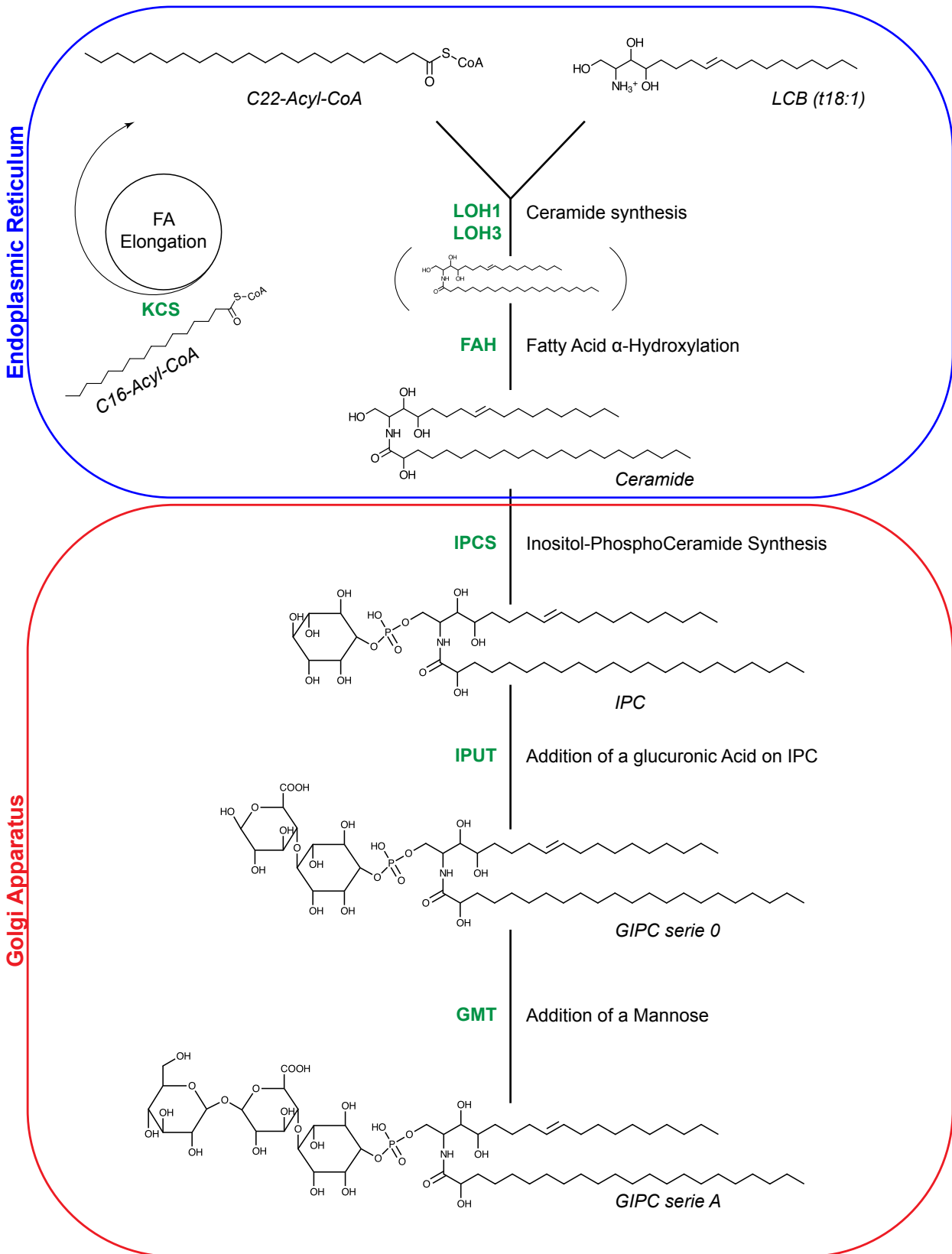


Figure 5: Simplified scheme of GIPC biosynthesis in *A. thaliana*. The biosynthesis of GIPC starts in the ER where there is the formation of a ceramide by the amidification of a LCB and the VLCFA after its elongation thanks to the elongase complex. The ceramide is then α -hydroxylated on the VLCFA and transported to the Golgi where an inositol is linked via a phosphate and several glycosylations occur to form first a glucuronic acid and then a mannose in *Arabidopsis thaliana*.

FA: Fatty Acid, KCS: 3-Ketoacyl-Coenzyme A Synthase, LCB: Long-Chain Base, LOH: Lag One Homologue, IPCS: Inositol PhosphorylCeramide Synthase, IPC: Inositol PhosphoCeramide, IPUT: Inositol Phosphorylceramide glucuronosyl-Transferase, GIPC: Glycosyl Inositol Phospho Ceramide, GMT: GIPC Mannosyl-Transferase

III. Results

A. Metazachlor: a new pharmacological tool to reduce the very-long-chain fatty-acid length of sphingolipids

The metazachlor is a chloroacetanilide herbicide used to prevent growth of weeds on rapeseed field, that inhibits the 3-Ketoacyl-Coenzyme A Synthases (KCSs). Used at nanomolar scale, lipidomic studies show it triggers a decrease of the length of the α -hydroxylated-Very-Long-Chain-Fatty-Acid (α VLCFA) which is mainly contained in sphingolipid pool, without any change in the total quantity of each classes of lipid (Wattelet-Boyer et al., 2016). Moreover, lipidomic studies highlight an enrichment of sphingolipids especially at plasma membrane (PM) and secretory vesicles (SVs) as compared to Clathrin-Coated Vesicles (CCVs) or Golgi apparatus (Gronnier et al., 2016; Wattelet-Boyer et al., 2016).

Sphingolipid biosynthesis occurs in two endomembrane compartments, the Endoplasmic Reticulum (ER) and the Golgi apparatus, described in figure 5. After the elongation of the acyl-CoA (from 16C up to 26C) by the KCSs, there is formation of a ceramide by linking an acyl-CoA (C > 18 carbons) to a Long-Chain Base (LCB) *via an amide bond* by the ceramide synthase LOH1, LOH2 and LOH3 (Markham et al., 2011). Plant sphingolipids have the same feature as yeast, 90% of them contain α -hydroxylated fatty-acids. At which step the α -hydroxylation of the fatty-acid occurs in plant still remains unclear. Nevertheless, as ceramide synthases do not use the α -FA as substrate *in vitro* it suggests that the α -hydroxylation occurs downstream of the ceramide formation (Lynch, 2000; Marquês et al., 2018). The addition of the headgroup composed by different sugars fixed on an inositol-phosphate occurs in the Golgi apparatus through the activity of Inositol PhosphorylCeramide Synthases (IPCSs), Inositol Phosphorylceramide Uronosyl-Transferase (IPUT) and GIPC Mannosyl-Transferase (GMT) that add, an inositol-phosphate, glucuronic acid and a mannose (in pollen, another sugar is added in *A. thaliana*), respectively (Wang et al., 2008; Mortimer et al., 2013; Rennie et al., 2014; Buré et al., 2014). Sphingolipids are probably transported to PM mainly *via* the SVs where there is an enrichment of α VLCFA-containing sphingolipids (Wattelet-Boyer et al., 2016).

Hence, sphingolipids probably traffic *via* secretory vesicles and may already play a role as well in protein secretion and sorting pathways. Indeed, when different genes implied in

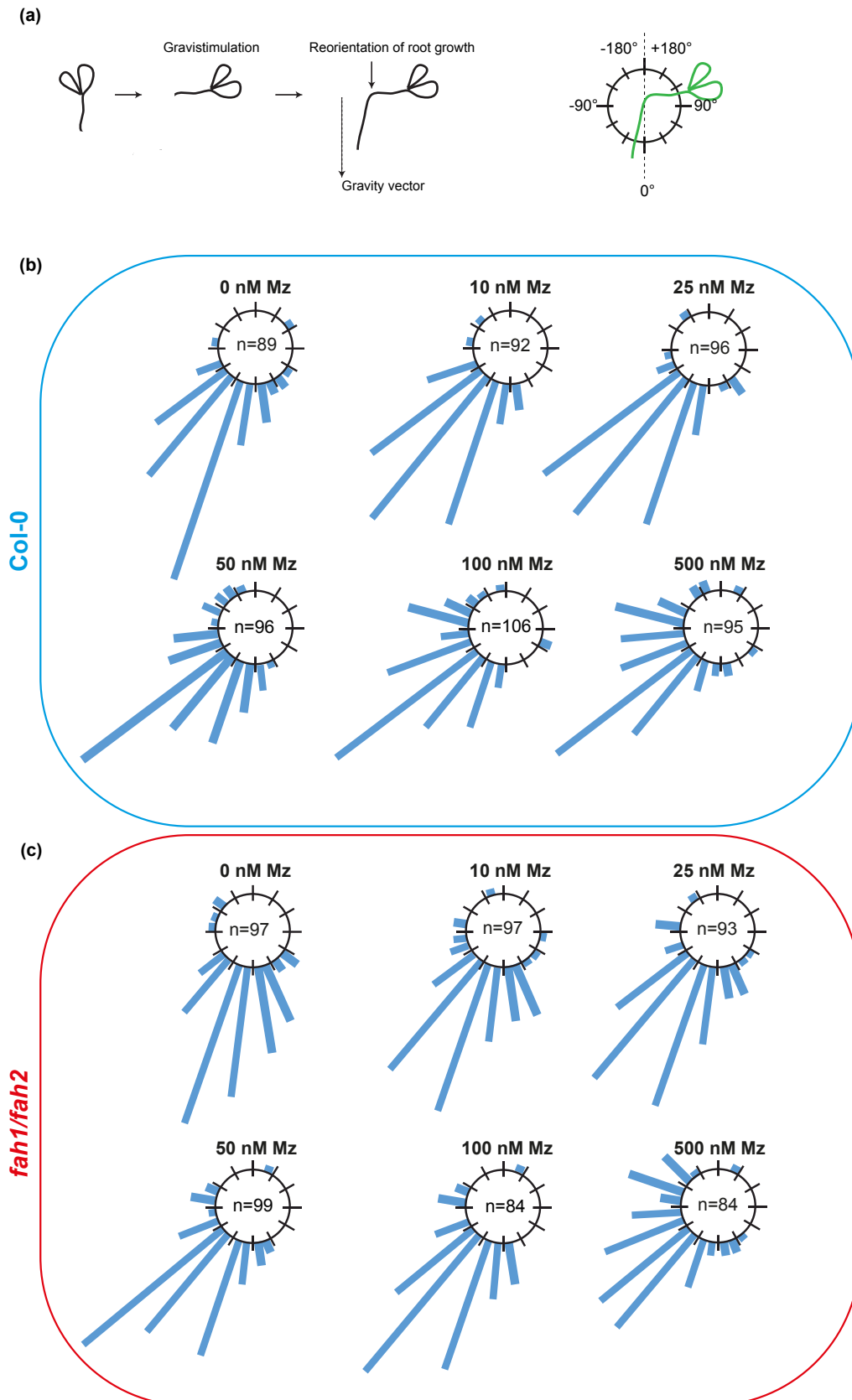


Figure 6: Metazachlor does not affect the α -hydroxylation in the GIPC biosynthesis. (a) Root angle curvature towards the new gravity vector 24h following a gravistimulation (turn the plate of 90°) is calculated, we then ranked the effective (n) into 15° angle-classes (0° was the exact direction of the new gravity vector) and represented each class of angles in a circular chart. The gravitropism response is affected at 50 nM metazachlor for the Col-0 plants (b). From this concentration, the root's reorientation is much less efficient. The double mutant *fah1/fah2* (c) has the same response pattern as the control condition.

the sphingolipid biosynthesis are *knock-down* or *knock-out*, some proteins localization at PM and secretion pathways are altered such as auxin carriers secretion (Lee et al., 2009; Markham et al., 2011; Wattelet-Boyer et al., 2016; Marquês et al., 2018). As sphingolipids are implied in the polar secretion of the polar auxin carrier PIN2 which is involved in the re-orientation of auxin fluxes during root response to gravity (gravitropism), we can measure an impact of sphingolipids in polar secretion using root gravitropism as a phenotypic readout. Root gravitropism allows a fast and inducible (gravistimulation) response which is transduced by the auxin fluxes through auxin carrier re-localization. My host team has shown that PIN2 polar secretory sorting depends on sphingolipids composition at SVs. Moreover, the PIN2 mutant *eir1* is resistant to metazachlor which indicates that the effect of metazachlor is partly effective through PIN2 (Wattelet-Boyer et al., 2016). Thus, the gravitropism is a good phenotypic readout for sphingolipid-mediated vesicle trafficking and cell polarity as it relies on the apical polarity of the auxin carrier PIN2.

To quantify root gravitropism, I measure *via* imageJ the last curvature of the root 24h after a gravistimulation (which consist of turning the plate 90°), when the roots are reoriented according to the new gravity vector (figure 6a). This new gravity vector is labeled as 0 while all the angles are ranked into 24 classes of 15° angles (0°:15°, 15°:30°, ...:180°). Thus, I represent the data on a circular chart by presenting on the left part, the angle classes in negative values to mark their reduce response (less gravi-response) and in contrary, the right part is positive due to an over gravi-response (figure 6a).

First, I tried six different concentrations of metazachlor on *Arabidopsis thaliana* ecotype Columbia-0 (Col-0) (figure 6b). Accordingly to what was found in the lab by Valérie Wattelet-Boyer, from 0nM to 10nM of metazachlor, the phenotypic responses are similar with an angle repartition around -30°:0°. However, at 25nM there is a small shift on the left that increase with the metazachlor concentration. From 50nM metazachlor, the gravitropism is totally spread which is consistent with a loss of gravity phenotype. This metazachlor range scale shows a dose response effect which reaches its maxima at 50nM. Together with results obtained by Valérie Wattelet-Boyer in the lab, these results underscore the role of the α -VLCFA-sphingolipids in the root gravitropism.

α -hydroxylation is characteristic of plant sphingolipids, hence, to look if the α -hydroxylation is important for root gravitropism response, I performed gravitropism assay in the *fah1fah2* double mutant knock down for *fah1* and knock out for *fah2* (König et al., 2012). It has been shown that the *fah1fah2* double mutant displays a reduce amount of α -VLCFA

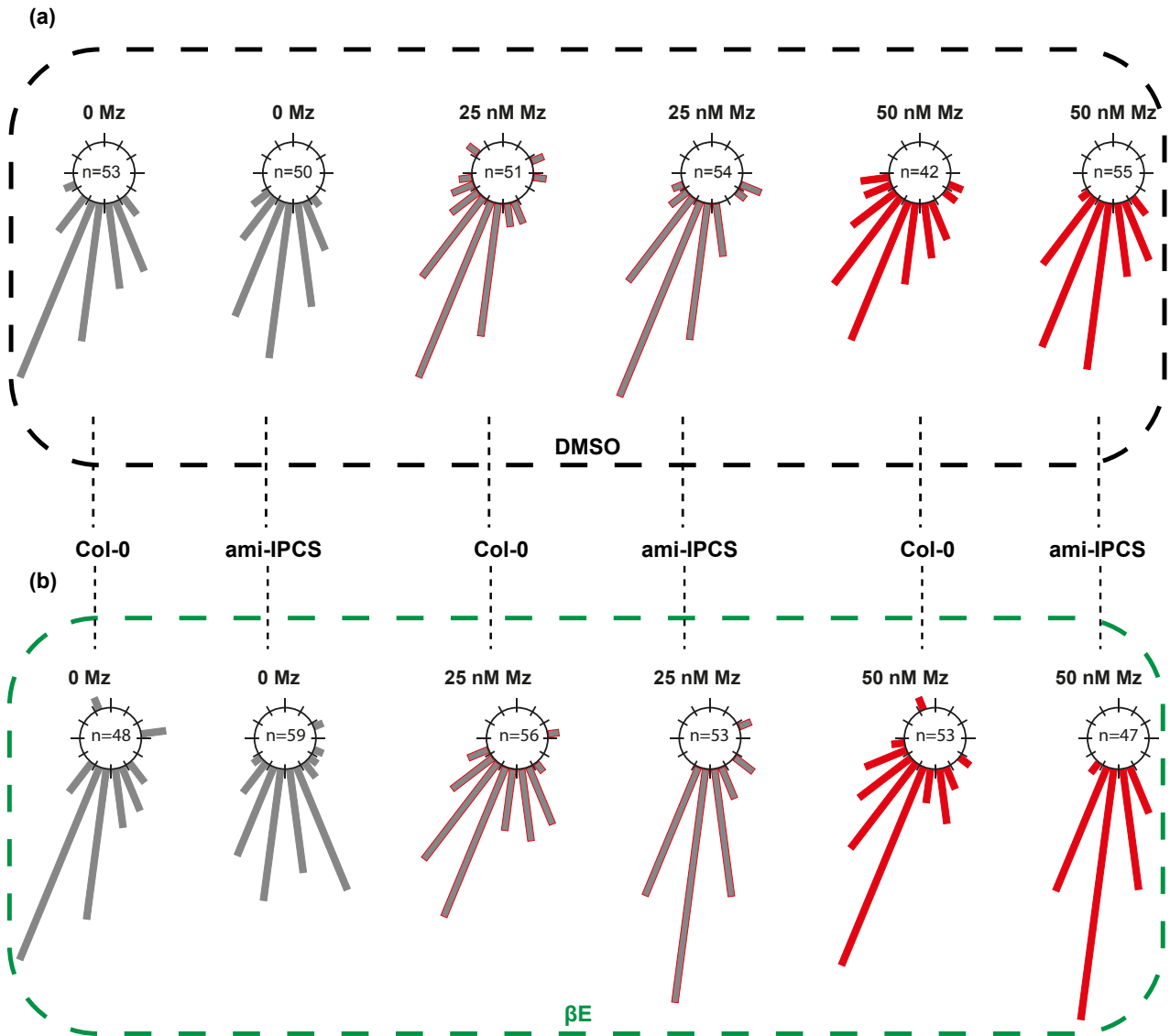


Figure 7: Knocking down IPCSs leads to a metazachlor resistance after gravitropism stimulation. Using inducible ami-IPCS (artificial micro-RNA targeting IPCS1 and IPCS2), we can mimic a *ipcs1/ipcs2* KD. The ami-IPCS construction is inducible by β -Estradiol (β E). Looking on the control condition with DMSO (a), there is no difference between the Col-0 and the ami-IPCS line. Whereas in the β E condition (b), there is a resistance of metazachlor treatment in the ami-IPCS induced plants. n, number of quantified roots, 6 days old seedlings.

(Nagano et al., 2012). Actually, the *fah1fah2* double mutant didn't display any root gravitropism phenotype compared to the wild-type in the control condition during the time of the experiment (figure 6c). Moreover, upon metazachlor treatment, there was no different gravi-response compared to metazachlor-treated wild-type. In both *fah1fah2* mutant and Col-0, higher the concentration of metazachlor is, lower the gravitropic response is. In the nutshell, as Col-0 and *fah1/fah2* have the same phenotypic response upon metazachlor, it means that metazachlor-induced gravitropism phenotype is independent of the α -hydroxylation.

On the other side, to look if the metazachlor-induced gravitropism phenotype is acting through a downstream step of the sphingolipid pathway, Valérie Wattelet-Boyer provided me an artificial micro-RNA (amiRNA) line she produced that targets both IPCS1 and IPCS2, and I characterize this line for gravi-response. This line has an amiRNA targeting both IPCS1 and IPCS2 under a β -Estradiol-inducible promoter. I used this line because both single complete knock-out mutants of either *ipcs1* or *ipcs2* have no phenotype and the double mutant *ipcs1/ipcs2* is seedling lethal (Wattelet-Boyer et al. unpublished results). Using this β -Estradiol inducible amiRNA line allows knocking down both IPCS1 and IPCS2 and getting an intermediate phenotype (Wattelet-Boyer et al. unpublished data).

The figure 7 shows the gravitropism responses under induction (β -Estradiol diluted in DMSO) and metazachlor treatment. As an induction-control condition, I did the metazachlor gravitropism assay on plate containing DMSO (figure 7a). As you can see, there is no difference between the wild-type and the amiIPCS in the induction-control condition which is not treated by β -Estradiol or metazachlor (figure 7a). At 25nM metazachlor, the wild-type and the amiIPCS plantlets react the same way, with a more spread gravitropism phenotype than the untreated conditions for both wild-type and amiIPCS. However, at 50nM, the angles of the wild-type roots are clearly more spread than the amiIPCS roots suggesting a possible effect of the amiIPCS construction already without β -Estradiol induction. When the lines are grown on inductive-medium (β -estradiol/DMSO, figure 7b), there is a clear resistance to metazachlor of the amiIPCS-induced lines compared to the wild-type, moreover the amiIPCS-induced plantlets seem to be more gravitropic upon metazachlor treatment than without metazachlor (figure 7b). These results were very encouraging but as I observed before a possible effect of the amiIPCS without β -Estradiol induction, I thought that this might reveals a low constitutive leak of the inducible promoter that could be activated by the DMSO. That would actually be reminiscent of the promoter leak in the DMSO condition that Valérie

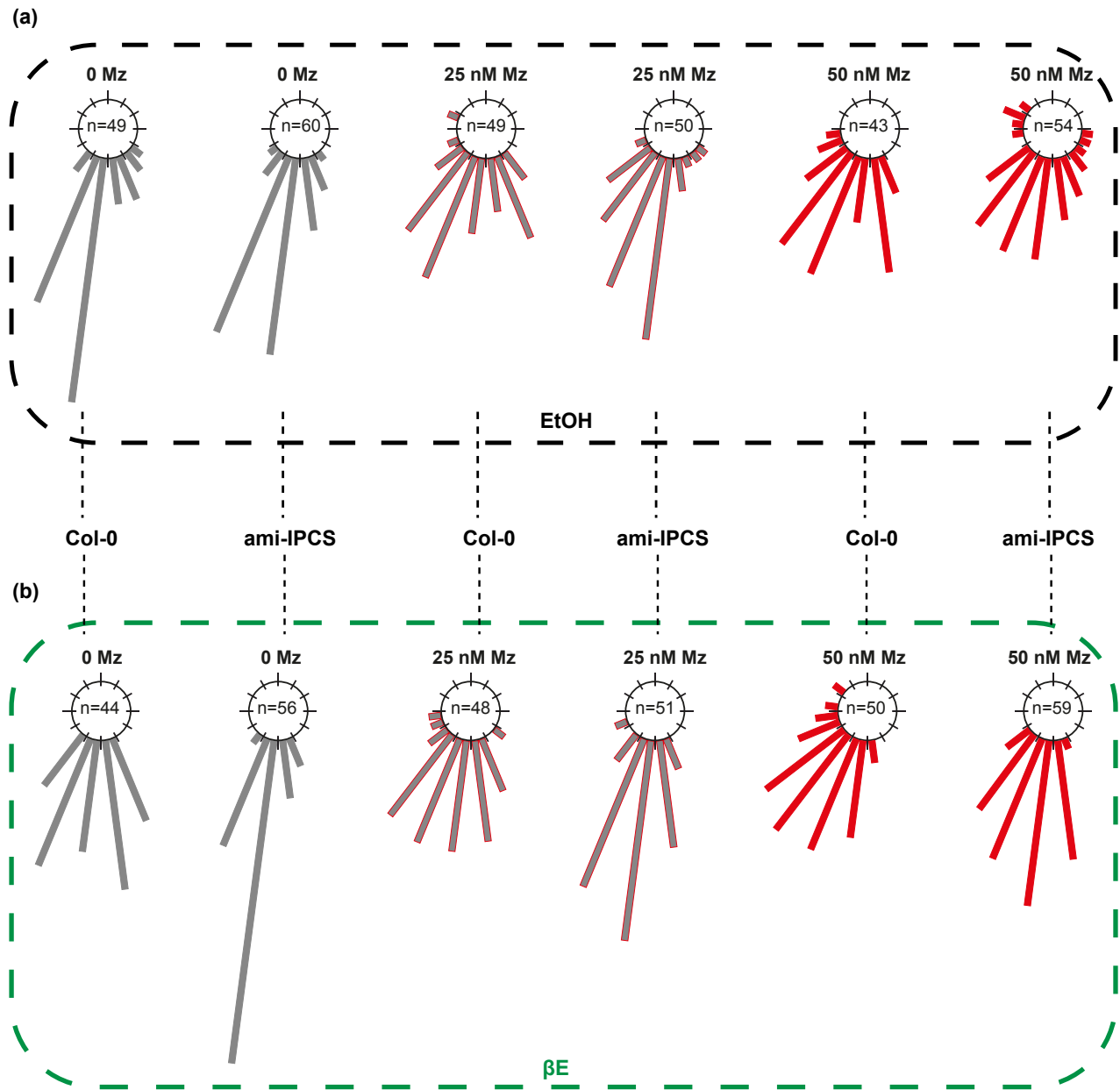


Figure 8: Knocking down IPCSs leads to a metazachlor resistance after gravitropism stimulation. Here, the β E is diluted in ethanol (EtOH) to see if the DMSO has an effect on the seedlings. Looking on the control condition with EtOH (a), there is no difference between the Col-0 and the ami-IPCS line. Whereas in the β E condition (b), there is a resistance of metazachlor treatment in the ami-IPCS induced plants compared to both non-induced amiIPCS and β E-induced wild-type. n, number of quantified roots, 6 days old seedlings

Wattelet-Boyer characterized in the laboratory when performing the quantitative PCR on these amiIPCS lines.

So, to avoid this possible DMSO-leak effect, I redid the gravitropism assay with β -Estradiol diluted in 96% ethanol (figure 8). In ethanol (EtOH) induction-control condition (figure 8a), the gravitropism phenotype is similar between Col-0 and amiIPCS with a normal repartition around the new gravity vector without metazachlor and a spread repartition upon metazachlor treatment. With β -Estradiol/EtOH, I still observe the metazachlor resistance in the induced amiIPCS root I found previously in β -Estradiol/DMSO induced amiIPCS (figure 8b). Upon metazachlor treatment and β -Estradiol induction, the amiIPCS root angles are less spread than the Col-0 or the non-induced amiRNA-IPCS at the same metazachlor concentration (figure 8).

Taken together (figure 7 and 8), these root gravitropism results suggest that the metazachlor-induced gravitropism phenotype may act mainly through the synthesis of Inositol-Phosphoryl-Ceramide (IPC) and be independent of the α -hydroxylation (figure 5). I could not look at the effect of metazachlor on mutants of sphingolipid biosynthesis steps downstream of IPC synthesis as the knock out mutant of the gene responsible of GIPC formation (by the addition of the glucuronic acid by IPUT1 enzyme) because a knock-out mutant of the corresponding gene is gametophyte lethal impeding to obtain a homozygous line (Rennie et al., 2014).

B. Identification of sphingolipid-dependent actors

To identify the actors depending on sphingolipids composition at TGN, we choose to perform proteomic analysis because the advantage of proteomic compared to transcriptomic or other -omic analysis is the identification of final products at precise compartments. Some years ago, proteomic analysis on TGN and other endomembrane compartment was done (Parsons et al., 2012; Drakakaki et al., 2012; Groen et al., 2014). However, these proteomic data were generated on plant cell culture or compartment purification in non-native condition that might lead to a compartment disruption (Parsons et al., 2012; Groen et al., 2014). Furthermore, the labeling of the proteins in both studies may causes proteins denaturation and modification. Nevertheless, proteomic analysis on the Syp61 compartment in native condition was already done in 2012 by Drakakaki et al. but they extracted the Syp61 compartment only

(Drakakaki et al., 2012). As we wanted to compare the different compartment proteomes of the Golgi apparatus and TGN sub-domains and determine the role of the sphingolipid's composition in these proteomes, we decided to do new proteomic analyses on TGN compartments using a called label-free LC-MS/MS. The proteomic label-free LC-MS/MS analysis was done by Stephane Claverol from the proteome's platform of the Functional Genomics Center of Bordeaux (CGFB). This mass spectrometry method aims to determine the relative amount of proteins in several biological samples. After trypsin digestion, the generated peptides are sent to Liquid Chromatography coupled to Mass Spectrometry (LC-MS) to measure with high precision the mass of peptides while a tandem MS run is done to acquire peptide identification (like a two-dimension electrophoresis). To sum up, this method allows uncoupling the quantification from the identification process. All the data created are analyzed *in silico* and confronted to databases (ARAPORT) to identify proteins.

1. Compartments extraction

Before starting proteomic analysis, the choice of vesicle markers came first. To identify the proteins of TGN compartments and Golgi, we chose the following protein-markers as compartment-baits:

- Syntaxin of Plant 61 (Syp61) which localizes at TGN and more precisely at Secretory Vesicles (SVs) (Kang et al., 2011) and is distinct from another TGN compartment labeled by RabA2a (Gendre et al., 2011; Boutte et al., 2013)
- Small Rab-GTPase A2a (RabA2a) which also localizes at TGN but at a different subdomains labeled by Clathrin-Heavy-Chain (CHC) (Wattelet-Boyer et al., 2016)
- Qb-SNARE Membrin12 (Memb12) which localizes at Golgi apparatus and colocalizes with the other Golgi marker Membrin11 that has been shown to localize at the cis-Golgi by electron microscopy (Uemura et al., 2004; Marais et al., 2015).

These three proteins were chosen as baits because their localization has been proved either by confocal imaging or by Transmission Electron Microscopy (TEM) immunolabeling. Thus, I used the Syp61-CFP as SVs bait, the RabA2a-YFP as Clathrin-Coated Vesicles (CCVs) bait and the Memb12-YFP as Golgi bait.

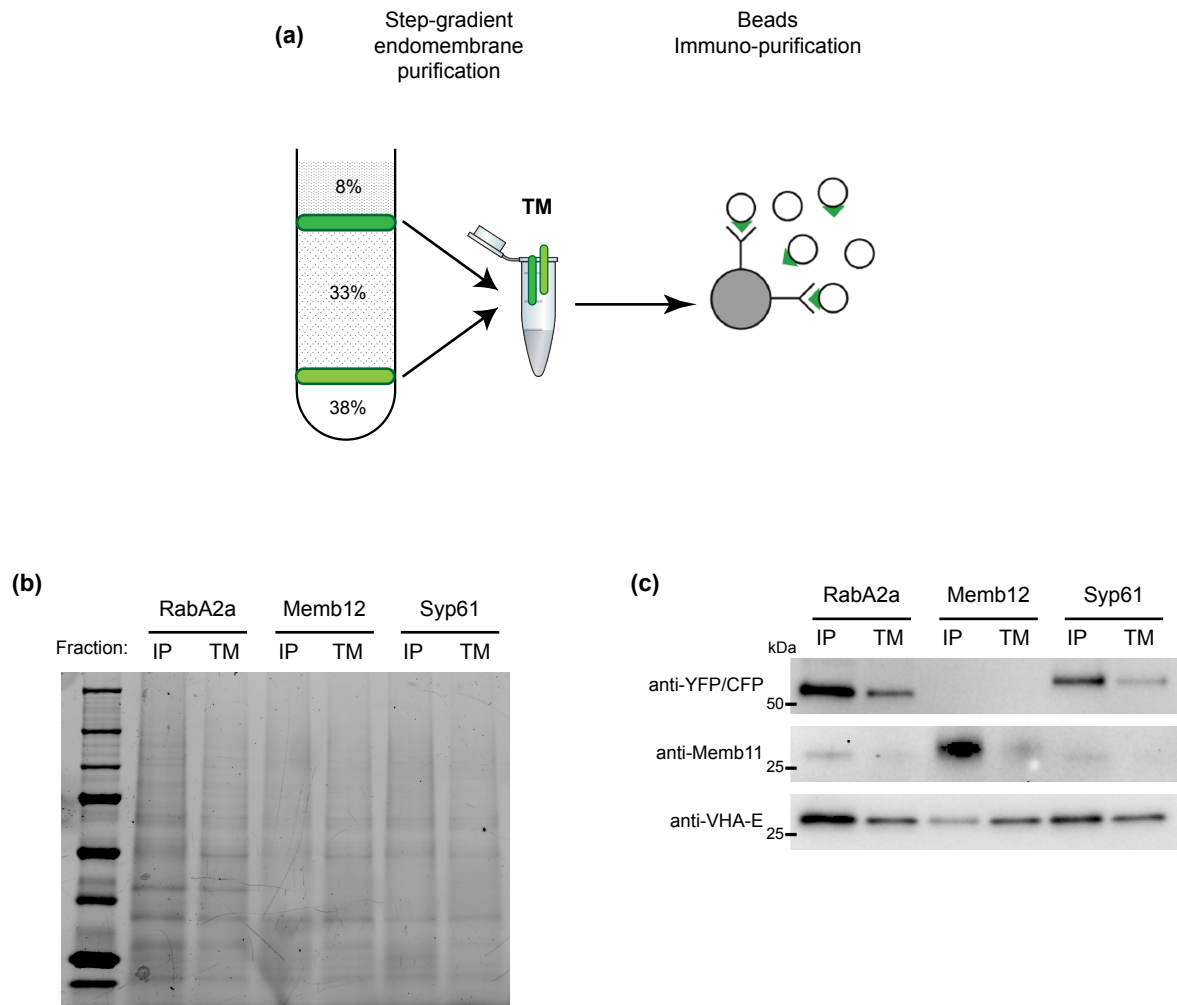


Figure 9: Immuno-purified vesicles fraction enrichment. **(a)** Immuno-purification (IP) of vesicle tagged by a fluorescent tag were done by incubating Total Membrane (TM) purified by a sucrose step-gradient centrifugation with magnetic beads coated with anti-tag antibodies. **(b)** Protein loading quantity checking from 3 IPs RabA2a, Memb12 and Syp61. For each IP, loading of the IP fraction and the TM fraction to verify the enrichment by western blotting **(c)** with 3 antibodies one anti-YFP/CFP, anti-Memb11 and the last anti-VHA-E. It shows the enrichment of each targeted IP compared to their TM fraction without contamination of the Golgi (anti-Memb11)

To extract the Syp61-, RabA2a- and Memb12-compartment, I grew the stable *Arabidopsis thaliana* lines (expressing the marker tagged with YFP or CFP) in liquid medium to increase the biomass and facilitate the harvesting. I grinded the seedlings in an extraction buffer without detergents (native condition) to keep the vesicles intact and complete, I loaded the mixture on a sucrose cushion, picked-up the floating fraction and subsequently built a sucrose step-gradient (with 38%, 33% and 8% sucrose as describe in figure 9a) to isolate the purified total membrane fraction (TM). I took both 8/33% and 33/38% to harvest all the purified endomembrane compartments. This TM fraction was then incubated with magnetic beads coupled with anti-GFP antibodies (recognizing both YFP and CFP) to purify the different compartments depending on the line used (Syp61-CFP, RabA2a-YFP or Memb12-YFP). All these steps were performed in native condition to avoid the disruption of the compartment and to lose their contents.

Before sending the immuno-purified (IP) fraction to proteomic analyses, I looked at their enrichment compared to the TM fraction. First, by using the stain-free technology developed by Bio-Rad[®], I equalized all the samples by measuring the total amount of proteins in each IP fractions and TM fractions. The stain-free gel uses the property of a molecule to enhance the fluorescence of tryptophan after UV-light activation. With this technology, we can quantify the amount of protein in the polyacrylamide gel and, with imageJ I measured the gray-value of each line and make a ratio to obtain the dilution factor to equalize the fractions between them (sample of stain-free equalized gel in figure 9b). With the freshly equalized fractions, I performed a new SDS-PAGE and then I blotted the gel on a PVDF membrane.

In the figure 9c, I checked the enrichment by using an antibody anti-GFP (recognizing YFP and CFP) for the RabA2a and Syp61 IPs and an anti-Memb11 for Memb12 IP. Due to a lack of volume for the IP fractions, we decided to no repeat the western blotting for quantification to save the fractions for proteomic analyses, but we can observe enrichment in each IP fraction as compared to the TM fraction. In the paper of Wattelet-Boyer et al., 2016 (See annex) and in the figure 9c, different western-blot were done. Sec21p and Membrin11 have been chosen as Golgi markers because immunolabeling electron microscopy of these two proteins proves their localization at the Golgi membrane (Pimpl et al., 2000; Marais et al., 2015). These two Golgi markers were found to be enriched in the Memb12 IP fraction by western-blot (Wattelet-Boyer et al., 2016). Furthermore, western-blot using an antibody targeting ECHIDNA, a well-known TGN/SVs marker (Gendre et al., 2011), shows an enrichment of ECHIDNA in the Syp61 fraction (Wattelet-Boyer et al., 2016).

Table 1: Proteome extract from Syp61 proteome. Red=proteins cloned and T-DNA mutant available, Orange=Proteins related to phosphoinositides (PIPs)

Accession	Unique peptides	Description	Control Mean	Metazachlo Mean	Ratio Mz/Ct	T-test
AT4G37310	2	cytochrome P450%2C family 81%2C subfamily H%2C polypeptide 1 - Chr4:17556152-17558833 REVERSE LENGTH=518 201604	30 348,85	166 278,81	5,48	0,08
AT2G04100	1	MATE efflux family protein - Chr2:1377020-1379051 REVERSE LENGTH=483 201604	6 879,06	31 161,71	4,53	0,01
AT2G30770	6	cytochrome P450 family 71 polypeptide - Chr2:13109909-13111988 REVERSE LENGTH=497 201604	566 928,90	2 295 681,87	4,05	0,01
AT1G71810	2	Protein kinase superfamily protein - Chr1:27002602-27007964 REVERSE LENGTH=692 201604	39 163,87	157 602,51	4,02	0,00
AT1G13090	2	multidrug resistance-associated protein 8 - Chr3:4203013-4208171 REVERSE LENGTH=1466 201604	38 622,30	153 232,31	3,97	0,01
AT4G08770	2	Peroxidase superfamily protein - Chr4:5598259-5600262 REVERSE LENGTH=346 201604	41 454,82	155 309,56	3,75	0,01
AT2G16660	4	Major facilitator superfamily protein - Chr2:7218930-7221592 REVERSE LENGTH=546 201604	497 013,55	1 688 037,35	3,40	0,01
AT5G44820	1	Nucleotide-diphospho-sugar transferase family protein - Chr5:18095795-18097558 REVERSE LENGTH=367 201604	51 580,90	172 808,03	3,35	0,01
AT3G59780	6	Rhodanese/Cell cycle control phosphatase superfamily protein - Chr3:22086906-22090324 FORWARD LENGTH=686 201604	260 141,93	853 943,16	3,28	0,05
AT3G60160	8	multidrug resistance-associated protein 9 - Chr3:22223829-22229195 REVERSE LENGTH=1506 201604	540 402,54	1 763 265,47	3,26	0,02
AT5G43760	7	3-ketoacyl-CoA synthase 20 - Chr5:17585903-17588486 FORWARD LENGTH=529 201604	1 201 615,7	3 873 764,33	3,22	0,01
AT3G14620	6	cytochrome P450%2C family 72%2C subfamily A%2C polypeptide 8 - Chr3:4914978-4916853 FORWARD LENGTH=515 201604	660 291,20	2 115 490,94	3,20	0,00
AT5G53550	2	YELLOW STRIPE like 3 - Chr5:21756081-21758776 FORWARD LENGTH=675 201604	91 169,67	289 280,52	3,17	0,03
AT4G01610	2	Cysteine proteinases superfamily protein - Chr4:694857-696937 FORWARD LENGTH=359 201604	76 958,47	239 886,31	3,12	0,05
AT4G39030	1	MATE efflux family protein - Chr4:18185740-18188898 FORWARD LENGTH=543 201604	31 863,45	85 963,88	2,70	0,11
AT4G28000	1	P-loop containing nucleoside triphosphate hydrolases superfamily protein - Chr1:23796887-23801240 REVERSE LENGTH=824 201604	8 319,25	17 910,69	2,15	0,43
AT4G27710	3	cytochrome P450%2C family 709%2C subfamily B%2C polypeptide 3 - Chr4:13828520-13830417 FORWARD LENGTH=518 201604	189 346,94	366 388,79	1,94	0,01
AT4G01100	7	adenine nucleotide transporter 1 - Chr4:477411-479590 FORWARD LENGTH=352 201604	1 072 886,9	2 071 769,07	1,93	0,08
AT1G51760	10	peptidase M20/M25/M40 family protein - Chr1:19199562-19201424 FORWARD LENGTH=440 201604	3 808 415,6	7 297 983,91	1,92	0,01
AT1G77510	25	PDI-like 1-2 - Chr1:29126742-29129433 FORWARD LENGTH=2014 201604	15 148 107,7	44 982 104,05	1,81	0,03
AT1G27980	11	dihydrospingosine phosphatase lyase - Chr1:9748812-9752618 FORWARD LENGTH=544 201604	5 396 080,3	9 784 490,49	1,81	0,02
AT2G21870	3	MALE GAMETOPHYTE DEFECTIVE 1 - Chr2:9320456-9322618 REVERSE LENGTH=240 201604	205 754,71	372 067,20	1,81	0,00
AT2G19450	2	membrane bound O-acyl transferase (MBOAT) family protein - Chr2:8426436-8429455 FORWARD LENGTH=520 201604	71 879,31	129 710,99	1,80	0,01
AT1G53240	26	Lactate/malate dehydrogenase family protein - Chr1:19854966-19856802 REVERSE LENGTH=341 201604	570 824,37	1 029 203,80	1,80	0,05
AT2G07707	3	Plant mitochondrial ATPase%2C F0 complex%2C subunit 8 protein - Chr2:3386292-3386768 FORWARD LENGTH=158 201604	191 090,16	344 015,51	1,80	0,15
AT4G26910	3	Dihydroliipoamide succinyltransferase - Chr4:13520127-13522889 REVERSE LENGTH=464 201604	120 899,45	217 580,85	1,80	0,00
AT2G15390	15	fucosyltransferase 4 - Chr2:6709345-6711044 REVERSE LENGTH=535 201604	3 866 150,3	6 955 280,25	1,80	0,01
AT5G05200	6	Protein kinase superfamily protein - Chr5:1544206-1547082 REVERSE LENGTH=540 201604	767 227,61	1 380 217,61	1,80	0,00
AT5G01500	25	thylakoid ATP/ADP carrier - Chr5:199017-201329 FORWARD LENGTH=415 201604	11 233 231,1	20 171 895,78	1,80	0,00
AT1G22510	2	E3 ubiquitin-protein ligase RNF170-like protein (DUF 1232) - Chr1:7951003-7952597 REVERSE LENGTH=185 201604	552 484,45	991 366,59	1,79	0,00
AT3G13930	5	Dihydroliipoamide acetyltransferase%2C long form protein - Chr3:4596240-4600143 FORWARD LENGTH=539 201604	623 314,22	1 117 581,58	1,79	0,06
AT3G48890	6	membrane-associated progesterone binding protein 3 - Chr3:18129669-18131353 FORWARD LENGTH=233 201604	5 703 248,7	10 213 606,13	1,79	0,01
AT4G38220	26	Peptidase M20/M25/M40 family protein - Chr4:17925251-17928919 FORWARD LENGTH=430 201604	20 130 601,3	35 813 737,53	1,78	0,03
AT5G15450	2	casein lytic protease B3 - Chr5:5014399-5018255 REVERSE LENGTH=968 201604	27 988,98	49 747,22	1,78	0,10
AT1G77130	4	plant glycogenin-like starch initiation protein 2 - Chr1:28979066-28981228 REVERSE LENGTH=618 201604	267 726,64	475 623,03	1,78	0,12
AT4G13770	41	cytochrome P450%2C family 83%2C subfamily A%2C polypeptide 1 - Chr4:7990682-7992282 REVERSE LENGTH=502 201604	40 650 794,7	72 163 472,8	1,78	0,00
AT5G20500	6	Glutaredoxin family protein - Chr5:6938652-6939665 FORWARD LENGTH=135 201604	3 127 259,2	5 546 644,86	1,77	0,02
AT2G24180	39	cytochrome p450 71b6 - Chr2:10281890-10283589 FORWARD LENGTH=503 201604	25 364 996,5	44 911 070,63	1,77	0,01
AT4G02580	3	NADH-ubiquinone oxidoreductase 24 kDa subunit - Chr4:1134586-1136906 FORWARD LENGTH=255 201604	240 642,12	425 849,74	1,77	0,12
AT3G46450	3	Sec14-Unk-3	153 261	260 897	1,70	0,09
AT3G48320	1	cytochrome P450%2C family 71%2C subfamily A%2C polypeptide 21 - Chr3:17891241-17892804 FORWARD LENGTH=490 201604	227 741,26	351 076,77	1,54	0,00
AT2G37710	1	receptor lectin kinase - Chr2:15814934-15816961 REVERSE LENGTH=675 201604	48 780,61	73 964,02	1,52	0,27
AT1G62200	1	Major facilitator superfamily protein - Chr1:22982147-22984334 REVERSE LENGTH=590 201604	92 019,04	137 545,82	1,49	0,00
AT1G74030	1	enolase 1 - Chr1:27839465-27841901 REVERSE LENGTH=477 201604	22 824,88	32 960,85	1,44	0,08
AT3G59770	4	SAC9	366 451	482 228	1,32	0,11
AT1G72175	1	E3 ubiquitin-protein ligase RNF170-like protein (DUF 1232) - Chr1:27157978-27159359 FORWARD LENGTH=185 201604	296 597,61	382 944,57	1,29	0,06
AT1G08750	3	Peptidase C13 family	500 067	616 838	1,23	0,04
AT5G19130	4	Gaa1-like family	288 377	344 441	1,19	0,08
AT1G70520	1	cysteine-rich RLK (RECEPTOR-like protein kinase) 2 - Chr1:26584888-26587334 REVERSE LENGTH=649 201604	117 222,00	137 520,08	1,17	0,32
AT3G51830	5	SAC8	641 288	742 551	1,16	0,31
AT1G04270	1	cytosolic ribosomal protein S15 - Chr1:1141852-1142960 REVERSE LENGTH=152 201604	302 753,17	350 532,19	1,16	0,79
AT1G63110	1	PIG-U	109 938	126 840	1,15	0,67
AT5G09510	1	Ribosomal protein S19 family protein - Chr5:2955698-2956554 REVERSE LENGTH=152 201604	86 099,62	96 358,99	1,12	0,83
AT1G58840	2	Sec14-Unk-4	285 180	315 184	1,11	0,52
AT3G02450	1	cell division protein ftsH - Chr3:502876-505030 FORWARD LENGTH=622 201604	18 821,43	20 608,79	1,09	0,85
AT3G17430	1	Nucleotide-sugar transporter family protein - Chr3:5966597-5968962 FORWARD LENGTH=375 201604	360 570,83	394 414,75	1,09	0,67
AT1G68000	1	PIS2	186 964	200 669	1,07	0,54
AT5G66020	24	SAC6/SAC7	9 491 492	10 026 512	1,06	0,31
AT2G39290	3	PGPS1	2 264 429	2 383 533	1,05	0,54
AT3G21690	3	MATE efflux family protein - Chr3:7638750-7641861 FORWARD LENGTH=506 201604	619 940,13	639 186,29	1,03	0,69
AT1G34120	2	IP5P1	105 482	100 241	0,95	0,75
AT1G01630	6	Sec14-Unk-5	1 573 049	1 378 674	0,88	0,36
AT1G17340	2	SAC5	281 123	231 479	0,82	0,13
AT3G19420	3	PTEN2A	362 153	291 257	0,80	0,21
AT2G22230	1	Thioesterase superfamily protein - Chr2:9450042-9451427 FORWARD LENGTH=220 201604	243 316,74	194 525,92	0,80	0,31
AT2G01690	14	VAC14	5 131 133	3 849 571	0,75	0,02
AT4G08690	4	Sec14-Unk-1	875 067	628 710	0,72	0,10
AT1G49340	3	PI4KA1	398 867	285 193	0,72	0,05
AT1G72160	7	PATL3	2 297 815	1 589 134	0,69	0,01
AT1G47550	3	exocyst complex component sec3A - Chr1:17457171-17463896 FORWARD LENGTH=887 201604	262 912,90	168 159,42	0,64	0,02
AT1G55020	1	lipoxigenase 1 - Chr1:20525798-20530143 FORWARD LENGTH=859 201604	210 469,35	134 509,97	0,64	0,15
AT3G03520	7	non-specific phospholipase C3 - Chr3:837972-840511 REVERSE LENGTH=523 201604	4 606 356,7	2 942 707,77	0,64	0,01
AT3G23280	2	hypothetical protein - Chr3:8321588-8324109 FORWARD LENGTH=462 201604	265 246,57	169 309,52	0,64	0,00
AT1G71695	3	Peroxidase superfamily protein - Chr1:26964359-26966557 FORWARD LENGTH=358 201604	288 063,11	183 559,09	0,64	0,02
AT3G11530	3	Vacuolar protein sorting 55 (VPS55) family protein - Chr3:3628801-3629885 REVERSE LENGTH=113 201604	2 601 609,8	1 656 527,51	0,64	0,09
AT3G12580	2	heat shock protein 70 - Chr3:3991487-3993689 REVERSE LENGTH=650 201604	128 576,53	81 807,79	0,64	0,33
AT4G31140	4	O-Glycosyl hydrolases family 17 protein - Chr4:15141581-15143188 FORWARD LENGTH=484 201604	1 850 055,1	1 176 930,89	0,64	0,01
AT1G09070	4	soybean gene regulated by cold-2 - Chr1:2927767-2928741 FORWARD LENGTH=324 201604	1 309 281,6	830 636,35	0,63	0,00
AT1G02500	4	S-adenosylmethionine synthetase 1 - Chr1:519037-520218 FORWARD LENGTH=393 201604	388 291,34	246 233,49	0,63	0,11
AT1G22280	2	phytochrome-associated protein phosphatase type 2C - Chr1:7874236-7875496 FORWARD LENGTH=281 201604	212 309,56	134 625,67	0,63	0,03
AT3G43220	1	SAC2/SAC3	93 102,78	58 877,20	0,63	0,00
AT1G75170	1	Sec14-Unk-2	27 405	17 058	0,62	0,26
AT2G20840	3	SAC4	500 349	305 421	0,61	0,00
AT4G30340	2	diacylglycerol kinase 7 - Chr4:14838465-14840941 REVERSE LENGTH=492 201604	720 329,60	436 958,08	0,61	0,02
AT3G51670	4	PATL6	1 222 614	736 223	0,60	0,00
AT1G22620	1	SAC1	103 653,17	61 992,22	0,60	0,00
AT3G02880	10	Leucine-rich repeat protein kinase family protein - Chr3:634819-636982 FORWARD LENGTH=627 201604	6 431 572,7	3 063 272,12	0,48	0,00
AT4G35790	17	phospholipase D delta - Chr4:16955774-16959875 REVERSE LENGTH=868 201604	5 024 153,9	2 385 391,73	0,47	0,00
AT1G45201	18	triacylglycerol lipase-like 1 - Chr1:17123889-17128462 FORWARD LENGTH=479 201604	24 725 891,1	11 735 687,53	0,47	0,01
AT1G75750	2	GAST1 protein homolog 1 - Chr1:28441813-28442284 REVERSE LENGTH=98 201604	98 582,74	46 714,96	0,47	0,09
AT1G66150	4	transmembrane kinase 1 - Chr1:24631503-24634415 FORWARD LENGTH=942 201604	704 115,01	333 473,03	0,47	0,00
AT5G61530	3	small G protein family protein / RhoGAP family protein - Chr5:24742630-24744586 FORWARD LENGTH=376 201604	694 269,12	322 944,12	0,47	0,00
AT5G35180	3	ENHANCED DISEASE RESISTANCE protein (DUF1336) - Chr5:13424538-13430831 FORWARD LENGTH=593 201604	582 615,36	270 048,59	0,46	0,03
AT4G09160	6	PATL5	855 339	281 057	0,33	0,01
AT1G22530	30	PATL2	26 374 221	6 660 038	0,25	0,00
AT1G30690	1	Sec14p-like phosphatidylinositol transfer family protein - Chr1:10888284-10890085 FORWARD LENGTH=540 201604	107 839,82	17 341,14	0,16	0,00

The vacuolar marker anti-VHA-E antibody which recognizes the VHA-E1, VHA-E2 and VHA-E3 subunits (Dettmer et al., 2006), reflects the secretory pathway of the V-ATPase from the TGN to the vacuole with a small enrichment in the RabA2a IP fraction (Wattelet-Boyer et al., 2016). Furthermore, there were no contaminations of the PM as there were no signals of the PM markers antibodies, PMA2 and PM-ATPase (two ATPases of the PM), in the three IP fraction (Wattelet-Boyer et al., 2016). I also tried the Clathrin Heavy-Chain (CHC) antibody however, as the CHC is a coat protein, we probably lost it during the vesicles extraction because I could not find it on my Western-blot. Altogether, these Western-blot results confirmed the efficiency of the vesicle immuno-purification protocol, without any or really few contamination from the vacuole and other membranes (Wattelet-Boyer et al., 2016).

2. Proteomic analyses

After 9 months of vesicle extraction and purification, all the IP fractions were sent to the CGFB to perform proteomic analysis using label-free LC-MS/MS. To be able to obtain reproducible results, the analysis was done on 4 experimental replicates for each condition. As describe before, this method relies on the tandem MS/MS which allows the identification and the quantification of each peptide separated by the upstream LC. The experimental replicates allow a normalization of each peptide and the results are presented as an excel table (simplified extract in table 1). The results give information on the gene identified as its accession number, its gene description, the number of unique peptides identified and other comparative data depending on the sample (treated with metazachlor or non-treated for example). However, I noticed that depending on the identified peptide, there may be several corresponding genes and accession numbers (like homologous genes or splicing variant or gene family). That might be a problem since *in silico* work as Gene Ontology or table manipulation to extract compartment specific proteins. To solve this problem, we had to think about an excel macro to count the number of genes (x) within one Excel cell and then create x lines and copy/paste the corresponding accession number one by one. Thanks to Clément Train from Lausanne University who made this macro for me, I could separate the data on each Excel cell, separate the accession numbers for which the peptide detected was common and then create Venn diagrams to identify compartment-specific proteins. I then performed abundance histograms for proteins we were interested in, after identification.

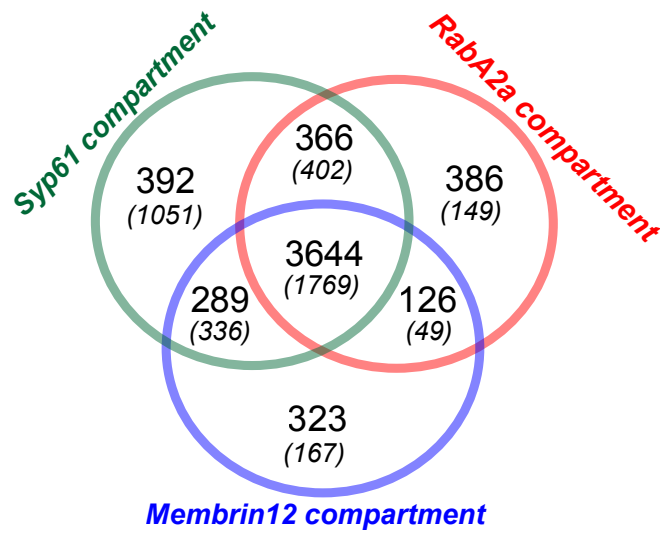


Figure 10: Venn diagram of the proteins compartment specificity. The Venn diagram is done according to the pivot table made by Excel to identify the compartment specificity of the identified proteins. (XXX) : Number of proteins before using the macro to separate the accession number

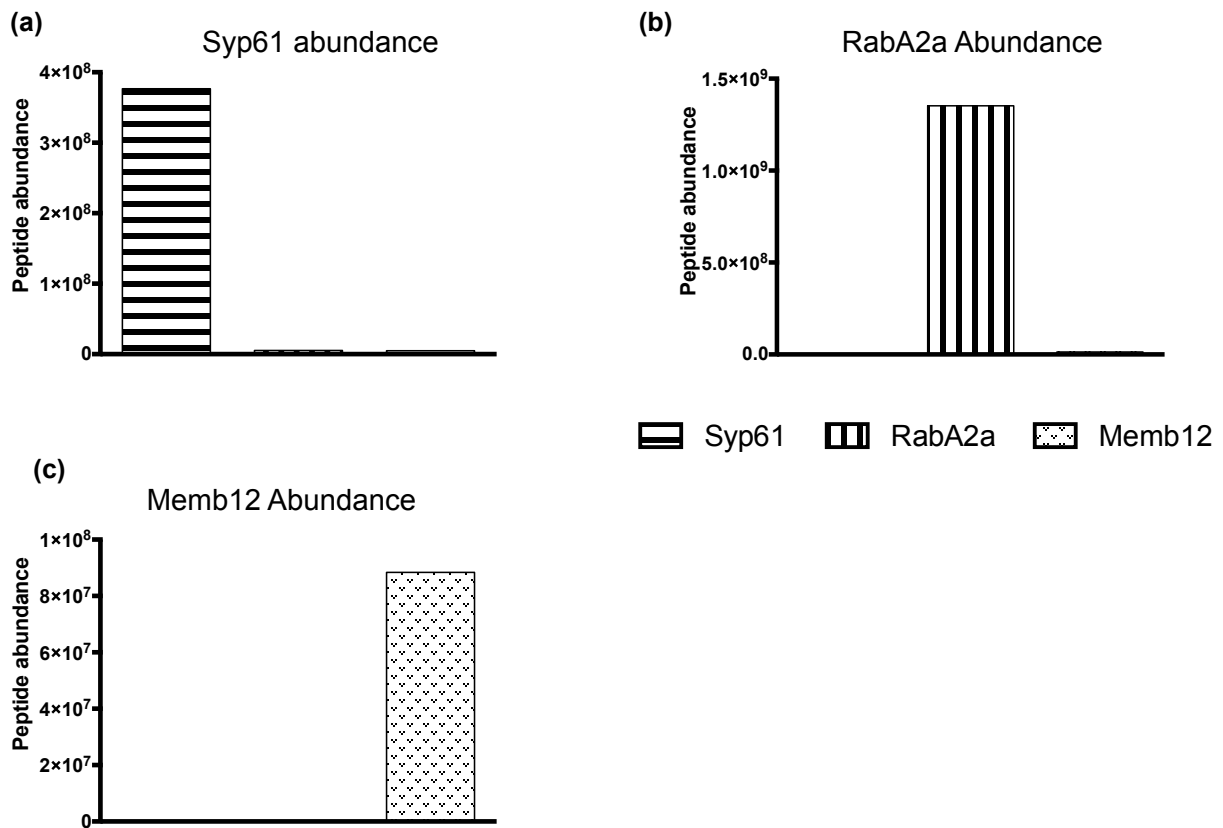


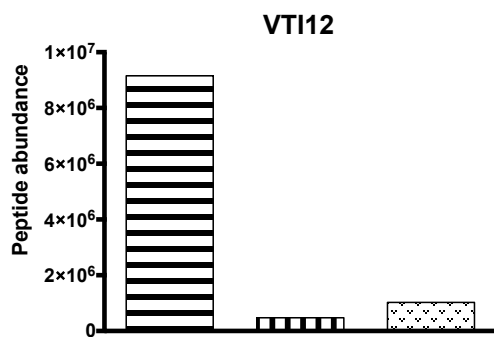
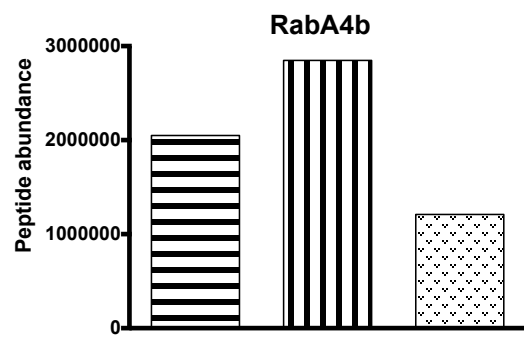
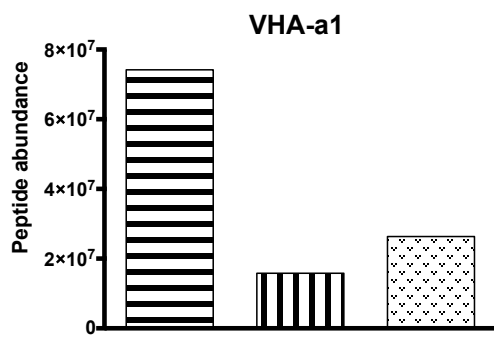
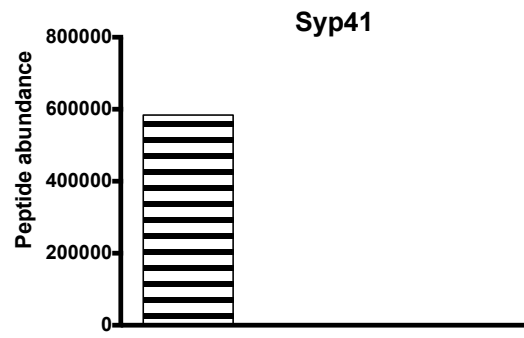
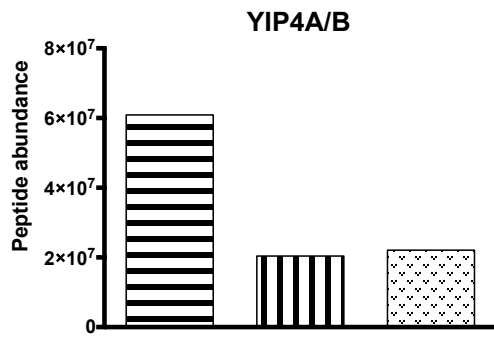
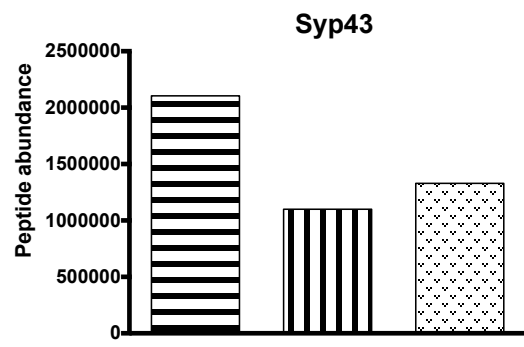
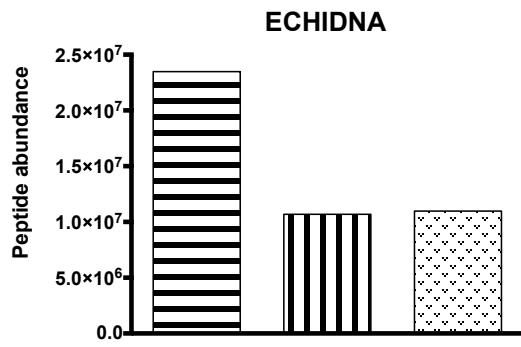
Figure 11: Each extracted compartment is enriched in their marker. Histogram graphs representing the abundance of the three proteins used as bait Syp61 (a), RabA2a (b) and Memb12 (c) enrichment in each proteome to validate the good immunopurification protocol.

Around 5,500 proteins have been identified in total. One of the aims of this proteomic analysis was to design an accurate proteome of the Syp61/SV, RabA2a/CCV and Memb12/Golgi. To identify the compartment-specific proteins, I used Excel software to make pivot table for each compartment. The protein distribution between the three compartments is plotted in the Venn diagram (figure 10). The numbers represent the amount of accessions found, and the ones in italic between brackets represent the number obtained with the same *in silico* processing before processing the data with the macro from Clément Train, however in both case the splice-variants are deleted. As you can see, there is a difference between the two processes. After the macro, I identified 70% more different accession numbers (splice-variants non-counted) whatever the compartment (from 3,900 to 5,500). The new proteomic table allows more complete identification to define the specific proteome of each compartment. In the Venn diagram, most of the genes are in common with the three compartments and around 350 genes are specific to each compartment. The Excel macro highlights the limitation of the software used for the proteomic analysis, because due to the several accession numbers that were sometimes found for one peptide identified, there was a loss of data. Without the macro, all the data (enrichment, number of detections, etc.) were linked to the first accession number and other possible accessions were not considered. Nevertheless, I managed to solve this problem with the use of the macro.

3. Extraction validation by proteomic analysis

Before sending the samples to proteomic analysis, I didn't look deeply in their purity by western-blot due to the small volume obtain after the extraction (35 μ L) and the volume needed for the proteomic analysis (20 μ L). Nonetheless, I checked by western-blot the enrichment of the targeted compartment using an anti-GFP antibody that recognize the compartment-specific marker, but I didn't look at other protein markers as I already did this in Wattelet-Boyer et al., 2016 on the fraction that served for lipid analyses.

However, while solving the number accession issue, I checked in my proteomics the abundance of already characterized proteins that could serve as markers to decipher further the specificity of purification of Syp61/SV, RabA2a/CCV and Memb12/Golgi fractions. First, I looked the proteins used as baits to purify the compartments: Syp61, RabA2a and Memb12 (Figure 11). As expected, each bait-protein is strongly enriched uniquely in its corresponding compartment Syp61 in Syp61/SV (Figure 11a), RabA2a in RabA2a/CCV (Figure 11b) or



 Syp61
  RabA2a
  Memb12

Figure 12: Abundance of SVs-localized proteins in Syp61/SV, RabA2a/CCV and Memb12/Golgi proteome. Histograms are representing the raw abundance of specific-peptides to each SV-localized proteins selected as markers: ECHIDNA, Syp43, YIP4A/B, Syp41, VhA-a1, RabA4b and VT112. These proteins are described to localize at TGN in the literature.

MEMBR12 in MEMBR12/Golgi (Figure 11c), confirming the IP specificity and purity. Nevertheless, it didn't prove that Syp61-, RabA2a- and Memb12-compartment are representative of the SV, CCV and Golgi apparatus respectively.

Therefore, to confirm this, I look at 23 proteins described in the literature to be localized at specific compartment, based on either confocal microscopy or TEM.

In the figure 12, I represented the abundance of 7 proteins localized at SV/EE according to the literature. ECHIDNA (ECH) is twice more abundant in Syp61 proteome than the other ones (RabA2a and Memb12), these result are in agreement with Gendre et al.'s work where they described ECH mostly colocalize with other SV markers (as VHA-A1, SYP41 or Syp61) and much less with TGN/CCV markers, like RabA2a (Gendre et al., 2011; Wattlelet-Boyer et al., 2016). The TGN marker SYP43 was found to mainly localize at SV which fits what was published before by confocal microscopy (Uemura et al., 2004) but I also identified its presence at RabA2a/CCV fraction. The non-negligible abundance level of SV markers in Memb12/Golgi proteome is probably representative of the secretory pathways through the Golgi apparatus up to TGN. The third SVs marker checked is the YPT/Rab GTPase Interacting Protein 4a/b (YIP4a/b) described to colocalize mainly with other SV markers (Syp61, VHA-a1, ECH) and much less with CCV marker or Golgi marker (Gendre et al., 2013). In the proteomic dataset, YIP4a/b's abundance is thrice more important in Syp61 proteome than in the two others, once more in accordance with the literature. On the other hand, the Syntaxin of Plant 41 (Syp41) is described to colocalize mainly with Syp61 (Sanderfoot et al., 2001). I found this protein to be exclusively present in Syp61 proteome.

Another TGN/SV marker used is the subunit a1 of the vacuolar H⁺-ATPase (VHA-a1) which, compared to the other subunits, localizes at TGN/SV (Dettmer et al., 2006). Indeed, I found VHA-a1 thrice more abundant in Syp61 proteome than both RabA2a and Memb12 proteome. Concerning RabA4b which is also described to localize at SV by Immunolabeling Electron Microscopy (IEM) but also at LE/MVB in pea, is 1.4 time more present in RabA2a proteome than Syp61 proteome (Kang et al., 2011; Inaba et al., 2001). This difference between the literature and my data could be explained by the fact that vesicles are very dynamics and RabA2a and Syp61 have been described as TGN subdomains and share a lot of proteins in common. Additionally, the localization of RabA4b has been described by IEM. IEM has some limits as it is much easier to found SVs in micrographs than CCVs. So, the distribution of RabA4b in my data is not discrediting my purification. The distribution of the last SV marker, VTI12 is reminiscent of immunochemical studies in which VTI12 is enriched

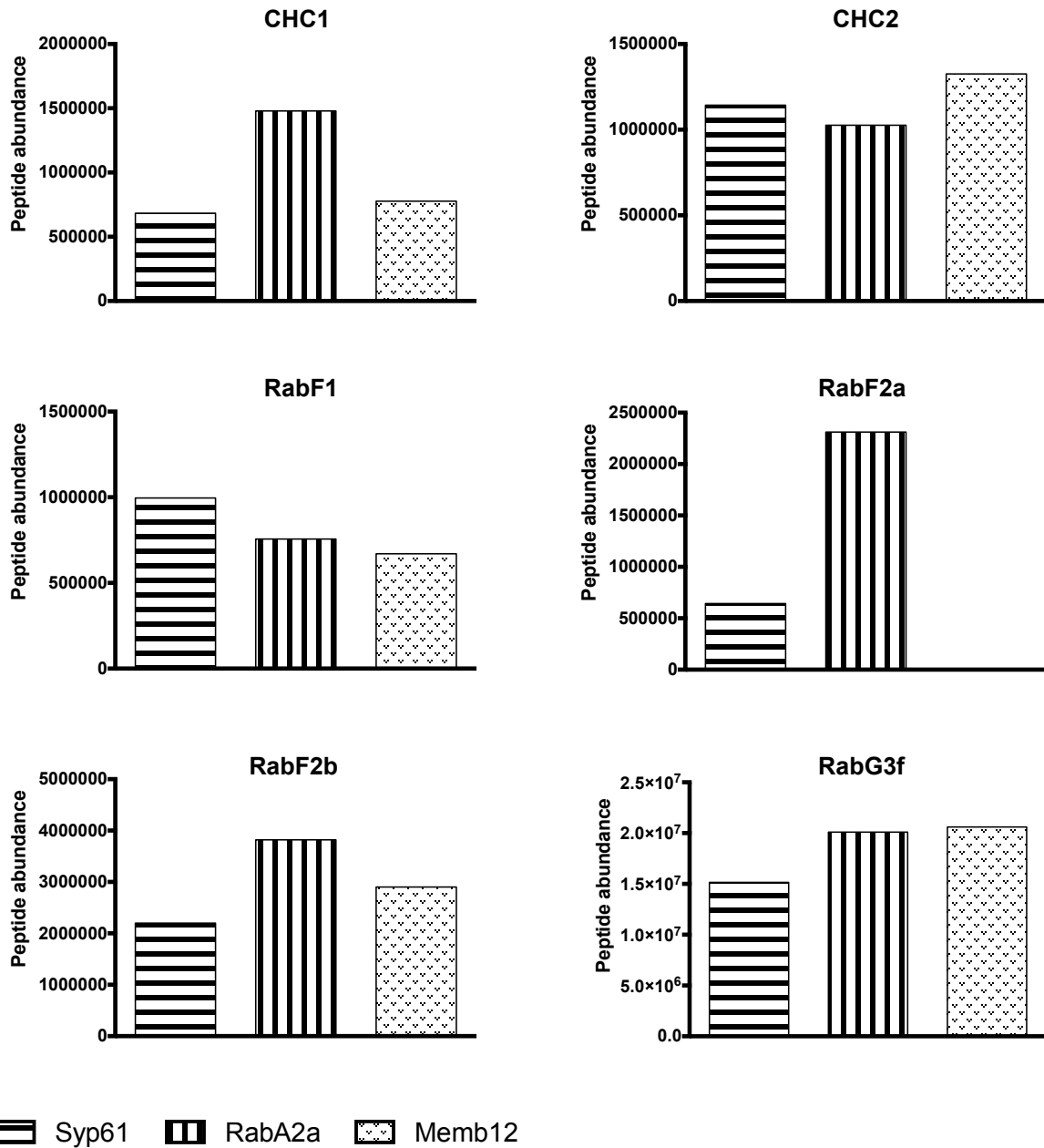


Figure 13: Abundance of CCV- and MVB/LE-localized proteins in Syp61/SV, RabA2a/CCV and Memb12/Golgi proteome. Histograms are representing the raw abundance of specific-peptides to each CCV- and MVB/LE-localized proteins selected as markers to control the good representativity of RabA2a as CCV bait. The two Clathrin Heavy Chains (CHCs) are Clathrin-Coated Vesicles (CCVs) marker while the Rab small-GTPase RabF1, RabF2a, RabF2b and RabG3f are mainly MultiVesicular Bodies (MVB) and Late Endosome (LE) marker.

in TGN compartment (Zheng et al., 1999; Sanderfoot et al., 2000, 2001; Surpin et al., 2003). Altogether (Figure 12), these abundance dataset of SV markers confirmed the enrichment of Syp61 fraction in SV markers suggesting that the Syp61 compartment is representative of SV compartment.

To check RabA2a/CCV IPs, I looked for either clathrin chains or Multi-Vesicular Body/Late Endosome (MVB/LE) markers as the trafficking pathway between TGN and MVBs is known to rely on clathrin, in the figure 13. It has been shown before that RabA2a strongly colocalize with Clathrin-Heavy-Chain 1 and 2 (CHC1 and CHC2) by immunolocalization with an antibody anti-CHC1 and CHC2 in *A. thaliana* root cells (Wattelet-Boyer et al., 2016). In my proteomics, both CHC1 and CHC2 abundance histogram show enrichment in RabA2a compartment, CHC1 is more abundant in RabA2a whereas CHC2 is dispersed between the three compartments. However, in the paper of Wattelet-Boyer et al., we showed that RabA2a colocalized strongly the CHC1 and CHC2 but not the other way around (i.e. that is CHC1 and CHC2 which colocalize strongly with RabA2a) meaning that CHC1 and CHC2 can colocalize with others markers as VHA-a1 and ECH for example (Boutte et al., 2013).

I also looked at MVB markers as trafficking from TGN to MVB is thought to depend on clathrin. RabF1 has been describe to localize mostly at MVBs (Multi-Vesicular Bodies) (Ueda et al., 2001). I found RabF1 in the three compartments (Memb12/Golgi, Syp61/SVs and RabA2a/CCVs) by proteomics. Another member of the RabF class (Rab5 plant homolog), RabF2a, which has been shown to localize mainly at MVBs as well, is 4 times more abundant in RabA2a/CCVs compartment than Syp61 compartment which is consistent with the known clathrin-mediated trafficking pathway from TGN to MVB/LE (Sohn et al., 2003). A last member of the RabF family, RabF2b, localizes mainly to MVB but as well, to a lesser extent, to TGN (Ueda et al., 2001; Jia et al., 2013). I found in my proteomic analysis RabF2b mostly present in RabA2a dataset but as well, to a lesser extent, in Syp61 and Memb12 proteomes. A last MVB marker I looked at is RabG3f (Rab-7 homolog), a characterized MVB/LE markers (Geldner et al., 2009) which is found enriched mostly in Memb12 and RabA2a proteomes. All these results show the existence of CCV-mediated pathway in the RabA2a compartment. However, it also underlines the dynamic of the TGN, with overlaps between the three compartments. TGN originates from the Golgi apparatus (Memb12 compartment) and, SV and CCV are TGN's subdomains. Hence, it's normal to find some markers described as

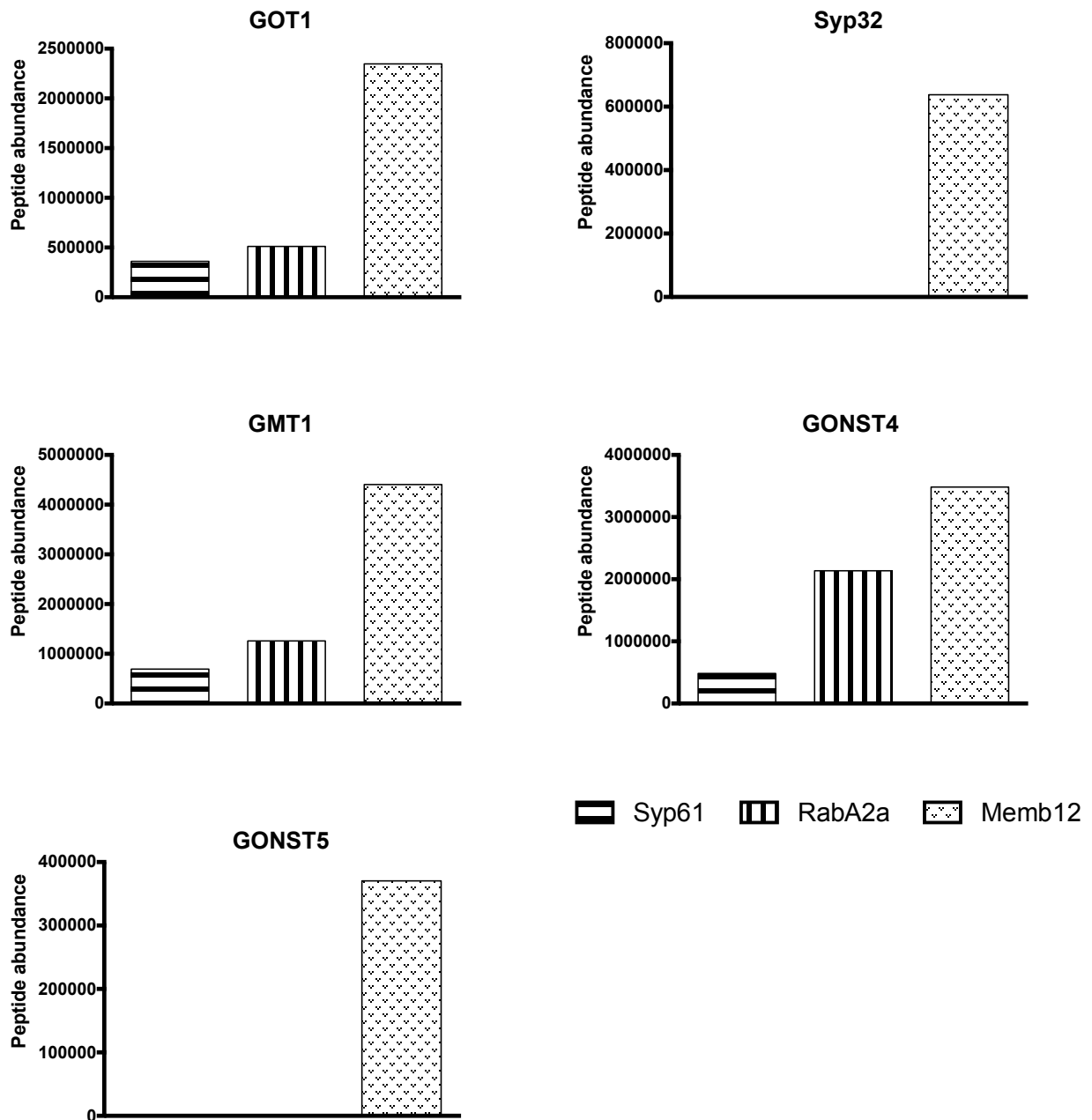
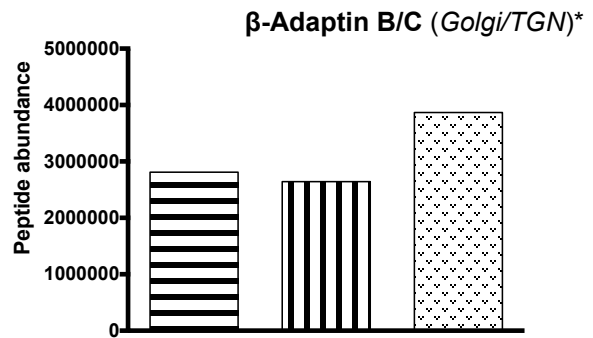
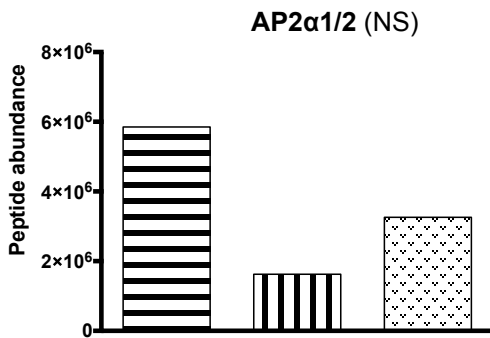
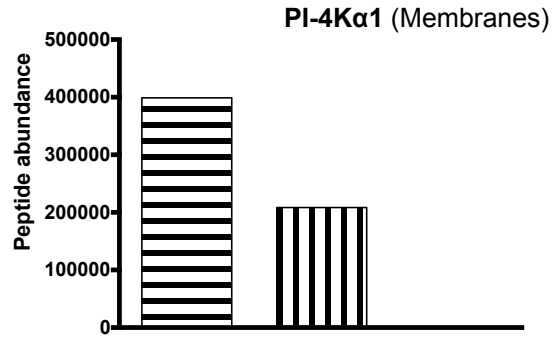
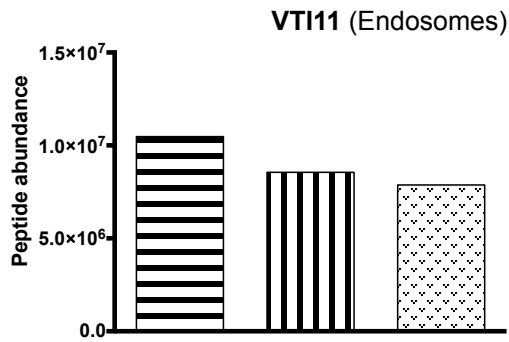



Figure 14: Abundance of Golgi-localized proteins in Syp61/SV, RabA2a/CCV and Memb12/Golgi proteome. Histograms are representing the raw abundance of specific-peptides to each Golgi-localized proteins selected as markers: GOT1, the syntaxin Syp32, the GIPC mannosyl transferase GMT1 and the Golgi-localized sugar transporters GONST4 and 5.

compartment-specific markers. In fact, the proteomic analysis has a higher detection threshold as confocal microscopy or TEM.

The Golgi markers abundances are also really clear; most Golgi markers are strictly specific to the Memb12 compartment (Figure 14). The GOT1 is used as Golgi marker, however there is no data in plant of its localization, it's based on its localization in *Saccharomyces cerevisiae* and sequence homology (Geldner et al., 2009; Conchon et al., 1999). GOT1 is 4 times more abundant in Memb12/Golgi IPs than the two other IPs (Syp61/SV and RabA2a/CCV). Another Golgi marker is the syntaxin Syp32, its localization is clear as Syp32 is only found in the Memb12 proteome, accordingly to previous work by confocal localization in protoplasts (Uemura et al., 2004; Rancour et al., 2002). GMT1 is another well characterized Golgi marker due to its mannosyl transferase activity in the sphingolipid biosynthesis pathway, it was first described in a work on dwarf mutant called ectopically parting cell (*epc* mutant) where they saw its localization in Golgi apparatus (Bown et al., 2007). Few years later, its name is changed in GMT1 according to its activity (Lombard et al., 2014). Its abundance in the Memb12 proteome is 4 times more enriched than the other compartments. The Golgi nucleotide-sugar transporters GONST4 and GONST5 are known to transport sugars from the cytosol to the lumen of the Golgi apparatus (Handford et al., 2004; Rautengarten et al., 2016). Between the Syp61-, RabA2a- and Memb12-proteomes, GONST4 is more abundant in Memb12 proteome (1.7 times more than RabA2a and 7 times more than Syp61 proteome) whereas GONST5 is present only in Memb12 proteome. These 5 Golgi markers are enriched in Memb12 proteome validating the choice of Memb12 as Golgi apparatus bait for the vesicle extraction.

I checked the abundance of other proteins which we thought might be of interest for our story and which we thought would inform us on how resolute the immuno-precipitation procedure is in yielding specific TGN sub-domains. The VTI12 homolog VTI11 is described to act in vesicle trafficking but to have a distinct localization from its homolog VTI12 (Zheng et al., 1999; Sanmartín et al., 2007). VTI11 colocalizes with other endomembrane-compartment proteins such as clathrin, VHA-a1 and Syp61 (Unpublished work from Jonsson K. and Boutté Y.) while VTI12 only colocalized with TGN marker. As showed in figure 15, VTI11 is equally found in all the proteome datasets comforting the unpublished work done before that suggested that VTI11 would equally localize to all TGN-subdomains (CCVs and SVs).



 Syp61
  RabA2a
  Memb12

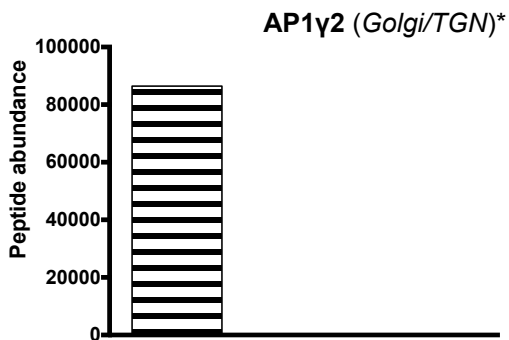


Figure 15: Abundance of compartment-localized proteins in Syp61/SV, RabA2a/CCV and Memb12/Golgi proteome. Histograms are representing the raw abundance of specific-peptide to each proteins described or supposed to be compartment-localized: the VTI12 homolog VTI11, the endomembrane-localized PI 4-kinase α1, and different adaptins implied in cargo formation. (*compartment*)* = Unpublished data or no imaging proofs

Another important protein for the follow-up of this manuscript and TGN sub-domains is the Phosphatidylinositol (PI) 4-kinase $\alpha 1$ (PI-4K $\alpha 1$) which phosphorylates the PI at on the 4th carbon of the inositol head to form PI4P. It has been shown before that the full PI-4K $\alpha 1$ protein localized to intracellular membranes (Stevenson-Paulik et al., 2003). The abundance data of my proteomics shows an enrichment of this protein mainly in Syp61/SV compartment (twice more than RabA2a/CCV compartment and no presence in Memb12/Golgi). This result is reminiscent of the presence of PI4P at TGN (Antignani et al., 2015) and suggest that PI4P could be more enriched at SVs subdomain of TGN as compare to CCV subdomain of TGN. Another important class to look at, from both trafficking machinery and TGN sub-domains point of view, is the Adaptor Proteins (AP or Adaptin) mostly known to be in charge of the selection of cargo, their secretion and vesicle formation (Hirst et al., 2011). From the complex 2, AP2 $\alpha 1/2$ are acting in Clathrin-Mediated Endocytosis, CME (McMahon and Boucrot, 2011) but its localization is described as cytosolic. The AP2 $\alpha 1/2$ is detected in the three compartments with a strong enrichment in Syp61/SV which could illustrate the CME transport from PM to TGN. The β -adaptin subunit B and C are also found in the three proteomes however, there is no strong enrichment in one particular compartment. The subunit γ of complex 1 adaptin is described in other organisms to localize at the TGN (Hirst et al., 2012) and I confirmed its presence only in Syp61 proteome.

Altogether (Figure 12-15), these abundance histograms confirm the choice of Syp61, RabA2a and Memb12 as bait for SV, CCV, and Golgi apparatus respectively. The TGN is considered as a central hub containing different subdomains where the release of SVs and CCVs occurs. These subdomains are marked by different markers as Syp61, RabA2a, ECH, VHA-a1, etc. which overlap partially. ECH is the best example as it localizes at TGN with Syp61, SYP41 and a little less with RabA2a (Gendre et al., 2013) while Syp61 and RabA2a colocalization is restricted. My proteomics allows comparing the abundance in each TGN sub-domains (SVs and CCVs) and Golgi apparatus, and I could see that most of the SV or CCV markers show a relatively small, but existing, overlap. Contrastingly, the Golgi markers are more often found only in the Memb12 proteome. These results could be explained by the plasticity of TGN sub-domains maturing from the Golgi.

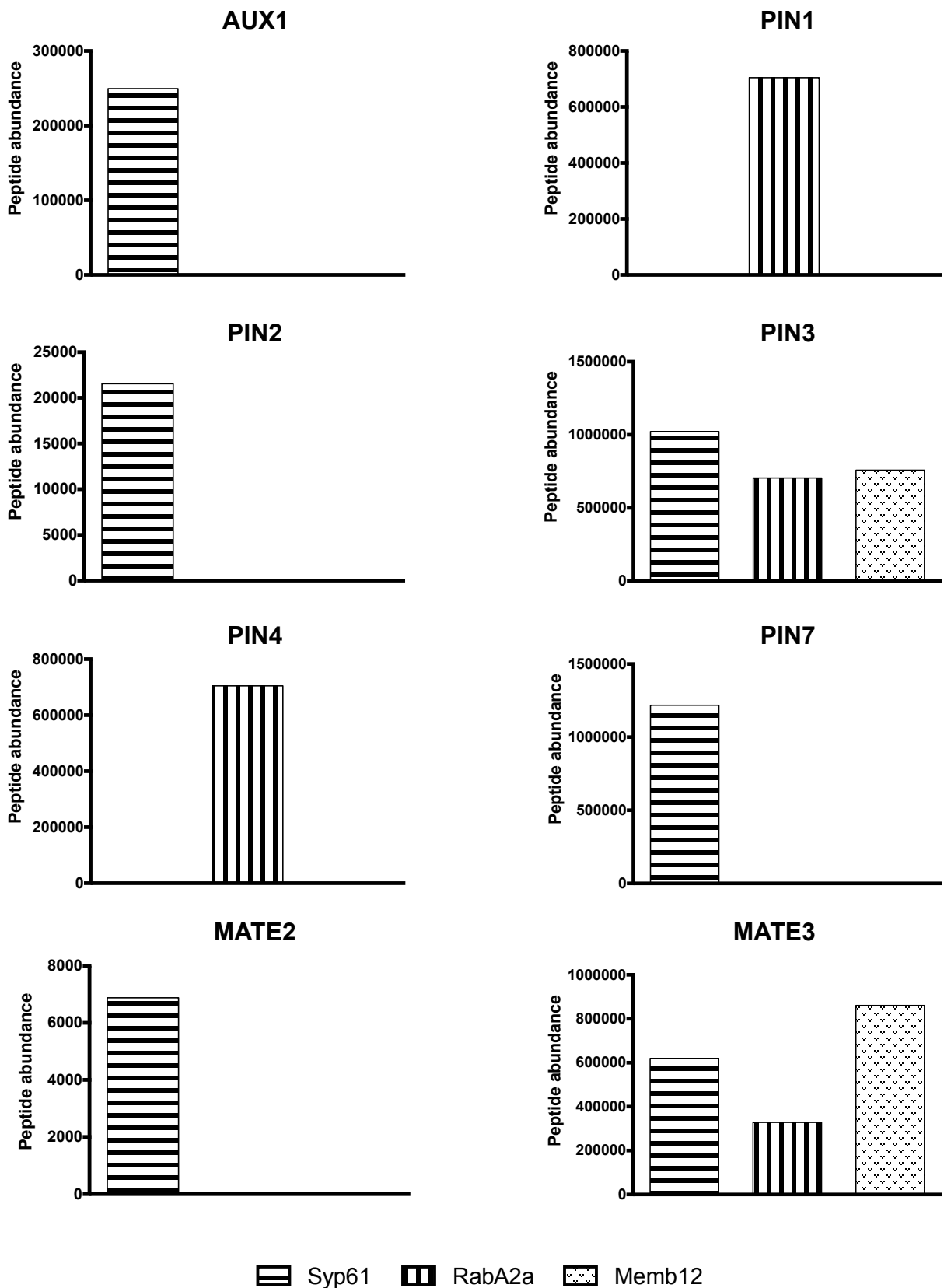


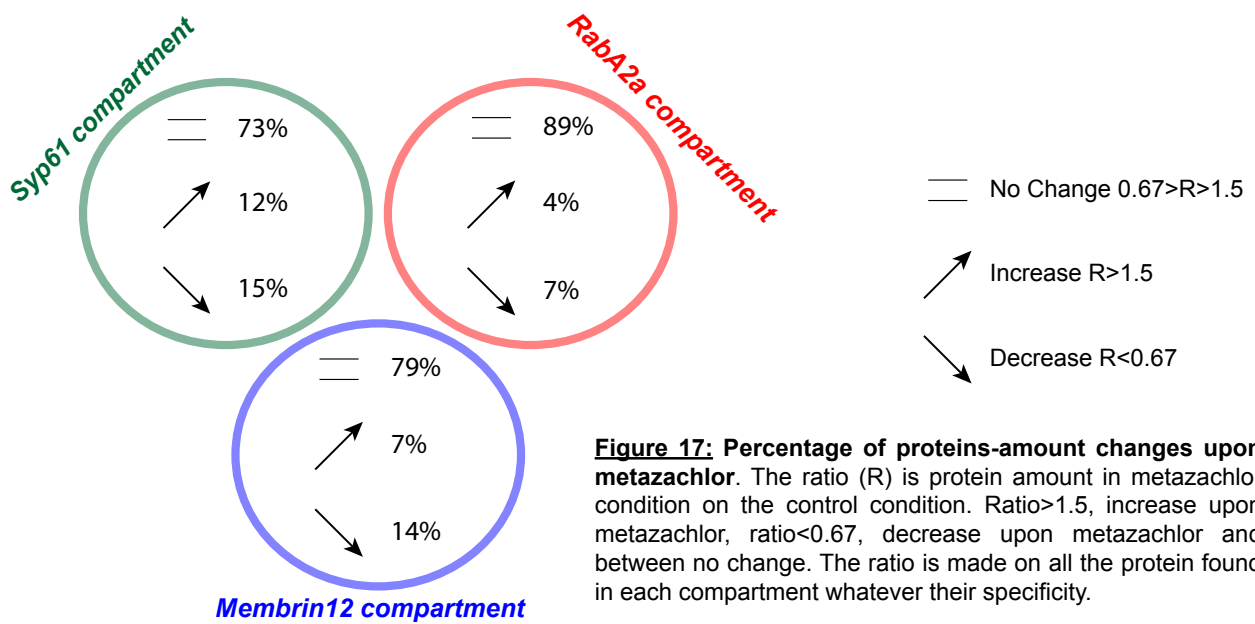
Figure 16: Carriers have compartment affinity. Raw abundance within the Syp61-, RabA2a- and Memb12-proteomes of six cargo proteins: the auxin carriers AUX1, PIN1, PIN2, PIN3, PIN4 and PIN7, and two others transmembrane proteins the MATE efflux carrier MATE2 and MATE3.

4. Cargos traffic through specific TGN sub-domains

The TGN is a place where occurs complex sorting mechanisms through different vesicles types (SV, CCV). One of the most obvious examples of this complexity is the auxin carriers secretory and recycling pathways. The auxin carriers have specific membrane localization (like basal, apical, all the PM, etc.) depending on the tissue (epidermis, cortex, meristem, etc.), the organ (root, hypocotyl, leaf, etc.) and the development stage (Petrášek and Friml, 2009). Some studies suggest a role of the TGN or endosomes in sorting pathways of auxin carriers (Geldner et al., 2001; Kleine-Vehn et al., 2006; Tanaka et al., 2009; Watelet-Boyer et al., 2016). In fact, by looking their abundance according to the compartments I immuno-precipitated, there is a quiet specific presence of each auxin carriers to specific TGN sub-domain (excepted for PIN3 which was found in the three compartments SVs, CVVs and Golgi, Figure 16). The three auxin carriers AUX1, PIN2 and PIN7 are Syp61/SV-specific protein, whereas PIN1 and PIN4 are RabA2a/CCV-specific. This difference in their compartmentation is reminiscent of the work of Kleine-Vehn J. et al. where they highlighted that AUX1 is using a different sorting pathway from PIN1 (Kleine-Vehn et al., 2006). On the other hand, PIN2 and AUX1 are present only in Syp61/SV proteome while Jaillais et al. showed that they do not localize at the same compartment upon BFA treatment (Jaillais et al., 2006). These results are not necessarily contradictory as the TGN/SVs-localized protein ECHIDNA has been shown to be involved in secretory sorting of AUX1 but not PIN2 (Gendre et al., 2011; Boutté et al, 2013). Hence, it could be that SVs host several secretory pathways.

Auxin carriers are transmembrane proteins and I looked if I could find other PM-localized transmembrane proteins in my IPs. MATE2 (as well named DETOXIFICATION6, DTX6) is a transmembrane PM transporter as PIN2 which is only enriched in Syp61/SV proteome highlighting that other cargo proteins undergo through specific compartment for their secretion like PIN2. Moreover, its homolog MATE3 (as well named DTX40) is, according to the MIND (Membrane-based Interactome Database) interacting strongly with PIN2 which is a really interesting observation for our study, although MATE3 does not display specific compartment localization in my IPs.

Altogether with the literature, it shows that the sorting mechanisms can occur at the same compartment but through different pathways, PIN2 and AUX1 are both found in Syp61/SV compartment however, they still use different molecular mechanisms for their correct sorting (Gendre et al., 2011; Boutte et al., 2013)



5. Identifying Sphingolipid-dependent actors at TGN

The secretory sorting of PIN2 relies on the FA's length of the sphingolipids at SV (Wattelet-Boyer et al., 2016). Modifying the FA's length using metazachlor, which lead to an accumulation of sphingolipids containing C16-, C20- and C22-acyl-chain and a decrease of sphingolipids containing C24- and C26-acyl-chain, results in an intracellular accumulation of PIN2 and a loss of its polarity (Wattelet-Boyer et al., 2016). To identify the actors acting in this sorting mechanism dependent on the FA's length, I extracted the Syp61/SV-, RabA2a/CCV- and Memb12/Golgi-compartments in metazachlor-treated seedlings and performed proteomic analysis at the same time than untreated seedlings. With the label-free proteomic analysis, I could compare the amount of proteins between control condition and upon metazachlor treatment. Thereby I could make the ratio of protein abundance in metazachlor treatment compared to protein abundance in control condition (Mz/Ct). We decided to define the following threshold: if $Mz/Ct > 1.5$ then the protein abundance increase upon metazachlor condition, if $Mz/Ct < 0.65$ then the protein decrease upon metazachlor treatment, and if $0.65 < Mz/Ct < 1.5$ then no change was observed between the two conditions.

The ratio is calculated using all the protein identified in each screen whatever their compartment's localization. In the figure 17, there are 563 proteins for which abundance increase upon metazachlor treatment specifically in Syp61/SV (181 specifically in RabA2a/CCV compartment and 307 specifically in Memb12/Golgi). Whereas 704 proteins decrease upon metazachlor treatment specifically in Syp61/SV, 317 specifically in RabA2a/CCV and 613 specifically in Memb12/Golgi. My results highlight that modifying the sphingolipid composition using metazachlor mainly impacts the Syp61/SV compartment where an enrichment of VLCFA-sphingolipid was observed previously in Wattelet-Boyer et al., 2016. Hence, we decided to focus on this proteome for further bioinformatics analyses.

As I am focused on the TGN sorting pathways, the Memb12/Golgi proteome was used in my project only to define the specific proteins at TGN subdomains (Syp61/SV and RabA2a/CCV). Having separated accession number allowed me to proceed with Gene Ontology (GO) analysis in order to identify proteins family or class that would be the most altered upon metazachlor treatment in Syp61/SV compartments. I did GO on the whole Syp61/SV proteome using Panther classification system (<http://pantherdb.org>) which

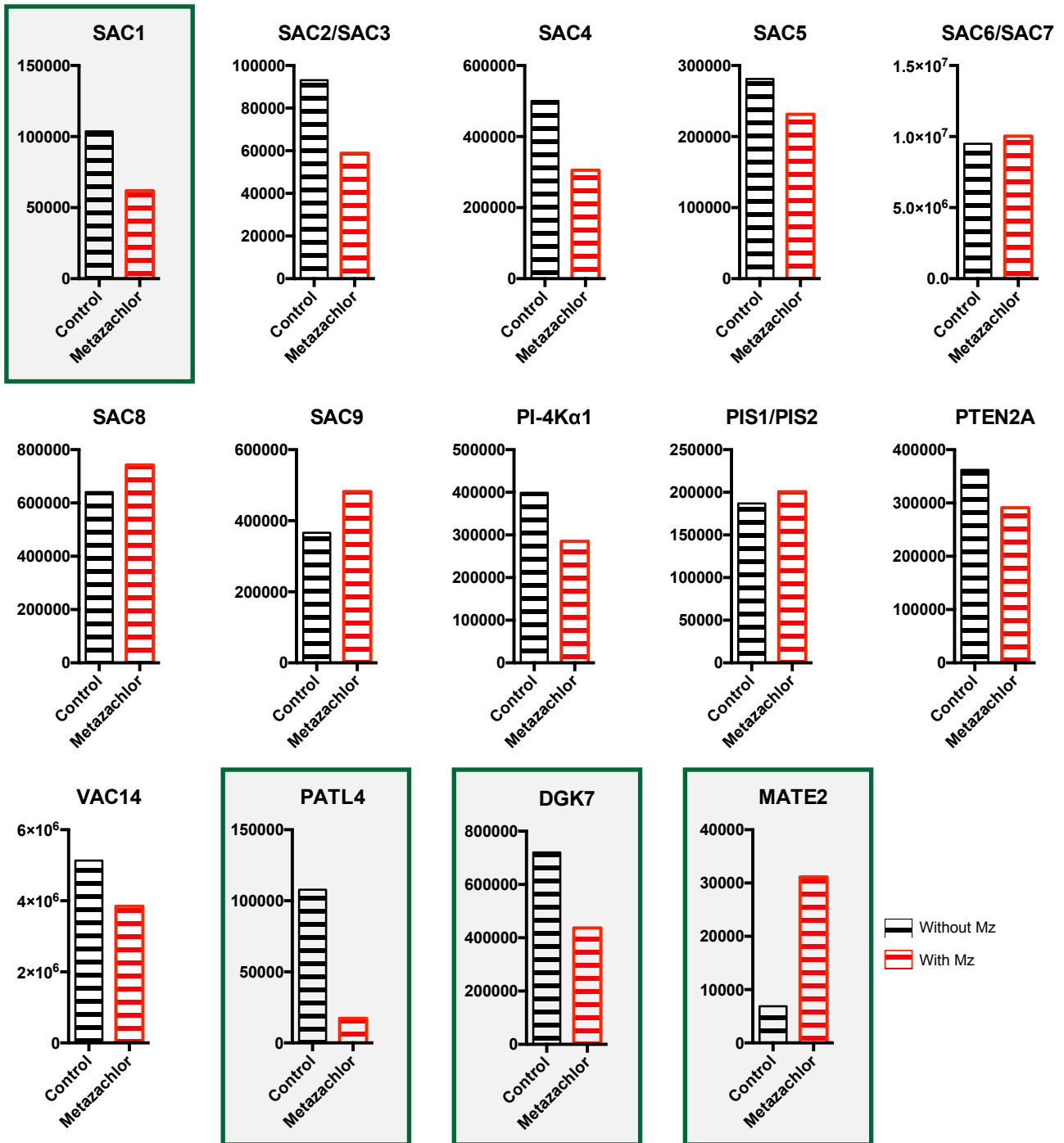


Figure 18: Abundance comparison of PIP-related proteins and selected proteins upon or not metazachlor treatment. The ones surrounded are the most sensitive to metazachlor by being either up- or down-regulated upon metazachlor treatment. They are already cloned by multisite Gateway.

PATL, PATELLIN; SAC, Suppressor of ACTin; PI-4Kα1, PI 4-Kinase α1; PIS, PI Synthase; PTEN2A, Phosphatase and TENSin homolog 2A; DGK7, Diacylglycerol Kinase 7

identified a nod of proteins linked to PhosphoInositides (PIPs) pathway (Table 1 highlighted lines).

Most of these PIP-related proteins are member of SAC proteins family (Suppressor of Actin). This family contains 9 different proteins SAC1 to SAC9 which I identified in Syp61/SV proteome. However, due to the detection method based on peptide identification, SAC2 and SAC3 shared the same identified peptides so I could not differentiate them, as for SAC6 and SAC7. All these SACs have an activity related to PIPs or assumed PIPs activity by similarity of sequence. The SAC1 protein have a PI_{3,5}P₂-5 phosphatase activity and was described to localize at the Golgi apparatus and vacuoles (Zhong et al., 2005). SAC2-SAC5 by similarity with SAC1 are expected to have the same activity *in vivo*, but there is no *in vitro* assay to confirm their activity (Nováková et al., 2014). The following SACs, SAC6 to SAC8 have still a hydrolase activity but on the PI₃P and PI₄P, and SAC7 has mainly a PI₄P phosphatase activity *in vitro* (Ton et al., 2005; Despres et al., 2003; Thole et al., 2008). And the last SAC, SAC9 is described to have a PI_{4,5}P₂ phosphatase activity as *sac9* mutant leads to an accumulation of PI_{4,5}P₂ in plants (Williams et al., 2005). By comparing abundances of the different SACs with or without metazachlor in Syp61/SV proteome (Figure 18), I could see that the SACs with a PI_{3,5}P₂ phosphatase activity (SAC1-SAC5) are decreased at SVs upon metazachlor treatment, whereas SAC6-SAC8 and SAC9, with respectively a PI₃P- and PI₄P-phosphatase, and a PI_{4,5}P₂ phosphatase activity, are increased at SVs upon metazachlor treatment. These PIP-related proteins are not the only ones found in the screen. I also identified a PI 4-kinase, the PI-4K α 1 known to add a phosphate on the 4th carbon of the PI and leads to the PI₄P formation (Stevenson et al., 1998; Stevenson-Paulik et al., 2003). My proteomics show that PI-4K α 1 is downregulated at SVs upon metazachlor treatment and that goes the same for PTEN2A, a protein that dephosphorylates the 3-phosphate of all PIP *in vitro* (Pribat et al., 2012). The PI synthases, PIS1 and PIS2 (Collin et al., 1999), are upregulated at SVs upon metazachlor treatment. The last PIP-related protein I found in my proteomic screen is a member of the PI_{3,5}P₂ regulator complex, VAC14 homolog. In yeast, VAC14 activates the FAB1 (a PI₃P 5-kinase) protein and controls the localization of a PI_{3,5}P₂ phosphatase at the vacuole (Rudge et al., 2004). Plants homologs of this complex are AtFAB1 kinase, which localizes at MVB/LE and the phosphatase SAC1, described to localize at TGN. This suggests that mechanism seems to be different than in yeast (Nováková et al., 2014).

The AtVAC14 mostly localizes at Syp61/SV according to the abundance data of my proteomics and its abundance decreases upon metazachlor (Figure 18). Altogether, these

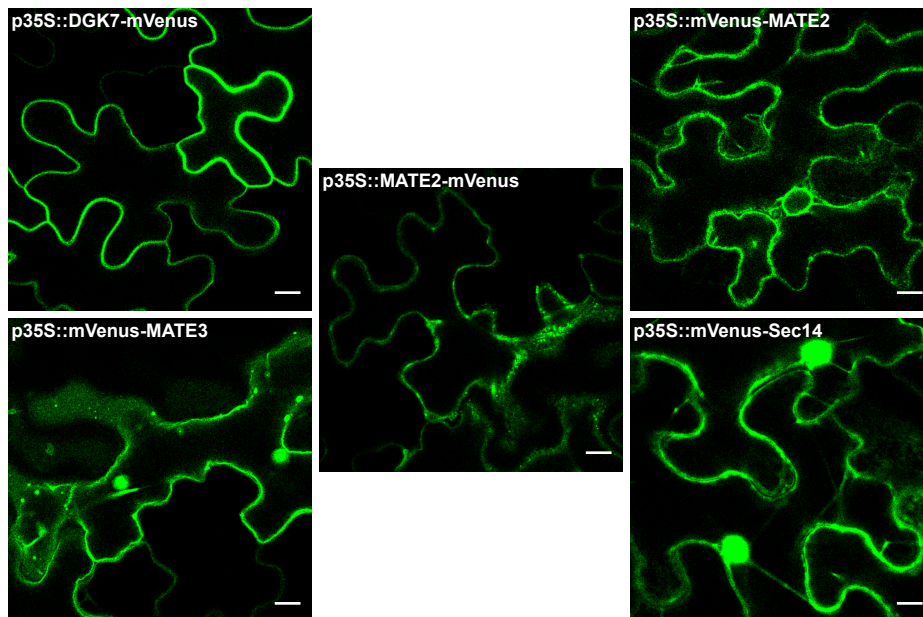


Figure 19: Localization of the selected proteins from the Syp61 proteome. Transient expression in *Nicotiana bethamiana* of 5 different constructions under the 35S constitutive promotor and tagged by mVenus in either C- or N-terminus end. DGK7 seems to be localized at the PM whereas the other constructions seem to be cytoplasmic and vesicular for MATE2 and MATE3 and cytoplasmic for Sec14p (PATL4). DGK7: DiacylGlycerol Kinase 7, PM: Plasma Membrane. Scale bar=10 μ M

results suggest a crosstalk between two different lipid classes: the sphingolipids and the PIPs. By changing the sphingolipid-FA composition, I modified PIP-related protein abundance in Syp61/SV compartment. Another type of PIP-related protein I found strongly decreased upon metazachlor treatment in Syp61/SV proteome, is the PATL4 (PATELLIN 4), a Sec14-like domain-containing protein. This domain is also called Sec14 phosphatidylinositol and phosphatidylcholine (PC) exchange and is well describe in yeast (Schaaf et al., 2008). Its function in plant was recently described (Huang et al., 2016) and highlight structural conserved PI/PC-binding/exchange activity. Another interesting protein identified in the screen is the diacylglycerol kinase 7, DGK7 that is the smallest DGKs described in plant with an DGK activity (Gómez-Merino et al., 2005). The DAG can be produced by the synthesis of inositol-phosphoceramide and, is also described in animal to recruits protein kinase D to activate the PI₄P synthesis, through PI 4-kinase (Baron and Malhotra, 2002; Hausser et al., 2005; Dippold et al., 2009; Capasso et al., 2017).

To confirm the localization of some proteins, we decided to clone them and transformed them in *Arabidopsis* for stable expression and in *Nicotiana* for transient expression.

C. Cloning of Syp61-proteome-selected proteins

To study the selected proteins (framed proteins in figure 18), the Multisite Gateway[®] technology was used to construct the plasmids in order to overexpress the gene and to check its subcellular localization. All the entry clones I have generated are listed in the table 2 and the final plasmid in the table 3. In this table, the transformation status in *Arabidopsis* is indicated. All the mVenus-tagged proteins transformed *in planta* are at the T₂ generation (and also for the SAC1 constructs tagged by TagRFP). Most of the constructions are under the constitutive promoter of Ubiquitin10 (pUB10) to avoid silencing due to a strong expression by 35S promoter (p35S). Nevertheless, I also used the p35S promoter to test the construction by transient expression in *Nicotiana benthamiana*. Moreover, I made N- and C- terminus tag position for each proteins, to be sure that the tag does not affect the protein localization and stability, and red (TagRFP) or yellow (mVenus) fusion to make crosses with other endomembrane marker lines like the WAVE lines (Geldner et al., 2009) and phosphoinositides fluorescent sensors PIPlines (Simon et al., 2014).

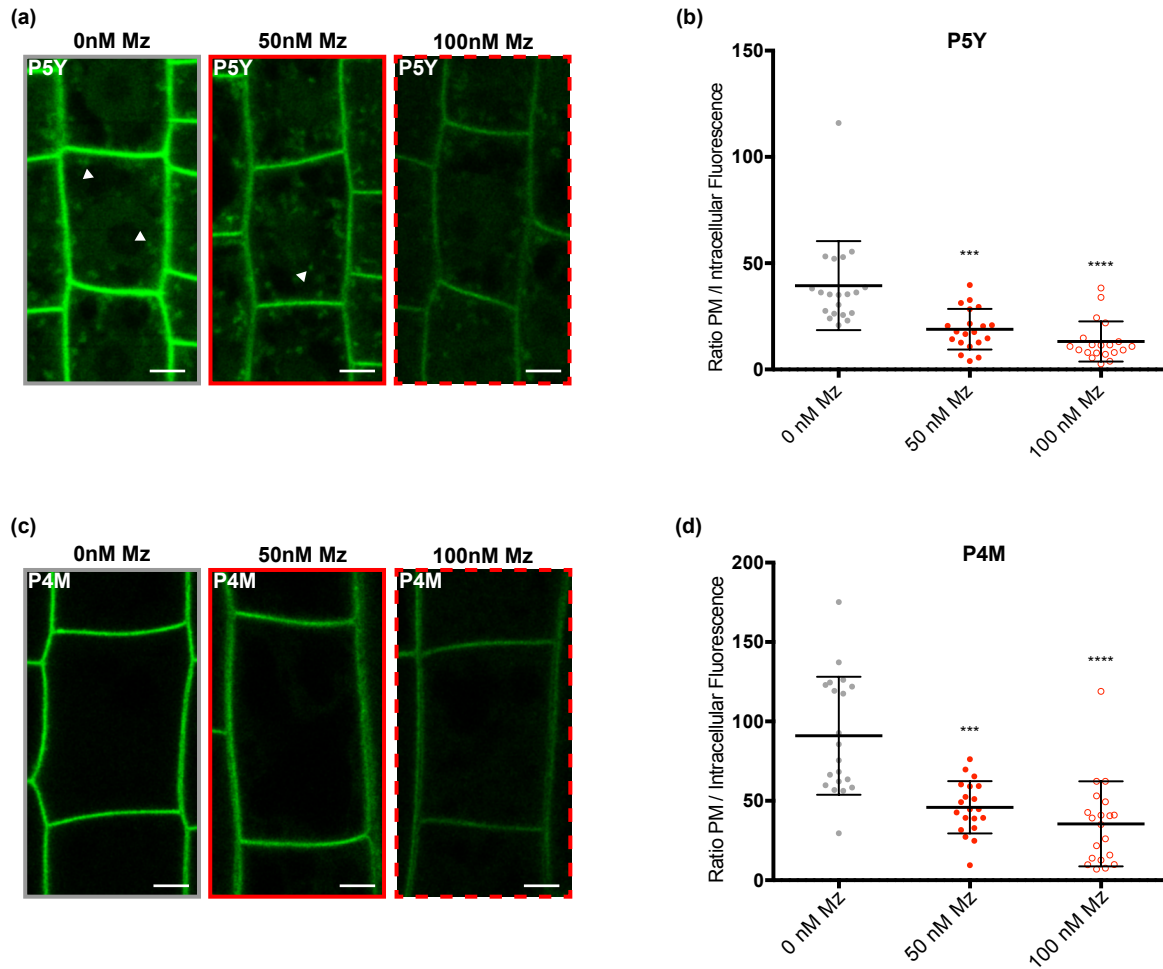


Figure 20: Decrease of PI₄P amount at plasma membrane upon metazachlor treatment. Confocal microscopy of root epidermal cells of PI₄P biosensor lines treated or not with metazachlor. One using the lipid-binding domain FAPP₁ tagged with mCitrine, the P5Y line (a) and the representation of the ratio between the the plasma membrane and the intracellular fluorescence underlying a strong decrease of the PI₄P at the plasma membrane (b). Similar results is observed with another biosensor line is observed in (c) using the lipid-binding domain P4M coupled with mCitrine too and the representation of the ratio between PM and intracellular fluorescence (d).

Statistic were done by Dunn's multiple comparisons test ***P-value<0.001, ****P-value<0.0001, n=20 measurements distributed over 20 roots for each experiment (3 biological replicates). All scale bar, 5μm. Errors bars are S.D.

While the *A. thaliana* stable lines were grown (transformation made by floral dipping), I transiently expressed in *N. benthamiana* some constructs to test them. As we know, transient expression in heterologous system does not necessarily reflect the homologous stable localization. In the figure 19, I showed by transient expression the localization of 5 proteins the DGK7, MATE2, MATE3, RhoGAP and Sec14p-like (PATL4) under the 35S promoter. Different localizations patterns appeared, DGK7 localized at the PM, the MATE2 and MATE3 localized in the cytosol and vesicular-like structure. Moreover, MATE2 localization changed whether the tag is in N- or C-terminus part of the protein. The C-terminus construct localized more at dotted structure whereas the N-terminus was more cytosolic. On the other hand, MATE3 might localize at bigger compartments than MATE2. The protein containing-Sec14p-like-domain was cytosolic too as I could observe the cytoplasmic sleeves. But as I said before, these results should be taken with high caution due to the heterologous system and the overexpression condition. Later on, in this manuscript, I will show homologous stable expression for one candidate of interest we decided to focus on due to the results I will now describe.

D. Metazachlor affects PIPs homeostasis

My proteomics results suggest that the sphingolipid composition could play a role in PIP homeostasis by changing the patterning of some PIP-related kinases and phosphatases in Syp61/SV compartment. To check if the metazachlor has an actual effect on PIP homeostasis, I used different fluorescent sensors lines for different PIPs that Yvon Jaillais (ENS Lyon) developed and called the PIPlines (Simon et al., 2014). The PIPlines are stable *A. thaliana* (Col-0) lines expressing fluorescent PIP biosensors. The fluorescent biosensors were constructed by a fusion of a fluorescent tag (mCitrine for the ones I used) and one or two Lipid-Binding Domain (LBD) specific to either PI3P, PI4P or PI4,5P2. Each construct is under the control of the ubiquitin 10 promotor (pUB10). Having 2xLBD in the biosensor increase the avidity of this one and allows better quantification. To be relevant, I took all the pictures with exactly the same confocal microscopy settings, biosensor by biosensor (laser power, resolution, detector gain; same tissue, etc.). I used 4 different lines: 2 lines recognizing the PI₄P: P5Y with 1xPH^{FAPP1} domain mCitrine-tagged and, P4M domain mCitrine-tagged, and 2 lines recognizing the PI₃P: P3Y containing PX^{P40}-mCitrine and P18Y containing mCitrine-2xFYVE^{HRS}.

1. Metazachlor alters PI₄P quantity at plasma membrane

Using the 2 different biosensor lines for PI₄P (P5Y and P4M), I quantified the PI₄P upon metazachlor treatment. Knowing that the PI₄P mainly localizes at the PM, I looked at the root epidermal cells of P5Y and P4M lines. Then, to be able to quantify the PM signal, I had to find the perfect spot which is defined by a perpendicular crop of the PM for at least 3 juxtaposed cells.

PI₄P displayed strong localization at the PM whatever the biosensor used (figure 20a and 20c) in control condition. As the 1xPH^{FAPP1} domain (P5Y, figure 20a) also binds to the TGN located protein ARF1, it explains the intracellular dots observed with the P5Y lines (He et al., 2011). The PM/intracellular ratio allows to normalize the measurements. As you can see in figure 20a and 20c, both P5Y and P4M signals at PM decrease upon metazachlor, even from 50nM metazachlor where the signal is already divided by 2, from 39.5 for control condition to 19 for 50nM metazachlor for P5Y (figure 20b, significant results) and from 100 to 46 for P4M (figure 20d, significant results). These results suggest a plausible effect of metazachlor on PI₄P synthesis and/or turnover as suggested by the decrease of PI-4K α 1 and the increase of SAC6-SAC8 (PI₄P phosphatase proteins) at TGN upon metazachlor treatment (figure 18).

2. Metazachlor gravitropism response is affected in the *pi4k β 1/pi4k β 2*

To check whether the metazachlor effect on the PI₄P could be link to the function of PI 4-Kinase localized at TGN, I used a double mutant for two PI 4-Kinases that are localized at TGN. I characterized the root phenotypic response after gravistimulation of the double mutant of the PI 4-kinases *pi4k β 1/pi4k β 2* which shows a lack of PI₄P (Antignani et al., 2015). The double mutant is a cross between two T-DNA insertion mutant lines, one on the PI 4-kinase β 1 locus and the other on PI 4-kinase β 2 locus. Before, I genotyped the double mutant plants to verify their zygoty. The genotyping results are grouped in the figure 21. The figure 21a represents the DNA gel electrophoresis after genotyping-PCR using two primers' couples, the forward and reverse one (F and R), targeting the T-DNA locus, and the other set of primer is the reverse and the left-border (LB) of the T-DNA sequence. If the plant is homozygote for the T-DNA insertion, I will obtain an amplicon just for the set LB/reverse, if it is heterozygote

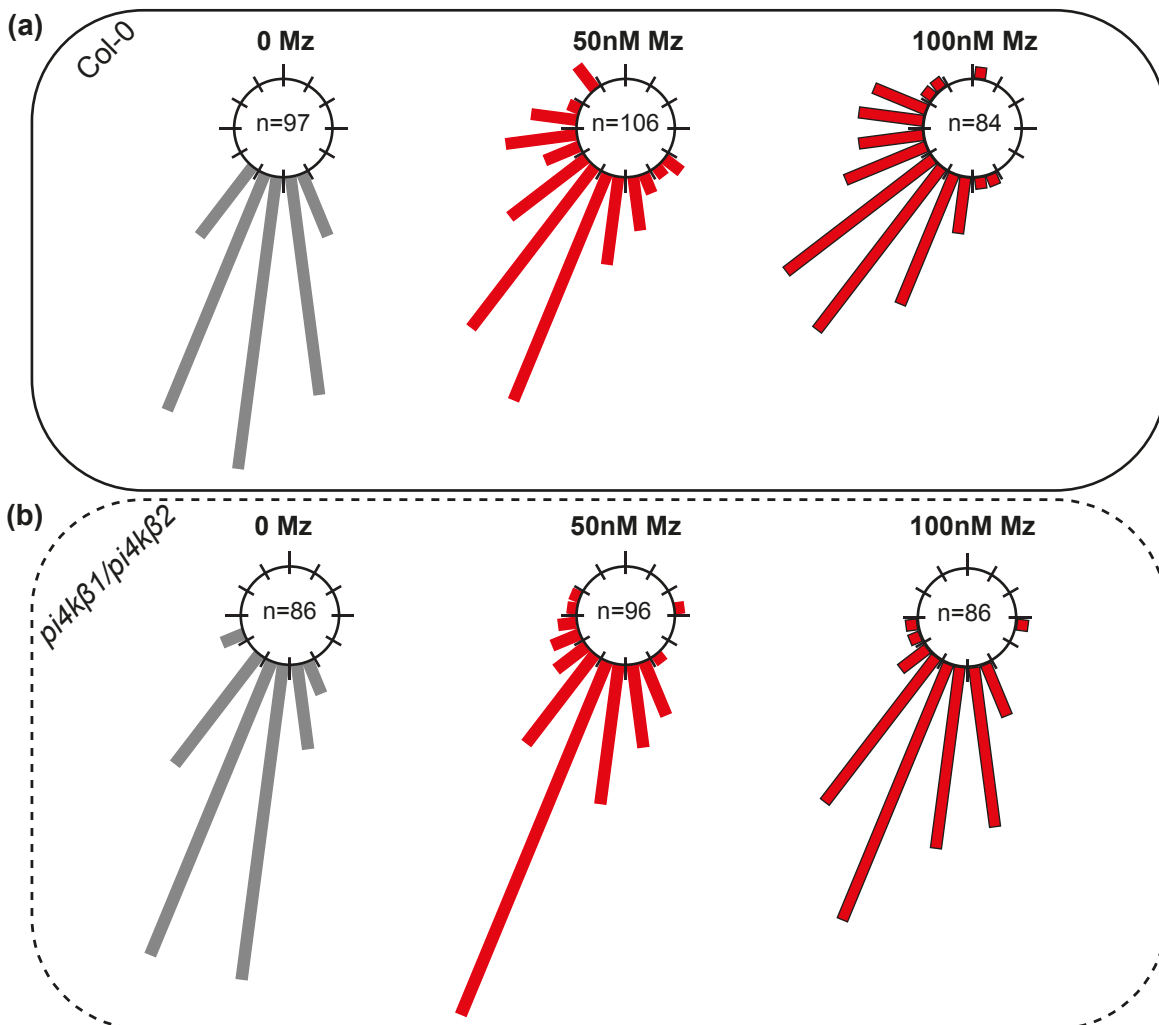


Figure 22: PI(4)P is involved in the metazachlor-induced gravitropism phenotype. Root reorientation upon 3 different concentration of metazachlor (0, 50 and 100 nM) of the wild-type Columbia-0 (a) and the double mutant *pi4kβ1/pi4kβ2* (b) which is resistant to metazachlor at the concentration of 100nM, the root are well-reorientated 24h after the gravistimulus.

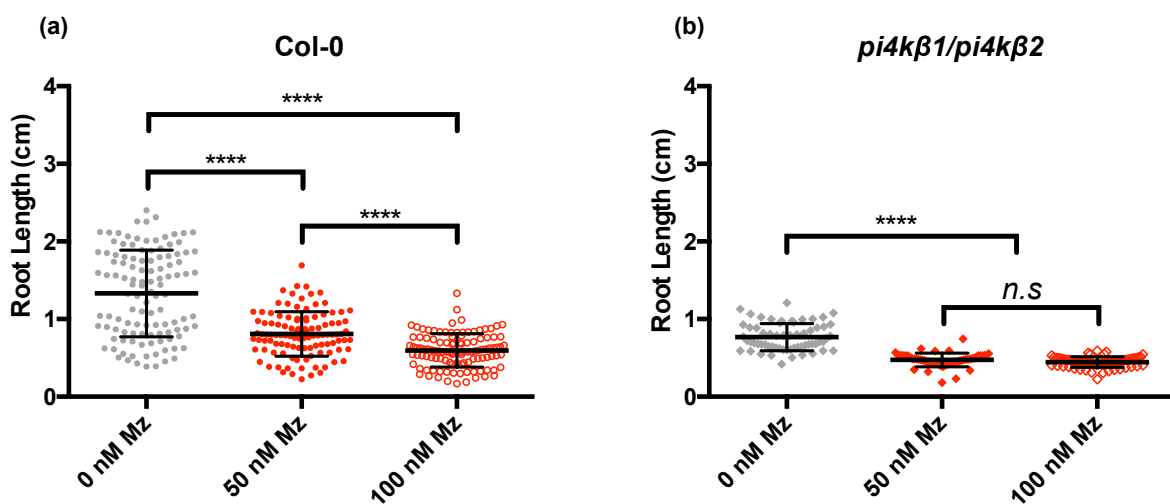


Figure 23: Metazachlor induces a root length decrease. Scatter dot plot representation of the root length upon metazachlor treatment on wild type Col-0 (a) and the double mutant *pi4kβ1/pi4kβ2* (b) which shows a slight resistance at 100nM metazachlor where the root length no longer decrease. $n > 60$ roots analysed per condition. Statistics were done by Dunn's multiple comparisons test, **** P -value < 0.0001 , *n.s.*: non significant.

an amplicon in both forward/reverse and LB/reverse will be obtained and finally, if this is a wild-type, an amplicon for the forward/reverse primers is only obtained. To make the reading easier, I sum up the results in the figure 21b, and on 22 plants genotyped, only 3 were not amplified well enough to conclude, so the seeds batch was considered to be homozygote. I also genotyped a triple mutant *pi4kβ1/pi4kβ2/sid2_1* (*sid2_1* is a mutation blocking the salicylic acid accumulation observed in the *pi4kβ1/pi4kβ2* double mutant) but, as you can see, in figure 21c, no homozygote plants have been identified.

The root reorientation after gravistimulation of the double mutant *pi4kβ1/pi4kβ2* is represented in the figure 22b. As you can see, the double mutant is less sensitive to metazachlor than the wild-type (figure 22a). Without metazachlor, both wild-type and double mutant lines displayed a normal reorientation of the root after the gravistimulation underlying that PI₄Kβ₁ and PI₄Kβ₂ are not absolutely required during root gravitropism. However, the *pi4kβ1/pi4kβ2* double mutant lines showed less sensitivity to metazachlor as the reorientation-angle are less spread than the wild-type (figure 22b). This resistance to metazachlor of the double mutant might suggest that the metazachlor-induced gravitropism phenotype is dependent on PI₄Kβ₁β₂-mediated PI₄P formation at TGN.

I also analyzed the root length upon metazachlor treatment (0, 50 and 100nM) of the double mutant line compared to wild-type (figure 23). Both plant lines analyzed, wild-type and double mutant, showed shorter roots upon metazachlor treatment. The wild-type has reduced root length upon metazachlor and higher the metazachlor concentration is, shorter the roots are (figure 23a). The double mutant *pi4kβ1/pi4kβ2* is also sensitive to the metazachlor regarding the root length, however, at 100nM metazachlor the root length no longer decreased (figure 23b). From these results, it seems than the metazachlor a slight effect on the double mutant, but this is not a dose-response effect like for the wild-type. More concentrations would have to be assessed as 25nM and 200nM to see whether the metazachlor effect on root length could be stronger.

Altogether, the root gravitropism analysis of the double mutant *pi4kβ1/pi4kβ2* upon metazachlor treatment shows that the metazachlor-induced gravitropism phenotype could be coupled to the PI-4K activity, as the *pi4kβ1/pi4kβ2* double mutant lines is more resistant to metazachlor than wild-type.

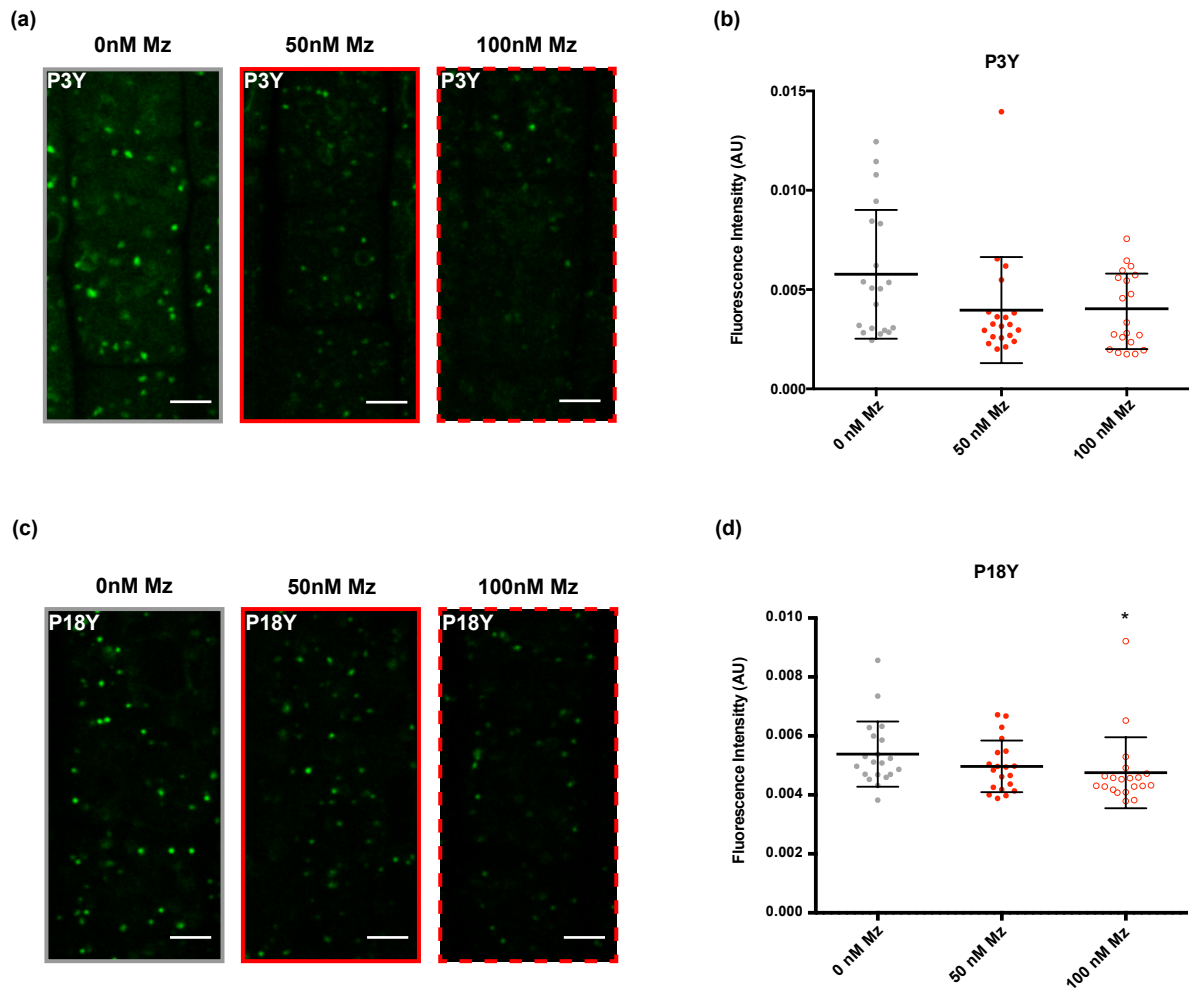


Figure 24: Decrease of PI₃P amount at vesicular compartment upon metazachlor treatment. Confocal microscopy of root epidermal cells of PI₃P biosensor lines treated or not with metazachlor. One using the lipid-binding domain PX^{P40} coupled with mCitrine, the P3Y line (a) and the representation of the fluorescence intensity showing a decrease upon metazachlor (b). With another biosensor line, the decrease of PI₃P upon metazachlor is still observed (c) using the double lipid-binding domain 2xFYVE^{HRS} coupled with mCitrine too and the representation of the fluorescence intensity (d). Statistic were done by Dunn's multiple comparisons test *P-value<0.05, n=20 measurements distributed over 20 roots for each experiment (3 biological replicates). All scale bar, 5μm. Errors bars are S.D.

3. PI₃P fluorescence intensity is decreased upon metazachlor treatment

As for PI₄P quantification, I use 2 different biosensor lines to quantify the PI₃P: the P3Y and the P18Y lines, 1xPX^{p40}-mCitrine and mCitrine-2xFYVE^{HRS} respectively. PI₃P is mainly localized at MVB/LE (Noack and Jaillais, 2017). To quantify intracellular dotted signal, I use imageJ[®] software and 3D Object Counter plugin to make a ratio between the intensity and the surface of the vesicle. For the P3Y biosensor line, the PI₃P amount is statistically not affected by metazachlor treatment (figure 24a and 24b). This might be due to the fact that 1xPX^{p40}-mCitrine is not avid enough to quantify all the PI₃P especially since it has 1xLBD (Simon et al., 2014). The avidity is based on the steric hindrance of the fluorescence tag linked to the LBD which blocks the recognition by another biosensor by hiding the lipids. Using the higher avidity biosensor P18Y (containing 2xLBD), there is less cytosolic-spready signal than P3Y in the control condition, supporting the avidity hypothesis (Figure 24). Moreover, upon metazachlor treatment, there is a significant decrease of the overall PI₃P quantity at 100nM metazachlor using the P18Y line. My results show that metazachlor affects PI₃P global quantity.

4. Metazachlor not only affect PI₃P overall quantity but also alters PI₃P localization pattern

The PIPs have specific localization within the cell. For example, the PM is enriched in PI₄P and PI_{4,5}P₂ whereas the tonoplast and the MVB/LE is enriched in PI₃P and PI_{3,5}P₂ (van Leeuwen et al., 2007; Singh et al., 2014; Posor et al., 2015; Casanova and Winckler, 2017; Noack and Jaillais, 2017). However, a small amount of PI₃P and PI₄P are found at the TGN meaning that there is a gradient between the TGN and the PM, but also between the TGN and the tonoplast (vacuolar membranes). Furthermore, my results show that metazachlor interferes with the PIP-related proteins (proteomics analysis), and the PI₃P and PI₄P level in intracellular compartments and PM, respectively (confocal microscopy). So, using cross line between PI₃P biosensor lines and endomembrane compartment markers, I look if the MVB/tonoplast localization of PI₃P is altered upon metazachlor. To quantify the colocalization between two dotted structure, I used the centroid (geometric center of vesicles) method (Bolte and Cordelières, 2006). With this method I could calculate the colocalization percentage of PI₃P with endomembrane compartment markers.

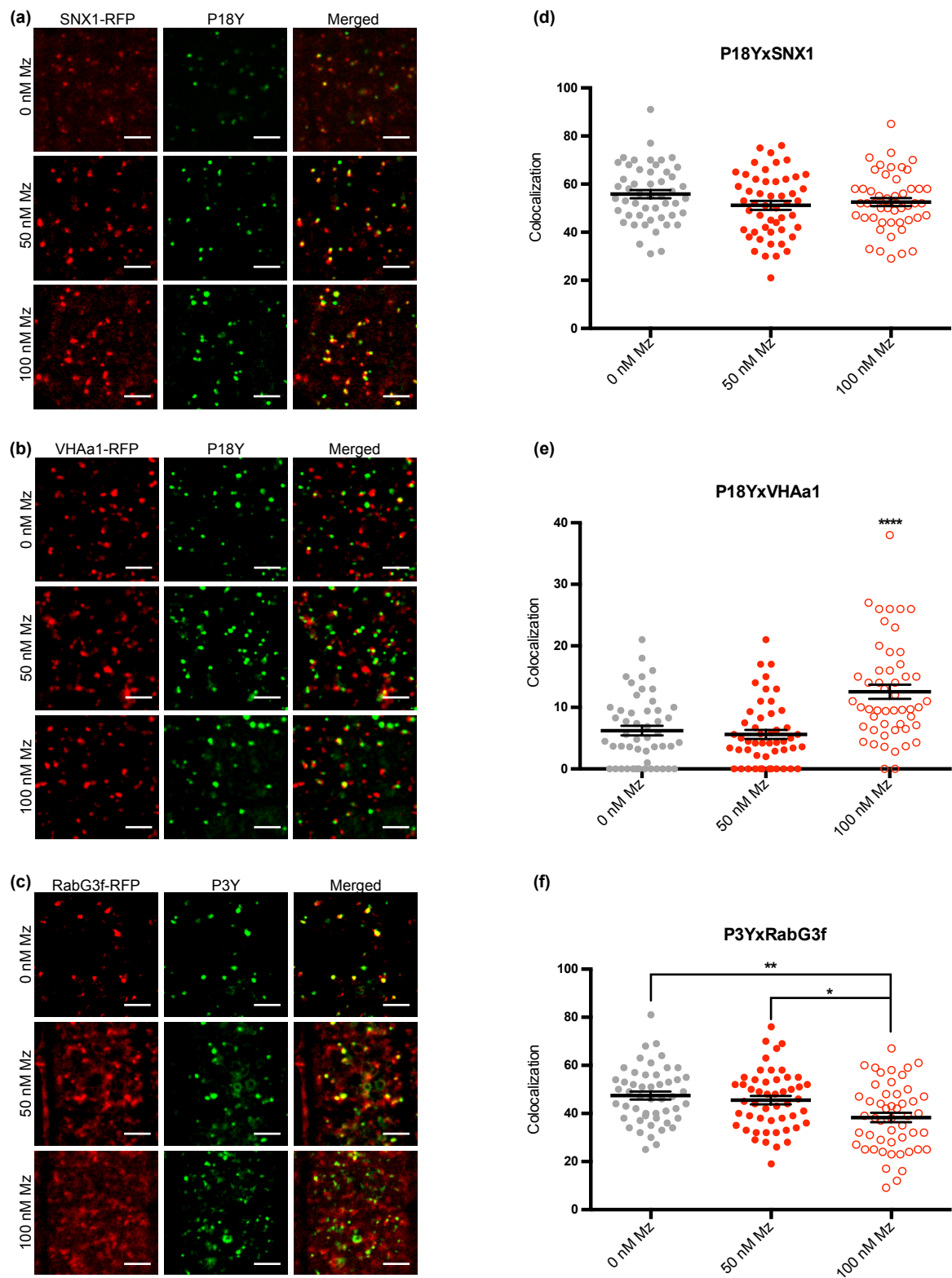


Figure 25: PI₃P localization changes upon metazachlor treatment. (a,c) PI₃P mostly localizes at MVBs using either (a) SNX1 or (c) RabG3f as MVBs markers. Upon metazachlor treatment, a decrease of PI₃P localization at MVBs is observed while using (c) RabG3f and not (a) SNX1, probably because SNX1 has a PI(3)P binding domain. (b) PI₃P do not localize at TGN in control condition, but upon metazachlor treatment, an increase of colocalization is observed between PI₃P and VHAa1. (d-f) Representation of colocalization upon metazachlor treatment between PI₃P and (d) SNX1, (e) VHAa1 or (f) RabG3f. *n*=50, 5 zones quantified per root, 10 roots analyzed per condition. Statistics were done by (e) Dunn's multiple comparisons test and (f) Tukey's multiple comparisons test, ***P*-value<0.01, ****P*-value<0.001, *****P*-value<0.0001. All scale bars, 5µm.

To check the PI₃P's localization, I took both biosensor lines (P3Y and P18Y) crossed with endomembrane markers: P18YxSNX1-RFP (Sorting Nexin 1, MVB marker (Viotti et al., 2010)), P18YxVHAa1-RFP (V-ATPase, TGN marker (Jaillais et al., 2008)) and P3YxRabG3f (Rab protein, MVBs marker (Geldner et al., 2009)). I measured the colocalization percentage upon 3 different metazachlor conditions (0, 50nM and 100nM) for each cross (figure 25). To quantify the colocalization, I took 5 different zones per root (the same zone for each quantification) and 10 roots per condition, and I applied the centroid colocalization method.

The colocalization between P18Y (mCitrine-2xFYVE^{HRS}) and SNX1-RFP doesn't change whatever the metazachlor concentration (figure 25a and 25d). Probably because SNX1 protein has been described to contain a PHOX domain that confers a PI₃P-binding ability (Ambrose et al., 2013). Hence, SNX1 could follow the PI₃P localization change. So, I tried another line with another MVB marker to be sure of this result.

Thus, I choose the MVB marker RabG3f-mCherry (Geldner et al., 2009) and the PI₃P biosensor, 1xPX^{P40}-mCitrine (P3Y). In the control condition (figure 25c and 25f), almost all the PI₃P's dots (green channel) colocalized with MVBs (red channel). Thus, these results are reminiscent of the work of Simon et al. in 2014 (Simon et al., 2014) where they showed PI₃P colocalizing with MVB markers. My co-localization results show that upon metazachlor, especially at 100nM, PI₃P localizes less at MVB/LE (figure 25f).

At last, when we look at the co-localization level of P18Y and VHAa1 (figure 25b and 25e), there is a weak co-localization at 0 and 50nM of metazachlor conditions. Nonetheless, a significant increase is observed at 100nM of metazachlor (twice more than 0 or 50nM of metazachlor). These results suggest that PI₃P might be stuck at TGN compartment upon metazachlor treatment.

Taking together, these results show that when the sphingolipid composition is changed by metazachlor, the PI₃P pool increase at TGN while it decreases at MVBs. Hence, the sphingolipid-FA composition might act on PIP homeostasis.

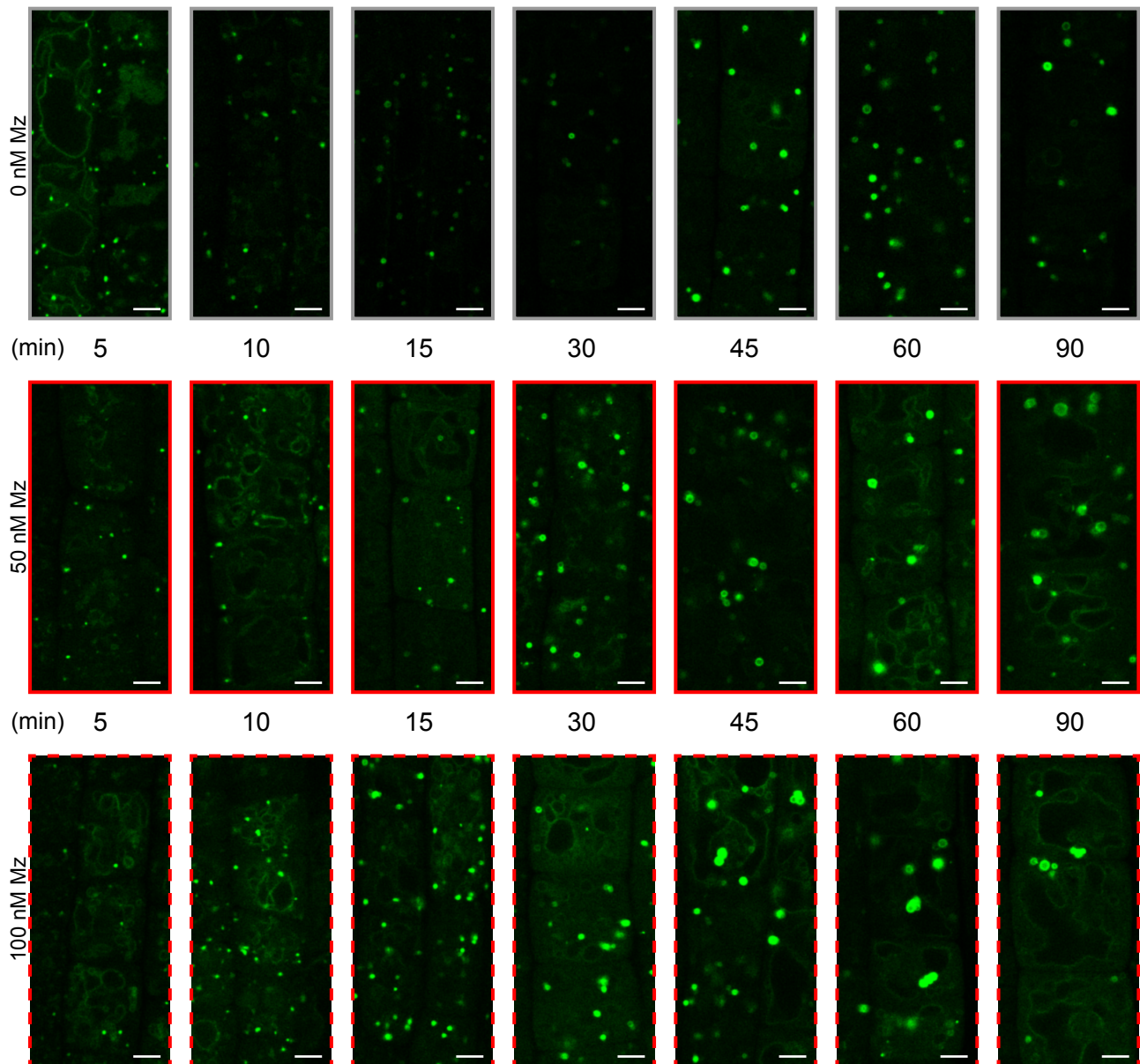


Figure 26: PI₃P's recovery upon wortmannin treatment is faster on metazachlor-pretreated seedling. Inhibition of the PI 3-kinase (PI3K) by wortmannin (33μM) cause a decrease of PI₃P pool (visualized thanks to the P18Y line). In control condition (top, 0 nM Mz), there is a strong decrease of fluorescence at the tonoplast and then at the vesicles signal marked by the PI₃P biosensor until 45min when occurs the recovery in donut-shaped structure probably *via* PI_{3,5}P₂ 5-phosphatase activity. For metazachlor conditions, there is no strong decrease and the PI₃P recovers at 30min for 50nM Mz (middle) or never decrease for 100nM Mz (bottom) meaning that the metazachlor seems to prevent the decrease of PI₃P upon wortmannin treatment. Root epidermal cells of 6 days old seedling, scale bar = 5μM

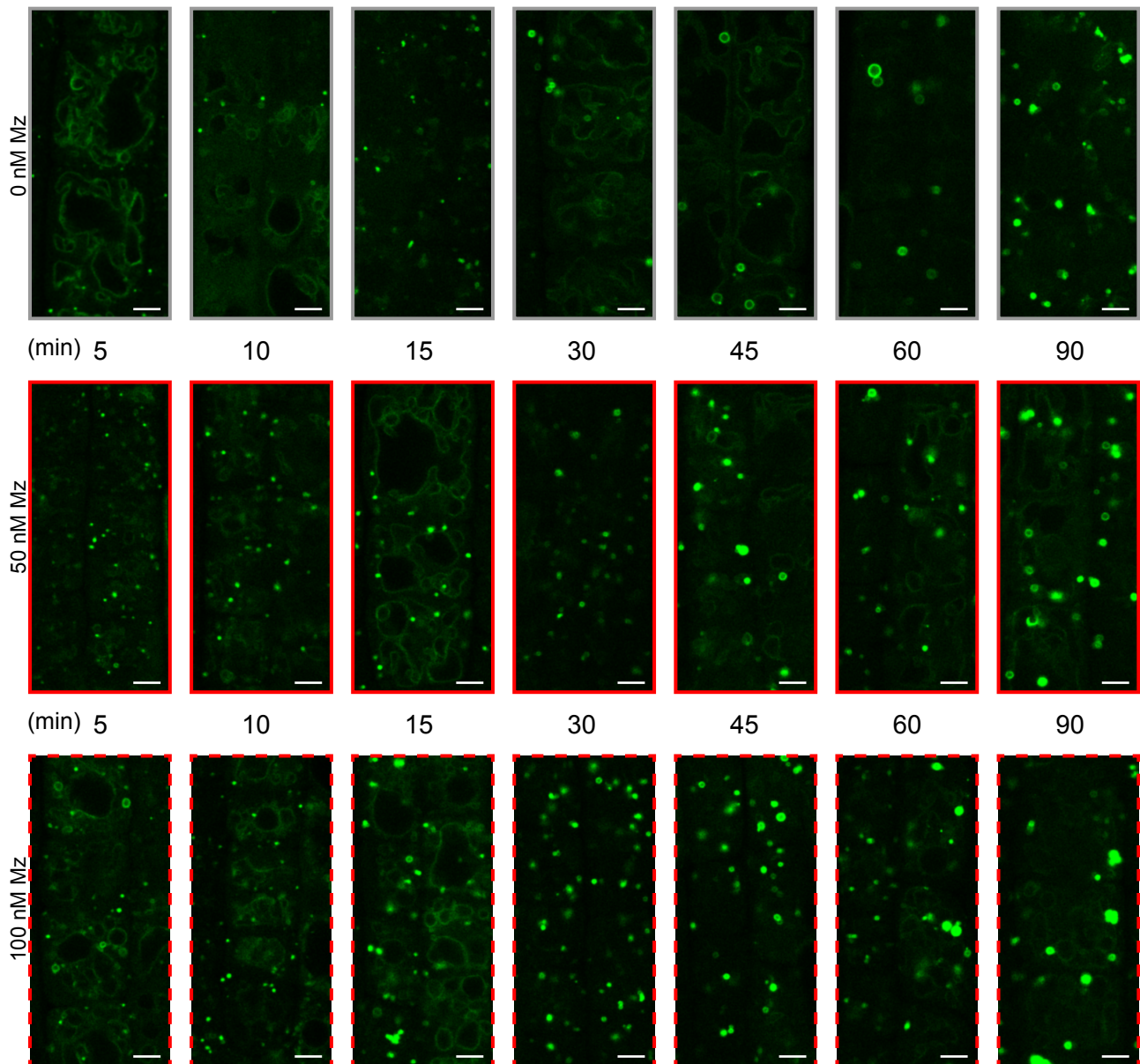


Figure 27: Metazachlor does not affect $PI_{3,5}P_2$ 5-phosphatase. Pre-treatment of the seedling during 2h in YM_{201636} ($1\mu M$) allows the inhibition of the $PI_{3,5}P_2$ 5-kinase leading to a decrease of the $PI_{3,5}P_2$ pool. After 2h of pre-treatment, the PI3K is inhibiting *via* wortmannin ($33\mu M$) treatment and different times of treatment are observed to identify the recovery of the PI_3P . In the control (top), the signal is lost starting by the tonoplast and then the vesicle. The recovery of PI_3P seems to be affected, delayed by YM_{201636} where the recovery starts after 60min (45min without YM_{201636}). While, with metazachlor, the PI_3P signal never decreases and the bigger vesicles appear already after 15min wortmannin treatment. Root epidermal cells of 6 days old seedling, scale bar = $5\mu M$

5. Metazachlor increases the PI₃P synthesis through a distinct pathway than the PI 3-kinase

Wortmannin (WN) is a PIPs kinases inhibitor that inhibits the PI 3-kinases or both PI 3-kinases and PI 4-kinases depending on the concentration used (1 μ M or 33 μ M, respectively) (Hirano et al., 2015). I used the 33 μ M concentration but looked only at PI₃P fluorescent probes. Hence, although I choose a concentration that inhibits both PI₄P and PI₃P, my analyses will show WN effect on the PI₃P pool only.

In my results, I could see a kinetic effect of WN on the PI₃P pool depending on the treatment time. I took pictures of P18Y lines with the confocal microscope at 7 different time points (figure 26) and I saw a fast decrease of PI₃P from 5 to 30min after WN incubation, in the control condition (without metazachlor). First, the tonoplast signal begins to disappear within 10min, and then the vesicle signal starts to fade slowly until a recovery of the signal at 45min after WN incubation. The recovered signal is different from the initial signal because the vesicles are larger and donuts-shaped as compared to untreated condition (without WN). This recovery might be due to the formation of PI₃P through the PI_{3,5}P₂ 5-phosphatases activity. Upon metazachlor treatment, the fast (from 5 to 30 min) WN-induced decrease of PI₃P signal was not observed and the PI₃P recovery (that occurs around 45 min in non-metazachlor treated seedlings) occurs earlier (Figure 26). Higher the metazachlor concentration is and faster the recovery begins. At 100nM I could not see any signal decrease whereas at 50nM, there is a slight decrease of the PI₃P signal.

To highlight this metazachlor effect on the PI₃P recovery, I performed this experiment by adding a 2h pre-treatment step with YM₂₀₁₆₃₆ to inhibit PI_{3,5}P₂ formation through the PI₃P 5-kinase (Hirano et al., 2017). As SAC1 (a PI_{3,5}P₂ 5-phosphatase) is decreased at TGN upon metazachlor treatment (figure 18), I thought that both YM₂₀₁₆₃₆ and metazachlor will block the recovery of PI₃P as the PI_{3,5}P₂ pool would be decreased by the YM₂₀₁₆₃₆. As expected, in the figure 27 I could see that the PI₃P recovery is a bit delayed by the YM₂₀₁₆₃₆ pre-treatment (top part, without metazachlor treatment). Upon metazachlor treatment combined with YM₂₀₁₆₃₆ pre-treated root, the WN-PI₃P recovery begins earlier than without metazachlor (Figure 27). Moreover, when we compare the PI₃P recovery upon metazachlor, without or with YM₂₀₁₆₃₆ pre-treatment (figure 26 and 27), I could not see strong change, both at 50nM or 100nM. Taking together these results suggest that the sphingolipid composition might have an effect on the PI₃P turnover, but this effect seems not to be related to the PI₃P formation *via* the PI_{3,5}P₂ dephosphorylation. However, YM₂₀₁₆₃₆ inhibits the PI₃P 5-kinase and not the

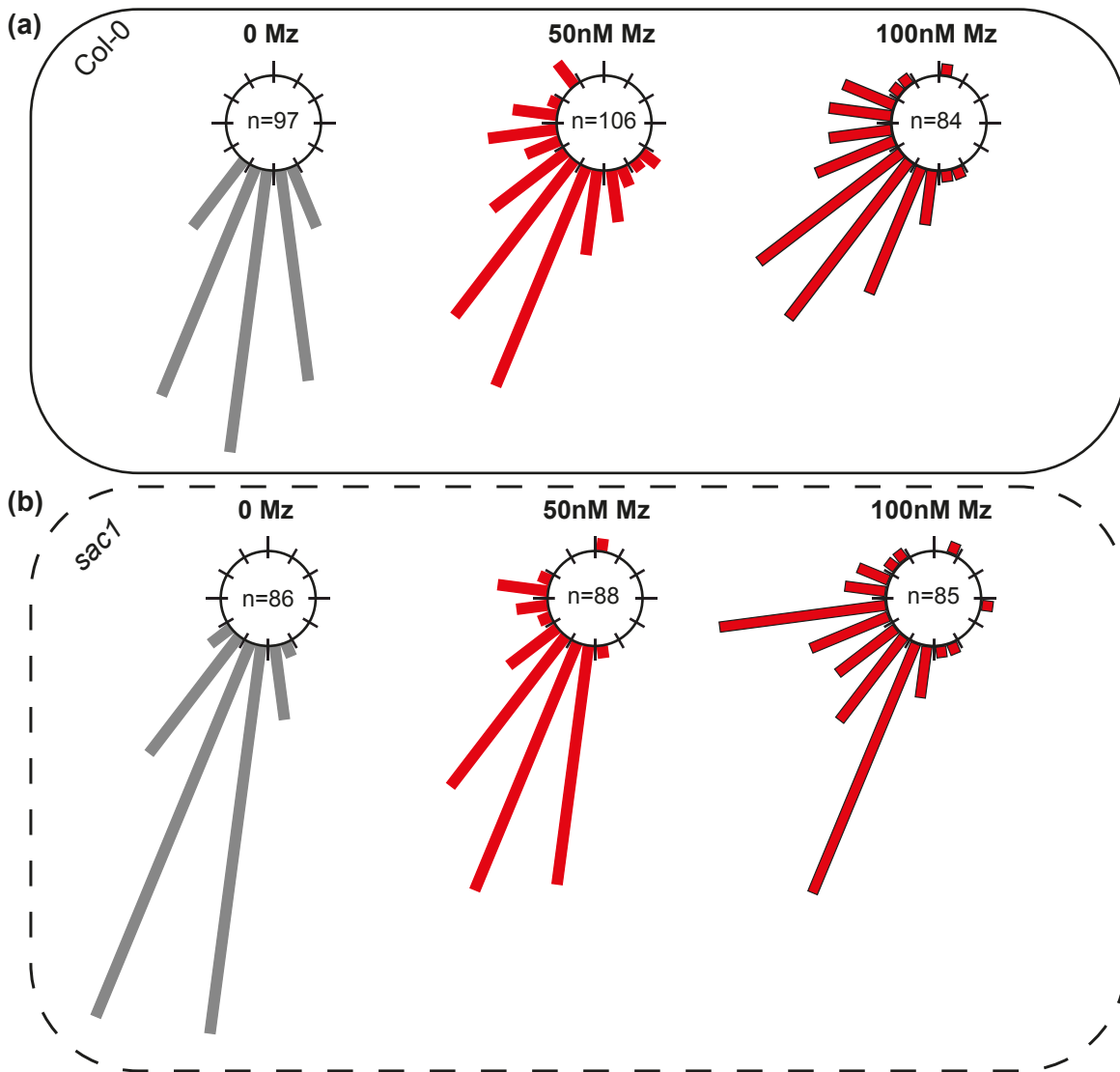


Figure 28: $PI_{3,5}P_2$ 5-phosphatase SAC1 is not involved in the metazachlor-induced gravitropism phenotype. Root reorientation 24h after gravistimulation upon 3 different concentration of metazachlor (0, 50 and 100 nM). The wild-type Columbia-0 (a) displays an altered reorientation with a spread repartition of the angle. The SAIL T-DNA mutant for *sac1* (b) have the same pattern than the wild-type with a spread repartition of the roots angle upon metazachlor treatment.

PI_{3,5}P₂ phosphatase. Hence, to have a direct evidence of sphingolipids effect on PI₃P through the PI_{3,5}P₂ phosphatase, I looked at a characterized PI_{3,5}P₂ 5-phosphatase: SAC1.

6. SAC1 function and localization is not impaired by metazachlor

So far, my results showed that when I block the biosynthesis of PI_{3,5}P₂ with YM₂₀₁₆₃₆ and the formation of PI₃P using WN, the PI₃P signal is not lost upon metazachlor and a faster recovery of the PI₃P signal is observed upon metazachlor (P18Y biosensor). Meanwhile, I observed in the proteomics that the SAC1 protein is decreased in Syp61/SV proteome upon metazachlor (figure 18). So, to conceal these data I ordered T-DNA insertion mutant to SAC1 locus in order to know whether the mutant could be more resistant or be hypersensitive to metazachlor. *sac1* KO lines is easy to phenotype because knocking out the gene induces a strong shoot gravitropism phenotype (Zhong et al., 2005).

When I obtained homozygote seeds of *sac1*, I performed gravitropism analyses to look if the *sac1* mutant is more sensitive or resistant to metazachlor than the wild-type (Col-0). In fact, the figure 28 did not show any difference between Col-0 and *sac1* mutant lines in respect to metazachlor treatment. The *ko* mutant has exactly the same metazachlor-induced gravitropism phenotype as the Col-0. Moreover, while looking at the root length upon metazachlor treatment (figure 29), *sac1* mutant shows the same response to metazachlor as the wild-type. First, by comparing each metazachlor condition, I thought that *sac1* was resistant to metazachlor as the root are longer than Col-0 but, when I calculated the decrease ratios from 0 to 50nM, 50nM to 100nM and 0 to 100nM, I saw that they are the same for both Col-0 and *sac1* lines (1.7, 1.4 and 2.3 respectively) meaning that the metazachlor effect is probably independent from SAC1 activity.

Another way to approach a potential impact of sphingolipids in SAC1 was to select plants expressing pUB10::SAC1-mVenus I generated previously (part III of this thesis). I looked at the localization of SAC1 in *A. thaliana* by confocal microscopy. I checked 8 independent *Arabidopsis thaliana* lines which did not displayed any phenotype for the construction pUB10::SAC1-mVenus. Only one line had a strong mVenus signal (figure 30). Surprisingly, this signal was localized at the tonoplast through 6 different roots analyzed for this line. SAC1 localization has been describe in 2005, with a vesicular-like-TGN localization (Zhong et al., 2005). So, there is a discrepancy of my results with what has been published before. However, in the published article, SAC1 was expressed under the 35S promotor and

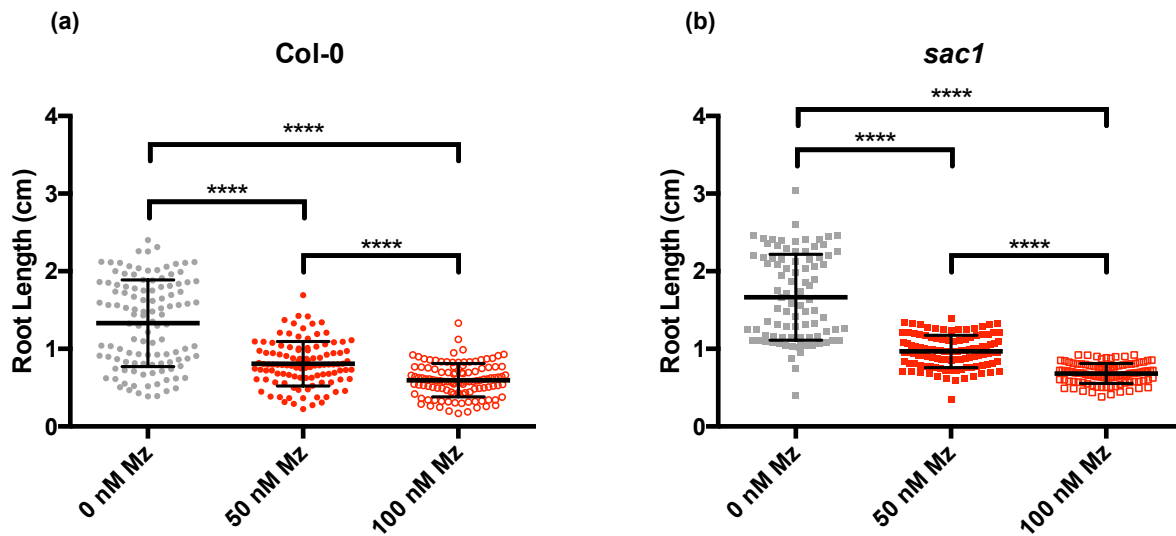


Figure 29: Metazachlor induces a root length decrease. Scatter dot representation of the root length upon metazachlor treatment on wild type Col-0 (a) and *sac1* mutant (SAIL T-DNA line)(b). Both Col-0 and *sac1* are sensitive to metazachlor showing the same decrease pattern meaning that the metazachlor effect is independent of the SAC1 activity. $n > 60$ roots analysed per condition. Statistics were done by Dunn's multiple comparisons test, **** P -value < 0.0001 .

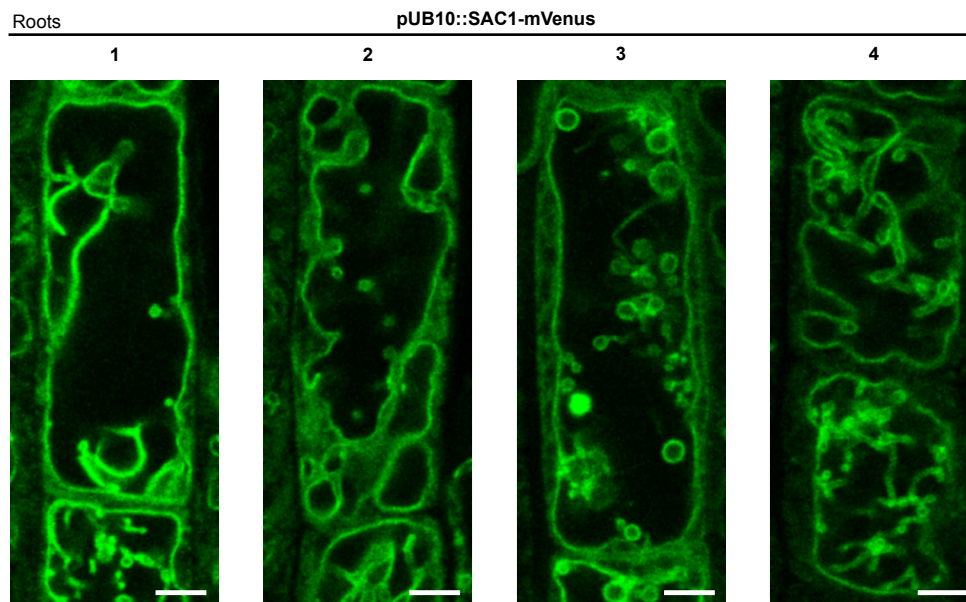


Figure 30: SAC1 seems to localize at the tonoplast in root epidermis cells of 4 independent *A. thaliana* stable lines expressing pUB10::SAC1-mVenus observed by confocal microscopy. SAC1: Suppressor of Actin 1 Scale bar = 5 μm

the localization was observed on 3-days-old seedling. Moreover, they did colocalization analyses in carrot protoplasts, so in a transient system heterologous to *Arabidopsis*. Thus, it could explain why my construction localizes at the tonoplast due to a less strong expression of SAC1 compared to the 35S promoter and due to that I expressed SAC1 is a stable homologous system. Other independent lines would have to be observed at confocal microscope to completely conclude on this experiment.

To underline whether SAC1 function is relevant for any PIPs-mediated trafficking steps, I crossed different endomembrane markers which were themselves crossed beforehand with PIPs biosensors, altogether in the *sac1* mutant. All the 14 crosses I made are plot in the annex 3. Unfortunately, I didn't look at the localization yet because I generated the F₂ and lack time to look at them at the time of writing my PhD thesis.

As I presented in the introduction, the cellular PIPs patterning is correlated to specific small GTPase Rab patterning. Hence, I looked at the Rab patterning at TGN/SVs upon metazachlor treatment in my proteomics.

E. Metazachlor affects Rab-GTPases patterning at TGN

The Rab small-GTPase family belongs to the super family of the Ras small-GTPase superfamily, composed by Ran-, Ras-, Rab-, Rho-, Arf-GTPase (Wennerberg, 2005). The Rab subfamily is involved in giving specificity to vesicle trafficking pathways and is divided in several sub-classes (Pereira-Leal and Seabra, 2000, 2001; Stenmark and Olkkonen, 2001). Their role in vesicle trafficking occurs at different level either at vesicle movement, vesicle fusion, tethering or cargo selection (Vernoud et al., 2003). Six classes are highly conserved between yeast, animal and plant kingdoms in term of localization, pathways and sequence homology, suggesting that a minimal Rab set is needed for the eukaryotic life. Moreover, the Rab display membrane localization due to a lipid anchor added mainly at the C-terminus part of the protein by prenylation. This prenylation fix either a geranylgeranyl or a farnesylfarnesyl anchor allowing the Rab to get attached on the membrane surface. Moreover, recent study highlights the remarkable capacity of this anchor to sense the membrane curvature, this sensitivity is due to the nature of the lipid anchor, their number and also the charge of the amino-acids surrounding the anchor (Kulakowski et al., 2018). As the Syp61/SV compartment is enriched in α VLCFA-containing GIPC and as sphingolipids participate in the

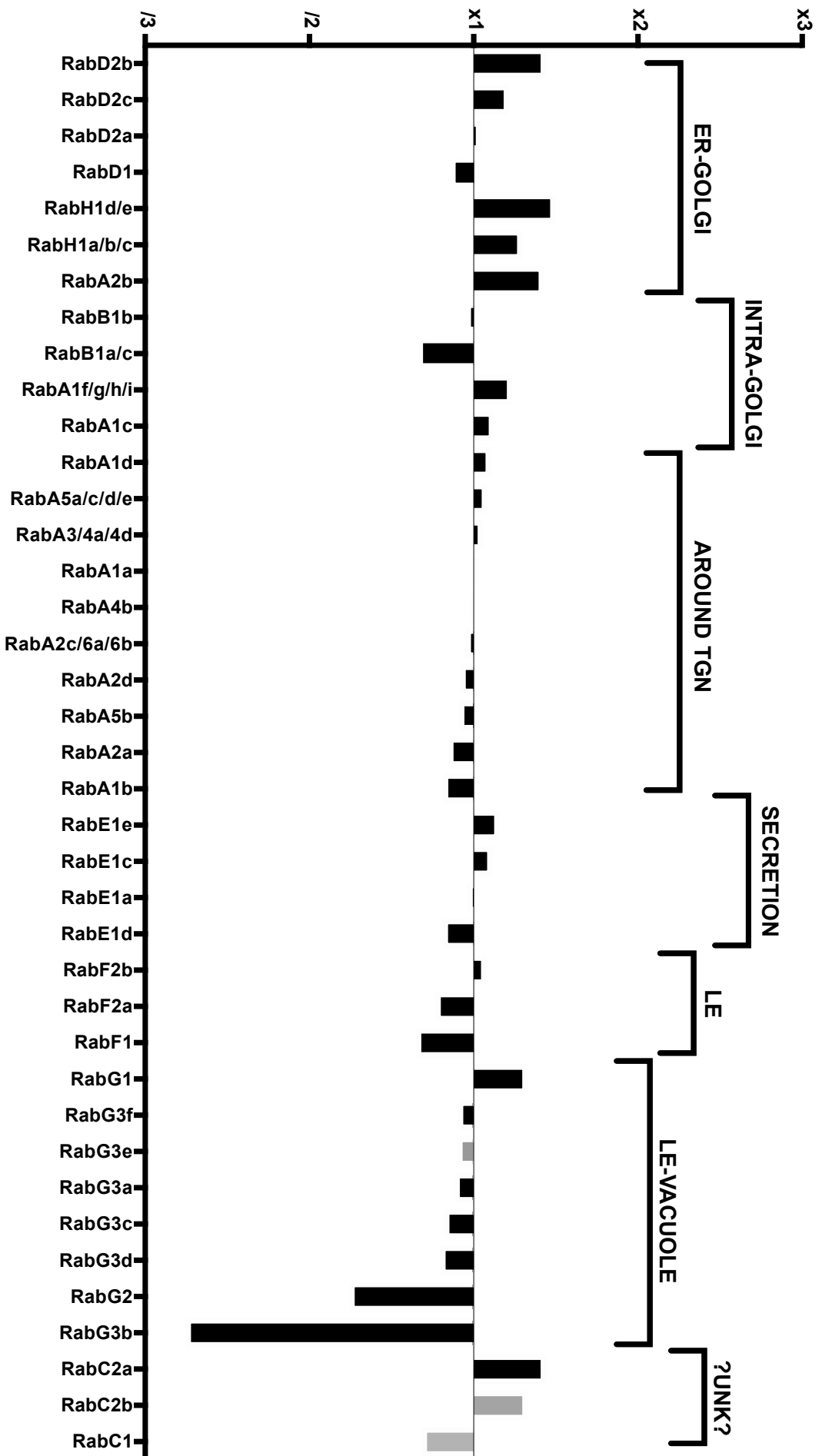


Figure 31: Rab patterning change in Syp61/SV compartment upon metazachlor. Enrichment fold upon metazachlor treatment, ratio calculated with the raw abundance of each RAB in metazachlor on control condition. The RAB are packed according their subcellular localization or prediction showing like a retention of the Golgi associated Rab as the maturation of the Syp61/SV is blocked. ER, Endoplasmic Reticulum; TGN, *trans*-Golgi Network; LE, Late Endosome; UNK, Unknown

L_o and L_d phase of membranes, it could as well be that sphingolipids play a role in the Rab patterning at Syp61/SV.

In fact, all the eight clades of plant Rab have been identified in the Syp61/SV proteome and they are ranked in the figure 31 according to the pathways they control (Rutherford and Moore, 2002; Vernoud et al., 2003). The histogram represents the effect of metazachlor on quantity of Rab found at TGN/SVs in term of enrichment or deprivation fold upon metazachlor. Amongst the 39 Rabs present in the Syp61/SV proteome, 18 Rabs are upregulated while 19 Rabs are downregulated when the sphingolipids composition in FA is altered by metazachlor. Interestingly, in the Rabs upregulated 11 Rabs (60%) are in charge of the anterograde or retrograde traffic between the ER and the Golgi/TGN. Some are involved in ER to *cis*-Golgi, some others in intra-Golgi transport and some others in Golgi to TGN trafficking (Rutherford and Moore, 2002). Furthermore, 90% of the Rabs which are decreased upon metazachlor are involved in post-TGN trafficking (LE, EE, vacuole, PM). It suggests that there is a possible blockage of the Rab patterning to keep the membrane identity closer to the pre-TGN Rabs composition

To confirm my findings on the sphingolipid impact on TGN-Rab patterning, I looked at the sub-cellular localization of the RabG3f which is a good Rab marker normally mostly localized at LE/MVBs and which was decreased at TGN upon metazachlor treatment in my IPs. In the figure 32, I extracted the red channel corresponding to RabG3f signal from the images that I got when I was looking P3Y colocalization with MVB. I could see in control condition (without metazachlor, figure 32a) a dotted signal reminiscent of the MVB signal tagged with RabG3f (Geldner et al., 2009). Upon metazachlor, my results indicated a loss of the dotted signal of RabG3f to a cytosolic-like localization (figure 32). Furthermore, the MVB-localization loss is linked to the metazachlor through a dose-response effect, the effect is stronger at 100 nM metazachlor than at 50 nM (figure 32). The quantification of the fluorescence intensity per μm^2 using 3D Object Counter plugin on imageJ confirmed this loss of dotted signal. This loss of MVB localization could be explained by the affinity of the lipid anchor to L_o or L_d membrane as suggest recently by Kulakowski et al. in 2018.

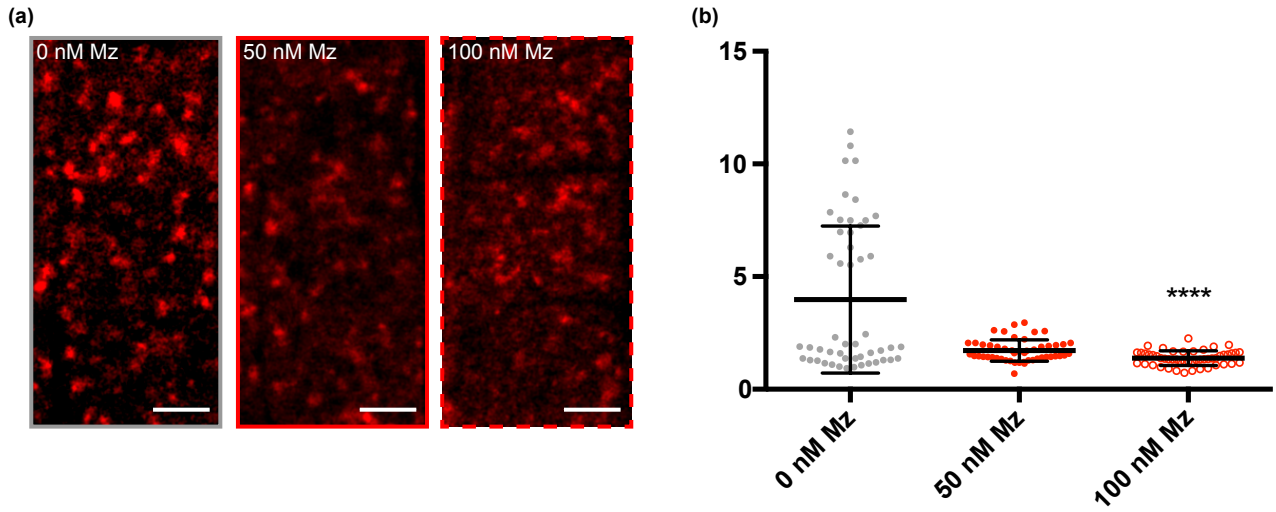


Figure 32: RabG3f loss of its vesicular localization upon metazachlor treatment. Epidermal root cells of *A. thaliana* lines expressing RabG3f tagged with mCherry (a). Without metazachlor, the signal is in dotted structure like MVB whereas upon metazachlor treatment there is an increase of cytosolic signal associated with a decrease a vesicular signal. These results are quantified in (b) with the representation of the fluorescence intensity per μm^2 (AU) showing a significant loss of vesicular signal at 100nM metazachlor. $n=50$ roots quantified. Statistics were done by Dunn's multiple comparisons test, **** P -value <0.0001

IV. Discussion

The development of methodologies to immuno-precipitate intact endomembrane compartments in the recent years has led to redefine our current knowledge of endomembrane trafficking in view of the identification of the whole protein content. Extraction of distinct subdomains of the TGN and isolation of the Golgi apparatus using immuno-precipitation has been used previously and reveals an enrichment of α VLCFAs-containing sphingolipids at SVs sites of TGN (Wattelet-Boyer et al., 2016). A proteomic analysis of these TGN subdomains was the next logical step to determine which proteins would be dependent on α VLCFAs-containing sphingolipids. Different proteomic analyses have been done by the past by Drakakaki G. et al., Parsons H. et al. and Groen A. et al. (in 2012 and 2014 for Groen A. respectively) on the Golgi apparatus and the TGN. They both used different proteomic methods that used either isotope tags labelling or non-native extraction protocols. In 2012, Harriet Parsons did a proteomic analysis on *A. thaliana* plantlets and cells suspension culture to identify the proteins from the Golgi apparatus and the TGN. To decipher the proteome, they did three different analyses, one using the LOPIT method (localization of organelle proteins by isotope tagging), a technique based on the identification of proteins localized at the same fraction/compartments by linear gradient and statistical pair-wise comparison of the different fractions (Dunkley et al., 2004). The second analysis was done on cell suspension too, but they separated the different compartments according to their charge at the membrane surface using the free-flow electrophoresis (FFE) and then performed proteomic analysis on the fractions obtained. The first analysis was done by Georgia Drakakaki on Syp61 compartment extracted by agarose-beads immunopurification (Drakakaki et al., 2012).

The proteomic analyses I have performed during my PhD bring a new thinner comparison between three immunopurified compartments, the Golgi apparatus and two distinct subdomains of TGN, the Syp61/SV and the RabA2a/CCV compartments. Using immuno-purification of compartments in native condition allowed for keeping intact vesicles and contents. The compartments were disrupted at the very last moment, after the immunopurification, to analyze them by LC-MS/MS label-free proteomic analyses. The label-free proteomics is clearly the most adapted method for these analyses as comparative quantitative data will be obtained for each sample. As show in the result (figure 7 to 12), the purity of the samples was checked either by western blotting or by looking at the abundance of compartment specific proteins directly in the results of my proteomic screen. Each fraction

was found to be highly enriched for the IP bait but also for already known proteins which localization at TGN or Golgi were characterized in previous publications. Hence, my immuno-purifications worked well. TGN compartment is, nowadays, described as a highly dynamic structure where endosomes could switch their identity quickly (Uemura et al., 2014). The proteome of the Syp61/SV and RabA2a/CCV show the same number of proteins specific to each compartment (around 400 proteins each), and show as well around 400 proteins in common, probably because the Syp61/SV and the RabA2a/CCV are both subdomains of the plant TGN that could get differentiated from a common set of membranes and share a part of their content between each other. Besides, most of the TGN subdomain markers are present in both Syp61/SV and RabA2a/CCV proteomes whereas the Golgi apparatus markers are mainly found in the Membl2/Golgi proteome. This might certainly underlines the maturation of TGN subdomains from the Golgi apparatus as there is no longer Golgi marker in the TGN subdomains, while the TGN subdomains (SV and CCV) share some markers. Last year, a study highlighted the behavior of each part of the Golgi complex upon Brefeldin A (BFA) treatment (Ito et al., 2017). In tobacco BY-2 cells, BFA treatment leads to the aggregation of the TGN and endosomes compartment, and the absorption of the Golgi apparatus in the ER. When the BFA is washed out, each compartment is reformed (Ito et al., 2012). Upon BFA treatment, the Golgi apparatus and TGN progress separately, both TGN and *cis*-Golgi form distinct aggregates while the medial/*trans* Golgi markers re-localize to the ER in BY-2 cells. In *A. thaliana* roots, the Golgi stacks surround TGN aggregates (Uemura et al., 2014). Furthermore, after the BFA washout, the recovery/rebuilding of the Golgi stacks and the TGN happen distinctly from each other. As some *cis*-Golgi relics did not mix with other Golgi markers under BFA treatment, this study suggest that the *cis*-Golgi compartment has to be distinct from the ER to initiate the formation of the Golgi stacks after the BFA wash-out. This study suggests an irreversible maturation from the ER to the Golgi apparatus, and from the Golgi apparatus to the TGN (Ito et al., 2017). This study is reminiscent from my proteomics results in which the different Golgi markers are specifically found in the Golgi proteome which suggest a strict and irreversible maturation of the Golgi in TGN compartment. While, both SV and CCV markers are found in both TGN subdomains but enriched in their corresponding compartment, facilitating a possible exchange or common maturation between the subdomains.

Besides the proteomes' differences between the endomembrane compartments, it is also known that a gradient of lipid concentration and composition is observed throughout the maturation of the different endomembranes. Furthermore, while the membranes mature from

the ER to the TGN, the concentration in sphingolipids increases (van Meer et al., 2008; Holthuis and Menon, 2014), due to the localization of sphingolipids biosynthesis enzymes at the end of the Golgi complex either in animal with sphingomyelin synthase SMS (Tafesse et al., 2013; Capasso et al., 2017) or in plant with IPCS (Wattelet-Boyer et al., unpublished data). As described in many papers and review, sphingolipids are localized at the outer leaflet of the PM where they act in antigens determination, blood groups, immune defense, pathogens specificity (Nachamkin et al., 2008; Ribeiro-Resende et al., 2010; Gault et al., 2010; Gronnier et al., 2016; Lenarčič et al., 2017; Gronnier et al., 2018). However, their involvement in vesicles trafficking was described relatively recently. The sorting of sphingolipids to the PM is described in cancerous HeLa cells to occur in specific vesicles, distinct from other vesicles transporting integral membrane secretory proteins (CD8 α , Deng et al., 2016). In plants, lipidomic of different TGN subdomains underlines an enrichment of sphingolipids in SYP61/SV too (Wattelet-Boyer et al., 2016). In addition, plant sphingolipids are composed by a specific fatty acid, a α VLCFA which is necessary for polar sorting of PIN2 (Wattelet-Boyer et al., 2016).

However, the diversity of sphingolipids is high, and it is not known whether the complexity of protein sorting relies, at least in part, on sphingolipids diversity. The sorting of PIN1 and AUX1, but not PIN2, is described to be dependent on the ceramides at the Rab2A/CCV compartment (Markham et al., 2011). Contrastingly, the PIN2 secretory sorting, but not PIN1 and AUX1 sorting, relies on the GIPC and GluCer composition at Syp61/SV ((Wattelet-Boyer et al., 2016, Supplemental Data). These two papers described two different sorting pathways, one relying on the ceramide-mediated recycling pathway at RabA2a/CCV and the other one implies the role of GIPC/Glucer in the secretory pathway of PIN2 at Syp61/SV (Markham et al., 2011; Wattelet-Boyer et al., 2016). Furthermore, Valérie Wattelet-Boyer showed that when the length of the α FA of the GIPC/GlcCer is inferior to 24 carbon atoms (using metazachlor treatment), the ultrastructure of the TGN is impaired, SVs are bigger and less tubular interconnections between SVs could be observed whereas the CCVs are not altered (Wattelet-Boyer et al., 2016). While, Markham J.E. showed that upon Fumonisin B1 (FB1, an inhibitor targeting the ceramide synthase LOH1 and LOH3) treatment, the VLCFA-containing ceramide decreases and the total LCB amount increases while no impact on the SVs/TGN ultrastructure could be observed (Markham et al., 2011). It might be that the CCVs/TGN ultrastructure is altered upon FB1 treatment, but this was not looked at in Markham et al., 2011. Both studies suggest the possible compartment-specificity of sphingolipids classes. Further lipidomic analysis have to be performed on the Syp61/SV

and RabA2a/CCV compartment to possibly identified a specific enrichment of the RabA2a/CCV in VLCFA-containing ceramide as compare to SVs/TGN for example.

Another interesting idea is that the tubular interconnection at the TGN might be the key of the PIN2 sorting because upon metazachlor treatment these tubular structures disappear almost completely. In animal cells, endosomal sorting of some proteins is described to occur in tubular structure between endosomes through the sorting nexins (SNXs) which could induced the membrane tubulation (Carlton et al., 2004; Traer et al., 2007). New technology in biophysics and bioinformatics allows a better understanding of sphingolipids properties inside the membrane. The length of the VLCFA of the sphingolipids is involved in the interdigitation of the two leaflet a membrane in plants (Pinto et al., 2008; Cacas et al., 2016). Interdigitation is a superposition of some carbons of the fatty acid chain, which is particularly long as for sphingolipids, with another fatty acid of a lipid localized at the opposite leaflet. In animal cells, the nanoclustering of GPI-anchored proteins at the outer leaflet of the PM is dependent on the grafting of a long acyl-chain on these proteins (Raghupathy et al., 2015). Moreover, this nanoclustering process of GPI-anchored proteins also depends on long acyl-chains of phosphatidylserine (PS) at the opposite inner leaflet of the PM (Raghupathy et al., 2015). Another example of the importance of the acyl-chain length in membrane interleaflet coupling is the lactosylceramide (LacCer) and Src family kinase Lyn coupling. In neutrophil cells, the very-long-chain fatty acids of the sphingolipid LacCer is instrumental in direct interaction between LacCer at the outer leaflet of the PM and Lyn kinase at the inner leaflet of the PM and for final activation of Lyn through phosphorylation (Chiricozzi et al., 2015).

Similar mechanisms are not yet described in plants, but it could explain in part the formation of microdomains in membranes. Unfortunately, the cell biology techniques used in animal cells are not always applicable on plant cells because the cells are surrounded by a cell wall blocking the incorporation of exogenous labeled analogs of sphingolipids. However, the development of lipid purification including GIPC has improved in the last years allowing biophysics experimentation to better understand the physic properties of plant sphingolipids (Carter and Koob, 1969; Buré et al., 2014; Lenarčič et al., 2017). The characterization of the GIPC properties is very important to refine the *in silico* analyses and improve our understanding of plant membranes because they are the most abundant lipids in plant membranes. Similarly to what was described in animal cells, plants' VLCFA of the sphingolipids could interact with some lipids at the opposite leaflet (inner leaflet), like very-

long-chain PS, or directly with some kinases, like what was described for Lyn, and leads to the formation of a L_o (liquid-ordered phase) in this opposite leaflet or leads to activation of a phosphorylation cascade that could be linked to phosphoinositides for example.

The L_o domains of membranes has been suggested recently to play a role in Rab small-GTPase recruitment at specific domain of the membrane (Kulakowski et al., 2018). Furthermore, *in vitro* experiments show a role for membrane electronegativity in specific recruitment of Rab35 which contains a positively-charged C-terminus end bypassing the affinity of the Rab geranylgeranyl prenylation for the L_d domain (Kulakowski et al., 2018). Nevertheless, this affinity of the Rab anchors to the membrane is not essential to their recruitment at the membrane as the Rabs have a lot of effectors facilitating their membrane localization (Kulakowski et al., 2018). According to my SYP61/SV proteomic data, there is an obvious effect of the sphingolipids (more precisely GIPC/GlcCer composition) on the Rab patterning in the SYP61/SV compartment. An interesting observation from my data was that the Rabs involved in the traffic before the TGN were increased at TGN upon metazachlor treatment while the Rabs involved in the trafficking after the TGN were decreased upon metazachlor treatment, and as I said before ‘further the endomembrane is going into the maturation from the ER to the TGN/PM, higher will be its amount in sphingolipids’ (van Meer et al., 2008; Holthuis and Menon, 2014). These results seem to highlight a plausible role of the sphingolipids in the recruitment on certain Rabs to facilitate the endomembrane maturation from the Golgi apparatus to endosomes. As the amount of sphingolipids increase during the endomembrane maturation from the ER to endosomes, the Rabs patterning could also follow this sphingolipids signature leading to a change in membrane identity and undergoing trafficking pathways. To confirm this hypothesis, the localization of different Rab has to be assessed upon metazachlor treatment. In my preliminary experiments, I observed a decrease of the vesicular localization of the RabG3f which is localized at LE/MVB. However, the experiment has to be completed and also more Rabs have to be observed. *In vitro* assay is important too, as the one done by Kulakowski (Kulakowski et al., 2018) to exclude the possible side effect of metazachlor. As the GIPC extraction is now available, construction of vesicles mimicking the different endosome membranes could be done and the affinity of the different Rab could be assessed as Kulakowski et al. did recently in 2018.

Amongst the Rab effectors in the Syp61/SV proteome, PIP-metabolizing enzymes are present, and their amount is changing upon metazachlor treatment. The decrease of different PI-kinases and the increase of PIPs phosphatases upon metazachlor treatment suggest a

decrease in the PIPs (PI₃P and PI₄P) that I confirmed by quantification of PI₃P and PI₄P by the use of PIPs biosensors (Simon et al., 2014) in *A. thaliana* root upon metazachlor treatment. Unlike the PI₄P localized at the PM, the PI₃P localization was changed when the GIPC composition was altered by metazachlor. Upon metazachlor, PI₃P were less localized at MVB/LE/tonoplast and more present at TGN/EE marked by VHA-a1. This result is quite interesting as couple years ago, researches underlined the maturation of LE from EE in animal cells and maturation of MVB/LE from TGN/EE in plant cells (Rink et al., 2005; Scheuring et al., 2011). This maturation in animals is associated with a mechanism called ‘Rab Conversion’ and this Rab conversion leads to PIPs composition modification. In fact, the animal EE membrane is composed by PI₃P and Rab5, the combination of the two recruits the Mon1-Ccz1 complex at EE membrane. The first one, Mon1 displaces the Rab5-GEF, Rabex-5 leading to a loss of Rab5 activity, and the second Ccz1 acts as a Rab7-GEF leading to the Rab7 activation. To further repress the Rab5 activity, a protein is recruited by Rab7 to take off the Rab5 from the new LE membrane (Nordmann et al., 2010; Casanova and Winckler, 2017). All this conversion is associated with a change in the PIP composition of the membrane as one of the Rab5 effector is a PI 3-kinase and one of the Rab7 effector is a PI₃P 5-kinase leading to the conversion of the PI₃P in PI_{3,5}P₂ from EE to LE (Poteryaev et al., 2010; Casanova and Winckler, 2017). Such a mechanism is not described yet in plants however, some data suggest its existence as the maturation of MVB/LE from TGN/EE is concomitant to the localization of the Rab5-like, RabF2b at TGN/EE membrane (Scheuring et al., 2011; Singh et al., 2014). In addition, in my thesis, I underlined an accumulation of PI₃P associated with a decrease and mislocalization of some Rab7-like proteins, with a loss of the vesicular localization of RabG3f. In plants, the dominant-negative of RabG3f displays a similar phenotype as the knock-out mutant of the PI₃P 5-kinase FAB1 (Cui et al., 2014; Hirano et al., 2017) suggesting that FAB1 might be an effector of the RabG3f (Hirano et al., 2015). However, this would have to be shown directly and, in general, the Rab conversion mechanisms still need to be explored in plant cells.

Nevertheless, some of my experiments highlight that metazachlor treatment prevents the PI₃P loss when PI₃P synthesis is inhibited by the PI 3-kinase inhibitor wortmannin (WN). This is unexpected as an alteration of the sphingolipid composition induces a decrease in the PI₃P quantity at LE/MVBs. WN treatment leads to a decrease of the PI₃P concentration at the beginning of the treatment and this is marked by the loss of PI₃P biosensor’s fluorescence. However, after 30-45min treatment a recovery of the PI₃P signal is observed in donut-like structures, probably due to the conversion PI_{3,5}P₂ in PI₃P (Jaillais et al., 2006; Hirano et al.,

2015). Metazachlor prevents the disappearance of PI₃P and higher the metazachlor concentration is, stronger the effect is. Furthermore, the PI₃P recovery does not seem to come from the PI_{3,5}P₂ pool as WN/metazachlor treatment experiment on YM₂₀₁₆₃₆ (inhibitor of PI_{3,5}P₂ synthesis from PI₃P) pre-treated plantlets does not change anything to the results. Consistently, *sac1* (conversion of PI_{3,5}P₂ to PI₃P) KO line is not hypersensitive or resistant to metazachlor as the gravitropism assays shown suggesting that the metazachlor effect on root gravitropism does not occur through SAC1 function. Of course, SAC1 could still be involved in the cellular phenotype observed (more PI₃P at TGN and less at MVBs) and this could be uncoupled from the gravitropism phenotype observed. Metazachlor acts not only on PI₃P homeostasis but as well on PI₄P turnover. My analysis of the metazachlor-induced gravitropism phenotype of the *pi4kβ1/pi4kβ2* double KO lines (Preuss et al., 2006) show a partial resistance to metazachlor suggesting that PI4Kβ1/2 could be sub-cellular targets of αVLCFA-sphingolipids. The WN experiment could be done as well on PI₄P biosensor lines because WN inhibits both PI 3- and PI 4-kinases (Gehrmann and Heilmeyer, 1998; Yue et al., 2001; Jaillais et al., 2006; Hirano et al., 2015). Moreover, crosses between the *pi4kβ1/pi4kβ2* double mutant with PIPlines and endomembranes markers could be done to see whether a defect in PI₄P composition alters the endosomal trafficking. I already did crosses in the *sac1* background to check whether the catalyses of PI_{3,5}P₂ into PI₃P is a limiting step in the PI₃P sub-cellular phenotype I observed upon metazachlor (PI₃P increase at TGN and WN-resistant loss of PI₃P), unfortunately again due to time limitations I did not analyze these crosses (Annex N°3).

I realize that my PhD raise a lot of questions that remain unanswered and 3 years was indeed a short time to address them completely. I would have like to get more time to at least determine whether the PIP homeostasis between TGN/EE and MVB/LE is either regulated by Rab conversion of Rab5-like (RabF2b for example) into Rab7-like (RabG3f for example) through the degree of membrane order and/or curvature of the membrane or regulated by possible lipid exchange through membrane contact site (MCS) between TGN/EE and MVB/LE. The last one is described in animal cells in the case of an exchange of PI₄P between endosomal membranes and ER membranes (Dong et al., 2016; Raiborg et al., 2016). To investigate whether TGN/EE and MVB/LE undergo MCS, *A. thaliana* lines expressing both tagged MVB-localized PI₃P-biosensor and TGN markers are available in the laboratory. Yoko Ito, a post-doc that started in the team in 2018, is currently analyzing MVB/TGN interactions in living cells using improved confocal resolution by airy-scan microscopy. Her results already showed that MVBs and TGN could be associated on a significant time scale but she

needs now to see whether metazachlor interfere with this process. Moreover, MVB/TGN association does not necessarily mean that they are exchanging PI₃P. This aspect of the work would need further experimental developments. These perspectives are really exciting because it would be the first time that these mechanisms would be described in plants in the endosomal network.

The question on the Rab conversion which is associated with the PIP conversion is not explored yet in plants. However recent discoveries seem to confirm its existence, the MON1/CCZ complex exists in plants (Cui et al., 2014). During a congress where I presented my work in a talk, the ENPER (European Network for Plant Endomembrane Research) 2018 meeting, a poster was presented on a protein called REAP. This protein is described as an effector of the plant Rab5-like protein, RabF2b. Interestingly, REAP protein also contains a PH domain that can bind to PIPs and/or small-GTPase (Lemmon, 2007). In this poster, Seung-won Choi (Takashi Ueda laboratory, Japan) has also presented that the protein co-localizes with RabF2b but only at the EE while no co-localization of REAP with RabF2b was observed at the MVBs. It will be interesting to have a look at Rab effectors I found in my proteomic analyses and find the ones containing a PIPs-binding site as they can bind PIPs and probably recruit a specific Rab at the membrane (Noack and Jaillais, 2017).

A tight lipid crosstalk between sphingolipids and PIP is already showed in animal cells, where sphingolipids increase the consumption of PI₄P leading to negative feedback of the sphingomyelin flow (Capasso et al., 2017). In plants, the PI₄P is probably produced in part at SVs through the recruitment of the PI4K β 1/2 which are RabA4b (Rab11-like) effectors (Preuss et al., 2006; Noack and Jaillais, 2017). Metazachlor treatment strongly affects the PI₄P quantity at the PM and overall, the double mutant *pi4k β 1/pi4k β 2* is resistant to metazachlor treatment. Altogether, these results suggest a connection between sphingolipids composition at SVs that could act on the PI₄P turnover. As for the impact of this PIPs turnover in protein sorting, the localization of PIN2 would need to be explored to further confirm whether polar sorting of PIN2 relies on PI₄P and sphingolipids crosstalk at TGN.

At the biochemical level, I did not explore in my PhD what would be the molecular nature of the PIPs/sphingolipids crosstalk. This would require performing *in vitro* assays by producing liposomes containing GIPC of different acyl-chain length. These experiments could as well give an idea on the affinity of the different Rab or PIP kinases for specific lipid composition as the interesting work done by Kulakowski et al. this year. Unfortunately, the limitation of liposome analysis is the absence of membrane asymmetry between the two

leaflets that is not reflecting the real nature of endomembrane and which is a strong issue when considering sphingolipids. Indeed sphingolipids are expected to locate in the luminal leaflet on TGN vesicles while phosphoinositides would locate at the cytoplasmic leaflet. However, a technique allows the study of lipid asymmetry using supported lipid bilayers that rely on a home-made asymmetric bilayer on mica plate (Visco et al., 2014). With asymmetric bilayers, the study on interdigitation is possible and we could maybe address the nature of the lipid which would interact with GIPC in the opposite leaflet. This would be precious information to start understanding the exact function of acyl-chain length of sphingolipids across a membrane. However, the membrane curvature could be one important aspect in this process. To mimic the vesicle curvature, nanoengineering to nano-mill the mica plate could be done to create on the surface of the mica plate vesicle-like structure to mimic the vesicle curvature at nano-scale (Cui and Zhang, 2017).

To conclude, these three years of study on the *trans*-Golgi network were really exciting and have led to the establishment of three compartment proteomes: the Golgi apparatus, the SYP61/SV and the RabA2a/CCV, and underlined the function of the length of the acyl-chain of sphingolipid in protein composition of those compartments, especially at SVs/TGN. The most impacted compartment was the SYP61/SVs where both the PIP-metabolizing pathway and the Rab small-GTPase patterning are altered when modifying the sphingolipid composition. These two features are described in animal cells to define the membrane identity of endomembrane compartments. However, we cannot only be based on the homology between animals and plants as the trafficking pathways are sometimes different. In particular, plants display specificity in TGN structure, function and dynamics that sum-up both secretion and endosomal recycling pathways. This difference probably relies, at least for some part, on how the lipids are locally generated and/or modified at precise TGN sub-domains. Hence, it would be crucial in the future to consider TGN maturation not only as a process that guide proteins to their final destination but also to consider it as a process in which lipid modifications drive and coordinate the whole process.

Finally, I could summarize my PhD by saying that I discovered a two-tales story between sphingolipids and phosphoinositides that might end-up in two-(very long) tails stories.

References

- Akkerman, M., Overdijk, E.J.R., Schel, J.H.N., Emons, A.M.C., and Ketelaar, T.** (2011). Golgi Body Motility in the Plant Cell Cortex Correlates with Actin Cytoskeleton Organization. *Plant Cell Physiol.* **52**: 1844–1855.
- Ambrose, C., Ruan, Y., Gardiner, J., Tamblyn, L.M., Catching, A., Kirik, V., Marc, J., Overall, R., and Wasteneys, G.O.** (2013). CLASP Interacts with Sorting Nexin 1 to Link Microtubules and Auxin Transport via PIN2 Recycling in *Arabidopsis thaliana*. *Dev. Cell* **24**: 649–659.
- Antignani, V., Klocko, A.L., Bak, G., Chandrasekaran, S.D., Dunivin, T., and Nielsen, E.** (2015). Recruitment of PLANT U-BOX13 and the PI4Kb1/b2 Phosphatidylinositol-4 Kinases by the Small GTPase RabA4B Plays Important Roles during Salicylic Acid-Mediated Plant Defense Signaling in *Arabidopsis*. *Plant Cell* **Vol. 27**: 243–261.
- Atmodjo, M.A., Hao, Z., and Mohnen, D.** (2013). Evolving Views of Pectin Biosynthesis.
- Barlowe, C., D’Enfert, C., and Schekman, R.** (1993). Purification and characterization of SAR1p, a small GTP-binding protein required for transport vesicle formation from the endoplasmic reticulum. *J. Biol. Chem.* **268**: 873–879.
- Baron, C.L. and Malhotra, V.** (2002). Role of diacylglycerol in PKD recruitment to the TGN and protein transport to the plasma membrane. *Science* (80-.). **295**: 325–328.
- Batoko, H., Zheng, H.Q., Hawes, C., and Moore, I.** (2000). A rab1 GTPase is required for transport between the endoplasmic reticulum and golgi apparatus and for normal golgi movement in plants. *Plant Cell* **12**: 2201–18.
- Beck, K.A., Keen, H., and Chern, J.B.** (1991). Interaction of Phosphoinositide Cycle Intermediates with the Plasma Membrane-associated Clathrin Assembly Protein AP-2 ” accompanying paper. *J. Biol. Chem.* **266**: 4442–4447.
- Becker, B. and Melkonian, M.** (1996). The secretory pathway of protists: spatial and functional organization and evolution. *Microbiol. Rev.* **60**: 697–721.
- Blümer, J., Rey, J., Dehmelt, L., Mazel, T., Wu, Y.-W., Bastiaens, P., Goody, R.S., and Itzen, A.** (2013). RabGEFs are a major determinant for specific Rab membrane targeting. *J. Cell Biol.* **200**: 287–300.
- Bolte, S. and Cordelières, F.P.** (2006). A guided tour into subcellular colocalization analysis in light microscopy.
- Boutte, Y., Jonsson, K., McFarlane, H.E., Johnson, E., Gendre, D., Swarup, R., Friml, J., Samuels, L., Robert, S., and Bhalerao, R.P.** (2013). ECHIDNA-mediated post-Golgi trafficking of auxin carriers for differential cell elongation. *Proc. Natl. Acad. Sci.* **110**: 16259–16264.
- Bown, L., Kusaba, S., Goubet, F., Codrai, L., Dale, A.G., Zhang, Z., Yu, X., Morris, K., Ishii, T., Evered, C., Dupree, P., and Jackson, S.** (2007). The ectopically parting cells 1-2 (*epc1-2*) mutant exhibits an exaggerated response to abscisic acid. *J. Exp. Bot.* **58**: 1813–1823.

- Buré, C., Cacas, J.L., Mongrand, S., and Schmitter, J.M.** (2014). Characterization of glycosyl inositol phosphoryl ceramides from plants and fungi by mass spectrometry. *Anal. Bioanal. Chem.* **406**: 995–1010.
- Cacas, J.-L. et al.** (2016). Revisiting Plant Plasma Membrane Lipids in Tobacco: A Focus on Sphingolipids. *Plant Physiol.* **170**: 367–84.
- Campa, C.C. and Hirsch, E.** (2017). Rab11 and phosphoinositides: A synergy of signal transducers in the control of vesicular trafficking. *Adv. Biol. Regul.* **63**: 132–139.
- Campelo, F., van Galen, J., Turacchio, G., Parashuraman, S., Kozlov, M.M., García-Parajo, M.F., and Malhotra, V.** (2017). Sphingomyelin metabolism controls the shape and function of the golgi cisternae. *Elife* **6**.
- Capasso, S. et al.** (2017). Sphingolipid metabolic flow controls phosphoinositide turnover at the *trans* -Golgi network. *EMBO J.* **36**: 1736–1754.
- Carlton, J., Bujny, M., Peter, B.J., Oorschot, V.M.J., Rutherford, A., Mellor, H., Klumperman, J., McMahon, H.T., and Cullen, P.J.** (2004). Sorting Nexin-1 Mediates Tubular Endosome-to-TGN Transport through Coincidence Sensing of High- Curvature Membranes and 3- Phosphoinositides. *Curr. Biol.* **93**: 43–46.
- Carter, H.E. and Koob, J.L.** (1969). Sphingolipids in bean leaves (*Phaseolus vulgaris*). *J. Lipid Res.* **10**: 363–369.
- Casanova, J.E. and Winckler, B.** (2017). A new Rab7 effector controls phosphoinositide conversion in endosome maturation. *J. Cell Biol.* **216**: 2995–2997.
- Casey, P.J. and Seabra, M.C.** (1996). Protein prenyltransferases. *J. Biol. Chem.* **271**: 5289–92.
- Chen, X. and Varki, A.** (2010). Advances in the biology and chemistry of sialic acids. *ACS Chem. Biol.* **5**: 163–176.
- Chiricozzi, E., Ciampa, M.G., Brasile, G., Compostella, F., Prinetti, A., Nakayama, H., Ekyalongo, R.C., Iwabuchi, K., Sonnino, S., and Mauri, L.** (2015). Direct interaction, instrumental for signaling processes, between LacCer and Lyn in the lipid rafts of neutrophil-like cells. *J. Lipid Res.* **56**: 129–141.
- Chow, C.-M., Neto, H., Foucart, C., and Moore, I.** (2008). Rab-A2 and Rab-A3 GTPases define a trans-golgi endosomal membrane domain in Arabidopsis that contributes substantially to the cell plate. *Plant Cell* **20**: 101–23.
- Clermont, Y., Rambourg, A., and Hermo, L.** (1995). Trans-Golgi network (TGN) of different cell types: Three-dimensional structural characteristics and variability. *Anat. Rec.* **242**: 289–301.
- Clough, S.J. and Bent, A.F.** (1998). Floral dip: a simplified method for Agrobacterium-mediated transformation of Arabidopsis thaliana. *Plant J.* **16**: 735–43.
- Collin, S., Justin, A.-M., Cantrel, C., Arondel, V., and Kader, J.-C.** (1999). Identification of AtPIS, a phosphatidylinositol synthase from Arabidopsis. *Eur. J. Biochem.* **262**: 652–658.
- Conchon, S., Cao, X., Barlowe, C., and Pelham, H.R.B.** (1999). Got1p and Sft2p: membrane proteins involved in traffic to the Golgi complex. *EMBO J.* **18**: 3934–3946.

- Crowley, K.S., Reinhart, G.D., and Johnson, A.E.** (1993). The signal sequence moves through a ribosomal tunnel into a noncytoplasmic aqueous environment at the ER membrane early in translocation. *Cell* **73**: 1101–15.
- Cui, D.D. and Zhang, L.C.** (2017). Nanomachining of materials: understanding the process through molecular dynamics simulation. *Adv. Manuf.* **5**: 20–34.
- Cui, Y., Zhao, Q., Gao, C., Ding, Y., Zeng, Y., Ueda, T., Nakano, A., and Jiang, L.** (2014). Activation of the Rab7 GTPase by the MON1-CCZ1 Complex Is Essential for PVC-to-Vacuole Trafficking and Plant Growth in Arabidopsis. *Plant Cell* **26**: 2080–2097.
- D’Angelo, G., Vicinanza, M., Di Campli, A., and De Matteis, M.A.** (2008). The multiple roles of PtdIns(4)P - not just the precursor of PtdIns(4,5)P₂. *J. Cell Sci.* **121**: 1955–1963.
- Dalton, A.J. and Felix, M.D.** (1956). A comparative study of the Golgi complex. *J. Biophys. Biochem. Cytol.* **2**: 79–84.
- Day, K.J., Staehelin, L.A., and Glick, B.S.** (2013). A Three-Stage Model of Golgi Structure and Function. *Histochem Cell Biol.* **6**: 247–253.
- Delevoeye, C., Miserey-Lenkei, S., Montagnac, G., Gilles-Marsens, F., Paul-Gilloteaux, P., Giordano, F., Waharte, F., Marks, M.S., Goud, B., and Raposo, G.** (2014). Recycling endosome tubule morphogenesis from sorting endosomes requires the kinesin motor KIF13A. *Cell Rep.* **6**: 445–454.
- Deng, Y., Rivera-Molina, F.E., Toomre, D.K., and Burd, C.G.** (2016). Sphingomyelin is sorted at the trans Golgi network into a distinct class of secretory vesicle. *Proc. Natl. Acad. Sci.* **113**: 6677–6682.
- Despres, B., Bouissonnie, F., Wu, H.-J., Gomord, V., Guilleminot, J., Grellet, F., Berger, F., Delseny, M., and Devic, M.** (2003). Three SAC1-like genes show overlapping patterns of expression in Arabidopsis but are remarkably silent during embryo development. *Plant J.* **34**: 293–306.
- Dettmer, W.J., Hong-Hermesdorf, A., Stierhof, Y.-D., and Schumacher, K.** (2006). Vacuolar H⁺-ATPase Activity Is Required for Endocytic and Secretory Trafficking in Arabidopsis. *Plant Cell* **18**: 715–730.
- Dick, G., Akslen-Hoel, L.K., Grøndahl, F., Kjos, I., and Prydz, K.** (2012). Proteoglycan synthesis and Golgi organization in polarized epithelial cells. *J. Histochem. Cytochem.* **60**: 926–35.
- Dippold, H.C. et al.** (2009). GOLPH3 bridges phosphatidylinositol-4-phosphate and actomyosin to stretch and shape the Golgi to promote budding. *Cell* **139**: 337–51.
- Dong, R., Saheki, Y., Swarup, S., Lucast, L., Harper, J.W., and De Camilli, P.** (2016). Endosome-ER Contacts Control Actin Nucleation and Retromer Function through VAP-Dependent Regulation of PI4P. *Cell* **166**: 408–423.
- Donohoe, B.S., Kang, B.-H., Gerl, M.J., Gergely, Z.R., McMichael, C.M., Bednarek, S.Y., and Staehelin, L.A.** (2013). Cis-Golgi cisternal assembly and biosynthetic activation occur sequentially in plants and algae. *Traffic* **14**: 551–67.
- Drakakaki, G., Van De Ven, W., Pan, S., Miao, Y., Wang, J., Keinath, N.F., Weatherly, B., Jiang, L., Schumacher, K., Hicks, G., and Raikhel, N.** (2012). Isolation

and proteomic analysis of the SYP61 compartment reveal its role in exocytic trafficking in Arabidopsis. *Cell Res.* **22**: 413–424.

Dunkley, T.P.J., Watson, R., Griffin, J.L., Dupree, P., and Lilley, K.S. (2004). Localization of Organelle Proteins by Isotope Tagging (LOPIT)*. *Mol. Cell. Proteomics* **3**: 1128–1134.

Duran, J.M. et al. (2012). Sphingomyelin organization is required for vesicle biogenesis at the Golgi complex. *EMBO J.* **31**: 4535–46.

Emr, S. et al. (2009). Journeys through the Golgi--taking stock in a new era. *J. Cell Biol.* **187**: 449–53.

Farquhar, M.G. and Palade, G.E. (1998). The Golgi apparatus: 100 years of progress and controversy. *Trends Cell Biol.* **8**: 2–10.

Farquhar, M.G. and Palade, G.E. (1981). The Golgi Apparatus (Complex)-(1954-1981) from Artifact to Center Stage. *J. Cell Biol.* **91**: 77–103.

Garnier, C. (1897). Les filaments basaux des cellules glandulaires. *Bibliogr. Anat.* **V**: 278–289.

Gault, C.R., Obeid, L.M., and Hannun, Y.A. (2010). An overview of sphingolipid metabolism: from synthesis to breakdown. *Adv. Exp. Med. Biol.* **688**: 1–23.

Gehrmann, T. and Heilmeyer, L.M.G. (1998). Review Phosphatidylinositol 4-kinases. *Eur. J. Biochem.* **370**.

Geldner, N., Déneraud-Tendon, V., Hyman, D.L., Mayer, U., Stierhof, Y.-D., and Chory, J. (2009). Rapid, combinatorial analysis of membrane compartments in intact plants with a multicolor marker set. *Plant J.* **59**: 169–178.

Geldner, N., Friml, J., Stierhof, Y.-D., Jürgens, G., and Palme, K. (2001). Auxin transport inhibitors block PIN1 cycling and vesicle trafficking. *Nature* **413**: 425–428.

Gendre, D. et al. (2011). Conserved Arabidopsis ECHIDNA protein mediates trans-Golgi-network trafficking and cell elongation. *Proc. Natl. Acad. Sci.* **108**: 8048–53.

Gendre, D., McFarlane, H.E., Johnson, E., Mouille, G., Sjödin, A., Oh, J., Levesque-Tremblay, G., Watanabe, Y., Samuels, L., and Bhalerao, R.P. (2013). Trans-Golgi network localized ECHIDNA/Ypt interacting protein complex is required for the secretion of cell wall polysaccharides in Arabidopsis. *Plant Cell* **25**: 2633–46.

Golgi, C. (1898). Intorno alla struttura della cellula nervosa. *Arch Ital Biol* **II**: 60–70.

Gómez-Merino, F.C., Arana-Ceballos, F.A., Trejo-Téllez, L.I., Skiryecz, A., Brearley, C.A., Dörmann, P., and Mueller-Roeber, B. (2005). Arabidopsis AtDGK7, the smallest member of plant diacylglycerol kinases (DGKs), displays unique biochemical features and saturates at low substrate concentration: the DGK inhibitor R59022 differentially affects AtDGK2 and AtDGK7 activity in vitro and alters plant growth and development. *J. Biol. Chem.* **280**: 34888–99.

Görlich, D., Prehn, S., Hartmann, E., Kalies, K.U., and Rapoport, T.A. (1992). A mammalian homolog of SEC61p and SECYp is associated with ribosomes and nascent polypeptides during translocation. *Cell* **71**: 489–503.

Grassé, P.-P. (1957). Ultrastructure, polarity and reproduction of Golgi apparatus. *C. R. Hebd. Seances Acad. Sci.* **245**: 1278–81.

- Griffiths, G. and Simons, K.** (1986). The trans Golgi network: Sorting at the exit site of the Golgi complex. *Science* (80-.). **234**: 438–443.
- Groen, A.J., Sancho-Andrés, G., Breckels, L.M., Gatto, L., Aniento, F., and Lilley, K.S.** (2014). Identification of Trans-Golgi Network Proteins in *Arabidopsis thaliana* Root Tissue. **13**: 763–76.
- Gronnier, J., Gerbeau-Pissot, P., Germain, V., Mongrand, S., and Simon-Plas, F.** (2018). Divide and Rule: Plant Plasma Membrane Organization. *Trends Plant Sci.* **23**: 899–917.
- Gronnier, J., Germain, V., Gouguet, P., Cacas, J.-L., and Mongrand, S.** (2016). GIPC: Glycosyl Inositol Phospho Ceramides, the major sphingolipids on earth. *Plant Signal. Behav.* **11**: e1152438.
- Gu, F., Crump, C.M., and Thomas, G.** (2001). Trans-Golgi network sorting. *Cell. Mol. Life Sci.* **58**: 1067–84.
- Hanada, K.** (2006). Discovery of the molecular machinery CERT for endoplasmic reticulum-to-Golgi trafficking of ceramide. *Mol. Cell. Biochem.* **286**: 23–31.
- Hanada, K., Kumagai, K., Tomishige, N., and Yamaji, T.** (2009). CERT-mediated trafficking of ceramide. *BBA - Mol. Cell Biol. Lipids* **1791**: 684–691.
- Handford, M.G., Sicilia, F., Brandizzi, F., Chung, J.H., and Dupree, P.** (2004). *Arabidopsis thaliana* expresses multiple Golgi-localised nucleotide-sugar transporters related to GONST1. *Mol. Genet. Genomics* **272**: 397–410.
- Hanna, M.G., Mela, I., Wang, L., Henderson, R.M., Chapman, E.R., Edwardson, J.M., Audhya, A., and Audhya, A.** (2016). Sar1 GTPase Activity Is Regulated by Membrane Curvature. *J. Biol. Chem.* **291**: 1014–27.
- Haubruck, H., Disela, C., Wagner, P., and Gallwitz, D.** (1987). The ras-related ypt protein is an ubiquitous eukaryotic protein: isolation and sequence analysis of mouse cDNA clones highly homologous to the yeast YPTJ gene.
- Haubruck, H., Prange', R., Vorgias, C., and Gallwitz, D.** (1989). The ras-related mouse ypt 1 protein can functionally replace the YPT1 gene product in yeast.
- Hausser, A., Storz, P., Märtens, S., Link, G., Toker, A., and Pfizenmaier, K.** (2005). Protein kinase D regulates vesicular transport by phosphorylating and activating phosphatidylinositol-4 kinase IIIbeta at the Golgi complex. *Nat. Cell Biol.* **7**: 880–6.
- He, J., Scott, J.L., Heroux, A., Roy, S., Lenoir, M., Overduin, M., Stahelin, R. V., and Kutateladze, T.G.** (2011). Molecular Basis of Phosphatidylinositol 4-Phosphate and ARF1 GTPase Recognition by the FAPP1 Pleckstrin Homology (PH) Domain. *J. Biol. Chem.* **286**: 18650–18657.
- Heung, L.J., Luberto, C., and Del Poeta, M.** (2006). Role of sphingolipids in microbial pathogenesis. *Infect. Immun.* **74**: 28–39.
- Hirano, T., Munnik, T., and Sato, M.H.** (2015). Phosphatidylinositol 3-Phosphate 5-Kinase, FAB1/PIKfyve Kinase Mediates Endosome Maturation to Establish Endosome-Cortical Microtubule Interaction in *Arabidopsis* 1[OPEN]. *Plant Physiol.* **169**: 1961–1974.
- Hirano, T., Stecker, K., Munnik, T., Xu, H., and Sato, M.H.** (2017). Visualization of Phosphatidylinositol 3,5-Bisphosphate Dynamics by a Tandem ML1N-Based

Fluorescent Protein Probe in Arabidopsis. *Plant Cell Physiol.*

Hirst, J., Barlow, L.D., Francisco, G.C., Sahlender, D.A., Seaman, M.N.J., Dacks, J.B., and Robinson, M.S. (2011). The fifth adaptor protein complex. *PLoS Biol.* **9**: e1001170.

Hirst, J., Borner, G.H.H., Antrobus, R., Peden, A.A., Hodson, N.A., Sahlender, D.A., and Robinson, M.S. (2012). Distinct and overlapping roles for AP-1 and GGAs revealed by the “knocksideways” system. *Curr. Biol.* **22**: 1711–6.

Holthuis, J.C.M. and Menon, A.K. (2014). Lipid landscapes and pipelines in membrane homeostasis. *Nature* **510**: 48–57.

Huang, J., Ghosh, R., Tripathi, A., Lonnfors, M., Somerharju, P., and Bankaitis, V.A. (2016). Two-ligand priming mechanism for potentiated phosphoinositide synthesis is an evolutionarily conserved feature of Sec14-like phosphatidylinositol and phosphatidylcholine exchange proteins. *Mol. Biol. Cell* **27**: 2317–2330.

Hutagalung, A.H. and Novick, P.J. (2011). Role of Rab GTPases in membrane traffic and cell physiology. *Physiol. Rev.* **91**: 119–149.

Ichikawa, S., Sakiyama, H., Suzuki, G., Jwa Hidari, K., and Hirabayashi, Y. (1996). Expression cloning of a cDNA for human ceramide glucosyltransferase that catalyzes the first glycosylation step of glycosphingolipid synthesis. *Proc. Natl. Acad. Sci.* **93**: 4638–4643.

Inaba, T., Nagano, Y., Nagasaki, T., and Sasaki, Y. (2001). Distinct Localization of Two Closely Related Ypt3/Rab11 Proteins

on the Trafficking Pathway in Higher Plants*. *J. Biol. Chem.* **277**: 9183–9188.

Ito, Y., Toyooka, K., Fujimoto, M., Ueda, T., Uemura, T., and Nakano, A. (2017). The trans-golgi network and the golgi stacks behave independently during regeneration after brefeldin A treatment in tobacco BY-2 cells. *Plant Cell Physiol.* **58**: 811–821.

Ito, Y., Uemura, T., Shoda, K., Fujimoto, M., Ueda, T., and Nakano, A. (2012). cis-Golgi proteins accumulate near the ER exit sites and act as the scaffold for Golgi regeneration after brefeldin A treatment in tobacco BY-2 cells. *Mol. Biol. Cell* **23**: 3203–14.

Jackson, C.L., Walch, L., and Verbavatz, J.M. (2016). Lipids and Their Trafficking: An Integral Part of Cellular Organization. *Dev. Cell* **39**: 139–153.

Jaillais, Y., Fobis-Loisy, I., Miège, C., and Gaude, T. (2008). Evidence for a sorting endosome in Arabidopsis root cells. *Plant J.* **53**: 237–247.

Jaillais, Y., Fobis-Loisy, I., Miège, C., Rollin, C., and Gaude, T. (2006). AtSNX1 defines an endosome for auxin-carrier trafficking in Arabidopsis. *Nature* **443**: 106–109.

Jean, S. and Kiger, A.A. (2012). Coordination between RAB GTPase and phosphoinositide regulation and functions. *Nat. Rev. Mol. Cell Biol.* **13**: 463–470.

Jia, T., Gao, C., Cui, Y., Wang, J., Ding, Y., Cai, Y., Ueda, T., Nakano, A., and Jiang, L. (2013). ARA7(Q69L) expression in transgenic Arabidopsis cells induces the formation of enlarged multivesicular bodies. *J. Exp. Bot.* **64**: 2817–29.

Käll, L., Canterbury, J.D., Weston, J., Noble, W.S., and MacCoss, M.J. (2007).

Semi-supervised learning for peptide identification from shotgun proteomics datasets. *Nat. Methods* **4**: 923–925.

Kang, B.H., Nielsen, E., Preuss, M.L., Mastronarde, D., and Staehelin, L.A. (2011). Electron Tomography of RabA4b- and PI-4Kb1-Labeled Trans Golgi Network Compartments in Arabidopsis. *Traffic* **12**: 313–329.

Kania, U., Fendrych, M., and Friml, J. (2014). Polar delivery in plants; commonalities and differences to animal epithelial cells. *Open Biol.* **4**: 140017–140017.

Kato, M., Muto, Y., Tanaka-Bandoh, K., Watanabe, K., and Ueno, K. (1995). Sphingolipid Composition in Bacteroides Species. *Anaerobe* **1**: 135–139.

Kleine-Vehn, J. et al. (2011). Recycling, clustering, and endocytosis jointly maintain PIN auxin carrier polarity at the plasma membrane. *Mol. Syst. Biol.* **7**: 540.

Kleine-Vehn, J., Dhonukshe, P., Sauer, M., Brewer, P.B., Wiśniewska, J., Paciorek, T., Benková, E., and Friml, J. (2008). ARF GEF-Dependent Transcytosis and Polar Delivery of PIN Auxin Carriers in Arabidopsis. *Curr. Biol.* **18**: 526–531.

Kleine-Vehn, J., Dhonukshe, P., Swarup, R., Bennett, M., and Friml, J. (2006). Subcellular trafficking of the Arabidopsis auxin influx carrier AUX1 uses a novel pathway distinct from PIN1. *Plant Cell* **18**: 3171–81.

Komba, S., Galustian, C., Ishida, H., Feizi, T., Kannagi, R., and Kiso, M. (1999). The First Total Synthesis of 6-Sulfo-de-N-acetylsialyl Lewis x Ganglioside :A Superior Ligand for Human L-Selectin. *Angew. Chemie Int. Ed.* **38**: 1131–1133.

König, S., Feussner, K., Schwarz, M., Kaefer, A., Iven, T., Landesfeind, M., Ternes, P., Karlovsky, P., Lipka, V., and Feussner, I. (2012). Arabidopsis mutants of sphingolipid fatty acid alpha-hydroxylases accumulate ceramides and salicylates. *New Phytol.* **196**: 1086–1097.

Kroesen, B.-J., Jacobs, S., Pettus, B.J., Sietsma, H., Kok, J.W., Hannun, Y.A., and de Leij, L.F.M.H. (2003). BcR-induced apoptosis involves differential regulation of C16 and C24-ceramide formation and sphingolipid-dependent activation of the proteasome. *J. Biol. Chem.* **278**: 14723–31.

Kulakowski, G., Bousquet, | Hugo, Manneville, J.-B., Bassereau, P., Goud, | Bruno, and Oesterlin, L.K. (2018). Lipid packing defects and membrane charge control RAB GTPase recruitment: *Traffic* **19**: 536–545.

Kumagai, K., Yasuda, S., Okemoto, K., Nishijima, M., Kobayashi, S., and Hanada, K. (2005). CERT mediates intermembrane transfer of various molecular species of ceramides. *J. Biol. Chem.* **280**: 6488–6495.

Ladinsky, M.S., Mastronarde, D.N., McIntosh, J.R., Howell, K.E., and Staehelin, L.A. (1999). Golgi structure in three dimensions: functional insights from the normal rat kidney cell. *J. Cell Biol.* **144**: 1135–49.

Lee, S.-B., Jung, S.-J., Go, Y.-S., Kim, H.-U., Kim, J.-K., Cho, H.-J., Park, O.K., and Suh, M.-C. (2009). Two Arabidopsis 3-ketoacyl CoA synthase genes, *KCS20* and *KCS2 / DAISY*, are functionally redundant in cuticular wax and root suberin biosynthesis, but differentially controlled by osmotic stress. *Plant J.* **60**: 462–475.

van Leeuwen, W., Vermeer, J.E.M., Gadella, T.W.J., and Munnik, T. (2007). Visualization of phosphatidylinositol 4,5-

bisphosphate in the plasma membrane of suspension-cultured tobacco BY-2 cells and whole *Arabidopsis* seedlings. *Plant J.* **52**: 1014–1026.

Lemmon, M. a (2007). Domains and Phosphoinositides. *Biochem. Soc. Symp.* **93**: 81–93.

Lenarčič, T. et al. (2017). Eudicot plant-specific sphingolipids determine host selectivity of microbial NLP cytolysins. *Science* **358**: 1431–1434.

Liberton, M., Page, L.E., O'Dell, W.B., O'Neill, H., Mamontov, E., Urban, V.S., and Pakrasi, H.B. (2013). Organization and flexibility of cyanobacterial thylakoid membranes examined by neutron scattering. *J. Biol. Chem.* **288**: 3632–40.

Lombard, V., Golaconda Ramulu, H., Drula, E., Coutinho, P.M., and Henrissat, B. (2014). The carbohydrate-active enzymes database (CAZy) in 2013. *Nucleic Acids Res.* **42**: D490-5.

Long, K.R., Yamamoto, Y., Baker, A.L., Watkins, S.C., Coyne, C.B., Conway, J.F., and Aridor, M. (2010). Sar1 assembly regulates membrane constriction and ER export. *J. Cell Biol.* **190**: 115–28.

Losev, E., Reinke, C.A., Jellen, J., Strongin, D.E., Bevis, B.J., and Glick, B.S. (2006). Golgi maturation visualized in living yeast. *Nature* **441**: 1002–1006.

Luschnig, C. et al. (2014). The dynamics of plant plasma membrane proteins: PINs and beyond. *Development* **141**: 2924–38.

Lynch, D. V. (2000). Enzymes of Sphingolipid Metabolism in Plants. *Methods Enzymol.* **311**: 130–149.

Mandon, E.C., Ehses, I., Rother, J., Van Echten, G., and Sandhoff, K. (1992).

Subcellular localization and membrane topology of serine palmitoyltransferase, 3-dehydrosphinganine reductase, and sphinganine N- acyltransferase in mouse liver. *J. Biol. Chem.* **267**: 11144–11148.

Marais, C., Wattelet-Boyer, V., Bouyssou, G., Hocquellet, A., Dupuy, J.W., Batailler, B., Brocard, L., Boutté, Y., Maneta-Peyret, L., and Moreau, P. (2015). The Qb-SNARE Memb11 interacts specifically with Arf1 in the Golgi apparatus of *Arabidopsis thaliana*. *J. Exp. Bot.* **66**: 6665–6678.

Markham, J.E., Li, J., Cahoon, E.B., and Jaworski, J.G. (2006). Separation and Identification of Major Plant Sphingolipid Classes from Leaves *. *J. Biol. Chem.* **281**: 22684–22694.

Markham, J.E., Molino, D., Gissot, L., Bellec, Y., Hématy, K., Marion, J., Belcram, K., Palauqui, J.-C., Satiat-JeuneMaître, B., and Faure, J.-D. (2011). Sphingolipids Containing Very-Long-Chain Fatty Acids Define a Secretory Pathway for Specific Polar Plasma Membrane Protein Targeting in *Arabidopsis*. *Plant Cell* **23**: 2362–2378.

Marquês, J.T., Marinho, H.S., Freire, R., and De Almeida, M. (2018). Sphingolipid hydroxylation in mammals, yeast and plants – an integrated view. *Prog. Lipid Res.* **71**: 18–42.

Martin, T.F.J. (2001). PI(4,5)P₂ regulation of surface membrane traffic. *Curr. Opin. Cell Biol.* **13**: 493–499.

Matsuura-Tokita, K., Takeuchi, M., Ichihara, A., Mikuriya, K., and Nakano, A. (2006). Live imaging of yeast Golgi cisternal maturation. *Nature* **441**: 1007–1010.

De Matteis, M.A. and Godi, A. (2004). PI-loting membrane traffic. *Nat. Cell Biol.* **6**: 487–492.

- De Matteis, M.A., Godi, A., and Corda, D.** (2002). Phosphoinositides and the Golgi complex. *Curr. Opin. Cell Biol.* **14**: 434–447.
- McMahon, H.T. and Boucrot, E.** (2011). Molecular mechanism and physiological functions of clathrin-mediated endocytosis. *Nat. Rev. Mol. Cell Biol.* **12**: 517–533.
- van Meer, G., Voelker, D.R., and Feigenson, G.W.** (2008). Membrane lipids: where they are and how they behave. *Nat. Rev. Mol. Cell Biol.* **9**: 112–24.
- Mesmin, B., Bigay, J., Polidori, J., Jamecna, D., Lacas-Gervais, S., and Antony, B.** (2017). Sterol transfer, PI4P consumption, and control of membrane lipid order by endogenous OSBP. *EMBO J.* **36**: e201796687.
- Milosevic, I., Giovedi, S., Lou, X., Raimondi, A., Collesi, C., Shen, H., Paradise, S., O'Toole, E., Ferguson, S., Cremona, O., and De Camilli, P.** (2011). Recruitment of endophilin to clathrin-coated pit necks is required for efficient vesicle uncoating after fission. *Neuron* **72**: 587–601.
- Mina, J.G., Okada, Y., Wansadhipathi-Kannangara, N.K., Pratt, S., Shams-Eldin, H., Schwarz, R.T., Steel, P.G., Fawcett, T., and Denny, P.W.** (2010). Functional analyses of differentially expressed isoforms of the Arabidopsis inositol phosphorylceramide synthase. *Plant Mol. Biol.* **73**: 399–407.
- Mollenhauer, H.H. and Morré, D.J.** (1994). Structure of Golgi apparatus.
- Mortimer, J.C. et al.** (2013). Abnormal Glycosphingolipid Mannosylation Triggers Salicylic Acid-Mediated Responses in *Arabidopsis*. *Plant Cell* **25**: 1881–1894.
- Nachamkin, I., Shadomy, S.V., Moran, A.P., Cox, N., Fitzgerald, C., Ung, H., Corcoran, A.T., Iskander, J.K., Schonberger, L.B., and Chen, R.T.** (2008). Anti-Ganglioside Antibody Induction by Swine (A/NJ/1976/H1N1) and Other Influenza Vaccines: Insights into Vaccine-Associated Guillain-Barré Syndrome. *J. Infect. Dis.* **198**: 226–233.
- Nagano, M., Takahara, K., Fujimoto, M., Tsutsumi, N., Uchimiya, H., and Kawai-Yamada, M.** (2012). Arabidopsis sphingolipid fatty acid 2-hydroxylases (AtFAH1 and AtFAH2) are functionally differentiated in fatty acid 2-hydroxylation and stress responses. *Plant Physiol.* **159**: 1138–48.
- Naka, T., Fujiwara, N., Yano, I., Maeda, S., Doe, M., Minamino, M., Ikeda, N., Kato, Y., Watabe, K., Kumazawa, Y., Tomiyasu, I., and Kobayashi, K.** (2003). Structural analysis of sphingophospholipids derived from *Sphingobacterium spiritivorum*, the type species of genus *Sphingobacterium*. *Biochim. Biophys. Acta* **1635**: 83–92.
- Naramoto, S., Sawa, S., Koizumi, K., Uemura, T., Ueda, T., Friml, J., Nakano, A., and Fukuda, H.** (2009). Phosphoinositide-dependent regulation of VAN3 ARF-GAP localization and activity essential for vascular tissue continuity in plants. *Development* **136**: 1529–38.
- Naslavsky, N., Rahajeng, J., Sharma, M., Jovic, M., and Caplan, S.** (2006). Interactions between EHD Proteins and Rab11-FIP2: A Role for EHD3 in Early Endosomal Transport. *Mol. Biol. Cell* **17**: 163–177.
- Ng, M.M., Dippold, H.C., Buschman, M.D., Noakes, C.J., and Field, S.J.** (2013). GOLPH3L antagonizes GOLPH3 to determine Golgi morphology. *Mol. Biol. Cell* **24**: 796–808.

- Noack, L.C. and Jaillais, Y.** (2017). Precision targeting by phosphoinositides: how PIs direct endomembrane trafficking in plants. *Curr. Opin. Plant Biol.* **40**: 22–33.
- Nordmann, M., Cabrera, M., Perz, A., Bröcker, C., Ostrowicz, C., Engelbrecht-Vandré, S., and Ungermann, C.** (2010). The Mon1-Ccz1 Complex Is the GEF of the Late Endosomal Rab7 Homolog Ypt7. *Curr. Biol.* **20**: 1654–1659.
- Nováková, P. et al.** (2014). SAC phosphoinositide phosphatases at the tonoplast mediate vacuolar function in Arabidopsis. *Proc. Natl. Acad. Sci. U. S. A.* **111**: 2818–23.
- Orci, L., Stamnes, M., Ravazzola, M., Amherdt, M., Perrelet, A., Söllner, T.H., and Rothman, J.E.** (1997). Bidirectional transport by distinct populations of COPI-coated vesicles. *Cell* **90**: 335–349.
- Di Paolo, G. and De Camilli, P.** (2006). Phosphoinositides in cell regulation and membrane dynamics. *Nature* **443**: 651–657.
- Papanikou, E. and Glick, B.S.** (2009). The yeast Golgi apparatus: insights and mysteries. *FEBS Lett.* **583**: 3746–51.
- Parsons, H.T., Drakakaki, G., and Heazlewood, J.L.** (2012). Proteomic dissection of the Arabidopsis Golgi and trans-Golgi network. *Front. Plant Sci.* **3**: 298.
- Pereira-Leal, J.Â.B. and Seabra, M.C.** (2001). Evolution of the Rab Family of Small GTP-binding Proteins. *J. Mol. Biol.* **313**: 889–901.
- Pereira-Leal, J.B. and Seabra, M.C.** (2000). The mammalian Rab family of small GTPases: definition of family and subfamily sequence motifs suggests a mechanism for functional specificity in the Ras superfamily 1. Edited by M. Yaniv. *J. Mol. Biol.* **301**: 1077–1087.
- Petrášek, J. and Friml, J.** (2009). Auxin transport routes in plant development. Primer.
- Pichler, H., Gaigg, B., Hrastnik, C., Achleitner, G., Kohlwein, S.D., Zellnig, G., Perktold, A., and Daum, G.** (2001). A subfraction of the yeast endoplasmic reticulum associates with the plasma membrane and has a high capacity to synthesize lipids. *Eur. J. Biochem.* **268**: 2351–2361.
- Pimpl, P., Movafeghi, A., Coughlan, S., Denecke, J., Hillmer, S., and Robinson, D.G.** (2000). In situ localization and in vitro induction of plant COPI-coated vesicles. *Plant Cell* **12**: 2219–36.
- Pinto, S.N., Silva, L.C., De Almeida, R.F.M., and Prieto, M.** (2008). Membrane domain formation, interdigitation, and morphological alterations induced by the very long chain asymmetric C24:1 ceramide. *Biophys. J.* **95**: 2867–2879.
- Porter, K.R., Claude, A., and Fullam, E.F.** (1945). A STUDY OF TISSUE CULTURE CELLS BY ELECTRON MICROSCOPY: METHODS AND PRELIMINARY OBSERVATIONS. *J. Exp. Med.* **81**: 233–46.
- Posor, Y., Eichhorn-Grünig, M., and Haucke, V.** (2015). Phosphoinositides in endocytosis. *Biochim. Biophys. Acta - Mol. Cell Biol. Lipids* **1851**: 794–804.
- Poteryaev, D., Datta, S., Ackema, K., Zerial, M., and Spang, A.** (2010). Identification of the switch in early-to-late endosome transition. *Cell* **141**: 497–508.
- Preuss, M.L., Schmitz, A.J., Thole, J.M., Bonner, H.K.S., Otegui, M.S., and Nielsen,**

- E. (2006). A role for the RabA4b effector protein PI-4K β 1 in polarized expansion of root hair cells in *Arabidopsis thaliana*. *J. Cell Biol.* **172**: 991–998.
- Preuss, M.L., Serna, J., Falbel, T.G., Bednarek, S.Y., and Nielsen, E.** (2004). The *Arabidopsis* Rab GTPase RabA4b Localizes to the Tips of Growing Root Hair Cells. *Plant Cell Online* **16**: 1589–1603.
- Pribat, A., Sormani, R., Rousseau-Guetin, M., Julkowska, M.M., Testerink, C., Joubès, J., Castroviejo, M., Laguerre, M., Meyer, C., Germain, V., and Rothan, C.** (2012). A novel class of PTEN protein in *Arabidopsis* displays unusual phosphoinositide phosphatase activity and efficiently binds phosphatidic acid. *Biochem. J.* **441**: 161–171.
- Raghupathy, R. et al.** (2015). Transbilayer lipid interactions mediate nanoclustering of lipid-anchored proteins. *Cell* **161**: 581–594.
- Raiborg, C., Wenzel, E.M., Pedersen, N.M., and Stenmark, H.** (2016). Phosphoinositides in membrane contact sites. *Biochem. Soc. Trans.* **44**: 425–430.
- Rambourg, A. and Clermont, Y.** (1990). Three-dimensional electron microscopy: structure of the Golgi apparatus. *Eur. J. Cell Biol.* **51**: 189–200.
- Rambourg, A., Clermont, Y., and Hermo, L.** (1979). Three-dimensional architecture of the Golgi apparatus in Sertoli cells of the rat. *Am. J. Anat.* **154**: 455–475.
- Rancour, D.M., Dickey, C.E., Park, S., and Bednarek, S.Y.** (2002). Characterization of AtCDC48. Evidence for multiple membrane fusion mechanisms at the plane of cell division in plants. *Plant Physiol.* **130**: 1241–53.
- Rautengarten, C., Ebert, B., Liu, L., Stonebloom, S., Smith-Moritz, A.M., Pauly, M., Orellana, A., Scheller, H.V., and Heazlewood, J.L.** (2016). The *Arabidopsis* Golgi-localized GDP-L-fucose transporter is required for plant development. *Nat. Commun.* **7**: 12119.
- Rennie, E.A. et al.** (2014). Identification of a sphingolipid α -glucuronosyltransferase that is essential for pollen function in *Arabidopsis*. *Plant Cell* **26**: 3314–25.
- Rennie, E.A., Hansen, S.F., Baidoo, E.E.K., Hadi, M.Z., Keasling, J.D., and Scheller, H. V.** (2012). Three Members of the *Arabidopsis* Glycosyltransferase Family 8 Are Xylan Glucuronosyltransferases. *Plant Physiol.* **159**: 1408–1417.
- Ribeiro-Resende, V.T., Ribeiro-Guimarães, M.L., Lemes, R.M.R., Nascimento, I.C., Alves, L., Mendez-Otero, R., Pessolani, M.C.V., and Lara, F.A.** (2010). Involvement of 9-O-Acetyl GD3 ganglioside in *Mycobacterium leprae* infection of Schwann cells. *J. Biol. Chem.* **285**: 34086–96.
- Rink, J., Ghigo, E., Kalaidzidis, Y., and Zerial, M.** (2005). Rab conversion as a mechanism of progression from early to late endosomes. *Cell* **122**: 735–749.
- Robert, S., Chary, S.N., Drakakaki, G., Li, S., Yang, Z., Raikhel, N. V., and Hicks, G.R.** (2008). Endosidin1 defines a compartment involved in endocytosis of the brassinosteroid receptor BRI1 and the auxin transporters PIN2 and AUX1. *Proc. Natl. Acad. Sci. U. S. A.* **105**: 8464–9.
- Róg, T., Orłowski, A., Llorente, A., Skotland, T., Sylvänne, T., Kauhanen, D., Ekroos, K., Sandvig, K., and Vattulainen, I.** (2016). Interdigitation of long-chain sphingomyelin induces coupling of membrane leaflets in a cholesterol

dependent manner. *Biochim. Biophys. Acta - Biomembr.* **1858**: 281–288.

Rossanese, O.W., Soderholm, J., Bevis, B.J., Sears, I.B., O'Connor, J., Williamson, E.K., and Glick, B.S. (1999). Golgi structure correlates with transitional endoplasmic reticulum organization in *Pichia pastoris* and *Saccharomyces cerevisiae*. *J. Cell Biol.* **145**: 69–81.

Roux, A., Cuvelier, D., Nassoy, P., Prost, J., Bassereau, P., and Goud, B. (2005). Role of curvature and phase transition in lipid sorting and fission of membrane tubules. *EMBO J.* **24**: 1537–1545.

Rudge, S.A., Anderson, D.M., and Emr, S.D. (2004). Vacuole size control: regulation of PtdIns(3,5)P₂ levels by the vacuole-associated Vac14-Fig4 complex, a PtdIns(3,5)P₂-specific phosphatase. *Mol. Biol. Cell* **15**: 24–36.

Ruiz-May, E., Kim, S.-J., Brandizzi, F., and Rose, J.K.C. (2012). The secreted plant N-glycoproteome and associated secretory pathways. *Front. Plant Sci.* **3**: 117.

Ruiz Rosquete, M., Davis, D.J., and Drakakaki, G. (2017). The plant Trans-Golgi Network. Not just a matter of distinction. *Plant Physiol.* **176**: pp.01239.2017.

Rutherford, S. and Moore, I. (2002). The Arabidopsis Rab GTPase family: Another enigma variation. *Curr. Opin. Plant Biol.* **5**: 518–528.

Saito, Y., Kimura, K., Oka, T., and Nakano, A. (1998). Activities of Mutant Sar1 Hydrolysis, and Cell-Free to the Golgi Apparatus. *J. Biochem.* **823**: 816–823.

Sanderfoot, A.A., Assaad, F.F., and Raikhel, N. V (2000). The Arabidopsis Genome. An Abundance of Soluble N-

Ethylmaleimide-Sensitive Factor Adaptor Protein Receptors 1.

Sanderfoot, A.A., Kovaleva, V., Bassham, D.C., and Raikhel, N. V. (2001). Interactions between Syntaxins Identify at Least Five SNARE Complexes within the Golgi/Prevacuolar System of the Arabidopsis Cell. *Mol. Biol. Cell* **12**: 3733–3743.

Sanmartín, M., Ordóñez, A., Sohn, E.J., Robert, S., Sánchez-Serrano, J.J., Surpin, M.A., Raikhel, N. V, and Rojo, E. (2007). Divergent functions of VTI12 and VTI11 in trafficking to storage and lytic vacuoles in Arabidopsis. *Proc. Natl. Acad. Sci. U. S. A.* **104**: 3645–50.

Scales, S.J., Pepperkok, R., and Kreis, T.E. (1997). Visualization of ER-to-Golgi transport in living cells reveals a sequential mode of action for COPII and COPI. *Cell* **90**: 1137–1148.

Schaaf, G., Ortlund, E.A., Tyeryar, K.R., Mousley, C.J., Ile, K.E., Garrett, T.A., Ren, J., Woolls, M.J., Raetz, C.R.H., Redinbo, M.R., and Bankaitis, V.A. (2008). Functional anatomy of phospholipid binding and regulation of phosphoinositide homeostasis by proteins of the sec14 superfamily. *Mol. Cell* **29**: 191–206.

Scheuring, D., Viotti, C., Krüger, F., Künzl, F., Sturm, S., Bubeck, J., Hillmer, S., Frigerio, L., Robinson, D.G., Pimpl, P., and Schumacher, K. (2011). Multivesicular bodies mature from the trans-Golgi network/early endosome in Arabidopsis. *Plant Cell* **23**: 3463–81.

Schnaar, R.L., Gerardy-Schahn, R., and Hildebrandt, H. (2014). Sialic Acids in the Brain: Gangliosides and Polysialic Acid in Nervous System Development, Stability,

Disease, and Regeneration. *Physiol. Rev.* **94**: 461–518.

Scott, C.C., Vacca, F., and Gruenberg, J. (2014). Endosome maturation, transport and functions. *Semin. Cell Dev. Biol.* **31**: 2–10.

Segev, N. (2001). Ypt/Rab GTPases: Regulators of Protein Trafficking. *Sci. Signal.* **2001**: re11-re11.

Segev, N., Mulholland, J., and Botstein, D. (1988). The Yeast GTP-Binding YPT1 Protein and a Mammalian Counterpart Are Associated with the Secretion Machinery.

Shibata, Y., Voeltz, G.K., and Rapoport, T.A. (2006). Rough Sheets and Smooth Tubules. *Cell* **126**: 435–439.

Shin, H.W. et al. (2005). An enzymatic cascade of Rab5 effectors regulates phosphoinositide turnover in the endocytic pathway. *J. Cell Biol.* **170**: 607–618.

Simon, M.L.A., Platre, M.P., Assil, S., Van Wijk, R., Chen, W.Y., Chory, J., Dreux, M., Munnik, T., and Jaillais, Y. (2014). A multi-colour/multi-affinity marker set to visualize phosphoinositide dynamics in Arabidopsis. *Plant J.* **77**: 322–337.

Simon, M.L.A., Platre, M.P., Marquès-Bueno, M.M., Armengot, L., Stanislas, T., Bayle, V., Caillaud, M.C., and Jaillais, Y. (2016). A PtdIns(4)P-driven electrostatic field controls cell membrane identity and signalling in plants. *Nat. Plants* **2**.

Simon, S.M. and Blobel, G. (1991). A protein-conducting channel in the endoplasmic reticulum. *Cell* **65**: 371–80.

Singh, M.K., Krüger, F., Beckmann, H., Brumm, S., Vermeer, J.E.M., Munnik, T., Mayer, U., Stierhof, Y.D., Grefen, C.,

Schumacher, K., and Jürgens, G. (2014). Protein delivery to vacuole requires SAND protein-dependent Rab GTPase conversion for MVB-vacuole fusion. *Curr. Biol.* **24**: 1383–1389.

Sohn, E.J., Kim, E.S., Zhao, M., Kim, S.J., Kim, H., Kim, Y.-W., Lee, Y.J., Hillmer, S., Sohn, U., Jiang, L., and Hwang, I. (2003). Rha1, an Arabidopsis Rab5 homolog, plays a critical role in the vacuolar trafficking of soluble cargo proteins. *Plant Cell* **15**: 1057–70.

Stanley, P. (2011). Golgi glycosylation. *Cold Spring Harb. Perspect. Biol.* **3**.

Stenmark, H. and Olkkonen, V.M. (2001). The Rab GTPase family. *Genome Biol.* **2**: 1–7.

Stevenson-Paulik, J., Love, J., and Boss, W.F. (2003). Differential regulation of two Arabidopsis type III phosphatidylinositol 4-kinase isoforms. A regulatory role for the pleckstrin homology domain. *Plant Physiol.* **132**: 1053–64.

Stevenson, J.M., Perera, I.Y., and Boss, W.F. (1998). A phosphatidylinositol 4-kinase pleckstrin homology domain that binds phosphatidylinositol 4-monophosphate. *J. Biol. Chem.* **273**: 22761–7.

Sugiki, T., Egawa, D., Kumagai, K., Kojima, C., Fujiwara, T., Takeuchi, K., Ichio Shimada, X., Hanada, K., and Takahashi, H. (2018). Phosphoinositide binding by the PH domain in ceramide transfer protein (CERT) is inhibited by hyperphosphorylation of an adjacent serine-repeat motif.

Surpin, M., Zheng, H., Morita, M.T., Saito, C., Avila, E., Blakeslee, J.J., Bandyopadhyay, A., Kovaleva, V., Carter, D., Murphy, A., Tasaka, M., and Raikhel,

N. (2003). The VTI Family of SNARE Proteins Is Necessary for Plant Viability and Mediates Different Protein Transport Pathways. *Plant Cell Online* **15**: 2885–2899.

Swarup, R. and Péret, B. (2012). AUX/LAX family of auxin influx carriers-an overview. *Front. Plant Sci.* **3**: 225.

Tafesse, F.G., Sanyal, S., Ashour, J., Guimaraes, C.P., Hermansson, M., Somerharju, P., and Ploegh, H.L. (2013). Intact sphingomyelin biosynthetic pathway is essential for intracellular transport of influenza virus glycoproteins. *Proc. Natl. Acad. Sci. U. S. A.* **110**: 6406–11.

Tanaka, H., Kitakura, S., De Rycke, R., De Groodt, R., and Friml, J. (2009). Fluorescence imaging-based screen identifies ARF GEF component of early endosomal trafficking. *Curr. Biol.* **19**: 391–7.

Thole, J.M., Vermeer, J.E.M., Zhang, Y., Gadella, T.W.J., Nielsen, E., and Nielsen, E. (2008). Root hair defective4 encodes a phosphatidylinositol-4-phosphate phosphatase required for proper root hair development in *Arabidopsis thaliana*. *Plant Cell* **20**: 381–95.

Thyberg, J. and Moskalewski, S. (1999). Role of Microtubules in the Organization of the Golgi Complex. *Exp. Cell Res.* **246**: 263–279.

Ton, J., Jakab, G., Toquin, V., Flors, V., Iavicoli, A., Maeder, M.N., Métraux, J.-P., and Mauch-Mani, B. (2005). Dissecting the beta-aminobutyric acid-induced priming phenomenon in *Arabidopsis*. *Plant Cell* **17**: 987–99.

Traer, C.J., Rutherford, A.C., Palmer, K.J., Wassmer, T., Oakley, J., Attar, N., Carlton, J.G., Kremerskothen, J., Stephens, D.J., and Cullen, P.J. (2007). SNX4 coordinates

endosomal sorting of TfnR with dynein-mediated transport into the endocytic recycling compartment. *Nat. Cell Biol.* **9**: 1370–1380.

Traving, C. and Schauer, R. (1998). Structure, function and metabolism of sialic acids. *Cell. Mol. Life Sci.* **54**: 1330–1349.

Ueda, T., Yamaguchi, M., Uchimiya, H., and Nakano, A. (2001). Ara6, a plant-unique novel type Rab GTPase, functions in the endocytic pathway of *Arabidopsis thaliana*. *EMBO J.* **20**: 4730–41.

Uemura, T., Suda, Y., Ueda, T., and Nakano, A. (2014). Dynamic behavior of the trans-golgi network in root tissues of *Arabidopsis* revealed by super-resolution live imaging. *Plant Cell Physiol.* **55**: 694–703.

Uemura, T., Ueda, T., Ohniwa, R.L., Nakano, A., Takeyasu, K., and Sato, M.H. (2004). Systematic Analysis of SNARE Molecules in *Arabidopsis*: Dissection of the post-Golgi Network in Plant Cells. *Cell Struct. Funct.* **29**: 49–65.

Vernoud, V., Horton, A.C., Yang, Z., and Nielsen, E. (2003). Analysis of the small GTPase gene superfamily of *Arabidopsis*. *Plant Physiol.* **131**: 1191–208.

Viotti, C. et al. (2010). Endocytic and Secretory Traffic in *Arabidopsis* Merge in the Trans-Golgi Network/Early Endosome, an Independent and Highly Dynamic Organelle. *Plant Cell* **22**: 1344–1357.

Visco, I., Chiantia, S., and Schwille, P. (2014). Asymmetric supported lipid bilayer formation via methyl- β -cyclodextrin mediated lipid exchange: Influence of asymmetry on lipid dynamics and phase behavior. *Langmuir* **30**: 7475–7484.

Wang, W. et al. (2008). An Inositolphosphorylceramide Synthase Is Involved in Regulation of Plant Programmed Cell Death Associated with Defense in Arabidopsis. *Plant Cell Online* **20**: 3163–3179.

Watanabe, Y., Nakajima, M., Hoshino, T., Jayasimhulu, K., Brooks, E.E., and Kaneshiro, E.S. (2001). A novel sphingophosphonolipid head group 1-hydroxy-2-aminoethyl phosphonate in *Bdellovibrio stolpii*. *Lipids* **36**: 513–9.

Wattelet-Boyer, V., Brocard, L., Jonsson, K., Esnay, N., Joubès, J., Domergue, F., Mongrand, S., Raikhel, N., Bhalerao, R.P., Moreau, P., and Boutté, Y. (2016). Enrichment of hydroxylated C24- and C26-acyl-chain sphingolipids mediates PIN2 apical sorting at trans-Golgi network subdomains. *Nat. Commun.* **7**: 12788.

Wennerberg, K. (2005). The Ras superfamily at a glance. *J. Cell Sci.* **118**: 843–846.

Williams, M.E., Torabinejad, J., Cohick, E., Parker, K., Drake, E.J., Thompson, J.E., Hortter, M., and DeWald, D.B. (2005). Mutations in the Arabidopsis Phosphoinositide Phosphatase Gene SAC9 Lead to Overaccumulation of PtdIns(4,5)P₂ and Constitutive Expression of the Stress-Response Pathway. *Plant Physiol.* **138**: 686–700.

Yee, B., Sagulenko, E., Morgan, G.P., Webb, R.I., Fuerst, J.A., Ward, N.L., and Greub, G. (2012). Electron tomography of the nucleoid of *Gemmata obscuriglobus*

reveals complex liquid crystalline cholesteric structure. *Front. Microbiol.* **3**.

Yue, J., Liu, J., and Shen, X. (2001). Inhibition of Phosphatidylinositol 4-Kinase Results in a Significant Reduced Respiratory Burst in Formyl-methionyl-leucyl-phenylalanine-stimulated Human Neutrophils. *J. Biol. Chem.* **276**: 49093–49099.

Zerial, M. and McBride, H. (2001). RAB PROTEINS AS MEMBRANE ORGANIZERS COGNATE. *Nat. Rev. Mol. Cell Biol.* **2**: 107–119.

Zhang, G.F. and Staehelin, L.A. (1992). Compartmentation of the Golgi Apparatus of Plant Cells' Immunocytochemical Analysis of High-Pressure Frozen-and Freeze-Substituted Sycamore Maple Suspension Culture Cells.

Zheng, H., Fischer Von Mollard, G., Kovaleva, V., Stevens, T.H., and Raikhel, N. V. (1999). The Plant Vesicle-associated SNARE AtVT11a Likely Mediates Vesicle Transport from the Trans-Golgi Network to the Prevacuolar Compartment. *Mol. Biol. Cell* **10**: 2251–2264.

Zhong, R., Burk, D.H., Nairn, C.J., Wood-Jones, A., Morrison, W.H., Ye, Z.-H., and Ye, Z.-H. (2005). Mutation of SAC1, an Arabidopsis SAC domain phosphoinositide phosphatase, causes alterations in cell morphogenesis, cell wall synthesis, and actin organization. *Plant Cell* **17**: 1449–66.

Annex 1

Seeds used

Endomembrane compartments markers Waves Lines (Geldner et al., 2009)

Lines in italic used to make crossing

Name	Accession Number	Protein	Compartment	Fluorophore
SYP61-CFP	AT1G28490	Syntaxin of plant 61	TGN-SV	CFP
Wave127Y	AT5G50440	Membrin 12	Golgi apparatus	YFP
RabA2a-YFP	AT1G09630	RabA2a	TGN-CCV	YFP
Wave3R	<i>At1g43890</i>	<i>RabC1</i>	<i>Post-Golgi</i>	<i>mCherry</i>
Wave5R	<i>At3g18820</i>	<i>RabG3f</i>	<i>MVB/LE</i>	<i>mCherry</i>
Wave7R	<i>At5g45130</i>	<i>RabF2a</i>	<i>MVB/LE</i>	<i>mCherry</i>
Wave13R	<i>At1g26670</i>	<i>Vesicle transport v-SNARE 12, VT112</i>	<i>TGN/EE</i>	<i>mCherry</i>
Wave18R	<i>At3g03180</i>	<i>Got1p</i>	<i>Golgi apparatus</i>	<i>mCherry</i>
Wave22R	<i>At3g24350</i>	<i>Syntaxin of plant 32</i>	<i>Golgi apparatus</i>	<i>mCherry</i>
Wave25R	<i>At3g11730</i>	<i>RabD1</i>	<i>Golgi/Endosome</i>	<i>mCherry</i>
Wave34R	<i>At4g18430</i>	<i>RabA1e</i>	<i>RE</i>	<i>mCherry</i>
VhaA1R	<i>At2g28520</i>	<i>V-type proton ATPase subunit a1</i>	<i>TGN/EE</i>	<i>tagRFP</i>
VhaA3R	<i>At4g39080</i>	<i>V-type proton ATPase subunit a3</i>	<i>Vacuole</i>	<i>tagRFP</i>
SNX1R	<i>At5g06140</i>	<i>Sorting nexin 1</i>	<i>MVB/LE</i>	<i>tagRFP</i>
PIN2-GFP	AT5G57090	Auxin efflux carrier PIN2	PM	GFP

Name	Lipid Binding Domain	Lipid Targeted	Fluorophore	Resistance	
P3Y	1xPX ^{p40}	PI ₃ P	Citrine	Basta	Ho
P18Y	2xFYVE ^{HRS}	PI ₃ P	Citrine	Basta	Ho
P5Y	1xFAPP1	PI ₄ P and ARF1	Citrine	Basta	Ho
P4M	1xP4M	PI ₄ P	Citrine	Basta	Ho
P24Y	2xPH ^{PLC}	PI _{4,5} P ₂	Citrine	Basta	Ho

Phosphoinositide Biosensor Lines from Yvon Jaillais (Simon et al., 2014)

Annex 2

Stable lines generated

Stable line of *Arabidopsis thaliana* generated using Multisite Gateway® technology and done by floral dip in the ecotype Columbia-0

<u>Name</u>	<u>Accession Number</u>	<u>Construction</u>	<u>Resistance</u>	<u>Generation</u>
B.1.28.17	AT1G22620	pUB10::SAC1-mVenus	BASTA	F2
K.1.9.29	AT1G22620	pUB10::mVenus-SAC1	KANA	F2
B.1.28.39	AT1G22620	pUB10::SAC1-tagRFP	BASTA	F2
B.1.38.29	AT1G22620	pUB10::tagRFP-SAC1	BASTA	F2
B.1.7.17	AT3G54020	pUB10::IPCS1-mVenus	BASTA	F1
B.1.20'.17	AT1G30690	pUB10::Sec14p-mVenus	BASTA	F1
B.1.24.17	AT3G21690	pUB10::MATE3-mVenus	BASTA	F1
B.1.26.17	AT2G04100	pUB10::MATE2-mVenus	BASTA	F1
B.1.9.15	AT3G54020	pUB10::mVenus-IPCS1	BASTA	F1
B.1.9.16	AT2G37940	pUB10::mVenus-IPCS2	BASTA	F1
B.1.9.21'	AT1G30690	pUB10::mVenus-Sec14p	BASTA	F1
B.1.9.23'	AT4G30340	pUB10::mVenus-DGK7	BASTA	F1
K.1.9.30	AT5G61530	pUB10::mVenus-RhoGAP	KANA	F1
B.1.24.39	AT3G21690	pUB10::MATE3-tagRFP	BASTA	F1
B.1.26.39	AT2G04100	pUB10::MATE2-tagRFP	BASTA	F1
B.1.20.39	AT1G30690	pUB10::Sec14p-tagRFP	BASTA	F1
B.1.22.39	AT4G30340	pUB10::DGK7-tagRFP	BASTA	F1
B.1.35.39	AT5G61530	pUB10::RhoGAP-tagRFP	BASTA	F1
B.1.38.25	AT3G21690	pUB10::tagRFP-MATE3	BASTA	F1
B.1.38.27	AT2G04100	pUB10::tagRFP-MATE2	BASTA	F1
B.1.38.21'	AT1G30690	pUB10::tagRFP-Sec14p	BASTA	F1
B.1.38.23'	AT4G30340	pUB10::tagRFP-DGK7	BASTA	F1
B.1.38.30	AT5G61530	pUB10::tagRFP-RhoGAP	BASTA	F1

Annex 3

Crosses

Crosses already available thanks to Yvon Jaillais (ENS, Lyon)

PIPline Crosses					
PIPline	PIP Targeted	Marker	Protein	Localization	Zygoty
P3Y	PI3P	W3R	RabC1	Post-Golgi	Ho/Ho
		W5R	RabG3f	MVB/LE	Ho/Ho
		W13R	VTI12	TGN/EE	
		W18R	Got1p	Golgi	
		W22R	SYP32	Golgi	
		W24R	RabA5d	RE	
		W34R	RabA1e	RE	
		VhaA1R		TGN/EE	Ho/Ho
		VhaA3R		Tonoplast	Ho/Ho
P5Y	PI4P	W3R	RabC1	Post-Golgi	Ho/Ho
		W5R	RabG3f	MVB/LE	Ho/Ho
		W7R	RabF2a	MVB/LE	Ho/Ho
		W13R	VTI12	TGN/EE	Ho/Ho
		W18R	Got1p	Golgi	Ho/Ho
		W22R	SYP32	Golgi	Ho/Ho
		W34R	RabA1e	RE	Ho/Ho
		VhaA3R		Tonoplast	Ho/Ho
P18Y	PI3P	W7R	RabF2a	MVB/LE	
		W13R	VTI12	TGN/EE	Ho/Ho
		W22R	SYP32	Golgi	Ho/Ho
		W25R	RabD1	Golgi/Endosome	Ho/Ho
		W34R	RabA1e	RE	Ho/Ho
		VhaA1R		TGN/EE	Ho/Ho
		VhaA3R		Tonoplast	Ho/Ho
		SNX1R		MVB/LE	Ho/Ho
P21Y	PI4P	W13R	VTI12	TGN/EE	
		VhaA1R		TGN/EE	

Crosses I made in mutant background *ipcs1/ipcs2* inducible line and *sac1* mutant line (SAIL_262_C03)

		Cross	Marker 1	Marker 2	Generation
Induc-RNA-IPCSs	pER8::amiRNA-IPCSs	P4M	PM		F2
		P3Y	PI3P		F2
		P5Y	PI4P		F2
		P7Y	PI4P		F2
		P14Y	PI(4,5)P2		F2
		P15Y	PI(4,5)P2		F2
		P18Y	PI3P		F1
		P24Y	PI(4,5)P2		F2
		1xLACT1	PM		F2
		1xLACT2	PM		F1
		3xFAPP1	PI4P		F2
		1xFAPP1 E50A	PI4P		F2
		1xFAPP1 E50A H54A	PI4P		F2
		pUB10::YFP-2xC1a L1			F1
		mCherry-1xLACT C2			F1
		p35S::YFP-C1a L11			F1
		mCit-1xLACT2 C2			F1
		P3YxW3R	PI3P	Post-Golgi	F1
		P3YxW5R	PI3P	MVB/LE	F1
		P3YxW22R	PI3P	Golgi	F1
		P3YxVhaA1R	PI3P	TGN/EE	F1
		P3YxVhaA3R	PI3P	Tonoplast	F1
		P5YxW3R	PI4P	Post-Golgi	F1
		P5YxW5R	PI4P	MVB/LE	F1
		P5YxW7R	PI4P	MVB/LE	F1
		P5YxW13R	PI4P	TGN/EE	F1
		P5YxW18R	PI4P	Golgi	F1
		P5YxW34R	PI4P	RE	F1
		P18YxW13R	PI3P	TGN/EE	F1
		P18YxW22R	PI3P	Golgi	F1
		P18YxW25R	PI3P	Golgi/Endosome	F1
		P18YxW34R	PI3P	RE	F1
		P18YxVhaA1R	PI3P	TGN/EE	F1
P18YxVhaA3R	PI3P	Tonoplast	F1		
P18YxSNX1R	PI3P	MVB/LE	F1		
<i>sac1</i>	SAIL_262_C03	P4M	PM		F1
		P24Y	PI(4,5)P2		F1
		PIN2-GFP	PIN2		F1
		P3YxW5R	PI3P	MVB/LE	F1
		P3YxW13R	PI3P	TGN/EE	F1
		P3YxVhaA1R	PI3P	TGN/EE	F1
		P5YxW5R	PI4P	MVB/LE	F1
		P5YxW7R	PI4P	MVB/LE	F1
		P5YxW13R	PI4P	TGN/EE	F1
		P5YxW18R	PI4P	Golgi	F1
		P5YxW22R	PI4P	Golgi	F1
		P18YxW22R	PI3P	Golgi	F1
		P18YxVhaA1R	PI3P	TGN/EE	F1
		P18YxSNX1R	PI3P	MVB/LE	F1

Annex 4

Primers Used

Code	Name	Sequence
P5248	attB1-PIN2-Fw	GGGGACAAGTTTGTACAAAAAAGCAGGCTGGatgatcaccggcaaagacatgtac
P5249	attB2-PIN2-Rv	GGGGACCACTTTGTACAAGAAAGCTGGGTGagcccaaaagaacgtagtagag
P5250	attB2r-PIN2-Fw	GGGGACAGCTTTCTGTACAAAGTGGGatgatcaccggcaaagacatgtac
P5251	attB3-PIN2-Rv	GGGGACAACCTTTGTATAATAAAGTTGGttaaagcccaaaagaacgtag
P5252	attB1-FKBP1-Fw	GGGGACAAGTTTGTACAAAAAAGCAGGCTGGatggcgctgcaagtcgagac
P5253	attB2-FKBP1-Rv	GGGGACCACTTTGTACAAGAAAGCTGGGTGttctagttcagtagttcc
P5254	attB2r-FKBP1-Fw	GGGGACAGCTTTCTGTACAAAGTGGGatggcgctgcaagtcgagac
P5255	attB3-FKBP1-Rv	GGGGACAACCTTTGTATAATAAAGTTGGtcattctagttcagtagttccacg
P5266	LB-GABI	ATATTGACCATCATACTCATTGC
P5267	LBb1.3-Salk	ATTTTGCCGATTTTCGGAAC
P5268	LB_6313R-Salk	TCAAACAGGATTTTCGCCTGCT
P5358	attB1-PIN2-Fw	GGGGACAAGTTTGTACAAAAAAGCAGGCTATatgatcaccggcaaagacatgtac
P5359	attB2-PIN2-Rv	GGGGACCACTTTGTACAAGAAAGCTGGGTTaagcccaaaagaacgtagtagag
P5360	attB2r-PIN2-Fw	GGGGACAGCTTTCTGTACAAAGTGGATatgatcaccggcaaagacatgtac
P5361	attB3-PIN2-Rv	GGGGACAACCTTTGTATAATAAAGTTGGttaaagcccaaaagaacgtagta
P5362	attB1-eGFP-Fw	GGGGACAAGTTTGTACAAAAAAGCAGGCTGGatggtgagcaagggcgagga
P5363	attB2-eGFP-Rv	GGGGACCACTTTGTACAAGAAAGCTGGGTGgaagttcaccttgatgccgttc
P5364	attB2r-eGFP-Fw	GGGGACAGCTTTCTGTACAAAGTGGATatggtgagcaagggcgagga
P5365	attB3-eGFP-Rv	GGGGACAACCTTTGTATAATAAAGTTGGttagaagttcaccttgatgccgttc
P5366	attB1-RFP-Fw	GGGGACAAGTTTGTACAAAAAAGCAGGCTGGatgtcagaactatcaaggaaaa
P5367	attB2-RFP-Rv	GGGGACCACTTTGTACAAGAAAGCTGGGTGtttatgtccaatttactagggaaa
P5368	attB2r-RFP-Fw	GGGGACAGCTTTCTGTACAAAGTGGATatgtcagaactatcaaggaaaa
P5369	attB3-RFP-Rv	GGGGACAACCTTTGTATAATAAAGTTGGttattatgtccaatttactaggg
P5370	LB3-4-SAIL	TAGCATCTGAATTTTCATAACCAATCTCGATACAC
P5371	MSBP1-Fw-PhSalk	aaactcagtcaccagcagcgcg
P5372	MSBP1-Rv-PhSalk	GCTCCTCCTCCGTGATCTCACCGA
P5373	MSBP1-Fw-PhGabi	ATGGCGTTAGAACTATGGCAAA
P5374	MSBP1-Rv-PhGabi	TCCTCCTGGTCCGTAGAACATC
P5375	MSBP2-Fw-Ph	ATCAAGGGCCAGATCTATGATG
P5376	MSBP2-Rv-Ph	AGGCAGTCTTTGCTTCGGAAGG
P5377	MSBP3-Fw-Ph	Tgtatgacttcggccctgttc
P5378	MSBP3-Rv-Ph	CCAACAACAGGGGAACCTTGATAGAAC
P5388	CACC-PIN2-Fw	CACCatgatcaccggcaaagacatgtac
P5389	PIN2-Rv	aagcccaaaagaacgtagtagag
P5402	CACC-eBFP2-Fw	CACCatggtgagcaagggcgag
P5403	eBFP2w/oSTOP-Rv	cttgtagctcgtccatgccgag
P5642	attB1-AT1G30690-Fw	GGGGACAAGTTTGTACAAAAAAGCAGGCTGGatgactgctgaagttaagg
P5643	attB2-AT1G30690-Rv	GGGGACCACTTTGTACAAGAAAGCTGGGTGggaagaggattcagctctgg
P5644	attB2r-AT1G30690-Fw	GGGGACAGCTTTCTGTACAAAGTGGGatgactgctgaagttaagg
P5645	attB3-AT1G30690-Rv	GGGGACAACCTTTGTATAATAAAGTTGGtcaggaagaggattcagctctgg
P5646	attB1-AT4G30340.1-Fw	GGGGACAAGTTTGTACAAAAAAGCAGGCTGGatggaggagacgccgagatc
P5647	attB2-AT4G30340.1-Rv	GGGGACCACTTTGTACAAGAAAGCTGGGTGttgccattgatcattaacg
P5648	attB2r-AT4G30340.1-Fw	GGGGACAGCTTTCTGTACAAAGTGGGatggaggagacgccgagatc
P5649	attB3-AT4G30340.1-Rv	GGGGACAACCTTTGTATAATAAAGTTGGtcattcgcattgatcattaacg
P5650	attB1-AT3G21690.1-Fw	GGGGACAAGTTTGTACAAAAAAGCAGGCTGGatggactcgtctccaaacg
P5651	attB2-AT3G21690.1-Rv	GGGGACCACTTTGTACAAGAAAGCTGGGTGttcaggaacaactctgtttc
P5652	attB2r-AT3G21690.1-Fw	GGGGACAGCTTTCTGTACAAAGTGGGatggactcgtctccaaacg
P5653	attB3-AT3G21690.1-Rv	GGGGACAACCTTTGTATAATAAAGTTGGtcattcaggaacaactctgt
P5654	attB1-AT2G04100.1-Fw	GGGGACAAGTTTGTACAAAAAAGCAGGCTGGatggaagatccactttattggg
P5655	attB2-AT2G04100.1-Rv	GGGGACCACTTTGTACAAGAAAGCTGGGTGagcaagttcattgccaatg

P5656	attB2r-AT2G04100.1-Fw	GGGGACAGCTTTCTGTACAAAGTGGGGatggaagatccacttttattggg
P5657	attB3-AT2G04100.1-Rv	GGGGACAACCTTTGTATAATAAAGTTGGTcaagcaagccattgccaaatg
P5658	attB1-AT1G22620.1-Fw	GGGGACAAGTTTGTACAAAAAGCAGGCTGGatggcgaaatcggaaaactc
P5659	attB2-AT1G22620.1-Rv	GGGGACCACTTTGTACAAGAAAGCTGGGTGaatgaccttcgggacctatc
P5660	attB2r-AT1G22620.1-Fw	GGGGACAGCTTTCTGTACAAAGTGGGGatggcgaaatcggaaaactc
P5661	attB3-AT1G22620.1-Rv	GGGGACAACCTTTGTATAATAAAGTTGGTtaaagaccttcgggacc
P5662	attB1-AT5G61530.1-Fw	GGGGACAAGTTTGTACAAAAAGCAGGCTGGatgccttctctcatctcac
P5663	attB2-AT5G61530.1-Rv	GGGGACCACTTTGTACAAGAAAGCTGGGTGcctccatacagtctcggtgc
P5664	attB2r-AT5G61530.1-Fw	GGGGACAGCTTTCTGTACAAAGTGGGGatgccttctctcatctcac
P5665	attB3-AT5G61530.1-Rv	GGGGACAACCTTTGTATAATAAAGTTGGTcacctccatacagtctcggtgc
P5765	CACC-PIN2-2.0-Fw	cacctctcgcggaaaaagtaa
P5766	PIN2-2.0-Rv	atcacctttgggtcgatcg
P5767	Half-attB1-PIN2-Fw	AAAAAGCAGGCTGGatgatcaccggcaagacatg
P5768	Half-attB2-PIN2-Rv	AGAAAGCTGGGTTccccaaaagaacgtagtagag
P5769	LB4-FLAG	CGTGTGCCAGGTGCCACGGAATAGT
P5795	Sec14p-G-Fw	AAGGATATCGAGCTTTGGGG
P5796	Sec14p-G-Rv	AGGAGCTGGGATTTTCGATGG
P5797	MATE3-G-GK84-Fw	CTCTTTAACCTCGCTGCACC
P5798	MATE3-G-GK84-Rv	CGTAGCCGTTGAGATATAAGCA
P5799	MATE3-G-SSSG-Fw	acacttctccgctacagaca
P5800	MATE3-G-SSSG-Rv	GTTGCTCCATTTGTCCAACCT
P5801	MATE2-G-Fw	tctttgtcactaaatcgccc
P5802	MATE2-G-Rv	CCGAGTCAAAGGTTGTTGCA
P5803	RhoGAP-G-Fw	aggtttgatgatcggattgct
P5804	RhoGAP-G-Rv	acattcttgcgagtaacttca
P5805	DGK7-G-GG-Fw	cggcccatatgtcacatct
P5806	DGK7-G-GG-Rv	AAGCTCACCGAGACATCCAA
P5807	DGK7-G-G-Fw	GGTCGTCATGGCTCTGTTCT
P5808	DGK7-G-G-Rv	TCGAGCAATGGAACCTAAAGT
P5809	DGK7-G-S-Fw	GGAGAAGTCGTTGATCCTCTC
P5810	DGK7-G-S-Rv	Cgtacacacaaaacaaaccag
P5811	SACdoPI-G-S03-Fw	gcttggttggttttgga
P5812	SACdoPI-G-S03-Rv	GTGCCTGCAAAATGTGAGAGA
P5813	SACdoPI-G-Sail-Fw	cggatactggagctcaagtt
P5814	SACdoPI-G-Sail-Rv	acCTGACAGAATTGGGCGTA
P5815	SACdoPI-G-S02-Fw	TGCAACTTGACTGGCTTTC
P5816	SACdoPI-G-S02-Rv	tgtacaaaagaacaaaagtgagg
P5825	attB4-pPIN2-Fw	GGGGACAACCTTTGTATAGAAAAGTTGGGactgaattcatgttttgaagga
P5826	attB1r-pPIN2-Rv	GGGGACTGCTTTTTTGTACAAACTTGGtttgattacttttccggcg
P5827	attB2r-tPIN2-Fw	GGGGACAGCTTTCTGTACAAAGTGGGGgttattatcaaaacgtatttgcaataaaagcg
P5828	attB3-tPIN2-Rv	GGGGACAACCTTTGTATAATAAAGTTGGTgggaggtgtatatgtgctga
P5829	Seq-DGK7-Fw	GAGACTAGCGATGCCTGAGT
P5830	Seq-DGK7-Rv	GCAGCCGCctaaacgataa
P5831	Seq-MATE3-Fw	TGTGACGAGTGAGAGGTGTC
P5832	Seq-MATE3-Rv	AGGACAGGTTGGATTCCGTT
P5833	Seq-SAC1-Fw	ttccgttgtttggcctcag
P5834	Seq-SAC1-Rv	GCCAGTCCAAGTTGCAGAAA
P5879	Xba1-eBFP-Fw	GATTCTAGAatggtgagcaagggcgag
P5880	Xba1-eBFP-Rv	TTATCTAGactgtacagctcgtccatgccggag
P5881	attB1-TagRFP-Fw	GGGGACAAGTTTGTACAAAAAGCAGGCTGGATGGTGTCTAAGGGCGAAGAG
P5882	attB2-TagRFP-Rv	GGGGACCACTTTGTACAAGAAAGCTGGGTGATTAAGTTTGTGCCCAAGTTTC
P5883	attB2r-TagRFP-Fw	GGGGACAGCTTTCTGTACAAAGTGGATATGGTGTCTAAGGGCGAAGAG
P5884	attB3-TagRFP-Rv	GGGGACAACCTTTGTATAATAAAGTTGGTCAATTAAGTTTGTGCCCAAG
P5885	attB3-PIN2-2.0-Rv	GGGGACAACCTTTGTATAATAAAGTTGGTtaaagccccaaaagaacgtagtagag
P5909	PINseq-Fw	aatcttcaaagtgacgtgttac
P5910	PINseq-Rv	CTTCCCGGTGACATGTTCTC
P5943	MATE2-G-Fw-2	atctctgcatgtagtgggtt

P5944	MATE2-G-Rv-2	ACCAAACCCTGAGTCTGGAG
P5945	RhoGAP-G-Fw-2	cgtcttcgtcgtctttgatcg
P5946	RhoGAP-G-Rv-2	GGCCGCctaaagagaaaaca
P5947	FKBP1-Xbal-Fw	TATTCTAGAatggcgctgcaagtcgagac
P5948	FKBP1-Xbal-Rv	CGGTCTAGAttctagtttcagtagttcc
P5949	FKBP1-KpnI-Fw	TATGGTACCatggcgctgcaagtcgagac
P5950	FKBP1-KpnI-Rv	CGGGGTACCttctagtttcagtagttcc
P5951	TagRFP/BFP2-Xbal-Fw	CTATCTAGAATGGTGTCTAAGGGCGAAGAG
P5952	TagBFP2-Xbal-Rv	GTCTCTAGAATTAAGCTTGTGCCCCAGTT
P5953	TagRFP/BFP2-KpnI-Fw	CTAGGTACCATGGTGTCTAAGGGCGAAGAG
P5954	TagBFP2-KpnI-Rv	GTCGGTACCATTAAGCTTGTGCCCCAGTT
P5955	attB1-TagRFP/BFP2-Fw	GGGGACAAGTTTGTACAAAAAGCAGGCTGGATGGTGTCTAAGGGCGAAG
P5956	attB2-TagRFP-Rv	GGGGACCACTTTGTACAAGAAAGCTGGGTGATTAAGTTTGTGCCCCAG
P5957	attB2r-TagRFP/BFP2-Fw	GGGGACAGCTTCTTGTACAAAGTGGATATGGTGTCTAAGGGCGAAG
P5958	attB3-TagRFP-Rv	GGGGACAACCTTTGTATAATAAAGTTGTCAATTAAGTTTGTGCCCC
P5959	attB2-TagBFP2-Rv	GGGGACCACTTTGTACAAGAAAGCTGGGTGATTAAGCTTGTGCCCCAG
P5960	attB3-TagBFP2-Rv	GGGGACAACCTTTGTATAATAAAGTTGTCAATTAAGCTTGTGCCCC
P5961	TagRFP-Xbal-Rv	GTCTCTAGAATTAAGTTTGTGCCCCAG
P5962	TagRFP-KpnI-Rv	GTCGGTACCATTAAGTTTGTGCCCCAG
P6004	MATE2-G-Fw-3	TCGAGACCTCTGTTCTTTCCA
P6005	MATE2-G-Rv-3	TTCTCTGTCTTGCCCTGGCA
P6006	RhoGAP-G-Fw-3	ttgatgcccgttgattgagttt
P6007	RhoGAP-G-Rv-3	CACATGATCACTGGAGCCAT
P6064	attB4-pMATE3	GGGGACAACCTTTGTATAGAAAAGTTGGGtacctgcataatgtcataa
P6065	attB1r-pMATE3	GGGGACTGCTTTTTTGTACAACTTGGgatgatgatggagatttgc
P6066	attB4-pMATE2	GGGGACAACCTTTGTATAGAAAAGTTGGGcggttctatgactacaatt
P6067	attB1r-pMATE2	GGGGACTGCTTTTTTGTACAACTTGGtatcttcttgagatcttt
P6068	attB1-mTagBFP2-NEW	GGGGACAAGTTTGTACAAAAAGCAGGCTGGATGAGCGAGCTGATTAAGGAG
P6069	attB2r-mTagBFP2-NEW	GGGGACAGCTTCTTGTACAAAGTGGATATGAGCGAGCTGATTAAGGAG
P6070	PIN2-GFP-Seq2-Fw	TTCTATTCTCCTCACGACA
P6071	PIN2-GFP-Seq2-Rv	attattagtacttacTTGAA
P6072	PIN2-GFP-SeqMid-Fw	GAAGGGCATCGACTTCAAGG
P6073	attB2r-Opt-eGFP-Fw	GGGGACAGCTTCTTGTACAAAGTGGGGATGGTATCCAAGGGTGAAG
P6074	attB3-Opt-eGFP-Rv	GGGGACAACCTTTGTATAATAAAGTTGGTTATTTATAGAGCTCGTCC
P6075	attB1-Opt-eGFP-Fw	GGGGACAAGTTTGTACAAAAAGCAGGCTGGATGGTATCCAAGGGTGAAG
P6076	attB2-Opt-eGFP-Rv	GGGGACCACTTTGTACAAGAAAGCTGGGTGTTTATAGAGCTCGTCCATA
P6077	attB4-pPIN1-Fw	GGGGACAACCTTTGTATAGAAAAGTTGGGtacctttatgatattaaa
P6078	attB1r-pPIN1-Rv	GGGGACTGCTTTTTTGTACAACTTGGcttttgttcgcccggagaag
P6079	attB2r-tPIN1-Fw	GGGGACAGCTTCTTGTACAAAGTGGGGagagatattacaaaacac
P6080	attB3-tPIN1-Rv	GGGGACAACCTTTGTATAATAAAGTTGGttagtgtaagataaagccc
P6170	FKBP1-EcoRI-Fw	TATGAATTcatggcgctgcaagtcgagac
P6171	FKBP1-EcoRI-Rv	CGGGAATTCtctagtttcagtagttcc
P6222	FKBP1-Fw	ATGGGCGTGCAGTCCGAG
P6223	FKBP1-Rv	GTTTCAGTAGTCCACGTCGA
P6318	attB4-pPIN1-Fw-bis	GGGGACAACCTTTGTATAGAAAAGTTGGGgcataatttgatgcaaaacatg
P6428	attB1-PIN1-Fw	GGGGACAAGTTTGTACAAAAAGCAGGCTGGATGATTACGGCGGGGACTT
P6429	attB2-PIN1-Rv	GGGGACCACTTTGTACAAGAAAGCTGGGTGTCATAGACCCAAGAGAATG
P6430	attB3-tPIN2-Rv2	GGGGACAACCTTTGTATAATAAAGTTGGgagtaataattgtacttgc
P6431	attB3-tPIN1-Rv2	GGGGACAACCTTTGTATAATAAAGTTGGtgatattttccttaag
P6432	attB2-PIN2/STOP-Rv	GGGGACCACTTTGTACAAGAAAGCTGGGTGTTAAAGCCCCAAAAGAACGT
P6441	PIN1-BfF-Fw	ACGGTGGTCCTGCTAAACCG
P6442	PIN1-AfTag-Rv	CTCATAGCCGCCGCAAAGC
P6467	eGFP-opt-Fw	ATGGTATCCAAGGGTGAAGAG
P6468	eGFP-opt-Rv	TTTATAGAGCTCGTCCATACC
P6469	eGFP-opt-KpnI-Fw	TATGGTACCATGGTATCCAAGGGTGAAGAG
P6470	eGFP-opt-KpnI-Rv	CGGGGTACCTTTATAGAGCTCGTCCATACC
P6471	51-RestPos-Fw	GTCCGTTTCATCTTCACATTG

P6472	51-RestPos-Rv	CAGCCATTACGCTCGTCATC
P6473	TagRFP-Rv	ATTAAGTTTGTGCCCCAGTTTGC
P6474	TagRFP-Fw	ATGGTGTCTAAGGGCGAAGAGC
P6517	attB1-At1g14820	GGGGACAAGTTTGTACAAAAAAGCAGGCTGGATGGAGGAAAGCCAAGAAC
P6519	attB1-At2g43160	GGGGACAAGTTTGTACAAAAAAGCAGGCTGGATGAAGAAAGTCTTCGGAC
P6521	attB1-At1g75170	GGGGACAAGTTTGTACAAAAAAGCAGGCTGGATGTTTCGCTGGAAGAATTC
P6523	attB1-At3g26990	GGGGACAAGTTTGTACAAAAAAGCAGGCTGGATGGGTAGTTCATTTAACGC
P6525	attB1-At1g27100	GGGGACAAGTTTGTACAAAAAAGCAGGCTGGATGGAGCTATTCACAAAAGG
P6527	attB2r-At1g75170	GGGGACAGCTTTCTTGACAAAAGTGGGGATGTTTCGCTGGAAGAATTC
P6528	attB3-At1g75170	GGGGACAACCTTTGTATAATAAAGTTGGTCAAGGGTGGTTTTGGATTG
P6529	attB2r-At1g14820	GGGGACAGCTTTCTTGACAAAAGTGGGGATGGAGGAAAGCCAAGAAC
P6530	attB3-At1g14820	GGGGACAACCTTTGTATAATAAAGTTGGCTAACATTATTGTTTGTAG
P6531	attB2r-At2g43160	GGGGACAGCTTTCTTGACAAAAGTGGGGATGAAGAAAGTCTTCGGAC
P6532	attB3-At2g43160	GGGGACAACCTTTGTATAATAAAGTTGGTTACCGGTATCCACCACC
P6533	attB2r-At3g26990	GGGGACAGCTTTCTTGACAAAAGTGGGGATGGGTAGTTCATTTAACGC
P6534	attB3-At3g26990	GGGGACAACCTTTGTATAATAAAGTTGGCTACTGGCGAGTGACAGGTG
P6535	attB2r-At1g27100	GGGGACAGCTTTCTTGACAAAAGTGGGGATGGAGCTATTCACAAAAGG
P6536	attB3-At1g27100	GGGGACAACCTTTGTATAATAAAGTTGGCTAGAGGCTCGCGCTGGAGG
P6537	LBa1	TGGTTCACGTAGTGGGCCATCG
P6538	B2-Fw	ATGAACGAAATTGGGTTCTCC
P6539	B2-Rv	AAACCTCCTTATCTTCCGCTG
P6540	B1-Fw	AGGACGTAACCAGAGGGGTAG
P6541	B2-Rv	CGTTGTGACCCGTCATTAATC
P6542	SID2-Fw	ACCCTAATTTGGATTTGGTGC
P6543	SID2-Rv	AGCTCTAGGCCTAGTTGCAGC
P6573	attB2-At1g14820w/STOP	GGGGACCACCTTTGTACAAGAAAGCTGGGTGAACATTATTGTTTGTAGAG
P6574	attB2-At2g43160w/STOP	GGGGACCACCTTTGTACAAGAAAGCTGGGTGCCGGTATCCACCACCATAGG
P6575	attB2-At1g75170w/STOP	GGGGACCACCTTTGTACAAGAAAGCTGGGTGAGGGTGGTTTTGGATTGGCTC
P6576	attB2-At3g26990w/STOP	GGGGACCACCTTTGTACAAGAAAGCTGGGTGCTGGCGAGTGACAGGTGTAATAG
P6577	attB2-At1g27100w/STOP	GGGGACCACCTTTGTACAAGAAAGCTGGGTGGAGGCTCGCGCTGGAGGGTAG
P6601	miRNA-SP-Fw	AGCTGTGCTCTCTCTCTGTCAATGAAGACTAATCTTTTTCTC
P6602	attB2r-miRNA-Fw	GGGGACAGCTTTCTTGACAAAAGTGGGGAGCTGTGCTCTCTCTCTGTCA
P6603	Linker-BFP2-Rv-P	ACCAGCACCCGCATTAAGCTTGTGCCCCAGTTTGC
P6604	Linker-FKBP-Fw-P	GCTGGTGTGGTATGGGCGTGCAAGTCGAGAC
P6605	attB3-Rv	GGGGACAACCTTTGTATAATAAAGTTG
P6622	attB3-KKRY-Rv	GGGGACAACCTTTGTATAATAAAGTTGGTCAATATCTTTTCTGTGC

ARTICLE

Received 20 Oct 2015 | Accepted 29 Jul 2016 | Published 29 Sep 2016

DOI: 10.1038/ncomms12788

OPEN

Enrichment of hydroxylated C24- and C26-acyl-chain sphingolipids mediates PIN2 apical sorting at *trans*-Golgi network subdomains

Valérie Wattelet-Boyer¹, Lysiane Brocard², Kristoffer Jonsson³, Nicolas Esnay¹, Jérôme Joubès¹, Frédéric Domergue¹, Sébastien Mongrand¹, Natasha Raikhel⁴, Rishikesh P. Bhalerao^{3,5}, Patrick Moreau^{1,2} & Yohann Boutté¹

The post-Golgi compartment *trans*-Golgi Network (TGN) is a central hub divided into multiple subdomains hosting distinct trafficking pathways, including polar delivery to apical membrane. Lipids such as sphingolipids and sterols have been implicated in polar trafficking from the TGN but the underlying mechanisms linking lipid composition to functional polar sorting at TGN subdomains remain unknown. Here we demonstrate that sphingolipids with α -hydroxylated acyl-chains of at least 24 carbon atoms are enriched in secretory vesicle subdomains of the TGN and are critical for *de novo* polar secretory sorting of the auxin carrier PIN2 to apical membrane of *Arabidopsis* root epithelial cells. We show that sphingolipid acyl-chain length influences the morphology and interconnections of TGN-associated secretory vesicles. Our results uncover that the sphingolipids acyl-chain length links lipid composition of TGN subdomains with polar secretory trafficking of PIN2 to apical membrane of polarized epithelial cells.

¹UMR 5200 Membrane Biogenesis Laboratory, CNRS-University of Bordeaux, Bâtiment A3 - INRA Bordeaux Aquitaine, 71 Avenue Edouard Bourlaux - CS 20032, 33140 Villenave d'Ornon, France. ²Bordeaux Imaging Center, UMS 3420 CNRS, US4 INSERM, University of Bordeaux, 33000 Bordeaux, France. ³Umeå Plant Science Centre, Department of Forest Genetics and Plant Physiology, Swedish University for Agricultural Sciences, SE-901 83 Umeå, Sweden. ⁴Center for Plant Cell Biology, Department of Botany and Plant Sciences, University of California, Riverside, California 92521, USA. ⁵College of Science, KSU, 11451 Riyadh, Saudi Arabia. Correspondence and requests for materials should be addressed to Y.B. (email: yohann.boutte@u-bordeaux.fr).

The *trans*-Golgi network (TGN) is a heterogeneous tubulo-vesiculated post-Golgi structure, which matures from the Golgi, with distinct membrane subdomains that aid in the sorting and segregation of cargos to different cell compartments such as the plasma membrane (PM), vacuole and endosomes. Importantly, TGN plays a central role in trafficking of cargo that is deposited to highly specialized domains of the cell, for example, lipids and proteins destined to apical membrane through polar delivery^{1–3}. Examples of such polar transport to apical membrane include the influenza virus haemagglutinin of Madin–Darby canine kidney cells and PIN2, an auxin efflux carrier localized to the apical membrane of root epithelial cells in plants^{4–6}. Sphingolipids (SLs) are proposed to play a key role in polar delivery of proteins to PM. This suggestion is based on several lines of evidence. For example, during the course of polarization of animal epithelial cells, fatty acids (FAs) chain length and hydroxylation of SLs increase⁷. In *Caenorhabditis elegans*, apico-basal polarity conversion is observed in mutants for FAs and SLs biosynthetic enzymes⁸. Moreover, in budding yeast, TGN-derived vesicles involved in polar exocytosis are enriched in SLs and sterols⁹. Although these data support a role of SLs in polarity and polar delivery of proteins to PM, how these lipids mediate polar secretory sorting from the TGN is currently not well understood.

In this study, we used the polarized epithelium of roots from the plant model *Arabidopsis thaliana* and took advantage of the well-established auxin efflux carrier PIN2 protein, for which the localization is polar at apical membrane of root epithelial cells⁶. In plants, coordination of morphogenesis heavily relies on the phytohormone auxin. Polar auxin transport allows directionality of short distance auxin fluxes and mediates concentration of auxin at defined areas of plants to modulate growth patterns and axes^{10–14}. Modulation of root growth axis in response to a change in gravity (gravitropism) is known to rely on apical polarity of PIN2 in root epidermal cells^{6,15,16}. Hence, attenuation of root gravitropism is a good readout for possible defects in apical polarity in root epithelial cells. PIN2 polarity at apical membrane is known to hinge on PM recycling, defined endocytosis at the edge of the polar domain and clustering of PIN2 in small domains of PM⁵. PM recycling of PIN2 is partly mediated by the Exo70A1 and sec8 proteins of the exocyst complex and the nucleotide exchange factor for ARF GTPases (ARF-GEF) GNL1, which localizes to the Golgi apparatus^{17,18}. Interestingly, PIN2 recycling at apical membrane is also dependent on the ARF GTPase ARF1A1C/BEX1, which localizes both to the Golgi apparatus and to TGN¹⁹. Hence, Golgi apparatus and TGN appear to be playing a central role in PM recycling of PIN2 and its apical polarity at PM. Intriguingly, fluorescence recovery after photobleaching experiments indicate that PIN2 is apically delivered through uncharacterized polar exocytosis/delivery mechanisms⁵.

Here we show that, in *Arabidopsis*, subdomains of TGN are distinguished by differences in SL and sterol composition. We show that TGN-associated secretory vesicles (SVs) are enriched in sterols and α -hydroxylated very-long-chain FAs (hVLCFAs) containing 24 (h24) or 26 (h26) atoms of carbon. Inversion of the FAs ≥ 24 /FAs ≤ 24 ratio within the pool of SLs, without interfering with global quantity of SLs, results in a loss of PIN2 polarity at apical membrane and *de novo* secretory blockage of PIN2 in SVs. Moreover, this inversion also has impacts on the morphology of TGN-associated SVs and tubular membrane interconnections established between SVs. Altogether, our results reveal a role for the length of α -hydroxylated acyl chains of SLs, enriched at TGN, in secretory trafficking to apical membrane of polarized epidermal cells.

Results

SVs subdomain of TGN is enriched in hVLCFAs of SLs. To investigate the role of SLs in polar exocytosis, we analysed distribution of SLs in TGN. In *Arabidopsis* root cells, the TGN population labelled by the syntaxin SYP61 is distinct from another TGN population labelled by the RAB-GTPase RAB-A2a^{20–23}. Ultra-structural analyses by electron tomography have shown that SYP61 localizes to SVs at TGN²⁴. Interestingly, a conserved protein ECHIDNA (ECH) strongly co-localizes with SYP61 but weakly with clathrin heavy chain (CHC)²², whereas RAB-A2a, but not SYP61, strongly co-localized with CHC (Fig. 1a–g). Hence, TGN-associated SVs are marked by SYP61/ECH, whereas TGN-associated clathrin-coated vesicles (CCVs) are marked by RAB-A2a and represent two distinct subdomains of TGN. We used an immuno-isolation procedure yielding highly purified intact TGN compartments²⁵ in transgenic *Arabidopsis* plants expressing either the TGN-localized syntaxin SYP61 fused to the fluorescent tag cyan fluorescent protein (CFP)²⁶ or RAB-A2a fused to yellow fluorescent protein (YFP)²⁰ (Fig. 1h). In addition, a Golgi marker, the Qb-SNARE Membrin12 (MEMB12) fused to YFP was used to isolate Golgi compartment^{27,28}. We performed co-localization analyses between MEMB12–YFP and the Golgi marker MEMB11, for which we characterized the localization at the Golgi apparatus previously by electron microscopy²⁹. Our results show a strong co-localization between MEMB12–YFP and MEMB11 (Supplementary Fig. 1a–c), indicating that MEMB12–YFP is a good marker to isolate Golgi apparatus. Moreover, co-localization between MEMB12–YFP and either ECH (Supplementary Fig. 1g–i) or CHC (Supplementary Fig. 1m–o) is low. Thus, Golgi labelled with MEMB12–YFP/MEMB11 are distinct from TGN-associated SVs labelled by SYP61–CFP/ECH and from TGN-associated CCVs labelled by RAB-A2a–YFP/CHC.

Western blottings of SYP61–CFP, MEMB12–YFP and RAB-A2a–YFP immunopurified (IP) fractions, loaded to equal amount (Supplementary Fig. 2a), using anti-green fluorescent protein (GFP) antibodies showed enrichment of targeted compartments in the IP output (beads coupled to GFP antibodies, IP) compared with the IP input (total membrane (TM) fraction; Fig. 1i). We estimated the fold enrichment by quantifying the mean intensity of signals obtained on western blotting and evaluated that SYP61–CFP compartment was 9.5 ± 0.2 (\pm indicates s.d., $n = 3$) fold enriched, MEMB12–YFP was 9.2 ± 0.4 (\pm indicates s.d., $n = 3$) fold enriched and RAB-A2a was 9.3 ± 0.3 (\pm indicates s.d., $n = 3$) fold enriched, as compared with the IP input (TM fraction). Importantly, TGN markers ECH (anti-ECH) and SYP61 (anti-SYP61) were enriched in SYP61–CFP IP fraction, whereas ECH was neither detected in MEMB12–YFP nor in RAB-A2a–YFP IP fractions (Fig. 1i) in agreement with previous data showing minimal co-localization between ECH and RAB-A2a or Golgi markers²¹. Furthermore, SYP61 protein was only weakly detected in MEMB12–YFP or RAB-A2a–YFP IP fractions (Fig. 1i), whereas the Golgi marker SEC21 (anti-SEC21) and the Golgi marker MEMB11 (anti-MEMB11) were both enriched in MEMB12–YFP IP fraction and only weakly detected in SYP61–CFP or RAB-A2a–YFP IP fractions (Fig. 1i). These results strongly suggest the successful separation of the TGN subdomain SYP61–CFP/ECH/SVs from either the TGN subdomain RAB-A2a–YFP/CCVs or the Golgi apparatus by the IP isolation protocol. We also tested the presence of V-ATPase of the VHA-E family using an antibody recognizing VHA-E1, VHA-E2 and VHA-E3 subunits, which localize both to vacuoles and TGN, reflecting the secretion pathway to vacuoles through TGN³⁰. We detected signals in SYP61, RAB-A2a or MEMB12 IPs, but as compared with the IP input (TM fraction) we did not detect any enrichment of VHA-E

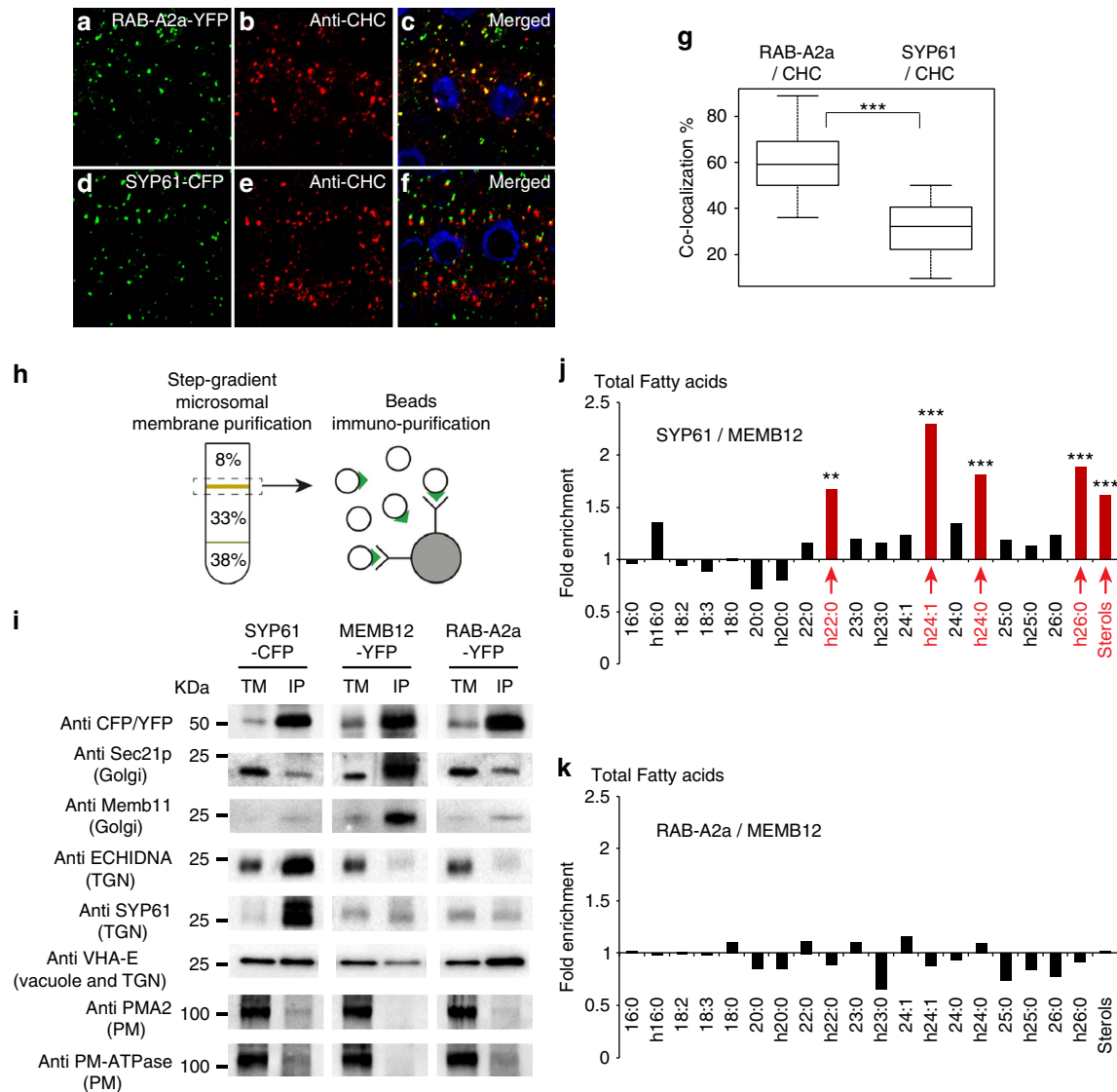


Figure 1 | TGN subdomain labelled by SYP61 is enriched in hVLCFAs and sterols as compared with Golgi or TGN subdomain RAB-A2a enriched for clathrin. (a–g) Immunolocalization of CHC (b,e) in *Arabidopsis* root epithelial cells expressing either the TGN marker RAB-A2a-YFP (a) or the TGN marker SYP61-CFP (d). Strong co-localization between RAB-A2a and CHC is detected in merged images (c), whereas weaker co-localization is visualized between SYP61 and CHC (f,g). Statistical analysis show highly significant difference between RAB-A2a/CHC co-localization and SYP61/CHC co-localization ($n = 50$ cells distributed over 10 roots for each experiment, 3 biological replicates). (h) Immunopurifications of SYP61-CFP-, MEMB12-YFP- and RAB-A2a-YFP-labelled compartments were performed by incubating a step-gradient-purified TM fraction with beads coated with anti-CFP/YFP antibodies. (i) Western blottings on IP SYP61-CFP-, RAB-A2a-YFP- and MEMB12-YFP-labelled intact vesicles. IP, beads-IP fraction; TM, input, step-gradient-purified TM fraction. As compared with the input (TM), anti-CFP/YFP antibodies revealed that all protein markers (SYP61-CFP, MEMB12-YFP or RAB-A2a-YFP) are enriched in their targeted IP compartments. Sec21p and MEMB11 markers of the Golgi apparatus are enriched in IP MEMB12-YFP-labelled Golgi but not in IP SYP61-CFP-labelled TGN or RAB-A2a-YFP-labelled TGN. The ECHIDNA and SYP61 markers of TGN-associated secretory vesicles are enriched in IP SYP61-CFP-labelled TGN but not in MEMB12-YFP-labelled Golgi or RAB-A2a-YFP-labelled TGN. V-ATPase VHA-E, which traffic through the TGN, is not enriched in SYP61-immunopurified or MEMB12-immunopurified fraction but is slightly enriched in IP RAB-A2a-YFP-labelled TGN. The PMA2 and PM-ATPase markers for PM are not enriched in any IP compartments. (j,k) Acyl-chain composition of the total pool of FAs contained in IP fractions. (j) As compared with MEMB12-YFP-labelled Golgi, SYP61-CFP-labelled TGN shows a significant enrichment (about 2-fold, $n = 11$ IPs for each compartment, 11 biological replicates for each compartment) in hVLCFAs h22:0, h24:1, h24:0, h26:0 and sterols. (k) As compared with MEMB12-YFP-labelled Golgi, RAB-A2a-YFP-labelled TGN does not display any enrichment in hVLCFAs or sterols ($n = 11$ IPs for each compartment, 11 biological replicates for each compartment). Statistics were done by two-sided Wilcoxon's rank-sum test, ** P -value < 0.01 , *** P -value < 0.001 . All scale bars, 5 μ m.

in SYP61 IPs, whereas VHA-E was even strongly depleted in Golgi MEMB12 IPs (Fig. 1i). Interestingly, enrichment of VHA-E was detected in RAB-A2a IPs, which is consistent with the description of clathrin-dependent trafficking from TGN to vacuoles^{31,32} and our previous finding that RAB-A2a strongly co-localizes with clathrin (Fig. 1a–c,g). To check PM

contamination we used two different ATPases of the PM: PMA2 and PM-H⁺-ATPase. As compared with IP input (purified TM fraction), very weak signal was detected for PMA2 and PM-H⁺-ATPase in SYP61, MEMB12 and RAB-A2a IP output fractions (beads coupled to GFP antibodies) (Fig. 1i). These results confirmed that PM contaminations were negligible in isolated

SYP61, RAB-A2a or MEMB12 populations. Altogether, these results indicate that IP allows high level of separation of SYP61/SVs, RAB-A2a and MEMB12/Golgi compartments.

Following the successful isolation of the SYP61-, RAB-A2a- and MEMB12-enriched IP fractions, we quantified lipids in these fractions by gas chromatography coupled to a mass spectrometer (GC-MS). As compared with GC coupled to a Flame ionization detector (GC-FID), we found that, when running the same mass (50 μ g) of individual FAs with various chain length in either GC-MS or GC-FID, areas of corresponding FA peaks were highly similar between GC-MS and GC-FID for all FAs chain length tested (Supplementary Fig. 2b). This validates the use of GC-MS to quantify FAs with diverse chain length. Our results show strong enrichment of the hVLCFAs h22:0, h24:1, h24:0 and h26:0 in SYP61-CFP IP fraction as compared with Golgi/MEMB12-YFP IP fraction (Fig. 1j). Enrichment of sterols was also observed in SVs/SYP61-CFP IP fraction compared with Golgi/MEMB12-YFP IP fraction (Fig. 1j). Interestingly, sterol and FAs composition of RAB-A2a-YFP were not different from that of the Golgi fraction (Fig. 1k). To identify which lipids contain h22:0, h24:1, h24:0 and h26:0, we then analysed FA composition of various lipid pools in *Arabidopsis* root. The FAs of glycerophospholipids contained only traces (2.3%) of α -hydroxylated FAs (hFAs; Fig. 2a,d). In contrast to glycerophospholipids, FAs of the SL glucosylceramide (GlcCer) contained 74% of hFAs (Fig. 2b,d). As in plants, glycosyl-inositol-phosphoryl-ceramides (GIPCs) are the most preponderant SLs³⁵, we also analysed FA composition within the pool of GIPCs. Our results indicated that in *Arabidopsis* root, FAs of GIPCs contained 83.5% of hFAs (Fig. 2c,d). In conclusion, our results suggest an enrichment of GIPCs and GlcCer rather than glycerophospholipids in SYP61 compartment of the TGN and, importantly, the h22:0, h24:1, h24:0 and h26:0 appears to dominate in the GIPCs and GlcCer in TGN/SYP61 compartment in the *Arabidopsis* roots.

Metazachlor alters hVLCFAs in the pool of SLs. Our data indicate that hVLCFAs are a characteristic defining feature of TGN/SYP61 compartments. Hence, we searched for pharmacological tools enabling us to modify chain-length composition of hFAs in SLs. Metazachlor, a chloracetamide-based herbicide, is a known inhibitor of VLCFA synthesis that directly targets the 3-ketoacyl CoA synthase (KCS) enzymes of the elongase complex, which condense two carbons at a time on a preexisting FAs chain³⁴. In this study, we found that metazachlor was an ideal tool to alter VLCFAs without decreasing the total quantity contained in each pools of lipids. Global analyses of FAs composition in *Arabidopsis* roots of 5-day-old seedlings revealed that 50 nM metazachlor strongly decreases h24:0, h24:1, h26:0 and h26:1 hFAs, whereas we observed an accumulation of h16:0 and h20:0 hFAs (Fig. 3a). Metazachlor also decreases non-hydroxylated 22:0 and 24:0 FAs and ω -hydroxylated 22:0 and 24:0 FAs (22:0 ω -OH and 24:0 ω -OH) (Fig. 3a). No effects of 50 nM metazachlor treatment is observed on C16- and C18-containing FAs (Fig. 3b), which are the most abundant FAs, suggesting that the *de novo* FAs synthesis is not altered by metazachlor. Our results show that when we summed up all types of FAs <24 (Fig. 3c) and all type of FAs >24 (Fig. 3d) atoms of carbon, we could clearly see that the FAs <24/FAs >24 ratio is inverted on metazachlor (Fig. 3c,d). The ratio FAs <24/FAs >24 (Fig. 3c,d) also suggests that hFAs are the most altered by metazachlor. As we show in Fig. 2d that hFAs are almost exclusively present in SLs, we guessed that metazachlor would target more the pool of SL than other lipids. Hence, to

check how specific metazachlor is towards distinct classes of lipids, we next analysed individual classes of lipids in *Arabidopsis* roots treated with 50 nM metazachlor.

Our results indicate that metazachlor neither alters the total quantity of individual sterols, nor the quantity of FAs from glycerophospholipids, GlcCer or GIPCs pools (Fig. 2e). In addition, metazachlor treatment did not induce formation of tri-acyl-glycerol (TAG), indicating that our conditions did not create any redistribution of lipid metabolism from membrane lipids to storage lipids (Supplementary Fig. 2c). Moreover, metazachlor did not alter FAs composition of dicarboxylic acids and fatty alcohols compounds (Fig. 3a), which are known to be contained in the suberin polymer³⁵. Instead, upon metazachlor we detected a strong decrease of h24:1, h24:0 and h26:0 in both GIPCs and GlcCer pools (Fig. 2b,c). Decrease of non-hydroxylated 24:0 was also observed in the pool of FAs of glycerophospholipids, but non-hydroxylated 24:0 FAs represent only 2% of the pool of glycerophospholipids (Fig. 2a), whereas they represent more than 10% of the pool of GIPCs (Fig. 2c). Concomitantly, accumulation of hFAs, for which acyl chain length is under 24 carbons (\leq h24), was observed on metazachlor treatment in pools of GlcCer and GIPC (Fig. 2b,c). Altogether, our results indicate that metazachlor is a unique tool to drastically invert the ratio between FAs \leq 24 and FAs \geq 24 within the pool of SLs (GlcCer and GIPCs) without decreasing their total quantity or significantly altering the pool of glycerophospholipids.

Metazachlor alters root gravitropism. In *A. thaliana*, modulation of root growth axis in response to change in gravity (gravitropism) is known to rely on apical polarity of PIN2 in epidermal cells^{6,15,16}. Hence, attenuation of gravitropic response provides a reliable readout for any defects in trafficking or polar localization of PIN2. To evaluate root gravitropism, we measured the angle formed between the root and the new gravity vector 24 h after a 90° turn (Fig. 4a). We ranked values into classes of 15° angles (0° was the exact direction of the new gravity vector) and represented every class of angles in a circular chart. Metazachlor treatment strongly altered the gravitropic response as measured by the reorientation of root growth axis after 24 h following gravistimulation (Fig. 4b,c and Supplementary Fig. 3a,b). Kinematic analyses showed that metazachlor-treated roots displayed very slight and slow response to change in the direction of gravity (Supplementary Fig. 3c). Importantly, 50 nM metazachlor did not strongly affect root length compared with mock-treated roots (Supplementary Fig. 3d). Thus, metazachlor effect on root graviresponse was not due to defect in root elongation *per se*.

Metazachlor targets KCS enzymes during gravitropism. Inhibition of activity of several KCS enzymes by metazachlor was previously shown by expressing a number of *Arabidopsis* KCS (KCS1, KCS2, KCS5/CER60, KCS6/CER6, KCS17, KCS18/FAE1 and KCS20) in yeast³⁴. As our study uses root gravitropism as a phenotypic readout for apical PIN2 polarity, we used publicly available micro-arrays data sets and previously published expression studies of KCS genes and found that among KCS enzymes targeted by metazachlor, KCS1, KCS2, KCS17 and KCS20 are highly expressed or expressed at medium level in primary roots^{36,37}. Moreover, we also found that KCS4 and KCS9 are highly expressed or expressed at medium level in primary roots^{36,37}. Previous studies have characterized reduction of C22- and C24-containing FAs accompanied by accumulation of C20-containing FAs in *kcs2,20* double knockout mutant and reduction of C24-containing FAs accompanied by accumulation of C20- and C22-containing FAs in *kcs9* knockout mutant^{38,39}.

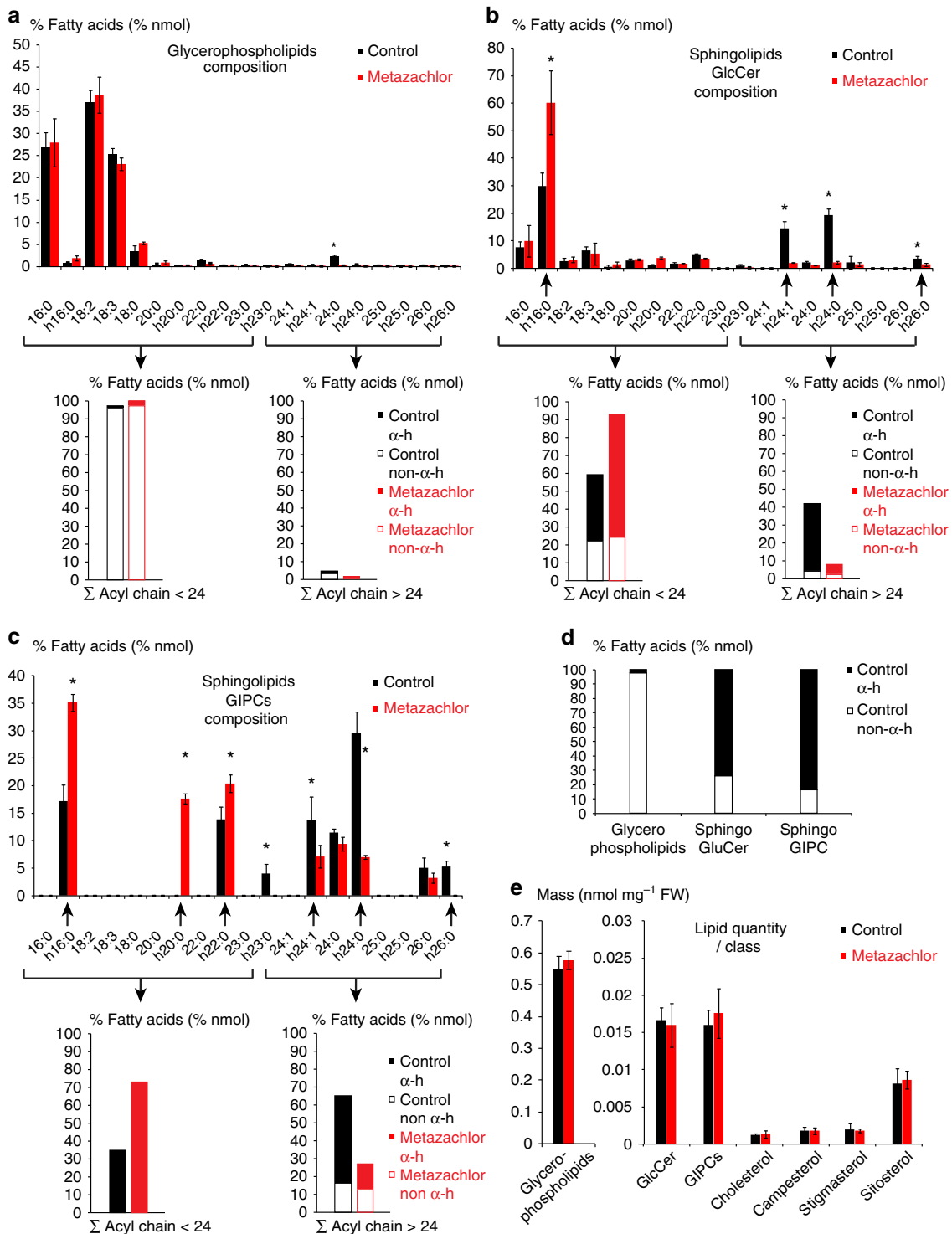


Figure 2 | hVLCFAs are almost specific of SLs and 50 nM metazachlor alters the composition of VLCFAs in the pool of SLs. In untreated *Arabidopsis* roots, the pool of FAs of glycerophospholipids (a) contains very few hFAs (d). Metazachlor significantly reduces the 24:0-containing FAs but does not alter the global composition of FAs of glycerophospholipids, which are mainly composed of C16- and C18-containing FAs. Arrowed brackets display the sum of <math>< 24</math> carbon atom-containing FAs and > 24 carbon atom-containing FAs. Each histogram is further divided in hFAs (α -h) and non-h FAs (non- α -h). The ratio between <math>< 24</math>- and > 24-FAs is not altered in the glycerophospholipids pool. (b,c) Contrastingly to glycerophospholipids, in untreated roots, FAs of GlcCer (b) and GIPCs (c) contain a substantial amount of hFAs (d). Interestingly, metazachlor strongly reduces α -hydroxylated h24:1, h24:0 and h26:0 and increases α -hydroxylated h16:0, h20:0 and h22:0 FAs of GlcCer and GIPCs pools. Arrowed brackets display the sum of <math>< 24</math> carbon atom-containing FAs and > 24 carbon atom-containing FAs. Each histogram is further divided in hFA α -h and non-hFA non- α -h. The ratio between <math>< 24</math>- and > 24-FAs is drastically inverted in both GlcCer and GIPCs pool. (e) Metazachlor neither alters the global quantity of FAs of the glycerophospholipids pool nor the global quantity of FAs of the GlcCer and GIPCs pools. Moreover, global quantities of individual sterols are not affected by metazachlor. Statistics were done by two-sided Wilcoxon's rank-sum test, * P -value < 0.05, $n = 4$ for each experiment, 4 biological replicates. Errors bars are s.d.

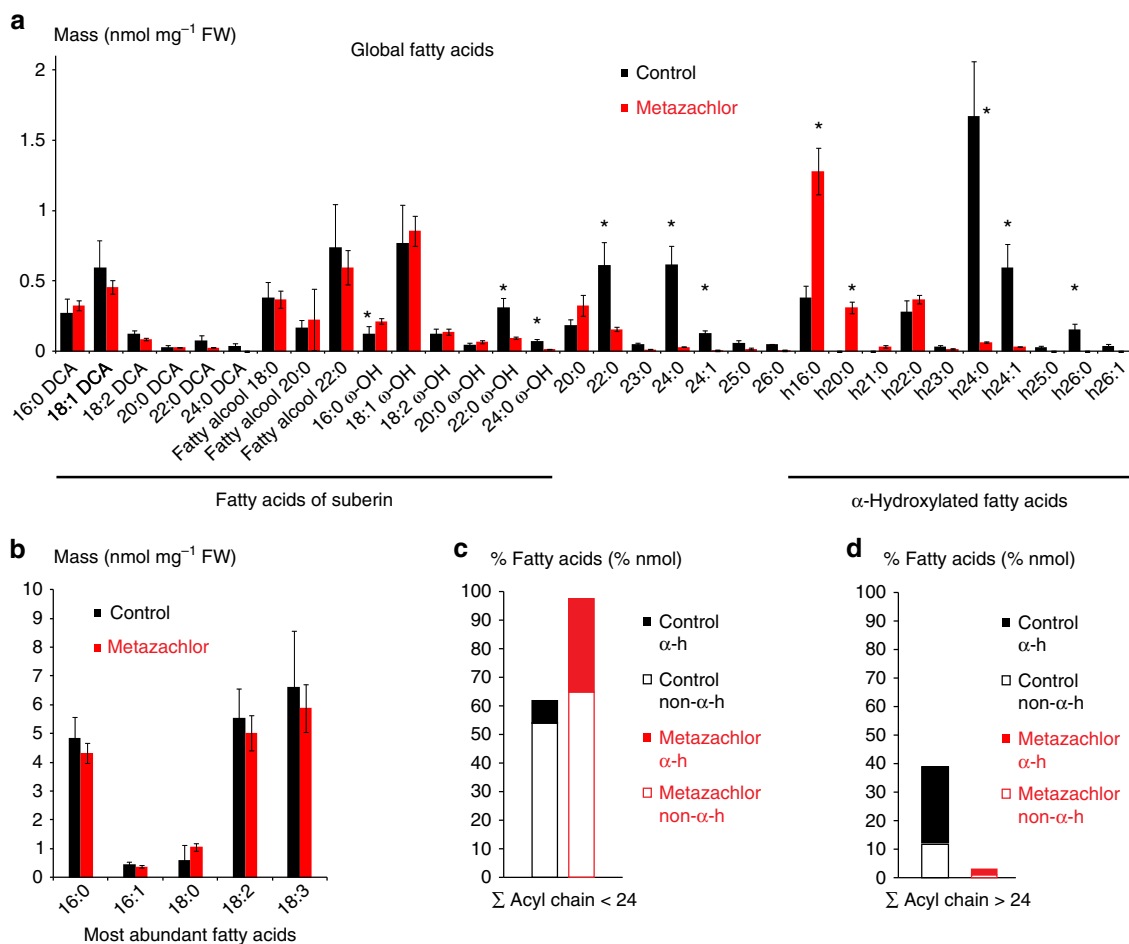


Figure 3 | Global FAs analysis reveals that metazachlor reduces all types of >24-FAs. (a) Global FAs of *Arabidopsis* roots in untreated (black) and metazachlor-treated (red) conditions. Compounds of the root suberin, dicarboxylic acid DCA and fatty alcohols are not altered by a 50 nM metazachlor treatment. However, ω -hVLCFAs, which are components are the root suberin, are significantly reduced on metazachlor. Non-hydroxylated C22 and C24-FAs, which are more abundant in GIPCs than in glycerophospholipids, are significantly reduced on metazachlor. hVLCFAs h22:0, h24:0, h24:1, h25:0, h26:0 and h26:1, almost exclusively present in GIPCs, are strongly reduced on metazachlor. Accumulation of h16:0 and h20:0 is observed on metazachlor. (b) Contrastingly to VLCFAs, metazachlor does not alter the quantity of C16- and C18-containing FAs ($n = 4$ for each experiment, 4 biological replicates). (c,d) Sums of <24 carbon atom-containing FAs (c) and > 24 carbon atom-containing FAs (d). Each histogram is further divided in hFAs (α -h) and non-hFAs (non- α -h). On metazachlor, the ratio between <24- and >24-FAs is drastically inverted. Statistics were done by two-sided Wilcoxon's rank-sum test, * P -value < 0.05, $n = 4$ for each experiment, 4 biological replicates. Error bars are s.d.

Hence, we analysed root gravitropism of *kcs9* single mutant and *kcs2,20* double mutant.

The *kcs9* single mutant or the *kcs2,20* double mutant do not display obvious root gravitropism phenotype in mock condition (Fig. 4d,f,h). However, root gravitropism defect is clearly seen when *kcs9* single mutant and *kcs2,20* double mutant are treated with 25 nM metazachlor (Fig. 4g,i), whereas wild-type roots do not significantly display gravitropism defect on 25 nM metazachlor treatment (Fig. 4d,e). To correlate root gravitropism phenotype and VLCFAs content, we quantified the total pool of VLCFAs and show that VLCFAs level is significantly and similarly reduced in roots of either *kcs9* single mutant, *kcs2,20* double mutant or 25 nM metazachlor-treated wild-type roots as compared with untreated wild type (Supplementary Fig. 4a). However, this level is far from being as low as a 50 nM metazachlor treatment on wild-type roots (Supplementary Fig. 4a). Contrastingly, a 25 nM metazachlor treatment on *kcs9* single mutant or the *kcs2,20* double mutant reduces VLCFAs content to similar level of a 50 nM metazachlor treatment on wild-type roots (Supplementary Fig. 4a). These results show that *kcs9* and *kcs2,20* double mutant are hypersensitive to metazachlor

with respect to VLCFAs level and gravireponse. This also suggests that KCS2, KCS20 and KCS9 are targets of metazachlor during root gravitropism, and that there is a threshold of VLCFAs quantity under which gravitropism defects are triggered. As we could not have the *kcs2,20,9* triple mutant available for this study, we cannot exclude that other KCS are also targeted by metazachlor during root gravitropism. However, root gravireponse of *kcs1*, *kcs4* or *kcs17* single mutants treated with 25 nM metazachlor is not different from their gravitropism phenotypes observed in mock conditions (Supplementary Fig. 4b–g). These results suggest that KCS1, KCS4 and KCS17 are not preferred targets of metazachlor in roots at the concentration used, although we cannot exclude the possibility that KCS1, 4 and 17 act redundantly and a triple mutant might be required to visualize an effect of a treatment with 25 nM metazachlor. Thus, our data suggests that KCS2, KCS20 and KCS9 are targeted by metazachlor in the roots. Interestingly, *kcs9* and *kcs2,20* double mutant have been shown to not only alter the level of VLCFAs and hVLCFAs but also the level of ω -hydroxylated-VLCFAs^{38,39}. Global FAs analysis performed on *Arabidopsis* roots treated with 50 nM metazachlor also showed that 22:0 ω -OH and 24:0 ω -OH were

reduced as compared with mock condition (Fig. 3a). To test whether 22:0 ω -OH and 24:0 ω -OH play a role in root gravitropism we used the *ralph/cyp86b1* mutant, which display almost complete absence of 22:0 ω -OH and 24:0 ω -OH in the root suberin without affecting the level of hFAs⁴⁰ (Supplementary Fig. 5a,b). Our results show that *ralph/cyp86b1* mutant does not display root gravitropism phenotype and is not hypersensitive to 25 nM metazachlor treatment (Supplementary Fig. 5c,d). These

results show that reduction of 22:0 ω -OH and 24:0 ω -OH does not attenuate gravitropism.

PIN2 localization and polarity depends on VLCFAs of SLs. We next used the AUX/IAA auxin-interaction domain DII fused to the fluorescent protein Venus (DII-venus) to visualize dynamic changes in cellular auxin distribution⁴¹. In untreated roots, 1 h gravistimulation resulted in a much weaker DII-venus fluorescent signal at the lower side of the root compared with the upper side of the root (Fig. 5a). In contrast, no such reduction in DII-venus fluorescent signal was observed in metazachlor-treated roots on gravistimulation (Fig. 5b,c). These results show that SL composition is important for auxin redistribution and gravitropic response. Auxin redistribution during root gravitropism is known to rely on the auxin influx carrier AUX1 and the auxin efflux carrier PIN2 (refs 6,15,16,42). Under control conditions, without metazachlor treatment, *aux1-21* or *pin2-eir1* mutants displayed similar response to gravistimulation (Fig. 5d,f). Interestingly, when the *aux1-21* mutant and the *pin2-eir1* mutant were subjected to metazachlor treatment, we could observe that metazachlor strongly enhances root gravitropism defect of the *aux1-21* mutant, while it only weakly enhanced *pin2-eir1* mutant phenotype (Fig. 5d–g). Although we cannot formally exclude the possibility that metazachlor treatment may target elements of gravitropic response in addition to PIN2, this appears less probable given the difference between *aux1-21* and *pin2-eir1* mutant response to metazachlor treatment. Importantly, we can conclude that modification of acyl-chain length of FAs by metazachlor targets a PIN2-mediated gravitropic response pathway rather than an AUX1-dependent pathway (Fig. 5d–g).

In agreement, we could not detect any changes in AUX1 localization on metazachlor treatment (Supplementary Fig. 6a,b). The ratio of fluorescence between the cell content and the whole PM (intracellular/PM) was identical for AUX1–YFP in metazachlor-treated roots compared with that in untreated roots (Supplementary Fig. 6c). Moreover, we did not detect any changes in localisation of PIN1 and PIN7 auxin efflux carriers, which are also involved in root gravitropism^{43,44} and which localize in a polar manner at the basal PM of cells (Supplementary Fig. 6d–l). PIN1–GFP either driven by its own promoter (pPIN1::PIN1–GFP) and expressed in vascular cells of roots (Supplementary Fig. 6d–f), or ectopically expressed in epidermal cells of roots using the promoter of PIN2 (pPIN2::PIN1–GFP2; Supplementary Fig. 6g–i), remained polarly localized at the basal membrane and did not display intracellular accumulation of PIN1–GFP on 50 nM metazachlor treatment (Supplementary Fig. 6d–i). Similarly, PIN7–GFP driven

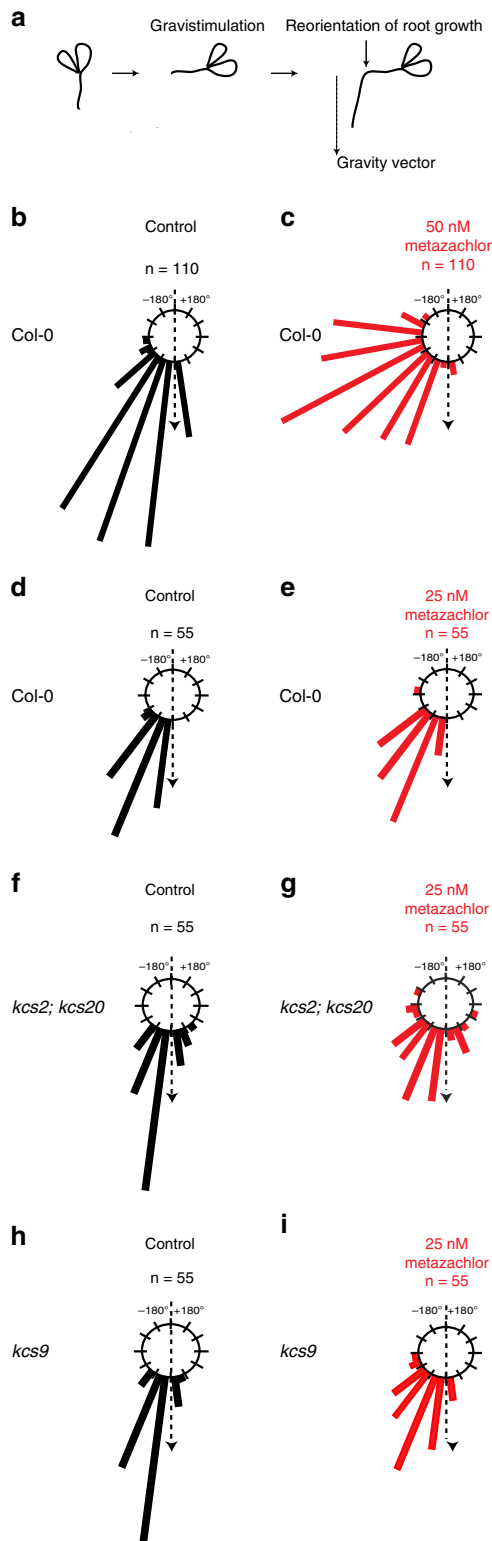


Figure 4 | Metazachlor alters root gravitropism and targets KCS9, KCS2 and KCS20.

(a) Root angle curvature towards the new gravity vector 24 h following a gravistimulation (turn the plate of 90°) is calculated, we then ranked the effective (n) into classes of 15° angles (0° was the exact direction of the new gravity vector) and represented each class of angles in a circular chart. (b) In untreated roots, reorientation of roots 24 h after a gravistimulation is very close to the gravity vector, whereas in 50 nM metazachlor-treated roots (c) this reorientation is much less efficient (n = 110 roots per experiment). (d–i) As compared with untreated roots (d), the *kcs2,20* double mutant (f) and *kcs9* single mutant (h) do not display gravitropism phenotype. On 25 nM metazachlor treatment, *kcs2,20* double mutant (g) and *kcs9* single mutant (i) display obvious root gravitropism phenotype, whereas wild-type roots treated with 25 nM of metazachlor (e) do not react. Hence, *kcs2,20* double mutant (f,g) and *kcs9* single mutant (h,i) are hypersensitive to metazachlor in respect to root gravitropism (n = 55 roots per experiment).

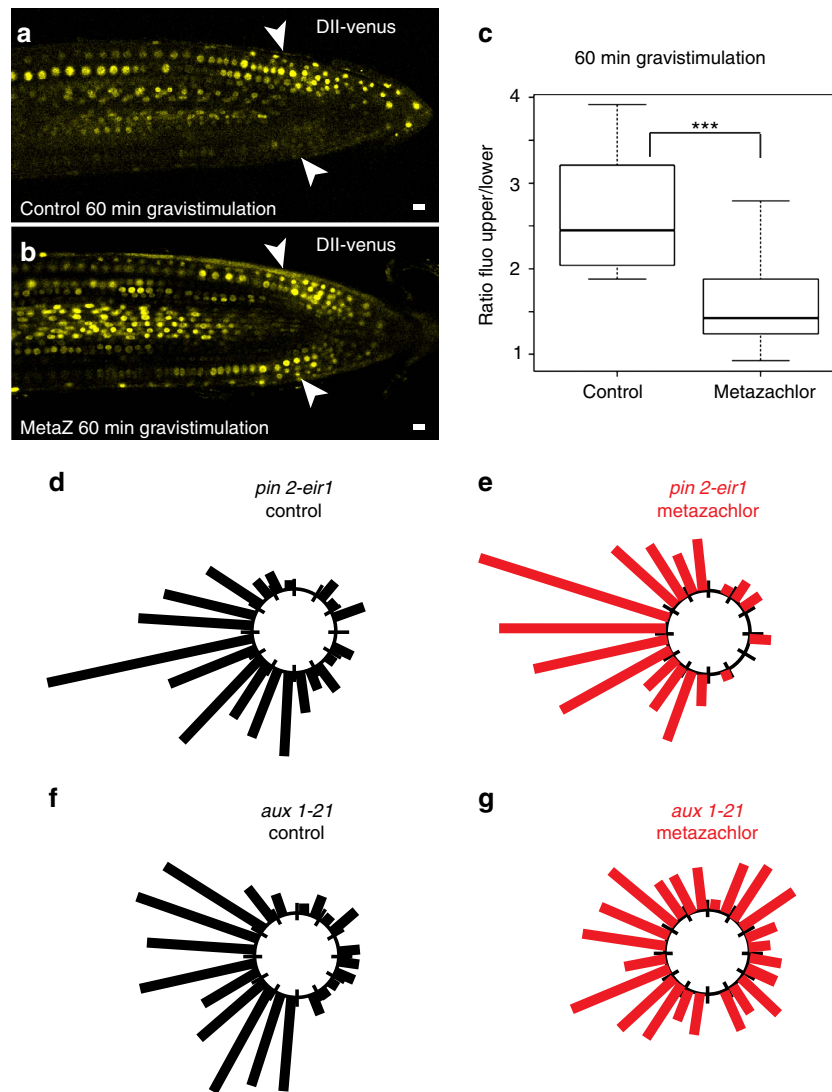


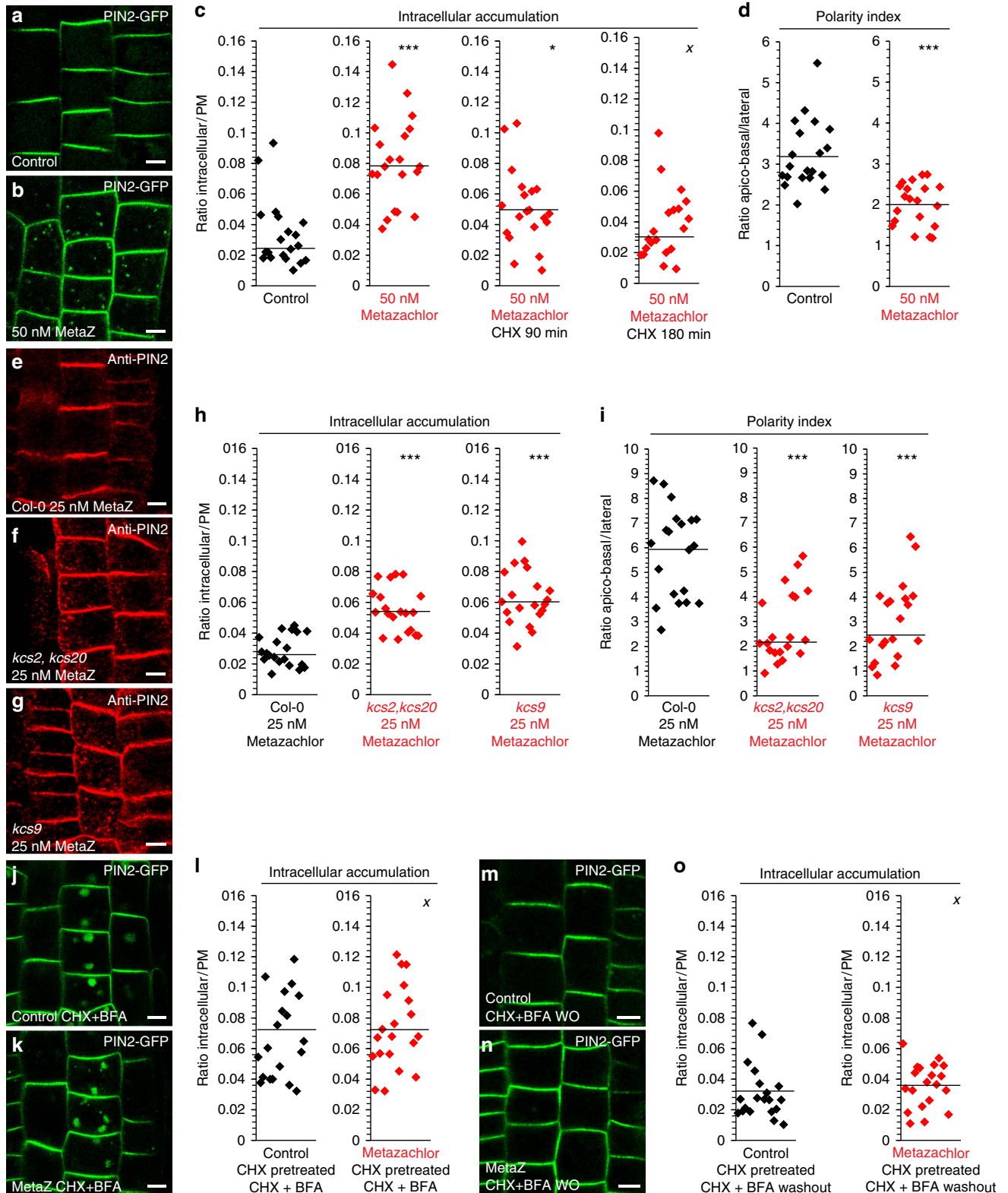
Figure 5 | Metazachlor alters auxin distribution during root bending partly through the auxin efflux carrier PIN2. (a,b) Dynamic auxin redistribution 60 min after a gravistimulation, visualized by DII-venus fusion, shows differential auxin distribution in untreated roots (a) with a higher concentration of auxin at the upper side of the root (a), whereas metazachlor-treated roots do not display this differential repartition of auxin after gravistimulation. (b,c) Quantification of signal intensities between the upper and lower side of gravistimulated roots clearly results in a highly significant difference ($n=10$ seedlings for each experiment over 3 biological replicates). (d-g) The auxin efflux carrier mutant *pin2-eir1* (d,e) and the auxin influx carrier mutant *aux1-21* (f,g) show similar phenotype in untreated roots (d,f) ($n=110$ root per genotype over 3 biological replicates). In metazachlor-treated roots, the *pin2-eir1* mutant (e) appears more resistant to metazachlor than the *aux1-21* mutant (g) ($n=110$ roots per genotype over 3 biological replicates). Statistics were done by two-sided Welch's two sample *t*-test, ****P*-value < 0.001. All scale bars, 10 μ m.

by its own promoter (pPIN7::PIN7-GFP) and expressed in vascular cells of roots also did not display localization defects when treated with 50 nM metazachlor (Supplementary Fig. 6j-l). In addition, in root epidermal cells the non-polar cargo SNARE protein NPSN12 fused to mCherry (Supplementary Fig. 6m-o) and the non-polar cargo aquaporin protein PIP1,4 fused to mCherry (Supplementary Fig. 6p-r) still localize at the PM and do not accumulate in intracellular compartments on 50 nM metazachlor treatment (Supplementary Fig. 6m-r). Contrastingly, in metazachlor-treated roots we observed a significant accumulation of the polar cargo PIN2-GFP in dotted structures and the ratio intracellular/PM was significantly higher compared with untreated roots (Fig. 6a-c). Accumulation of PIN2 in intracellular compartments was also detected in *kcs9* single mutant (Fig. 6e,g,h) and *kcs2,20* double mutant (Fig. 6e,f,h) treated with 25 nM metazachlor, the concentration at which

gravireponse is significantly attenuated in these mutants compared with wild type (Fig. 4d-i). In contrast, we did not detect intracellular accumulation of PIN2 in mock-treated *kcs9* single mutant or *kcs2,20* double mutant (Supplementary Fig. 7a-d) in agreement with the absence of root gravitropism phenotype in mock-treated *kcs9* single mutant or *kcs2,20* double mutants (Fig. 4d,f,h). Next, we investigated whether metazachlor impinges on polar localization of PIN2 as well (Fig. 6a,b,d). The ratio between fluorescence at apico-basal PM and lateral PM was significantly reduced for PIN2-GFP on metazachlor treatment (Fig. 6d). Moreover, PIN2 polarity at PM was also altered in *kcs9* single mutant (Fig. 6e,g,i) and *kcs2,20* double mutant (Fig. 6e,f,i) treated with 25 nM metazachlor. Together, these results show that PIN2 polarity at apical PM and PIN2 secretory trafficking at TGN are dependent on FAs ≥ 24 -acyl-chain length of SLs at the TGN.

VLCFAs of SLs are crucial for PIN2 secretory sorting at TGN. It has been shown earlier that TGN is a compartment where both secretory and endocytic/recycling pathways intersect^{30,45}. Hence, accumulation of PIN2 in intracellular compartment might be due to either alteration of secretion or alteration of endocytosis/recycling. Strikingly, treatment with the protein biosynthesis

inhibitor cycloheximide (CHX) nearly abolished PIN2-GFP accumulation in TGN/SYP61 compartments in wild-type seedlings treated with 50 nM metazachlor (Fig. 6c). These results strongly suggest that metazachlor blocks PIN2 secretory trafficking at TGN rather than PIN2 endocytosis at PM. However, it is still possible that attenuation of PIN2 polarity by metazachlor



may be due to metazachlor targeting endocytosis/recycling at the TGN. Therefore, we next addressed whether metazachlor affects PIN2 endocytosis/recycling. To visualize PIN2 endocytosis, we pretreated seedlings with CHX to exclude visualization of *de novo* synthesized PIN2-GFP. Seedlings were next treated with CHX and BrefeldinA (BFA), which induces intracellular accumulation of endocytosed PIN2-GFP in so-called 'BFA bodies'^{46,47} (Fig. 6j). We quantified that the ratio intracellular/PM increases identically between seedlings treated with metazachlor and metazachlor-free control (Fig. 6j–l). Moreover, when BFA was washed out, the ratio intracellular/PM decreased to the same level between metazachlor-treated and untreated seedlings (Fig. 6m–o). Previously, it has been shown that some types of SLs are involved in endocytosis and PM recycling of AUX1 and PIN1 potentially through RAB-A2a compartments that could then be considered as putative recycling endosomes⁴⁸. Our results suggest that modification of acyl chain length of SLs has impacts on *de novo* PIN2 delivery to apical PM without perturbing PIN2 endocytosis or PIN2 recycling.

Next, we identified which endomembrane compartment PIN2-GFP labelled on metazachlor treatment. Our results indicated that PIN2-GFP-labelled structures strongly co-localized with the TGN/SVs marker SYP61-CFP (Fig. 7a–c,p). PIN2-GFP-labelled structures also strongly co-localized with the RAB protein RAB-A5d fused to mCherry (Fig. 7d–f,p). Co-localization of RAB-A5d-mCherry with either the TGN/SVs marker ECHIDNA (ECH) or the TGN/CCVs marker CHC further indicated that RAB-A5d rather locates at SVs site of TGN (Supplementary Fig. 8a–c,g) rather than CCVs sites of TGN (Supplementary Fig. 8d–f,g). Hence, we could confirm with two independent markers that PIN2 accumulates at SVs sites of TGN on metazachlor. On metazachlor, only weak co-localization of PIN2 was observed with either the Golgi marker MEMB12 fused to mCherry (Fig. 7j–l,p) or with another Golgi marker, the syntaxin SYP32, fused to mCherry (Fig. 7m–o,p). Co-localization of PIN2-GFP-labelled structures and CLC-mOrange was higher than that observed for Golgi markers but much lower than what we observed for the two markers of SVs (Fig. 7g–i,p). Furthermore, metazachlor treatment did not abolish the separation of TGN from Golgi membranes as we did not detect a change in the amount of co-localization between the Golgi marker MEMB12-YFP with either the TGN/SVs marker ECH (Supplementary Fig. 1g–l,s) or the TGN/CCVs marker CHC (Supplementary Fig. 1m–r,s).

Altogether, these results suggest that on modification of acyl-chain length of SLs, PIN2 accumulates in a TGN subdomain labelled by SYP61 but not in a TGN subdomain labelled by clathrin or in the Golgi apparatus. These results are also consistent with the enrichment of hVLCFAs, which are almost exclusively contained in SLs (Fig. 2b,c), observed in immunoprecipitated SYP61 compartments compared with RAB-A2a or Golgi compartments observed in Fig. 1j,k.

Metazachlor alters the morphology of SVs at TGN. Although TGN is still able to separate from Golgi apparatus in metazachlor-treated roots, we investigated whether metazachlor would alter TGN ultrastructure. Using high-pressure freezing and freeze substitution we could clearly see by transmission electron microscopy that alteration of acyl-chain length of SLs by metazachlor resulted in morphology alteration of TGN. We focused on elongating cells, which are more difficult to preserve than meristematic cells but in which we clearly saw PIN2 localization defects. Moreover, cells in the elongation zone of the root mediate differential cell growth during root gravitropism and allow the bending of the root⁴⁹. In untreated cells, TGN appeared tubulovesiculated and SVs seemed to bud off from TGN tubules, while being progressively released (Fig. 8a). Contrastingly, in metazachlor-treated cells SVs of TGN appeared more swollen and seemed to remain in cluster (Fig. 8e). Quantification showed that in untreated cells the average diameter of SVs at TGN comprised between 60 and 100 nm (Fig. 8b). Contrastingly, average diameter of SVs in metazachlor-treated roots was rather comprised between 90 and 260 nm (Fig. 8f). Similar defects were also observed in roots chemically fixed with glutaraldehyde (Supplementary Fig. 9a,b), suggesting that enlarged diameter of SVs in metazachlor-treated roots were not due to potential ice crystals that could appear during the high-pressure freezing and freeze substitution procedure. In addition, we could observe in roots fixed by high-pressure freezing that although SVs were interconnected with tubules at TGN in untreated cells (Fig. 8c,d), metazachlor-treated cells hardly displayed SV-interconnecting tubules (Fig. 8g,h). These data show that acyl-chain length ≥ 24 of SLs is important for the machinery involved in regulating the size of SVs and the TGN membrane tubule network.

Discussion

To date, distinct subdomains of TGN have been recognized based on non-overlapping localization of TGN proteins, for example, SYP61 and RAB-A2a in plants. Our data now reveal that subdomains of TGN are not only marked by distinct proteins but also display differential distribution of SLs. We demonstrate that differential enrichment of hFAs that contain acyl-chain length ≥ 24 , almost exclusively present in SLs, are required for polar secretory sorting of apical-localized proteins, for example, PIN2 without affecting endocytosis or recycling. This is somehow reminiscent to what has been shown in yeast for the export from the endoplasmic reticulum (ER) of some glycosylphosphatidylinositol (GPI)-anchored proteins, which is sphingolipid dependent⁵⁰. The explanation of this sorting was proposed to be based on the chemical/physical properties of SLs and GPI anchored proteins, which produce specific associations and subsequently constitute specific endoplasmic reticulum export sites where other proteins could be excluded⁵⁰. Such specific SL-protein

Figure 6 | Reduction of VLCFAs alters apical polarity and secretory trafficking of PIN2 but not endocytosis and PM recycling of PIN2. (a–c) Compared with untreated cells (a), 50 nM metazachlor-treated cells (b) display intracellular accumulation of PIN2-GFP in endomembrane compartments. (c) Quantifications of fluorescence intensity ratios between the intracellular content and whole PM show a significant intracellular accumulation of PIN2-GFP in metazachlor-treated cells that is prevented by a pretreatment with 50 μ M CHX from already 90 min pretreatment. (d) Quantifications of fluorescence intensity ratios between the apical-basal membranes and lateral membranes clearly indicate a significant loss of PIN2 polarity. (e–i) Compared with wild-type roots treated with 25 nM metazachlor (e) *kcs2,20* double mutant (f) and *kcs9* single mutant (g) display intracellular accumulation of anti-PIN2 (Alexa647) in endomembrane compartments and loss of PM polarity of PIN2. (h) Quantifications of fluorescence intensity ratios between the intracellular content and whole PM. (i) Quantifications of fluorescence intensity ratios between the apical-basal membranes and lateral membranes. (j–l) 50 μ M BFA treatment, after a 50 μ M CHX pretreatment, show no significant differences (l) in PIN2-GFP accumulation from the PM to the so-called intracellular 'BFA bodies' between untreated cells (j,l) and metazachlor-treated cells (k,l), revealing that PIN2 endocytosis is not altered by metazachlor. (m–o) Washout of BFA in presence of CHX after a 50 μ M CHX pretreatment and 50 μ M BFA treatment show no significant differences (o) in PIN2 redistribution at PM from 'BFA bodies' between untreated cells (m,o) and metazachlor-treated cells (n,o). Statistics were done by two-sided Wilcoxon's rank-sum test, ^X*P*-value > 0.05, **P*-value < 0.05, ****P*-value < 0.001, *n* = 200 cells distributed over 20 roots for each experiment (3 biological replicates). All scale bars, 5 μ m.

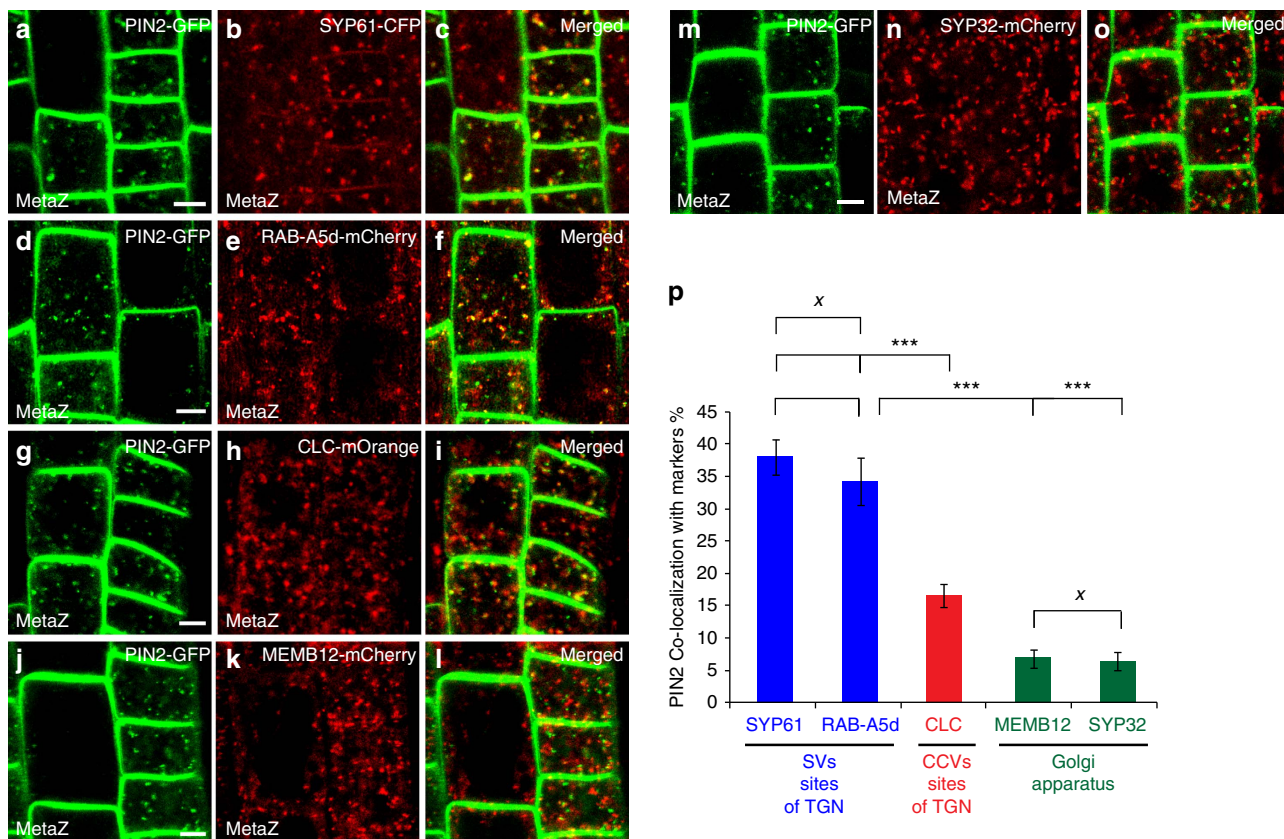


Figure 7 | Metazachlor accumulates PIN2 at SVs sites of TGN. (a–o) Co-localization of endomembrane compartments labelled by PIN2-GFP (a,d,g,j,m) and either SYP61-CFP-labelled TGN-associated SVs (b), RAB-A5d-mCherry-labelled TGN-associated SVs (e), CLC-mOrange-labelled TGN-associated CCVs (h), MEMB12-mCherry-labelled Golgi apparatus (k) or SYP32-mCherry-labelled Golgi apparatus (n) on 50 nM metazachlor. (c,f,i,o) Merged pictures of corresponding pictures. (g) Quantification of co-localization events show a strong match of PIN2 with TGN-associated-SYP61/RAB-A5d-SVs, whereas weak co-localization is detected with MEMB12/SYP32-Golgi. (p) Co-localization values of SYP61/RAB-A5d with PIN2 and MEMB12/SYP32 with PIN2 are highly different. PIN2 co-localizes at medial level with TGN-associated-CLC-Clathrin vesicles but is significantly different from co-localization of PIN2 with SYP61/RAB-A5d. Statistics were done by two-sided Kruskal-Wallis rank sum test, xP -value > 0.05, $^{***}P$ -value < 0.001, $n = 40$ cells distributed over 10 roots for each experiment (3 biological replicates). All scale bars, 5 μ m. Errors bars are s.e.m.

interactions were also recently demonstrated between a transmembrane protein and a C18-acyl-chain sphingomyelin species in animal cells⁵¹. In this study, we suggest that chemical/physical properties of acyl-chain length ≥ 24 of SLs govern PIN2 sorting at TGN. This could be achieved either by lipid-protein interactions as discussed above or by lipid-lipid interactions, or both. Indeed, at biochemical level it is well known that enrichment of SLs and sterols creates lateral auto-segregation of these lipids in micro-domains, for which the thickness and order of the bilayer is higher compared with the rest of the membrane^{52–56}. It is hypothesized that these differential membrane properties aid in membrane sorting of proteins but underlying mechanisms are not known. Our study now shows that acyl-chain length ≥ 24 of SLs play a key role in apical delivery of secretory cargo from TGN. In model membranes, it has been shown that C24-containing SLs display a distinct phase behaviour and membrane packing as compared with C16-containing SLs, which are mostly phase separated⁵⁷. Interestingly, C24-acyl chain of SLs can interdigitate with FAs of the opposing monolayer⁵⁸. Therefore, interdigitation of acyl-chain length ≥ 24 of SLs could contribute to segregation of PIN2 at TGN. The observation that specific subdomains of TGN are enriched in VLCFA-containing SLs, and that perturbing this distribution leads to defects in TGN structure and function indicates that subcompartmentalization of TGN hinges on the nature and the length of the acyl chain of SLs. Indeed, phase

separation induced by acyl-chain length of SLs is also directly linked to the shape of membranes, for example, vesicle versus tubule⁵⁹. In addition, VLCFAs of SLs were shown to favour tubular structures due to their ability to form interdigitated phases⁶⁰. Hence, concentration of VLCFA-containing SLs at the subdomain of the TGN where apical sorting occurs is fully consistent with the idea that phase separation at TGN is crucial to sorting. Our electron microscopy supports this hypothesis, as we observe less tubules versus vesicles when the length of acyl chains of SLs is shortened by metazachlor. Altogether, our results provide evidence for distinct SLs content of TGN subdomains and the importance of the length of acyl chains of SLs for polar sorting of proteins at TGN.

Methods

Plant material and growth conditions. The *A. thaliana* ecotype Colombia-0 (Col-0) and the following mutants were used: *pin2-eir1* (ref. 15), *aux1-21* (ref. 61), *kcs9* (ref. 38), *kcs2,20* (ref. 39), *kcs1* (GABI Kat GK-312G10), *kcs4* (SALK_095739C), *kcs17* (GABI Kat GK-128C11) and *ralph/cyp86b1* (ref. 40). The following transgenic fluorescent protein marker lines in Col-0 were used: pRAB-A2a::YFP-RAB-A2a²⁰, pSYP61::CFP-SYP61 (ref. 26), pUBQ10::YFP-MEMB12 (ref. 28), pUBQ10::mCherry-MEMB12 (ref. 28), pUBQ10::mCherry-RAB-A5d²⁸, pUBQ10::mCherry-SYP32 (ref. 28), pUBQ10::mCherry-NPSN12 (ref. 28), pUBQ10::mCherry-PIP1;4 (ref. 28), p35s::DII-venus⁴¹, pPIN2::PIN2-GFP⁶², pPIN1::PIN1-GFP¹², pPIN2::PIN1-GFP2 (ref. 13), pPIN7::PIN7-GFP¹¹ and pAUX1-AUX1-YFP⁶³. The p35s::CLC-mOrange fusion was in Wassilewskija background⁶⁴. Seeds were sown on half Murashige and Skoog (MS) agar medium plates (0.8% plant agar, 1% sucrose and 2.5 mM morpholinoethanesulfonic acid

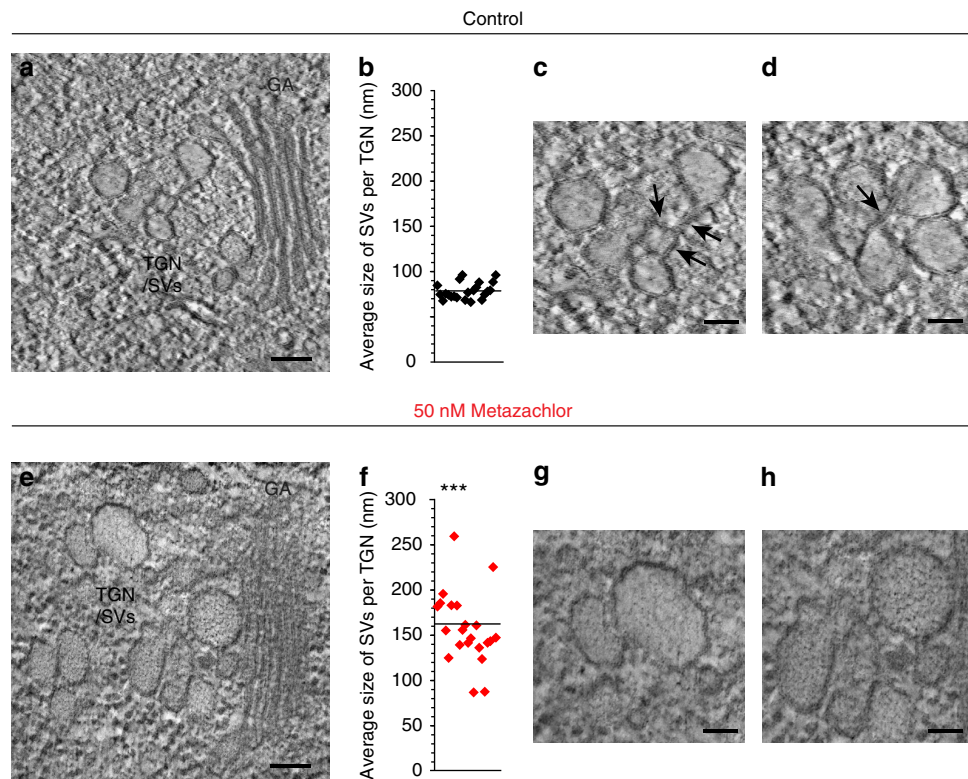


Figure 8 | Metazachlor alters TGN-associated SVs morphology and tubular interconnections at TGN. Transmission electron microscopy (TEM) of TGN membrane structures in *Arabidopsis* root treated (e–h) or not (a–d) with metazachlor. (a) Untreated cell showing Golgi apparatus (GA) and the SVs visible as a tubulo-vesiculated membrane network (SVs/TGN) at the *trans*-side of the Golgi. (e) Metazachlor-treated cell (50 nM) showing Golgi apparatus and swollen TGN-associated SVs. (b,f) Quantification show that the average diameter of SVs per TGN is around 80 nm in untreated cells (b), while being around 160 nm in metazachlor-treated cells ($n = 22$ TGN for each for each experiment over 3 biological replicates, statistics were done by two-sided Welch’s two-sample *t*-test, ****P*-value < 0.001). (f,c,d) Magnification from a displaying tubular interconnections (black arrows) between SVs at TGN in untreated cells. (g,h) Magnification from e displaying larger SVs without tubular interconnections detected between them. Scale bars, 100 nm (a,e) and 50 nm (c,d,g,h).

(Sigma) pH 5.8 with KOH, left at 4 °C for 2 days and then grown in 16 h light/8 h darkness for 5 days before all experiments exception made for gravitropism assays (described hereafter) and when obtaining plant material for immunoprecipitation (described hereafter).

Inhibitor treatments. For metazachlor (Greyhound Chromatography and Allied Chemicals) treatment, seedlings were grown on MS plates containing the drug at 50 nM in most experiments, except when specified. Metazachlor was added from a 100 mM stock in dimethylsulfoxide, an intermediate stock concentration at 100 μ M was used extemporarily to make the plates. For cycloheximide (CHX) and BFA treatments, seedlings were treated in liquid medium (LM) containing 1 \times MS, 1% sucrose, 2.5 mM morpholinoethanesulfonic acid pH 5.8. In BFA experiments, seedlings were first pretreated with 50 μ M CHX (Sigma) for 90 min and then treated with 50 μ M CHX and 50 μ M BFA for 90 min. Washout experiments were performed by washing in LM implemented with 50 μ M CHX for 90 min.

Immunocytochemistry and confocal laser scanning microscopy. Whole-mount immunolabelling of *Arabidopsis* root was performed as described⁶⁵. In brief, seedlings were fixed in 4% paraformaldehyde dissolved in MTSB (50 mM PIPES, 5 mM EGTA, 5 mM MgSO₄ pH 7 with KOH) for 1 h at room temperature (RT) and washed three times with MTSB. Roots were cut on superfrost slides (Menzel Gläser, Germany) and dried at RT. Roots were then permeabilized with 2% Driselase (Sigma), dissolved in MTSB for 30 min at RT, rinsed four times with MTSB and treated with 10% dimethylsulfoxide + 3% Igepal CA-630 (Sigma), and dissolved in MTSB for 1 h at RT. Aspecific sites were blocked with 5% normal donkey serum (NDS, Sigma) in MTSB for 1 h at RT. Primary antibodies, in 5% NDS/MTSB, were incubated overnight at 4 °C and then washed four times with MTSB. Secondary antibodies, in 5% NDS/MTSB, were incubated 1 h at RT and then washed four times with MTSB. Antibody dilutions were as follows: rabbit anti-CHC (Agriser, AS10 690) 1/300, rabbit anti-PIN2 (ref. 66) 1/1,000; rabbit anti-MEMB11 (ref. 29) 1/300, TRITC-coupled donkey anti-rabbit IgG (Jackson Immunoresearch, 711-025-152) 1/300 and AlexaFluor 647 (A647)-coupled donkey anti-rabbit IgG (Jackson Immunoresearch, 711-605-152) 1/300. Confocal laser

scanning microscopy was performed using Leica TCS SP5 AOBs and Leica TCS SP8 AOBs systems (Leica). For live-cell imaging, seedlings were mounted with LM medium between one 24 \times 50 mm coverslip and one 24 \times 24 mm coverslip separated with double-sided tape. Co-localization analyses were performed using geometrical object-based method⁶⁷ and the JACoP plug-in of ImageJ⁶⁸ (<http://rsb.info.nih.gov/ij/plugins/track/jacop.html>). Briefly, the distance between centroids of green-labelled and red-labelled objects was calculated for all possible combination. When the distance between two labelled structures is below the resolution limit of the objective (200 nm), the co-localization was considered as true. Laser excitation lines for the different fluorophores were 405 nm for 4,6-diamidino-2-phenylindole, 458 nm for CFP, 488 nm for GFP, 514 nm for YFP and venus, 561 nm for mCherry and TRITC, and 633 nm for A647. Fluorescence emissions were detected at 410–480 nm for 4,6-diamidino-2-phenylindole, 465–515 nm for CFP, 521–600 nm for GFP, YFP and venus, 566–650 nm for mCherry and TRITC, and 643–740 nm for A647. In multi-labelling acquisitions, detection was in sequential line-scanning mode with a line average of 4. An oil-corrected \times 63 objective, numerical aperture = 1.4 (HCX PL APO CS 63.0x1.40 OIL UV) was used in immunolabelling and live-cell imaging experiments.

Immunoprecipitation of intact TGN and Golgi compartments. The method is based on previously published TGN immuno-isolation procedure with some modifications²⁵. In brief, *Arabidopsis* seedlings are grown in 250 ml of LM in 500 ml flasks for 9 days under 120 r.p.m. shaking and 16 h light/8 h darkness cycle. Seedlings are transferred to a mortar pre-cooled on ice and then grinded with a pillar in three times more (w/v) vesicle isolation buffer: HEPES 50 mM pH 7.5, 0.45 M sucrose, 5 mM MgCl₂, 1 mM dithiothreitol, 0.5% PVP (Sigma) and 1 mM phenylmethylsulfonyl fluoride. The homogenate is then filtered through a Miracloth mesh and centrifuged at 1,600 *g* for 20 min. The supernatant is transferred to a new tube and centrifuged two more times at 1,600 *g* for 20 min. Supernatant is then loaded on 38% sucrose cushion (the sucrose is dissolved in 50 mM HEPES pH 7.4) and centrifuged at 150,000 *g* for 3 h at 4 °C. The total pool of membranes is located at the interface between the sucrose and the supernatant. After removing the supernatant, a step-gradient sucrose is built on the top of the membrane interface with 33 and 8% sucrose solutions (dissolved in 50 mM HEPES

pH 7.4) successively. Tubes are centrifuged overnight at 150,000 g at 4 °C. A band of membranes appears at the 33/8% sucrose interface and is harvested, diluted in 2–3 volume of 50 mM HEPES pH 7.4, centrifuged at 150,000 g for 2 h at 4 °C and resuspended in the resuspension buffer (50 mM HEPES pH 7.4, 0.25 M sucrose, 1.5 mM MgCl₂, 150 mM NaCl, 1 mM phenylmethylsulfonyl fluoride and protease inhibitor cocktail from Sigma). This resuspended fraction is the TM fraction we used as input for the IPs. Immunoprecipitation was performed with magnetic Dynabeads coupled to proteinA according to the manufacturer's instructions (Invitrogen). For each IP, 150 µl of beads were first washed with PBS-Tween (137 nM NaCl, 2.7 nM KCl, 10 nM Na₂HPO₄, 1.8 nM KH₂PO₄ and 0.02% Tween-20), then incubated with 15 µl of rabbit anti-GFP antibodies (Invitrogen, A-11122) for 1 h with shaking at 4 °C. After one PBS-Tween wash, beads are equilibrated in the resuspension buffer for 10 min on ice. Beads bound the anti-GFP antibodies are then incubated with 1 ml of purified TM extract for 1 h with shaking at 4 °C. After incubation, eight washes are performed with 1 ml of resuspension buffer for 5 min with shaking at 4 °C for each wash. Beads bound to targeted vesicles are eventually resuspended in 50 µl of resuspension buffer.

Western blottings of IP fractions. Polyacrylamide gels were casted using the TGX Stain-Free FastCast premixed acrylamide solution manufactured by Bio-Rad. After gel activation, proteins were visualized and imaged using a ChemiDoc MP imaging system (Bio-Rad). Initial step-gradient-purified TM fractions (IP input) and beads-IP fractions (IP output) were loaded at equal quantity on SDS-PAGE gel and subjected to western blotting. To equally load TM fractions and IPs fractions, we quantified the whole individual tracks using ImageJ software and adjusted the quantity of proteins loaded in each track to reach equal loading. For western blotting, the following antibodies and dilutions were used: mouse anti-GFP recognizing CFP, GFP and YFP (Roche, 118144600001) 1/1,000, rabbit anti-Sec21p (Agrisera, AS08 327) 1/1,000, rabbit anti-Memb11 1/1,000 (ref. 29), rabbit anti-ECH²¹ 1/1,000, rabbit anti-SYP61 (ref. 69) 1/1,000, rabbit anti-V-ATPase (VHA-E) 1/2,000 (Agrisera, AS07 213), rabbit anti-PMA2 (ref. 70) 1/1,000 and rabbit anti-H⁺ PM-ATPase (Agrisera, AS07 260) 1/1,000. Secondary antibodies were as follows: goat anti-mouse IgG-HRP conjugate (1/3,000, Bio-Rad, 1721011) and goat anti-rabbit IgG-HRP conjugate (1/5,000, Bio-Rad, 1706515). Pictures were acquired using a ChemiDoc MP imaging system (Bio-Rad). To calculate the IP efficiency, quantifications of intensities were done using the ImageJ software on pictures in which signals were white and background black. Boxes of exact same size were positioned on signals of the IP input line (TM fraction) and IP output (beads immunopurification) on anti-CFP/YFP blots. Uncropped pictures of full western blottings displaying enrichment of targeted compartments in IPs is available in Supplementary Fig. 2b.

Characterization of lipid composition. For acyl-chain characterization of lipids from beads-IP fractions and global FAs analyses from roots, 25 µl of beads extracts or fresh roots were directly incubated with 1 ml of 5% sulfuric acid solution in methanol (implemented with standards: 5 µg ml⁻¹ of C17:0 and 5 µg ml⁻¹ of h14:0) for transesterification (exchange of the organic group of esterified/amidified FAs by the methyl group of methanol). Transesterification is made overnight at 85 °C and leads to production of FAs methyl esters (FAMES). FAMES are then extracted by adding 1 ml of NaCl 2.5% and 1 ml of hexane 99%. After vigorous shaking and centrifugation at 700 g for 5 min at RT, the higher phase is collected, placed in a new tube and buffered with 1 ml of 100 mM Tris, 0.09% NaCl pH 8 with HCl. After vigorous shaking and centrifugation at 700 g for 5 min at RT, the higher phase is collected, placed in a new tube and evaporated with needles evaporating pan. Then, 200 µl of N,O-Bis(trimethylsilyl)trifluoroacetamide + 1% trimethylsilyl (BSTFA + 1% TMCS, Sigma) were added and incubated at 110 °C for 20 min. After evaporation, FAMES are resuspended in 100 µl of 99% hexane and run on GC-MS. For sterols characterization from beads-IP fractions, 25 µl of beads extracts were directly incubated with 1 ml chloroform/methanol (2:1) (implemented with the standard: 5 µg α-cholestanol) for 2 h at RT. Lipid extract was then washed with 1 ml 0.9% NaCl, vigorously shaken and centrifuged at 700 g for 5 min at RT. The organic (lower) phase is collected and evaporated. Then, a saponification is performed on the lipid extract by incubating with 1 ml 99% ethanol and 100 µl of 11 N KOH for 1 h at 80 °C. After incubation, 1 ml of 99% hexane and 2 ml of water are added. After vigorous shaking and centrifugation at 700 g for 5 min at RT, the higher phase is collected, placed in a new tube and buffered with 1 ml of 100 mM Tris, 0.09% NaCl pH 8 with HCl. After evaporation, sterols are incubated with 200 µl BSTFA + 1% TMCS, at 110 °C for 20 min. After evaporation, sterols are resuspended in 100 µl of 99% hexane and run on GC-MS.

For lipid characterization in *Arabidopsis* roots, lipids were extracted using methyl-*tert*-butyl ether (MTBE) as described previously⁷¹ and separated by high-performance thin-layer-chromatography (HPTLC). In brief, *Arabidopsis* roots were collected and incubated in 1 ml of boiling isopropanol for 10 min. Samples were then grinded in 5 ml of MTBE/methanol/water (10/3/2.5) in a glass potter and then transferred into a glass tube (called A). Samples were then heated at 60 °C for 30 min. Next, 3–4 ml of NaCl 0.9% was added to tube A and, after a vigorous shaking, was incubated another time at 60 °C for 30 min and then centrifuged at 700 g for 5 min at RT. The upper phase of tube A was collected and transferred into a new tube (called B). To the lower phase of the tube A, 3–4 ml of 100% MTBE was added. After shaking and centrifugation at 700 g for 5 min at RT, the upper phase

of tube A was collected and added to tube B where the upper phase was saved previously. After evaporation of tube B, lipids were resuspended in chloroform/methanol/water (3/6/0.8).

For GlcCer separation, lipids were separated by HPTLC using the following migration solvent: methyl acetate, *n*-propanol/chloroform/methanol/0.25% KCl (2.5/2.5/2.5/1/0.9). For GIPCs, MTBE-dried extract was first de-esterified (to remove glycerophospholipids) by dissolving in 2 ml of 33% methylamine solution in ethanol/water (7:3 v/v) and incubating at 50 °C for 1 h. After hydrolysis the sample was dried and dissolved with heating and gentle sonication in chloroform/methanol/water (3/6/0.8). Then, lipids were separated by HPTLC impregnated with freshly prepared 0.2 M ammonium acetate dissolved in methanol. The migration solvent for GIPCs migration was as following: chloroform/methanol/NH₄OH 4 N (in water) (9/7/2). Following this migration, glycerophospholipids were collected at the top of the plate and GIPCs were collected at the bottom of the plate. For both GlcCer and GIPCs separations, plates were run emptied with respective migration solvent before the loading of the plate. For both GlcCer and GIPCs, lipids on plate were stained with primuline. Pictures were acquired using a ChemiDoc MP imaging system (Bio-Rad). GlcCer and GIPCs spots were scratched off from plates and used for further analyses for acyl-chain composition using the above described procedure to produce FAMES followed by GC-MS analyses.

We always normalized non-hydroxylated FAs using heptadecanoic acid (17:0) and normalized hydroxylated FAs using 2-hydroxyltetradecanoic acid (h14:0). As GC-MS is measuring a mass of compound and not a number of molecules, we used the molecular weight of each individual FAs (that were transesterified to volatized FAs in GC and resulted in FAMES) to calculate the FAs content, expressed either as nmol% (when compared to the total pool of FAs) or nmol mg⁻¹ fresh weight (when compared with the weight of starting material).

To quantify TAGs and DAGs lipids, roots from 5-day-old seedlings were grinded and homogenized in 1 ml of CHCl₃-MeOH (2/1) in sintered glass tubes. Lipid extracts were then washed three times by an aqueous solution containing 0.9% of NaCl. After solvent evaporation, lipid extracts were resuspended in 100 µl of CHCl₃-MeOH (1/1). TAGs were separated from other lipids on HPTLC silica plates (silica gel 60 F 254, Merck, Germany) eluted with Hexane/Diethylether/acetic acid (90/15/2). Identification of lipids was done using lipid standards from Aventi Lipids (USA) and lipid quantification was performed by densitometry analysis⁷² using a TLC scanner 3 (CAMAG). The amounts (µg) of lipids were determined by using standard curves established with the standard lipids.

Root gravitropism assays and DII-venus visualization. Seedlings were grown on agar plates, cultured vertically at 22 °C under a 16 h light/8 h dark cycle for 3 days. They were then transferred to darkness under the same growth condition and incubated for a further 24 h, maintaining the same growth plate orientation. Next, plates were turned counter-clockwise through 90° and incubated vertically in the dark for 24 h under the same growth conditions. Photographs were then taken and the angle formed between the root tip and the new gravity vector was measured using ImageJ Software. For kinematic analyses seedlings were photographed starting from the gravistimulation at 1 h intervals for 24 h using a Canon D50 without infrared filter, remotely controlled by Canon Remote. The angles were ranked into twelve 15° negative values classes (from -180 to 0) and into twelve 15° positive values classes (from 1 to 180). Percentage from the total number of roots angles measurements was charted per class. Data presented in gravitropism charts were pooled from three independent experiments.

For DII-venus visualization, live imaging was performed 60 min after gravistimulation. Fluorescence at the root tip was acquired using strictly identical acquisition parameters (laser power, photomultiplier, offset, zoom factor and resolution) between the treated and untreated line. Fluorescence intensity was measured on the two opposite sides of the root using LAS AF Live Software. Background fluorescence was subtracted. Finally ratio between upper side and lower side was calculated.

Transmission electron microscopy. High-pressure freezing was performed on root of 5-day-old plants with a LEICA EM-PACT1 device. To easily separate the frozen samples of the high-pressure freezing carrier, the supports were previously coated with 2% phosphatidylcholine. As cryoprotectant we used a solution of 20% BSA diluted in LM implemented or not with 50 nM metazachlor. Freeze-substitution steps were achieved in a LEICA AFS2 system as follows: -90 °C during 72 h in acetone with 2% OsO₄ and 0.1% uranyl acetate, the temperature was then increased at the rate of 3 °C h⁻¹ until -50 °C was reached. Then, washings in acetone followed by washings in ethanol were performed. The embedding step was progressively achieved in the lowicryl resin HM20 (EMS) at -50 °C before the resin was polymerized under ultraviolet during 48 h at -50 °C followed by 48 h at 20 °C.

Chemical fixation of roots was performed on 5-day-old *Arabidopsis* roots that were fixed for 1 h in paraformaldehyde 1% + glutaraldehyde 3% dissolved in 0.1 M cacodylate buffer (pH 7.2), rinsed, incubated with tannic acid (0.1% in water) for 30 min, rinsed, postfixed in 1% OsO₄ in phosphate buffer 1 h, rinsed, dehydrated through an ethanol series and impregnated in increasing concentrations of SPURR⁷³ resin over a period of 2 days before being polymerized at 70 °C for 19 h.

For transmission electron microscopy observations, ultrathin sections of 70 nm thicknesses were made and imaged using a transmission electron microscopy FEI Tecnai G2 Spirit TWIN 120kV equipped with a CCD 16Mpixels Eagle 4k.

Statistics. All data analysed were unpaired (samples independent from each other). Normal distribution (Gaussian distribution) of data set was tested using Shapiro-Wilk normality test. On data normally distributed, sample homoscedasticity was assessed using Bartlett test before performing parametric tests. On data that were not normally distributed (or on data sets for which $n < 10$), non-parametric tests were performed. To compare two data sets, Welch two sample *t*-test was performed on data set normally distributed, whereas Mann-Whitney test was used as non-parametric test. To compare multiple data sets, Kruskal-Wallis test was used as non-parametric test. Tukey's test was used as a single-step multiple comparison procedure to find means significantly different from each other. All statistical tests were two-tailed (two-sided test). All statistical analyses were performed with R i386 3.1.0 software. *P*-values were as follows: $\chi^2 P$ -value > 0.05 (nonsignificant), $*P < 0.05$, $**P < 0.01$ and $***P < 0.001$. Variances between each group of data were either represented in box plot or by the s.d. Sample sizes to ensure adequate power were as follows: co-localization experiments $n =$ at least 40, lipid analyses on immunoprecipitated compartments $n =$ at least 10, lipid analyses on *Arabidopsis* roots $n =$ at least 4, root gravitropism assays $n =$ at least 50, single localization in *Arabidopsis* roots $n =$ at least 20 roots.

Data availability. The authors declare that all data supporting the findings of this study are available within the article and its Supplementary Information files or are available from the corresponding author on request.

References

- van Meer, G., Stelzer, E. H., Wijnaendts-van-Resandt, R. W. & Simons, K. Sorting of sphingolipids in epithelial (Madin-Darby canine kidney) cells. *J. Cell Biol.* **105**, 1623–1635 (1987).
- Simons, K. & van Meer, G. Lipid sorting in epithelial cells. *Biochemistry* **27**, 6197–6202 (1988).
- Gleeson, P. A., Lock, J. G., Luke, M. R. & Stow, J. L. Domains of the TGN: coats, tethers and G proteins. *Traffic* **5**, 315–326 (2004).
- Rodriguez-Boulán, E., Paskiet, K. T., Salas, P. J. & Bard, E. Intracellular transport of influenza virus hemagglutinin to the apical surface of Madin-Darby canine kidney cells. *J. Cell Biol.* **98**, 308–319 (1984).
- Kleine-Vehn, J. *et al.* Recycling, clustering, and endocytosis jointly maintain PIN auxin carrier polarity at the plasma membrane. *Mol. Syst. Biol.* **7**, 540 (2011).
- Müller, A. *et al.* AtPIN2 defines a locus of *Arabidopsis* for root gravitropism control. *EMBO J.* **17**, 6903–6911 (1998).
- Sampaio, J. L. *et al.* Membrane lipidome of an epithelial cell line. *Proc. Natl Acad. Sci. USA* **108**, 1903–1907 (2011).
- Zhang, H. *et al.* Apicobasal domain identities of expanding tubular membranes depend on glycosphingolipid biosynthesis. *Nat. Cell Biol.* **13**, 1189–1201 (2011).
- Klemm, R. W. *et al.* Segregation of sphingolipids and sterols during formation of secretory vesicles at the *trans*-Golgi network. *J. Cell Biol.* **185**, 601–612 (2009).
- Sabatini, S. *et al.* An auxin-dependent distal organizer of pattern and polarity in the *Arabidopsis* root. *Cell* **99**, 463–472 (1999).
- Friml, J. *et al.* Efflux-dependent auxin gradients establish the apical-basal axis of *Arabidopsis*. *Nature* **426**, 147–153 (2003).
- Benková, E. *et al.* Local, efflux-dependent auxin gradients as a common module for plant organ formation. *Cell* **115**, 591–602 (2003).
- Wisniewska, J. *et al.* Polar PIN localization directs auxin flow in plants. *Science* **312**, 883 (2006).
- Grienenstein, V. A., Xu, J., Marée, A. F., Hogeweg, P. & Scheres, B. Auxin transport is sufficient to generate a maximum and gradient guiding root growth. *Nature* **449**, 1008–1013 (2007).
- Luschign, C., Gaxiola, R. A., Grisafi, P. & Fink, G. R. EIR1, a root-specific protein involved in auxin transport, is required for gravitropism in *Arabidopsis thaliana*. *Genes Dev.* **12**, 2175–2187 (1998).
- Rahman, A. *et al.* Gravitropism of *Arabidopsis thaliana* roots requires the polarization of PIN2 toward the root tip in meristematic cortical cells. *Plant Cell* **22**, 1762–1776 (2010).
- Drdova, E. J. *et al.* The exocyst complex contributes to PIN auxin efflux carrier recycling and polar auxin transport in *Arabidopsis*. *Plant J.* **73**, 709–719 (2013).
- Teh, O. K. & Moore, I. An ARF-GEF acting at the Golgi and in selective endocytosis in polarized plant cells. *Nature* **448**, 493–496 (2007).
- Tanaka, H. *et al.* BEX1/ARF1A1C is required for BFA-sensitive recycling of PIN auxin transporters and auxin-mediated development in *Arabidopsis*. *Plant Cell Physiol.* **55**, 737–749 (2014).
- Chow, C. M., Neto, H., Foucart, C. & Moore, I. Rab-A2 and Rab-A3 GTPases define a *trans*-golgi endosomal membrane domain in *Arabidopsis* that contributes substantially to the cell plate. *Plant Cell* **20**, 101–123 (2008).
- Gendreau, D. *et al.* Conserved *Arabidopsis* ECHIDNA protein mediates *trans*-Golgi-network trafficking and cell elongation. *Proc. Natl Acad. Sci. USA* **108**, 8048–8053 (2011).
- Boutté, Y. *et al.* ECHIDNA-mediated post-Golgi trafficking of auxin carriers for differential cell elongation. *Proc. Natl Acad. Sci. USA* **110**, 16259–16264 (2013).
- Doyle, S. M. *et al.* An early secretory pathway mediated by GNOM-LIKE 1 and GNOM is essential for basal polarity establishment in *Arabidopsis thaliana*. *Proc. Natl Acad. Sci. USA* **112**, E806–E815 (2015).
- Kang, B. H., Nielsen, E., Preuss, M. L., Mastronarde, D. & Staehelin, L. A. Electron tomography of RabA4b- and PI-4K β 1-labeled *trans*-Golgi network compartments in *Arabidopsis*. *Traffic* **12**, 313–329 (2011).
- Drakakaki, G. *et al.* Isolation and proteomic analysis of the SYP61 compartment reveal its role in exocytic trafficking in *Arabidopsis*. *Cell Res.* **22**, 413–424 (2012).
- Robert, S. *et al.* Endosidin1 defines a compartment involved in endocytosis of the brassinosteroid receptor BRI1 and the auxin transporters PIN2 and AUX1. *Proc. Natl Acad. Sci. USA* **105**, 8464–8469 (2008).
- Uemura, T. *et al.* Systematic analysis of SNARE molecules in *Arabidopsis*: dissection of the post-Golgi network in plant cells. *Cell Struct. Funct.* **29**, 49–65 (2004).
- Geldner, N. *et al.* Rapid, combinatorial analysis of membrane compartments in intact plants with a multicolor marker set. *Plant J.* **59**, 169–178 (2009).
- Marais, C. *et al.* The Q β -SNARE Memb11 interacts specifically with Arf1 in the Golgi apparatus of *Arabidopsis thaliana*. *J. Exp. Bot.* **66**, 6665–6678 (2015).
- Dettmer, J., Hong-Hermesdorf, A., Stierhof, Y. D. & Schumacher, K. Vacuolar H $^{+}$ -ATPase activity is required for endocytic and secretory trafficking in *Arabidopsis*. *Plant Cell* **18**, 715–730 (2006).
- Song, J., Lee, M. H., Lee, G. J., Yoo, C. M. & Hwang, I. *Arabidopsis* EPSIN1 plays an important role in vacuolar trafficking of soluble cargo proteins in plant cells via interactions with clathrin, AP-1, VTI11, and VSRI. *Plant Cell* **18**, 2258–2274 (2006).
- Sauer, M. *et al.* MTV1 and MTV4 encode plant-specific ENTH and ARF GAP proteins that mediate clathrin-dependent trafficking of vacuolar cargo from the *trans*-Golgi network. *Plant Cell* **25**, 2217–2235 (2013).
- Buré, C., Cacas, J. L., Mongrand, S. & Schmitter, J. M. Characterization of glycosyl inositol phosphoryl ceramides from plants and fungi by mass spectrometry. *Anal. Bioanal. Chem.* **406**, 995–1010 (2014).
- Tresch, S., Heilmann, M., Christiansen, N., Looser, R. & Grossmann, K. Inhibition of saturated very-long-chain fatty acid biosynthesis by mefluidide and perfluidone, selective inhibitors of 3-ketoacyl-CoA synthases. *Phytochemistry* **76**, 162–171 (2012).
- Vishwanath, S. J. *et al.* Suberin-associated fatty alcohols in *Arabidopsis*: distributions in roots and contributions to seed coat barrier properties. *Plant Physiol.* **163**, 1118–1132 (2013).
- Hruz, T. *et al.* Genevestigator v3: a reference expression database for the meta-analysis of transcriptomes. *Adv. Bioinformatics* **2008**, 420747 (2008).
- Joubès, J. *et al.* The VLCFA elongase gene family in *Arabidopsis thaliana*: phylogenetic analysis, 3D modelling and expression profiling. *Plant Mol. Biol.* **67**, 547–566 (2008).
- Kim, J. *et al.* *Arabidopsis* 3-ketoacyl-coenzyme a synthase9 is involved in the synthesis of tetracosanoic acids as precursors of cuticular waxes, suberins, sphingolipids, and phospholipids. *Plant Physiol.* **162**, 567–580 (2013).
- Lee, S. B. *et al.* Two *Arabidopsis* 3-ketoacyl CoA synthase genes, KCS20 and KCS2/DAISY, are functionally redundant in cuticular wax and root suberin biosynthesis, but differentially controlled by osmotic stress. *Plant J.* **60**, 462–475 (2009).
- Compagnon, V. *et al.* CYP86B1 is required for very long chain omega-hydroxyacid and alpha, omega -dicarboxylic acid synthesis in root and seed suberin polyester. *Plant Physiol.* **150**, 1831–1843 (2009).
- Brunoud, G. *et al.* A novel sensor to map auxin response and distribution at high spatio-temporal resolution. *Nature* **482**, 103–106 (2012).
- Marchant, A. *et al.* AUX1 regulates root gravitropism in *Arabidopsis* by facilitating auxin uptake within root apical tissues. *EMBO J.* **18**, 2066–2073 (1999).
- Xi, W., Gong, X., Yang, Q., Yu, H. & Liou, Y. C. Pin1At regulates PIN1 polar localization and root gravitropism. *Nat. Commun.* **7**, 10430 (2016).
- Kleine-Vehn, J. *et al.* Gravity-induced PIN transcytosis for polarization of auxin fluxes in gravity-sensing root cells. *Proc. Natl Acad. Sci. USA* **107**, 22344–22349 (2010).
- Viotti, C. *et al.* Endocytic and secretory traffic in *Arabidopsis* merge in the *trans*-Golgi network/early endosome, an independent and highly dynamic organelle. *Plant Cell* **22**, 1344–1357 (2010).
- Grebe, M. *et al.* *Arabidopsis* sterol endocytosis involves actin-mediated trafficking via ARA6-positive early endosomes. *Curr. Biol.* **13**, 1378–1387 (2003).
- Men, S. *et al.* Sterol-dependent endocytosis mediates post-cytokinetic acquisition of PIN2 auxin efflux carrier polarity. *Nat. Cell Biol.* **10**, 237–244 (2008).

48. Markham, J. E. *et al.* Sphingolipids containing very-long-chain fatty acids define a secretory pathway for specific polar plasma membrane protein targeting in *Arabidopsis*. *Plant Cell* **23**, 2362–2378 (2011).
49. Dyson, R. J. *et al.* Mechanical modelling quantifies the functional importance of outer tissue layers during root elongation and bending. *New Phytol.* **202**, 1212–1222 (2014).
50. Muñoz, M. & Riezman, H. Trafficking of glycosylphosphatidylinositol anchored proteins from the endoplasmic reticulum to the cell surface. *J. Lipid Res.* **57**, 352–360 (2016).
51. Contreras, F. X. *et al.* Molecular recognition of a single sphingolipid species by a protein's transmembrane domain. *Nature* **481**, 525–529 (2012).
52. Baumgart, T. *et al.* Large-scale fluid/fluid phase separation of proteins and lipids in giant plasma membrane vesicles. *Proc. Natl Acad. Sci. USA* **104**, 3165–3170 (2007).
53. Simons, K. & Ikonen, E. Functional rafts in cell membranes. *Nature* **387**, 569–572 (1997).
54. Lingwood, D., Ries, J., Schuille, P. & Simons, K. Plasma membranes are poised for activation of raft phase coalescence at physiological temperature. *Proc. Natl Acad. Sci. USA* **105**, 10005–10010 (2008).
55. Kaiser, H. J. *et al.* Order of lipid phases in model and plasma membranes. *Proc. Natl Acad. Sci. USA* **106**, 16645–16650 (2009).
56. Grosjean, K., Mongrand, S., Beney, L., Simon-Plas, F. & Gerbeau-Pissot, P. Differential effect of plant lipids on membrane organization: specificities of phytosphingolipids and phytosterols. *J. Biol. Chem.* **290**, 5810–5825 (2015).
57. Školová, B. *et al.* Different phase behavior and packing of ceramides with long (C16) and very long (C24) acyls in model membranes: infrared spectroscopy using deuterated lipids. *J. Phys. Chem. B.* **118**, 10460–10470 (2014).
58. Grant, C. W., Mehlhorn, I. E., Florio, E. & Barber, K. R. A long chain spin label for glycosphingolipid studies: transbilayer fatty acid interdigitation of lactosyl ceramide. *Biochim. Biophys. Acta* **902**, 169–177 (1987).
59. Roux, A. *et al.* Role of curvature and phase transition in lipid sorting and fission of membrane tubules. *EMBO J.* **24**, 1537–1545 (2005).
60. Pinto, S. N., Silva, L. C., Futerman, A. H. & Prieto, M. Effect of ceramide structure on membrane biophysical properties: the role of acyl chain length and unsaturation. *Biochim. Biophys. Acta* **1808**, 2753–2760 (2011).
61. Bennett, M. J. *et al.* *Arabidopsis* AUX1 gene: a permease-like regulator of root gravitropism. *Science* **273**, 948–950 (1996).
62. Xu, J. & Scheres, B. Dissection of *Arabidopsis* ADP-RIBOSYLATION FACTOR 1 function in epidermal cell polarity. *Plant Cell* **17**, 525–536 (2005).
63. Swarup, R. *et al.* Structure-function analysis of the presumptive *Arabidopsis* auxin permease AUX1. *Plant Cell* **16**, 3069–3083 (2004).
64. Konopka, C. A., Backues, S. K. & Bednarek, S. Y. Dynamics of *Arabidopsis* dynamin-related protein 1C and a clathrin light chain at the plasma membrane. *Plant Cell* **20**, 1363–1380 (2008).
65. Boutté, Y. & Grebe, M. Immunocytochemical fluorescent *in situ* visualization of proteins in *Arabidopsis*. *Methods Mol. Biol.* **1062**, 453–472 (2014).
66. Abas, L. *et al.* Intracellular trafficking and proteolysis of the *Arabidopsis* auxin-efflux facilitator PIN2 are involved in root gravitropism. *Nat. Cell Biol.* **8**, 249–256 (2006).
67. Boutte, Y., Crosnier, M. T., Carraro, N., Traas, J. & Satiat-Jeunemaitre, B. The plasma membrane recycling pathway and cell polarity in plants: studies on PIN proteins. *J. Cell Sci.* **119**, 1255–1265 (2006).
68. Bolte, S. & Cordelières, F. P. A guided tour into subcellular colocalization analysis in light microscopy. *J. Microsc.* **224**, 213–232 (2006).
69. Sanderfoot, A. A., Kovaleva, V., Bassham, D. C. & Raikhel, N. V. Interactions between syntaxins identify at least five SNARE complexes within the Golgi/prevacuolar system of the *Arabidopsis* cell. *Mol. Biol. Cell* **12**, 3733–3743 (2001).
70. Morsomme, P., Dambly, S., Maudoux, O. & Boutry, M. Single point mutations distributed in 10 soluble and membrane regions of the Nicotiana plumbaginifolia plasma membrane PMA2 H + -ATPase activate the enzyme and modify the structure of the C-terminal region. *J. Biol. Chem.* **273**, 34837–34842 (1998).
71. Matyash, V., Liebisch, G., Kurzchalia, T. V., Shevchenko, A. & Schwudke, D. Lipid extraction by methyl-tert-butyl ether for high-throughput lipidomics. *J. Lipid Res.* **49**, 1137–1146 (2008).
72. Macala, L. J., Yu, R. K. & Ando, S. Analysis of brain lipids by high performance thin-layer chromatography and densitometry. *J. Lipid Res.* **24**, 1243–1250 (1983).
73. Spurr, A. R. A low-viscosity epoxy resin embedding medium for electron microscopy. *J. Ultrastruct. Res.* **26**, 31–43 (1969).

Acknowledgements

We gratefully acknowledge K. Schumacher (University of Heidelberg, Germany), I. Moore (University of Oxford, UK), T. Vernoux (ENS, Lyon, France), M. Bennett (University of Nottingham, UK), J. Friml (Institute of Science and Technology, Austria), S. Bednarek (University of Wisconsin-Madison, USA) and Mi Chung Suh (Chonnam National University, Korea) for sharing published research materials that were important for this study. We warmly acknowledge Christian Luschig for the generous gift he made of the rabbit PIN2 antibody that was essential for this work. This work was supported by a grant co-funded by 'initiative d'excellence de l'Université de Bordeaux (IdEx Bordeaux)' and the French National Research Center (CNRS) to Y.B. We acknowledge the French National Research Agency (ANR) for programme blanc 'PANACEA' NT09_517917, contract to S.M. and 'ACETOTRYP' 2010 BLAN 1319 03 contract to P.M. R.P.B. was funded by grants from Knut and Alice Wallenberg foundation. We kindly acknowledge the engineers from Bordeaux Imaging Center Facility (BIC, UMS 3420 CNRS, U4 INSERM), member of the France-BioImaging infrastructure supported by the French National Research Agency (ANR-10-INBS-04, <<Investments for the future>>), where the Microscopy was performed and CGFB Bordeaux Metabolome Facility-MetaboHUB (ANR-11-INBS-0010; http://www.biomemb.cnrs.fr/page_8.html), where lipidomic analyses were performed.

Author contributions

All gravitropism assays were performed by V.W.-B. Kinematic analysis was done by K.J. Co-localizations were performed by V.W.-B, K.J. and Y.B. DII-venus experiment was done by V.W.-B. Single localizations of auxin carriers were performed by Y.B. Immunoprecipitations and western blottings were done by Y.B. and N.E. All lipid analyses were performed by J.J., F.D., S.M., P.M. and Y.B. Electron microscopy was performed by L.B. All statistical analyses were run by V.W.-B. The manuscript was written by Y.B. with contributions of S.M., N.R., R.P.B. and P.M. Funding important for this study was obtained by S.M., N.R., R.P.B., P.M. and Y.B. Research was designed by Y.B.

Additional information

Supplementary Information accompanies this paper at <http://www.nature.com/naturecommunications>

Competing financial interests: The authors declare no competing financial interests.

Reprints and permission information is available online at <http://npg.nature.com/reprintsandpermissions/>

How to cite this article: Watelet-Boyer, V. *et al.* Enrichment of hydroxylated C24- and C26-acyl-chain sphingolipids mediates PIN2 apical sorting at *trans*-Golgi network subdomains. *Nat. Commun.* **7**:12788 doi: 10.1038/ncomms12788 (2016).



This work is licensed under a Creative Commons Attribution 4.0 International License. The images or other third party material in this article are included in the article's Creative Commons license, unless indicated otherwise in the credit line; if the material is not included under the Creative Commons license, users will need to obtain permission from the license holder to reproduce the material. To view a copy of this license, visit <http://creativecommons.org/licenses/by/4.0/>

© The Author(s) 2016

LA PROTÉOMIQUE DE SOUS-DOMAINES DU *TRANS*-GOLGI NETWORK RÉVÈLE UN LIEN ENTRE LES SPHINGOLIPIDES ET LES PHOSPHOINOSITIDES CHEZ LES PLANTES

La polarité cellulaire est une caractéristique commune à tous les organismes. Jusqu'à récemment, il était assumé que la sécrétion de protéines vers des domaines polaires de la cellule végétale se faisait de façon non polarisée, mais ce point de vue a été re-étudié, la sécrétion est polarisée mais la dynamique, les voies de trafic empruntées et les mécanismes sont toujours inconnus. Précédemment, mon laboratoire d'accueil a caractérisé un enrichissement en sphingolipides contenant des acides gras à très longues chaînes (VLCFAs) au niveau d'un sous-domaine du trans-Golgi Network (TGN) appelé Vésicules de Sécrétions (SVs). Plus précisément, il a été montré que la longueur des acides gras des sphingolipides jouait un rôle critique dans la sécrétion du transporteur d'auxine PIN2 des SVs vers des domaines polaires de la membrane plasmique. Pendant ma thèse, je me suis intéressé à la question suivante : comment les sphingolipides agissent-ils au TGN? En identifiant le protéome des SVs, ainsi qu'en utilisant des outils génétiques et pharmacologiques en combinaison avec la visualisation de marqueurs lipidiques, j'ai pu identifier que les sphingolipides agissent sur l'homéostasie des phosphoinositides en mettant en avant un lien fonctionnel entre ces deux classes de lipides au sein de la cellule végétale. En utilisant un set de marqueurs des phosphoinositides (PIPs), j'ai pu montrer que les sphingolipides ciblent principalement le phosphatidyl-inositol-3-phosphate, PI(3)P et le phosphatidyl-inositol-4-phosphate, PI(4)P. De plus, mon analyse protéomique a montré que la localisation d'un ensemble de protéines liées aux PIPs était diminuée dans les SVs/TGN immunopurifiées quand la composition des sphingolipides est altérée. Mes résultats nous forcent à revoir notre vision de la dynamique des lipides au niveau des membranes, et suggère l'idée que la dynamique de remodelage de la composition d'une classe de lipide, les phosphoinositides, peut être modulée par une autre classe de lipide, les sphingolipides.

Mots clés : *trans*-Golgi Network, Protéomique, Sphingolipides, Phosphoinositides, Vésicules

PROTEOMICS OF *TRANS*- GOLGI NETWORK SUBDOMAINS REVEAL A LIPID CROSSTALK BETWEEN SPHINGOLIPIDS AND PHOSPHOINOSITIDES IN PLANTS

Cell polarity is a defining feature of all organisms. Until very recently, it was thought that delivery of proteins to polar domains of root epidermal cells plasma membrane was non-polar, but this view has been re-examined, the delivery is polar but the dynamics, the paths taken, and the mechanisms are unknown. My host team previously characterised an enrichment of Very-Long-Chain-Fatty-Acids (VLCFAs)-containing sphingolipids at the site of secretory vesicles (SVs) sub-domain of the trans-Golgi Network (TGN). Moreover, the length of sphingolipids acyl-chain was found to play a critical role in secretory sorting of the auxin carrier PIN2 from SVs-associated TGN to apical polar domain of the plasma membrane (PM). During my PhD, I addressed the following question: how sphingolipids act at SVs/TGN? Using proteomics of SVs, genetics and pharmacological tools in combination with visualisation of lipid probes we could identify that sphingolipids act on phosphoinositides (PIPs) homeostasis establishing a new functional link between these two lipids in plant cells. Using a set of multi-affinity fluorescent PIPs probes I could show that sphingolipids target phosphatidylinositol-3-phosphate (PI3P) and phosphatidylinositol-4-phosphate (PI4P). Moreover, my proteomic analyses show that several PIPs-related proteins are downregulated in immuno-purified TGN-associated SVs when the sphingolipid composition is altered pharmacologically. My results force the reassessment of our view of lipid membranes dynamics and highlight the idea that dynamic remodelling of the composition of one lipid class, the phosphoinositides, can be modulated by another lipid class, the sphingolipids.

Keywords: *trans*-Golgi Network, Proteomic, Sphingolipids, Phosphoinositides, Vesicles

Unité de recherche

Laboratoire de Biogenèse Membranaire, UMR 5200, CNRS, Domaine de la Grande Ferrade INRA
Aquitaine